UNIVERSITEIT GENT

FACULTEIT **WETENSCHAPPEN**

COMPUTATIONAL DYNAMICAL SYSTEMS ANALYSIS:

BOGDANOV-TAKENS POINTS AND AN ECONOMIC MODEL

BASHIR AL-HDAIBAT

AL-HDAIBAT COMPUTATIONAL DYNAMICAL SYSTEMS ANALYSIS 2015

UNIVERSITEIT GENT

Faculty of Science

Department of Applied Mathematics, Computer Science and Statistics

COMPUTATIONAL DYNAMICAL SYSTEMS ANALYSIS:

BOGDANOV-TAKENS POINTS AND AN ECONOMIC MODEL

by

BASHIR AL-HDAIBAT

Supervisors: Prof. Dr. Willy Govaerts

Prof. Dr. Yuri A. Kuznetsov (Utrecht University)

Thesis submitted in fulfillment of the requirements for the degree of

Doctor of Science: Mathematics

December 2015

COMPUTATIONAL DYNAMICAL SYSTEMS ANALYSIS: BOGDANOV-TAKENS POINTS AND AN ECONOMIC MODEL

by

Bashir Al-Hdaibat[1]

Public defence on December 10, 2015

Supervisors:

Prof. Willy Govaerts[1]
Prof. Yuri A. Kuznetsov[2,4]

Examination committee:

Prof. Marnix Van Daele[1] (chair)
Prof. Peter De Maesschalck[3]
Prof. Hans De Meyer[1]
Prof. Hil Meijer[4]
Prof. Hans Vernaeve[5]

---

[1] Department of Applied Mathematics, Computer Science and Statistics, Ghent University, Ghent, Belgium.
[2] Department of Mathematics, Utrecht University, Utrecht, The Netherlands.
[3] Department of Mathematics and Statistics, Hasselt University, Hasselt, Belgium.
[4] Department of Mathematics, University of Twente, Enschede, The Netherlands.
[5] Department of Mathematics, Ghent University, Ghent, Belgium.

Abstract

The subject of this thesis is the bifurcation analysis of dynamical systems (ordinary differential equations and iterated maps). A primary aim is to study the branch of homoclinic solutions that emerges from a Bogdanov-Takens point. The problem of approximating such branch has been studied intensively but neither an exact solution was ever found nor a higher-order approximation has been obtained. We use the classical "blow-up" technique to reduce an appropriate normal form near a Bogdanov-Takens bifurcation in a generic smooth autonomous ordinary differential equations to a perturbed Hamiltonian system. With a regular perturbation method and a generalization of the Lindstedt-Poincaré perturbation method, we derive two explicit third-order corrections of the unperturbed homoclinic orbit and parameter value. We prove that both methods lead to the same homoclinic parameter value as the classical Melnikov technique and the branching method. We show that the regular perturbation method leads to a "parasitic turn" near the saddle point while the Lindstedt-Poincaré solution does not have this turn, making it more suitable for numerical implementation. To obtain the normal form on the center manifold, we apply the standard parameter dependent center manifold reduction combined with the normalization, using the Fredholm solvability of the homological equation. By systematically solving all linear systems appearing from the homological equation, we correct the parameter transformation existing in the literature. The generic homoclinic predictors are applied to explicitly compute the homoclinic solutions in the Gray-Scott kinetic model. The actual implementation of both predictors in the MATLAB continuation package MatCont and five numerical examples illustrating its efficiency are discussed. Besides, the thesis discusses the possibility to use the derived homoclinic predictor of generic ordinary differential equations to continue the branches of homoclinic tangencies in the Bogdanov-Takens map.

The second part of this thesis is devoted to the application of bifurcation theory to analyze the dynamic and chaotic behaviors of a nonlinear economic model. The thesis studies the monopoly model with cubic price and quadratic marginal cost functions. We present fundamental corrections to the earlier studies of the model and a complete discussion of the existence of cycles of period 4. A numerical continuation method is used to compute branches of solutions of period 5, 10, 13 and 17 and to determine the stability regions of these solutions. General formulas for solutions of period 4 are derived analytically. We show that the solutions of period 4 are never linearly asymptotically stable. A nonlinear stability criterion is combined with basin of attraction analysis and simulation to determine the stability region of the 4-cycles. This corrects the erroneous linear stability analysis in previous studies of the model. The chaotic and periodic behavior of the monopoly model are further analyzed by computing the largest Lyapunov exponents, and this confirms the above mentioned results.

The content of this thesis has been published in or submitted for publication, see [2], [3], [107], [92] and [91].

Introduction

Dynamical systems theory is one of the classical topics in mathematics. It deals with the continuous- and discrete-time behavior of mathematical objects, primarily differential equations (ordinary and partial) and difference equations (maps). The theory mainly focuses on analyzing the behavior of such objects and examining its dependence on the parameters. The space in which the objects (states) live is called the state space (*phase space*) of the dynamical system while the parameters live in the *parameter space*. In the case of autonomous ordinary differential equations (ODEs), the solution starting at an initial point x defines a curve in the phase space passing through x. The collection of all curves corresponding to different initial conditions in the phase space forms the phase portrait. In general the phase portrait provides a global qualitative picture of the dynamics of the dynamical systems based on the value of the parameters. If we vary some of the parameters, the phase portrait may change qualitatively. This phenomenon is called a *bifurcation*. The study of dynamical systems so leads to the topic of bifurcation theory. In this field one studies the qualitative changes in the phase portrait, e.g., the appearance or disappearance of equilibria, periodic orbits or more complicated features such as chaos. Similar to dynamical systems theory, bifurcation theory uses ideas and methods from the qualitative theory of differential/difference equations, linear algebra theory, group theory, singularity theory and computer-assisted study of differential/difference equations. Bifurcation theory is considered as one of the richest interdisciplinary subjects in applied mathematics. The theory is used not only in many traditional sciences like physics, astronomy, chemistry, biology, medicine and engineering but also in economics, sociology and physiology.

This thesis focuses on the study of the bifurcations in dynamical systems (ODEs and maps). The main focus is on the dynamics near the Bogdanov-Takens (BT) bifurcation. This bifurcation plays an important role in the study of dynamical systems since it implies global (homoclinic) bifurcations as well as two local (limit point and Andronov-Hopf) bifurcations. The approximation of the local bifurcations near the BT bifurcation point is standard. A more interesting problem is to construct the homoclinic bifurcation curve along which the homoclinic orbit shrinks to the BT point while tracing the homoclinic bifurcation curve. For this problem, no exact analytic solution is possible. The present thesis provides not only a novel construction of the homoclinic bifurcation near a BT point of a generic system of ODEs but also a software implementation (MatCont) to study this type of bifurcation. Along this we apply basic linear algebra theory, perturbation techniques, continuation techniques and computer software packages (MATLAB R2015a, Maple 18 and Wolfram Mathematica 10). Since the bifurcation structure near a fixed point of BT type of maps is similar to but more complicated than the case of ODEs, the thesis also discusses the homoclinic structure in the BT map, i.e., *the normal form of the 1:1 resonance bifurcation*.

It is known that a BT point is a regular point for the continuation problem of the fold curve as well as of the Andronov-Hopf curve (if the Andronov-Hopf curve is defined by requiring that there are two eigenvalues summing up to zero). So one can use the standard continuation methods [70] to continue these curves in two parameters. The difficult case is to continue homoclinic orbits starting from a BT point. In this case, the problem is regular near the BT point but not at the BT point itself. So with a small nonzero step away, ε, form the BT point, it should be possible to derive a special predictor based on asymptotics for the bifurcating parameter values and the corresponding small homoclinic orbits in the phase space. The idea of starting homoclinic orbits near a BT point in planar systems with the help of Melnikov's method was developed by Rodriguez *et al.* [114]. Beyn [15] treated the general n-dimensional problem. He derived the first asymptotics, i.e., *a homoclinic predictor*, of the homoclinic solutions near a generic BT point. If we assume that a generic n-dimensional ODE has a BT point, then by the existence of the parameter-dependent two-dimensional center manifold near the bifurcation, the problem of approximating the homoclinic solution splits naturally into two sub-problems: (a) derive the asymptotics for the smooth normal form on the two-dimensional center manifold; (b) transform the approximate homoclinic orbit into the phase- and parameter-space of the original n-dimensional ODE. The general first step in solving sub-problem (a) is to perform a singular rescaling (based on a small non-zero step away from the BT point) that brings the two-dimensional normal form into a Hamiltonian system (with known explicit homoclinic solution) plus a small perturbation. Then one can use several methods to obtain an asymptotic expression for

the parameter values corresponding to the perturbed homoclinic orbit. One possibility is to apply the classical Melnikov technique [78] or the equivalent branching method [15] to derive a first-order approximation for the homoclinic bifurcation curve in parameter space and a zero-order approximation for the homoclinic orbit in phase space. The sub-problem (b) can either be solved with a Lyapunov-Schmidt method [15], or using a parameter-dependent center manifold reduction combined with the normalization and based on the Fredholm solvability applied to the homological equation [16].

The present thesis revisits both sub-problems (in reversed order). For the sub problem (a), we use the regular perturbation (R-P) method to derive the second-order approximation to the homoclinic bifurcation curve and to obtain explicit first-, second- and third-order corrections of the unperturbed homoclinic orbit, see also [91, 92]. This approximation involves a "parasitic turn" in the homoclinic solution near the saddle point. Actually, as the perturbation parameter ε increases, the higher-order corrections in ε quickly become larger than the zero-order approximation and then the expansion breaks down for larger time-spans. Therefore, we use a generalization of the Lindstedt-Poincaré perturbation (L-P) method to derive an accurate third-order homoclinic approximation of the unperturbed homoclinic orbit (see [2]). The predicted orbits based on the L-P method not only "nearly" coincide with the actual homoclinic situation but also approach the saddle along the correct direction. It is known that the standard L-P method for oscillators removes secular terms by a linear time-rescaling dependent on a small parameter which allows to eliminate unbounded terms and to obtain a solution valid for all time. In our case, we use a nonlinear time-rescaling dependent on the perturbation parameter ε to remove the "parasitic turn" near the saddle-point rather than secular terms. This improves the prediction in the phase space. For the sub-problem (b), we correct the parameter transformation presented in [15, 16]. This is achieved by systematically solving all linear systems appearing from the homological equation. By collecting all these results, we formulate an accurate homoclinic predictor at a generic BT bifurcation.

The old versions of MatCont [51, 52] use the incorrect homoclinic predictor given in [15, 16]. In practice, the initialization of the homoclinic continuation from a BT point often fails. So the new predictors are implemented in MatCont and proved to be more robust than the previous one. We show how to use the new predictors to explicitly (not only numerically) derive an accurate approximation for the homoclinic solution in ODEs (as an example we study the homoclinic solutions in the Gray-Scott kinetic model).

For maps things are different. In the maps case the parameters that correspond to the transverse homoclinic orbits (or simply *the homoclinic orbits*) are located inside a sector,

instead of forming a curve in the ODE case. This sector, i.e., *the homoclinic zone* [66], is bounded by two curves, i.e., *the homoclinic tangencies curves*, where the homoclinic trajectories intersect tangentially. The idea of continuing branches of homoclinic orbits and homoclinic tangencies, given a good starting point, was developed in [17, 18]. To find such a point, the algorithm in [85] can be used in the case of planar maps if an asymptotic of the homoclinic parameters exists. This algorithm consists of finding a finite number of intersection points of the stable and unstable manifolds of the saddle, i.e., *the connecting orbit*, by computing the manifolds from a local approximation near the saddle [59]. These points can be continued in one parameter until the limit point is detected, which corresponds to a tangency of the stable and unstable manifolds. Continuation of such a limit point in two parameters gives the homoclinic tangency structure. Therefore, if a good asymptotic of the homoclinic parameter exists, then one can use the numerical method described above to compute the homoclinic tangencies bifurcations.

It is known that the map is exactly (up to a certain order of terms) the time-1 flow of a system of ODEs. Although the exact bifurcation structure is different for the map and its approximating ODE, the usage of the ODE provides information that is hardly available by the analysis of the map alone. The thesis describes two methods to approximate the BT map by a system of ODEs, namely, the interpolating technique and the method of Picard iteration. Using the homoclinic predictor in Chapter 3, we derive an asymptotic of the homoclinic parameter of the approximating system. Further, we use this asymptotic to predict the homoclinic bifurcation that appear in the BT map. The new asymptotic is proved to be more accurate than the asymptotic of the homoclinic parameter presented in [26, 34, 64, 126]. We show how to use the new asymptotic to compute the branches of the homoclinic tangencies in the BT map.

In the second part of the thesis, we aim to apply bifurcation theory and difference equation theory to study the dynamic behavior of a nonlinear market model (the monopoly model). This model is based on cubic price and quadratic marginal functions [111, 112]. The recent literature still deals with simplified versions of the monopoly model, cf. [1, 8, 98, 104], and none of them analyzes the dynamic behavior of the monopoly model in detail. These versions are far from reality since the market dynamics should be described by a higher-order polynomials. A numerical continuation analysis, Lyapunov stability analysis and numerical simulations are used to study the periodic and chaotic behaviors that arise in this model. In this study, we use the continuation and bifurcation package MatContM and the computer software packages MATLAB and Maple.

T. Puu [111, 112] provides incomplete information on the existence of cycles of period 4 and the chaotic behavior in his model. We reconsider the dynamic monopoly model. We present fundamental corrections to the study presented in [112]. We prove the existence of solutions of period 5, 10, 13, 17. A general formula for two cycles of period 4 is derived. We prove that one of them is always unstable while the stability region of the second 4-cycle is larger than the one obtained in [112] which is based on an incorrect linear stability analysis. The chaotic behavior of the monopoly model is studied by computing the largest Lyapunov exponents.

Outline of thesis

This thesis is divided into two parts. The first part is dedicated to the study of the homoclinic solutions rooted at a generic BT point of an ODE and the homoclinic structures of the BT map. The second (smaller) part is an application of bifurcation theory to a monopoly model.

Chapter 1 recalls some basic concepts related to the qualitative theory of differential and difference equations along with notions and terminology in dynamical systems (continuous and discrete) and bifurcation theory. Basic results and definitions related to the linear stability analysis, multivariate Taylor expansion, Jordan canonical form, center manifolds and normal forms, local and global (homoclinic) bifurcations, Melnikov's method for homoclinic bifurcations, periodic orbits, chaotic behavior and Lyapunov exponents are discussed.

Chapter 2 provides a description of the bifurcation diagram of the BT bifurcation. We describe the parameter-independent center manifold for a generic smooth family of autonomous ODEs at the critical parameter value (i.e., at the BT point). Further, by normal form theory, the dynamics in the parameter-dependent center manifold is transformed to *the critical BT normal form*. However, the interesting dynamical behavior happens in the neighborhood of the critical parameter value, so the parameter dependence is introduced in the critical normal form (by constructing a *versal deformation*) such that we get the so-called *BT topological normal form*. By adding the (usually ignored) cubic terms in the BT topological normal form, we obtain *the smooth BT normal form*. This normal form will be used to derive a correct second-order approximation for the homoclinic bifurcation rooted at a generic BT point in Chapter 3. The complete bifurcation diagram of the topological normal form is discussed. Using the standard parameter-dependent center manifold reduction combined with the normalization, that is based on the Fredholm solvability of the homological equation, we derive a quantitative relation between orbits of the smooth BT normal form and of the original system. This relation will be used in Chapter 3 to transfer the homoclinic approximation in the smooth BT normal form back to the original n-dimensional system. Finally, we discuss the existence of the BT bifurcation in the Gray-Scott kinetic model.

Chapter 3 contains the most important results of the thesis. Second-order homoclinic predictors at a generic BT bifurcation are presented. We use the classical "blow-up" technique to reduce the smooth BT normal form to a Hamiltonian system (with known explicit homoclinic solution) plus a small perturbation. First, with the R-P method, we derive explicit first-, second- and third-order corrections of the perturbed homoclinic orbit and parameter value. We fix the phase of the solution by applying two different conditions (a point phase condition and an integral phase condition). This leads to different approximations to the homoclinic orbits in the phase space and the same homoclinic curve in parameter space. An extensive numerical comparison in the state space is presented. However, in general the R-P method leads to a "parasitic turn" near the saddle point. So we apply the L-P method to approximate the homoclinic solution. We prove that the L-P method leads to the same homoclinicity conditions as the classical Melnikov technique, the branching method and the R-P method. A numerical comparison is presented to illustrate the accuracy of the asymptotic for the L-P and R-P method. This proves that the homoclinic asymptotic based on the L-P method does not have a "parasitic turn", making it more suitable for numerical implementation. By the parameter-dependent center manifold reduction that we derived in Chapter 2, we provide the explicit computation formulas for the second-order homoclinic predictor to a generic n-dimensional ODEs. The results of this Chapter are applied to derive an explicit approximation to the homoclinic solutions in the Gray-Scott kinetic model.

Chapter 4 discusses the implementation and computational algorithms to continue the homoclinic orbits in two free parameters. We show how to use the computed homoclinic asymptotics in Chapter 3 to calculate the initial homoclinic cycle so as to continue homoclinic orbits starting from a BT point. We derive an important relation between the geometric amplitude of the homoclinic orbit and the initial choice of the perturbation parameter. We also present an extra parameter that can be used to find a suitable finite time interval where the continuation problem will converge. The new homoclinic predictors are implemented in the MATLAB continuation package MatCont. This implementation includes the computation of the smooth BT normal form coefficients. Five examples with multi-dimensional state spaces are included, namely, the Morris-Lecar model, a predator-prey model with constant rate harvesting, CO-oxidation in platinum model, an indirect field oriented control model and the extended Lorenz-84 model.

Chapter 5 describes two methods to approximate the BT map by a system of ODEs, namely, the interpolating technique and the method of Picard iteration. We present an improved asymptotic for the homoclinic parameter in the BT map by (i) considering all the second-order terms of the coordinates and parameter in the computation of the approximating system using the method of Picard iteration, (ii) applying the results in Chapter 3 on the

BT bifurcation of ODEs to obtain an improved asymptotic of the homoclinic bifurcation in the approximating system. We show how to use the new asymptotic parameter to continue branches of homoclinic tangencies in the BT map. In this way we obtain the whole homoclinic structure of the BT map. We derive an asymptotic formula for the homoclinic parameter at a generic BT point of maps by applying the standard parameter-dependent center manifold reduction combined with the normalization, that is based on the Fredholm solvability of the homological equation. By systemically solving all linear systems appearing from the homological equation, we correct the parameter transformation existing in the literature.

Chapter 6 is a study of a dynamic monopoly model. Some preliminary results are presented including corrections to the fixed point stability analysis presented in [112]. By simulations, the existence of solutions of period 4, 5, 10, 13, 17 and the chaotic behavior are investigated. Continuation and bifurcation analysis is used to get information about the stability of 5, 10, 13, 17-cycles under parameter variation. In all regions, further period-doubling bifurcations are found which implies the existence of orbits with higher periods as well. A general formula for solutions of period 4 is derived. Among other things, we discuss the symmetry properties of these solutions. The analytical stability analysis for the 4-cycles proves that they are never linearly asymptotically stable. Therefore, the stability of the 4-cycle is investigated by studying the effect of small displacements in the direction of the eigenvector corresponding to the eigenvalue located at the stability boundary. This work, combined with simulation and the basin of attraction analysis for the 4-cycle allows us to determine the stability region of the 4-cycle. This region is larger than the one obtained in [111, 112] which is based on an incorrect linear stability analysis. Two methods to compute the largest Lyapunov exponent are discussed. Further, we analyze the chaotic behavior of the monopoly model by the largest Lyapunov exponents. This analysis confirms the results in the earlier sections.

Chapter 7 and 8 collect the conclusions of the previous chapters and suggestions for further research, respectively.

The content of this thesis has been published or is submitted for publication, see [2], [3], [107], [92] and [91].

Contents

CHAPTER 1

Preliminaries

In this introductory chapter we provide the major definitions, notions and facts of the dynamical system theory that will be used in the remainder of this thesis. Most of the material cited in this chapter are based on [23, 41, 78, 88, 109].

1.1 Dynamical systems

Consider the following system of ODEs of the form

$$\begin{cases} \dfrac{dx_1}{dt} = f_1(x_1, \ldots, x_n, \alpha_1, \ldots, \alpha_p), \\ \dfrac{dx_2}{dt} = f_2(x_1, \ldots, x_n, \alpha_1, \ldots, \alpha_p), \\ \qquad \vdots \\ \dfrac{dx_n}{dt} = f_n(x_1, \ldots, x_n, \alpha_1, \ldots, \alpha_p), \end{cases} \tag{1.1}$$

dependent on the parameters $\alpha_i \in \mathbb{R}$, which describes a motion in an n-dimensional state (phase) space $\mathbb{R}^n$, where each f_j is assumed to be sufficiently smooth. Introduce a phase vector $x \in \mathbb{R}^n$ and a parameter vector $\alpha \in \mathbb{R}^p$ with coordinates $x = (x_1, \ldots, x_n)$ and $\alpha = (\alpha_1, \ldots, \alpha_p)$. With an abuse of notation we write

$$f_i(x, \alpha) = f_i\left(x_1, \ldots, x_n, \alpha_1, \ldots, \alpha_p\right), \quad i = 1, 2, \ldots, n.$$

Thus the system (1.1) can be written in the form

$$\begin{cases} \dfrac{dx_1}{dt} = f_1(x,\alpha), \\ \dfrac{dx_2}{dt} = f_2(x,\alpha), \\ \qquad \vdots \\ \dfrac{dx_n}{dt} = f_n(x,\alpha). \end{cases} \tag{1.2}$$

The function f_i can be regarded as the i^{th} component of the vector-valued function $f(x,\alpha)$ defined by

$$f(x,\alpha) = (f_1(x,\alpha), \ldots, f_n(x,\alpha)).$$

Then the system (1.2) can be written in compact form as

$$\dot{x} := \frac{dx}{dt} = f(x,\alpha). \tag{1.3}$$

The unique solution $x(t)$ of (1.3) with initial condition $x(t_0) = x_0$ for a fixed value of α, $\alpha = \alpha_0$, defines a C^k-mapping[†]

$$\varphi_{\alpha_0}^t : \mathbb{R}^n \to \mathbb{R}^n,$$

which transforms $x_0 \in \mathbb{R}^n$ into some state $x(t) \in \mathbb{R}^n$ at time t:

$$\varphi_{\alpha_0}^t(x_0) = x(t).$$

This map is called the flow determined by (1.3). From now, we drop the subscript α_0 to simplify writing.

Definition 1.1. *A continuous-time dynamical system is a triplet* $\{\mathbb{R}, \mathbb{R}^n, \varphi^t\}$, *where* $\varphi^t : \mathbb{R}^n \to \mathbb{R}^n$ *is a local flow parametrized by* $t \in \mathbb{R}$ *and satisfying the properties*

(1) For all $x_0 \in \mathbb{R}^n$ *the equation* $\varphi^0(x_0) = x_0$ *holds,*

(2) For all $x_0 \in \mathbb{R}^n$ *and* $t, s \in \mathbb{R}$ *the relation* $\varphi^{t+s}(x_0) = \varphi^t o \varphi^s(x_0)$ *holds, where the composition symbol "o" means*

$$\varphi^t o \varphi^s(x_0) = \varphi^t(\varphi^s(x_0)).$$

Similarly, the notion of discrete-time dynamical systems can be introduced as follows

[†] C^k means that the map $\varphi_{\alpha_0}^t$ has the same smoothness as the R.H.S. of (1.3).

Definition 1.2. *A discrete dynamical system is a triplet* $\{\mathbb{Z}, \mathbb{R}^n, \varphi^k\}$*, where* $\varphi^k : \mathbb{R}^n \to \mathbb{R}^n$ *is a local flow parametrized by* $k \in \mathbb{Z}$ *and satisfying the properties*

(1) For all $x_0 \in \mathbb{R}^n$ *the equation* $\varphi^0(x_0) = x_0$ *holds,*

(2) For all $x_0 \in \mathbb{R}^n$ *and* $k, m \in \mathbb{Z}$ *the relation* $\varphi^{k+m}(x_0) = \varphi^k o \varphi^m(x_0)$ *holds.*

If we consider φ^t as the flow map of a continuous-time dynamical system, then the (time-1) map φ^1 defines an *invertible* discrete-time dynamical system. An example of discrete-time dynamical system is an n-dimensional map which can be written in compact form as

$$x_{k+1} = f(x_k, \alpha), \tag{1.4}$$

where $x_k = (x_{k,1}, x_{k,2}, \ldots, x_{k,n}) \in \mathbb{R}^n$, $\alpha \in \mathbb{R}^p$, $k \in \mathbb{Z}$ denotes the time and the vector-valued function $f : \mathbb{R}^n \times \mathbb{R}^p \to \mathbb{R}^n$ is assumed to be sufficiently smooth. It thus follows that

$$x_k = f^k(x_0, \alpha_0)$$

where f^k denotes a k-fold compositions of f to (x_0, α_0), $f^k = \underbrace{fofo\ldots of}_{k-\text{times}}$.

Definition 1.3. *A dynamical system* $\{T, \mathbb{R}^n, \varphi^t\}$*, where* T *is a time set (*$T = \mathbb{R}$ *or* $T = \mathbb{Z}$*), is called topologically equivalent to a dynamical system* $\{T, \mathbb{R}^n, \phi^t\}$ *if there is a homeomorphism*[†] $h : \mathbb{R}^n \to \mathbb{R}^n$ *mapping orbits of the first system onto orbits of the second system, preserving the direction of time.*

The *orbit* (or trajectory) of φ^t starting at x_0 is an ordered subset of the state space X,

$$Or(x_0) = \{x \in X : x = \varphi^t(x_0), \text{ for all } t \in T\}.$$

In the study of dynamical systems, we are mostly interested in a special class of orbits, namely the *invariant sets*.

Definition 1.4. *Let* $\Omega \subset \mathbb{R}^n$ *be a set in the state space of a dynamical system* $\{T, \mathbb{R}^n, \varphi^t\}$*.* Ω *is said to be invariant under the dynamical system if for any* $x_0 \in \Omega$ *we have* $\varphi^t(x_0) \in \Omega$ *for all* $t \in T$*.*

An example of invariant sets is *the equilibria*.

[†] A continuous map with continuous inverse is called *homeomorphism*.

Definition 1.5. *A point $x = x_0$ at $\alpha = \alpha_0$ is called an equilibrium (a fixed point) if $\varphi^t(x_0) = x_0$ for all $t \in \mathbb{R}$ (for all $t \in \mathbb{Z}$).*

Another example of invariant sets is a *periodic orbits* which is defined as follows

Definition 1.6. *[88] A cycle or periodic orbit Γ is an orbit that for each point $x_0 \in \Gamma$ holds that $\varphi^t(x_0) \neq x_0$ and $\varphi^{t+T_0}(x_0) = \varphi^t(x_0)$ with some $T_0 > 0$, for all $t \in \mathbb{R}$. The minimal T_0 with this property is called the period of the cycle Γ. A cycle of a continuous-time dynamical system, in a neighborhood of which there are no other cycles, is called a limit cycle.*

Note that, for a given equilibrium solution (x_0, α_0) one can always move it to the origin, $(0,0)$, by a change of coordinates, so from now we assume $(0,0)$ to be an equilibrium for (1.3).

1.2 Taylor expansion, linear stability analysis

At $x = 0$, $\alpha = 0$ the Taylor expansion of (1.3) can be expressed as

$$\begin{aligned} f(x,\alpha) = {} & Ax + J_1\alpha + \frac{1}{2}B(x,x) + A_1(x,\alpha) + \frac{1}{2}J_2(\alpha,\alpha) + \frac{1}{6}C(x,x,x) + \frac{1}{2}B_1(x,x,\alpha) \\ & + \mathcal{O}\left(\|x\|\|\alpha\|^2 + \|\alpha\|^3\right) + \mathcal{O}\left(\|(x,\alpha)\|^4\right), \end{aligned} \tag{1.5}$$

where $A = f_x(x,\alpha)|_0$ denotes the Jacobian matrix evaluated at $(0,0)$, $J_1 = f_\alpha(x,\alpha)|_0$ and B, A_1, J_2, C, B_1, ... are vector-valued functions with n components. The i^{th} component of these functions are defined by

$$\begin{cases} B_i(x,y) = \displaystyle\sum_{j,k=1}^{n} \frac{\partial^2 f_i(\xi,\mu)}{\partial\xi_j\partial\xi_k}\Big|_0 x_j y_k, & A_{1,i}(x,\alpha) = \displaystyle\sum_{j=1}^{n}\sum_{k=1}^{p} \frac{\partial^2 f_i(\xi,\mu)}{\partial\xi_j\partial\mu_k}\Big|_0 x_j \alpha_k, \\ J_{2,i}(\alpha,\delta) = \displaystyle\sum_{j,k=1}^{p} \frac{\partial^2 f_i(\xi,\mu)}{\partial\mu_j\partial\mu_k}\Big|_0 \alpha_j\delta_k, & C_i(x,y,z) = \displaystyle\sum_{j,k,l=1}^{n} \frac{\partial^3 f_i(\xi,\mu)}{\partial\xi_j\partial\xi_k\partial\xi_l}\Big|_0 x_j y_k z_l, \\ B_{1,i}(x,y,\alpha) = \displaystyle\sum_{j,k=1}^{n}\sum_{l=1}^{p} \frac{\partial^3 f_i(\xi,\mu)}{\partial\xi_j\partial\xi_k\partial\mu_l}\Big|_0 x_j y_k \alpha_l, & \dots . \end{cases} \tag{1.6}$$

For a fixed value of α, the terms J_1, $A_1(x,\alpha)$, $J_2(\alpha,\alpha)$, $B_1(x,x,\alpha)$ ... need not be considered and we have,

$$\dot{x} = Ax + \mathcal{O}(\|x\|^2). \tag{1.7}$$

Near $x = 0$ the terms $\mathcal{O}(\|x\|^2)$ are negligible so that we may try to approximate (1.7) by the linear part, i.e., $\dot{x} = Ax$. It is possible to transform the matrix A to an "almost" diagonal form. This form is known as the Jordan canonical form.

Theorem 1.1 (**The Jordan Canonical form**). *Let A be a real matrix with k real eigenvalues and $n-k$ complex eigenvalues. Then there exists a non-singular matrix P such that the matrix $J = P^{-1}AP$ is a block diagonal matrix of the form $J = diag[J_1, \ldots, J_s]$. The elementary Jordan blocks $J = J_r$, $r = 1, \ldots s$ are either of the form $J = diag[\lambda, \ldots, \lambda] + N$ for λ one of the real eigenvalues of A or of the form $J = diag[D, \ldots, D] + N_2$ for $\lambda = a + ib$ (complex eigenvalues of A), where N is the nilpotent matrix with ones on the super-diagonal and zero elsewhere, $D = \begin{pmatrix} a & -b \\ b & a \end{pmatrix}$ and N_2 is the nilpotent matrix with $\begin{pmatrix} 1 & 0 \\ 0 & 1 \end{pmatrix}$ on the super-diagonal and zero elsewhere.*

Hence, the general solution $x(t)$ with an initial condition x_0 is obviously given by

$$x(t) = x_0\, P \left\{ \text{diag}\left[e^{tJ_j}\right] \right\} P^{-1},$$

where if λ is a real eigenvalue of A and $J_j = J$ is an $m \times m$ matrix then

$$e^{tJ} = e^{\lambda t} \begin{pmatrix} 1 & t & \ldots & \frac{t^{m-1}}{(m-1)!} \\ 0 & 1 & \ldots & \frac{t^{m-2}}{(m-2)!} \\ \vdots & \vdots & \ddots & \vdots \\ 0 & 0 & & 1 \end{pmatrix}.$$

Similarly, if $\lambda = a + ib$ and $J_j = J$ is a $2m \times 2m$ matrix then

$$e^{tJ} = e^{at} \begin{pmatrix} R & Rt & \ldots & \frac{Rt^{m-1}}{(m-1)!} \\ 0 & R & \ldots & \frac{Rt^{m-2}}{(m-2)!} \\ \vdots & \vdots & \ddots & \vdots \\ 0 & 0 & & R \end{pmatrix}.$$

where $R = \begin{pmatrix} \cos(bt) & -\sin(bt) \\ \sin(bt) & \cos(bt) \end{pmatrix}$. In general, it is clear that if $\Re(\lambda)$ is negative then every element of e^{tJ} decays to zero and if $\Re(\lambda) > 0$, then some elements of e^{tJ} diverge to ∞.

Definition 1.7. *An equilibrium point is said to be hyperbolic if the Jacobian matrix has no eigenvalues on the imaginary axis.*

Two invariant sets are associated to a hyperbolic equilibrium $x = 0$ at some fixed value of α, namely the stable and unstable sets of 0 given by $W^s = \left\{x \middle| \varphi^t(x) \to 0, t \to +\infty\right\}$, $W^u = \left\{x \middle| \varphi^t(x) \to 0, t \to -\infty\right\}$, respectively. Note that if we perturb the system (1.3) slightly, then the hyperbolic equilibrium point cannot disappear, nor can another equilibrium point be born near it. Indeed the following theorem holds:

Theorem 1.2. *Consider a family of autonomous ODEs*

$$\dot{x} = \frac{dx}{dt} = f(x, \varepsilon), \quad 0 < \varepsilon \ll 1,$$

such that at $\varepsilon = 0$ there exists a hyperbolic equilibrium point $x = 0$. Then the system has a unique hyperbolic equilibrium x_ε in a small neighborhood of 0 for all small ε.

Definition 1.8. *Two maps $x \mapsto f(x)$ and $y \mapsto g(y)$, $f, g : \mathbb{R}^n \to \mathbb{R}^n$, are called topologically conjugate if there is a homeomorphism $y = h(x)$, $h : \mathbb{R}^n \to \mathbb{R}^n$, such that $f = h^{-1} \circ g \circ h(x)$ for all $x \in \mathbb{R}^n$.*

We note that the conjugacy in the previous definition can be localized at some fixed point p and q if there are an open neighborhoods $U \subset \mathbb{R}^n$ of p and $V \subset \mathbb{R}^n$ of q, and a homomorphism $h : U \to V$ that satisfies $f = h^{-1} \circ g \circ h(x)$ for all $x \in U$ such that $f(x) \in U$ and $q = h(p)$.

Theorem 1.3 (Hartman and Grobman). *Let $x = 0$ be a hyperbolic fixed point of (1.3) at some fixed value of α, and φ^t denote the flow of (1.3). Then there is a neighborhood Ω of 0 such that φ^t is locally topologically conjugate to the flow generated by the linear system $\dot{x} = Ax$.*

Therefore, the dynamics in the neighborhood of a hyperbolic equilibrium point are guaranteed to be "simple". Thus the stability of the hyperbolic equilibrium point is determined completely by the eigenvalues of the matrix A.

Lemma 1.4. *An equilibrium of a continuous-time dynamical system is locally asymptotically stable if for all eigenvalues λ of the Jacobian matrix holds that $\Re(\lambda) < 0$. If for at least one eigenvalue holds that $\Re(\lambda) > 0$, the equilibrium is unstable.*

As for the continuous-time dynamical systems, the following holds for a discrete-time dynamical system.

Definition 1.9. *A fixed point is said to be hyperbolic if the Jacobian matrix has no eigenvalues with magnitude equal to one.*

Lemma 1.5. *A fixed point of a discrete-time dynamical system is locally asymptotically stable if all eigenvalues μ of the Jacobian matrix have magnitude smaller than one. If for at least one eigenvalue holds that the magnitude is larger than one, the fixed point is unstable.*

1.3 Center manifold and normal forms

The Hartman-Grobman theory shows that the local behavior of the flow near a hyperbolic equilibrium point is determined by the linearized flow. In this section we discuss a results for determining the stability and qualitative behavior in a neighborhood of a nonhyperbolic equilibria. Assume that (1.7) has a nonhyperbolic equilbrium at $x = 0$, and further assume that there are n_- eigenvalues with $\Re(\lambda) < 0$, n_0 with $\Re(\lambda) = 0$, and no eigenvalues with $\Re(\lambda) > 0$ [†] ($n_- + n_0 = n$). Let T be a non-singular matrix such that

$$J = T^{-1}AT = \begin{pmatrix} J_c & 0 \\ 0 & J_s \end{pmatrix},$$

where J_c and J_s are the blocks in the diagonal matrix whose diagonals contain the eigenvalues with $\Re(\lambda) = 0$ and $\Re(\lambda) < 0$, respectively.

Write

$$x = T \begin{pmatrix} u \\ v \end{pmatrix}, \quad u \in \mathbb{R}^{n_0}, \quad v \in \mathbb{R}^{n_-}.$$

Thus (1.7) becomes

$$\begin{pmatrix} \dot{u} \\ \dot{v} \end{pmatrix} = J \begin{pmatrix} u \\ v \end{pmatrix} + \begin{pmatrix} g_1(u,v) \\ g_2(u,v) \end{pmatrix}.$$

where $g_1(u,v)$ and $g_2(u,v)$ are the first n_0 and last n_- components, respectively, of the vector $T^{-1}\mathcal{O}(\|T\,(u,v)\,\|^2)$.

[†] If the matrix A has n_+-eigenvalues with positive real part, then $x = 0$ is unstable with an n_+-dimensional unstable manifold.

Theorem 1.6 (Center manifold theorem). *There exists an invariant C^k-center manifold*

$$W^c(0) = \{\,(u,v) \in \mathbb{R}^{n_0} \times \mathbb{R}^{n_-} \,|\, v = H(u),\ \|u\| < \delta,\ H(0) = 0,\ \frac{\partial}{\partial u} H(0) = 0\},$$

for δ sufficiently small, which satisfies

$$\frac{\partial}{\partial u} H(u)\,(J_c u + g_1(u, H(u))) = J_s H(u) + g_2(u, H(u)).$$

Once $H(u)$ is determined, the system describing the dynamics on the center manifold is given by the following n_0-dimensional system

$$\dot{u} = J_c u + g_1(u, H(u)). \tag{1.8}$$

The center manifold is exponentially attractive. So, to understand what happens to the system around the non-hyperbolic equilibrium point, it is sufficient to investigate what happens in the center manifold. In this way, the study of a high-dimensional dynamical system can be reduced to the study of a low-dimensional center manifold.

To write (1.8) in the simplest form, i.e., *the critical normal form*, that is easier to analyze, we first rearrange terms in (1.8),

$$\dot{u} = J_c u + g_1^2(u) + \mathcal{O}(\|u\|^3), \tag{1.9}$$

where $g_1^2(u)$ is a real n_0-dimension vector whose components are homogenous polynomials of degree 2 in u, *i.e.*, $g_1^2(u) \in \mathcal{H}^2$. Then we apply a near-identity transformation of coordinates[†]

$$u = w + z_2(w), \quad z_2(w) \in \mathcal{H}^2, \tag{1.10}$$

where the coefficients of $z_2(w)$ are unknown and to be determined. Substituting (1.10) into (1.9) gives

$$\left(I + \frac{\partial}{\partial w} z_2(w)\right) \dot{w} = J_c w + J_c z_2(w) + g_1^2(w) + \mathcal{O}(\|w\|^3) \tag{1.11}$$

For sufficiently small w, $\left(I + \frac{\partial}{\partial w} z_2(w)\right)^{-1}$ exists. By the binomial theorem we have

$$\left(I + \frac{\partial}{\partial w} z_2(w)\right)^{-1} = I - \frac{\partial}{\partial w} z_2(w) + \left(\frac{\partial}{\partial w} z_2(w)\right)^2 + \dots\ .$$

[†]This method originated in the Ph.D thesis of Poincaré [110].

Thus (1.11) becomes

$$\dot{w} = J_c w + J_c z_2(w) - \left(\frac{\partial}{\partial w} z_2(w)\right) J_c w + g_1^2(w) + \mathcal{O}(\|w\|^3) \tag{1.12}$$

The second-order terms $J_c z_2(w) - \left(\frac{\partial}{\partial w} z_2(w)\right) J_c w + g_1^2(w)$ can be simplified (or, in the ideal case, removed) by solving the *homological equation*,

$$\left(\frac{\partial}{\partial w} z_2(w)\right) J_c w - J_c z_2(w) = g_1^2(w), \tag{1.13}$$

for the unknown coefficients of $z_2(w)$. After possible elimination of terms, we can write (1.9) in the critical normal form,

$$\dot{w} = J_c w + S_2(w) + \mathcal{O}(\|w\|^3).$$

If $S_2(w) \neq 0$ then it is referred to as the *resonance* vector which contains the second-order terms that cannot be eliminated by the nonlinear transformation (1.10). As we mentioned before, in the ideal case $S_2(w) = 0$. In general it is possible to generalize this method to simplify the $g_1^r(u) \in \mathcal{H}^r$ terms of (1.8), see, for example, [6, 7, 25, 109, 131] for more detail.

1.4 Equilibria and their bifurcations

For a fixed value of α, assume that φ^t is a flow of (1.3) that is uniquely determined by an initial condition x_0. The collection of orbits corresponding to various initial conditions of (1.3) in phase space forms the so-called phase portrait. The phase portrait provides information about the qualitative behavior such as whether an attraction or a repeller present in (1.3). If α is varied slightly, then it may happen that the new phase portrait is *nonequivalent* to the original one. In this case the corresponding parameter value $\alpha = \alpha_c$ is called a *bifurcation* point, where a bifurcation is said to occur.

Definition 1.10. *The appearance of a topologically nonequivalent phase portrait under variation of a parameter is called a bifurcation.*

The bifurcation diagram shows the topologically nonequivalent strata in parameter space, together with their corresponding phase portraits. The minimal number of parameters that have to be varied for the detection of the bifurcation is called the codimension of a bifurcation (codim). Bifurcations are said to be *local* if they occur in an arbitrary small neighborhood

of the equilibrium; otherwise they are said to be *global*. To study what happens to (1.3) as α varies near the bifurcation value $\alpha = \alpha_c$, the standard approach is used. This approach has several steps (see for example [6, 88] for further details):

(1) **Reduction:** Restrict (1.3) at the bifurcation parameter $\alpha = \alpha_c$ to the appropriate center manifold (the parameter-independent center manifold).

(2) **Normalization:** Simplify the dynamics in the center manifold by computing the critical normal form for the bifurcation.

(3) **Unfolding:** Introduce small terms (linear and possibly nonlinear) into the critical normal form for the bifurcation to describe the effects of varying α away from α_c. This yields *the model system* for the bifurcation.

(4) **Equating:** Prove that (1.3) is locally (near $\alpha = \alpha_c$) topological equivalent to the model system. The model system then is called *the topological normal form*.

Codimension 1 bifurcations of equilibria

In particular, we are interested in the local bifurcation that occurs when one parameter change causes the stability of an equilibrium to change.

Definition 1.11. *The bifurcation associated with the appearance of a simple real eigenvalue $\lambda = 0$ is called a limit point bifurcation (LP) (or fold or saddle-node bifurcation).*

The limit point bifurcation corresponds with a collision and disappearance of two equilibria, a stable and an unstable one, when crossing the bifurcation parameter value $\alpha = \alpha_c$. At the bifurcation value a saddle-node equilibrium appears. The topological normal form at the limit point bifurcation is given by the one-dimensional system

$$\dot{w} = \beta + a_{\mathbf{LP}} w^2, \quad w \in \mathbb{R}.$$

where $a_{\mathbf{LP}} \neq 0$ is the normal form coefficient and β is the unfolding parameter.

Definition 1.12. *The bifurcation corresponding to the presence of a simple conjugate pair of eigenvalues satisfying $\Re(\lambda) = 0$ ($\lambda = \pm i\omega_0$) is called an Andronov-Hopf bifurcation (H).*

The topological normal form at the Hopf bifurcation is given by the two-dimensional system

$$\dot{z} = (i\omega_0 + \beta)\, z + l_1 z|z|^2, \quad z \in \mathbb{C},$$

where β is the unfolding parameter and $l_1 \neq 0$[†]. At the Andronov-Hopf point a periodic orbit is born and there is an exchange of stability of the equilibrium. A stable periodic orbit is born from a stable equilibrium if l_1 is negative, in which case the Andronov-Hopf bifurcation is supercritical or soft. Otherwise, the periodic orbit is unstable and coexists with the stable equilibrium, which corresponds with a subcritical or hard bifurcation.

Codimension 2 bifurcations of equilibria

Codim-2 bifurcation points are points where curves corresponding to codim-1 bifurcations intersect transversally or tangentially. In generic system (1.3) only five codim-2 bifurcations of equilibria are possible [88]. We list them in Table 1.1. Note that the coefficients a_{LP} and l_1 appear in the normal forms of the limit point and Andronov-Hopf bifurcation, respectively. The eigenvalues mentioned in the table are assumed to be the only ones for which $\Re(\lambda) = 0$.

1.5 Homoclinicity in two-dimensional vector-field

In this section, we discuss the existence of homoclinic bifurcation [‡] in two-dimensional systems (as in the BT normal form for ODEs and maps). So we restrict to the study of existence of a homoclinic orbit in (1.3) when $n = 2$ and the parameter α is assumed to be fixed.

Definition 1.13. *An orbit Γ starting at a point $x \in \mathbb{R}^n$ is called a homoclinic orbit to the equilibrium point $x = 0$ of system (1.3) if for some parameter values $\varphi^t x \to 0$ as $t \to \pm\infty$.*

In general, there are two invariant sets related to homoclinic orbits, namely the stable and unstable manifolds. These manifolds are tangent to the stable (generalized) eigenspace, corresponding to the union of all eigenvalues λ of A with $\Re(\lambda) < 0$, and the unstable (generalized) eigenspace, corresponding to the union of all eigenvalues λ of A with $\Re(\lambda) > 0$, respectively. Depending on the type of equilibrium and the correspond invariant sets there are many kinds of homoclinic orbits (for further details, see for example [16, 32, 33, 47]):

[†] l_1 is called the first Lyapunov coefficient.

[‡] Homoclinic bifurcation is a global bifurcation.

Name	Properties	The model system[a]
Cusp (C)	$\lambda = 0,\ a_{\rm LP} = 0$	$\dot{w} = \beta_1 + \beta_2 w + c w^3, \quad c \in \mathbb{R},$
Bogdanov-Takens (BT)	$\lambda_{1,2} = 0$	$\begin{pmatrix} \dot{w}_0 \\ \dot{w}_1 \end{pmatrix} = \begin{pmatrix} w_1 \\ \beta_1 + \beta_2 w_1 + a w_0^2 + b w_0 w_1 \end{pmatrix}, \quad (a,b) \in \mathbb{R}^2,$
Generalized-Hopf (GH)	$\lambda_{1,2} = \pm i\omega_0,\ l_1 = 0$	$\dot{z} = (\beta_1 + i\omega_0) z + \beta_2 z\lvert z\rvert^2 + l_2 z\lvert z\rvert^4, \quad l_2 \in \mathbb{R},$
Zero-Hopf (ZH)	$\lambda_1 = 0,\ \lambda_{2,3} = \pm i\omega_0$	$\begin{pmatrix} \dot{w} \\ \dot{z} \end{pmatrix} = \begin{pmatrix} \beta_1 + b(\beta) w^2 + c(\beta)\lvert z\rvert^2 \\ (\beta_2 + i\omega(\beta)) z + d(\beta) w z + e(\beta) w^2 z \end{pmatrix} + \mathcal{O}(\lVert (w,z,\bar{z})\rVert^4),$ b, c, ω, e are real functions, d is a complex function.
Hopf-Hopf (HH)	$\lambda_{1,2} = \pm i\omega_1,\ \lambda_{3,4} = \pm i\omega_2$	$\begin{pmatrix} \dot{z}_0 \\ \dot{z}_1 \end{pmatrix} = \begin{pmatrix} (\beta_1 + i\omega_1) z_0 + P_{12} z_0 \lvert z_1\rvert^2 + \frac{1}{2} P_{11} z_0 \lvert z_0\rvert^2 + \frac{1}{4} S_1 z_0 \lvert z_1\rvert^4 + i R_1 z_0 \lvert z_0\rvert^4 \\ (\beta_2 + i\omega_2) z_1 + P_{21} z_1 \lvert z_0\rvert^2 + \frac{1}{2} P_{22} z_1 \lvert z_1\rvert^2 + \frac{1}{4} S_2 z_1 \lvert z_0\rvert^4 + i R_2 z_1 \lvert z_1\rvert^4 \end{pmatrix}$ $\mathcal{O}(\lVert (z_0, \bar{z}_0, z_1, \bar{z}_1)\rVert^6),$ P_{jk}, S_k are complex, R_k are real.

Table 1.1: Codim-2 bifurcations of equilibria. See [16, 87, 88] for background information and notation used.

[a] For the cusp, Bogdanov-Takens and generalized-Hopf bifurcations, the model system is the topological normal form. In the model systems: $w \in \mathbb{R}$, $(w_0, w_1) \in \mathbb{R}^2$, $z \in \mathbb{C}$, $(z_0, z_1) \in \mathbb{C}^2$ and $\beta = (\beta_1, \beta_2) \in \mathbb{R}^2$ are the unfolding parameters.

Codimension 1 homoclinic bifurcations:
Homoclinic to hyperbolic-saddle, Homoclinic to saddle-node.

Codimension 2 homoclinic bifurcations:
Non-central Homoclinic to saddle-node, Neutral saddle, Neutral saddle-focus, Neutral bi-focus, Shilnikov-Hopf, Double real stable leading eigenvalue, Double real unstable leading eigenvalue, Neutrally-divergent saddle-focus (stable), Neutrally-divergent saddle-focus (unstable), Three leading eigenvalues (stable), Three leading eigenvalues (unstable), Orbit-flip with respect to the stable manifold, Orbit-flip with respect to the unstable manifold, Inclination-flip with respect to the stable manifold, Inclination-flip with respect to the unstable manifold.

1.5.1 Melnikov's method for homoclinic orbits

Consider the following two-dimensional system of ODEs of the form

$$\begin{pmatrix} \dot{x} \\ \dot{y} \end{pmatrix} = \begin{pmatrix} y \\ f(x) \end{pmatrix} + \varepsilon \begin{pmatrix} g_1(x,y) \\ g_2(x,y,\tau) \end{pmatrix}, \quad 0 < \varepsilon \ll 1,$$

or, equivalently, in a vector-field form:

$$X = X_h + \varepsilon X_p, \tag{1.14}$$

where

$$X_h = y\,\partial x + f(x)\,\partial y, \quad X_p = g_1(x,y)\,\partial x + g_2(x,y,\tau)\,\partial y,$$

f, g_1, g_2 are sufficiently smooth and τ is referred to as a homoclinic bifurcation parameter. Assume that

(1) There exists $k \in \mathbb{R}$ such that $h(x,y) := \frac{1}{2}y^2 - \int_0^x f(z)\,dz - k = 0$ defines a homoclinic loop to a hyperbolic saddle point ρ_0. This loop is explicitly known and it is defined by $L_0(t) = (x_0(t),\, y_0(t))$.

(2) For ε small, the vector-field (1.14) possesses a homoclinic orbit at the critical value $\tau = \tau_c(\varepsilon)$.

To obtain information about the homoclinic solution of (1.14) when $\varepsilon \neq 0$, one needs to approximate it by perturbation (asymptotic) techniques. According to these techniques, the homoclinic solution can be approximated by the first few terms of an asymptotic expansion in the phase space, $(x,y) = (x_0,y_0) + \varepsilon(x_1,y_1) + \varepsilon^2(x_2,y_2) + \mathcal{O}(\varepsilon^3)$, together with an expansion

of the homoclinic bifurcation parameter, $\tau = \tau_0 + \varepsilon\tau_1 + \varepsilon^2\tau_2 + \mathcal{O}(\varepsilon^3)$. A detailed discussion of different perturbation approaches to find asymptotics for the homoclinic solution of (1.14) -with explicitly given f, g_1, g_2- will be presented in Chapter 3.

We start with basic perturbation results. Since the fixed point ρ_0 is hyperbolic it will continue to exist in the vector-field (1.14) for ε small, say ρ_ε. However, the stable and unstable manifolds $W^s(\rho_\varepsilon)$, $W^u(\rho_\varepsilon)$ of ρ_ε will in general not coincide and hence there is no homoclinic orbit to ρ_ε. The distance between $W^s(\rho_\varepsilon)$, $W^u(\rho_\varepsilon)$ can be approximated by the Melnikov method [78, 106, 131]. Further we can use this approximation to compute the critical homoclinic parameter $\tau_c(\varepsilon) \approx \tau_0$ where the distance between the stable and unstable manifolds vanishes. Let $L^s_\varepsilon(t)$, $L^u_\varepsilon(t)$ be the trajectories lying in $W^s(\rho_\varepsilon)$, $W^u(\rho_\varepsilon)$, respectively, which can be expressed as follows (see [78, Lemma 4.5.2])

$$\begin{cases} L^s_\varepsilon(t) = L_0(t) + \varepsilon L^s_1(t) + \mathcal{O}(\varepsilon^2),\ t \in [0,\infty)\,, \\ L^u_\varepsilon(t) = L_0(t) + \varepsilon L^u_1(t) + \mathcal{O}(\varepsilon^2),\ t \in (-\infty,0]\,, \end{cases} \tag{1.15}$$

where $L^{s,u}_i(t) = (x^{s,u}_i(t),\, y^{s,u}_i(t))$ are uniformly bounded in the indicate intervals. As shown in Figure 1.1, we assume that the saddle point ρ_0 to be at the origin. Then for fixed $t = 0$ (i.e., at $\gamma_0 = L_0(0)$) the displacement vector d between $W^s(\rho_\varepsilon)$, $W^u(\rho_\varepsilon)$ is given by: $d(0) = \gamma_0^+ - \gamma_0^-$ and hence

$$d(0) = L^u_\varepsilon(0) - L^s_\varepsilon(0) = \varepsilon\,(L^u_1(0) - L^s_1(0)) + \mathcal{O}(\varepsilon^2). \tag{1.16}$$

On the other hand, the unit normal vector v to the unperturbed homoclinic orbit at γ_0 is given by

$$v = \frac{\left(\frac{\partial h}{\partial x}, \frac{\partial h}{\partial y}\right)}{\sqrt{\left(\frac{\partial h}{\partial x}\right)^2 + \left(\frac{\partial h}{\partial y}\right)^2}} = \frac{\big(-f(x_0(0)), y_0(0)\big)}{\sqrt{f^2(x_0(0)) + y_0^2(0)}}. \tag{1.17}$$

By projecting the distance vector $d(0)$ onto the unit normal vector v, we obtain the following distance function between the stable and unstable separatists of the flow generated by (1.14):

$$\Delta(0) = \varepsilon\,\langle v, d(0)\rangle + \mathcal{O}(\varepsilon^2). \tag{1.18}$$

Hence,

$$\Delta(0) = \varepsilon\left(\frac{\Delta^u(0) - \Delta^s(0)}{\sqrt{f^2(x_0(0)) + y_0^2(0)}}\right) + \mathcal{O}(\varepsilon^2), \tag{1.19}$$

where $\Delta^{u,s}(0) = y_0(0)y_1^{u,s}(0) - f(x_0(0))x_1^{u,s}(0)$. Note that, the ε-term of (1.19) vanishes if $\Delta^u(0) = \Delta^s(0)$. We define the *Melnikov function* as

$$M(0) = \Delta^u(0) - \Delta^s(0). \tag{1.20}$$

If the time t is no longer assumed to be 0, we can rewrite (1.20) as a function of time t,

$$M(t) = \Delta^u(t) - \Delta^s(t), \tag{1.21}$$

where $\Delta^{u,s}(t) = y_0(t)y_1^{u,s}(t) - f(x_0(t))x_1^{u,s}(t)$. To simplify (1.20), differentiate (1.21) with respect to t to obtain

$$\frac{d}{dt}\Delta^{u,s}(t) = y_0(t)\dot{y}_1^{u,s}(t) + \dot{y}_0(t)y_1^{u,s}(t) - f(x_0(t))\dot{x}_1^{u,s}(t) - f'(x_0(t))\dot{x}_0(t)x_1^{u,s}(t). \tag{1.22}$$

The components $\dot{x}_1^{u,s}(t)$, $\dot{y}_1^{u,s}(t)$ can be computed as follows. Substituting (1.15) into (1.14) with the expansions for

$$f(x_\varepsilon^{u,s}(t)) = f(x_0(t)) + \varepsilon f'(x_0(t))x_1^{u,s}(t) + \mathcal{O}(\varepsilon^2), \tag{1.23}$$

$$g_1(x_\varepsilon^{u,s}(t), y_\varepsilon^{u,s}(t)) = g_1(x_0(t), y_0(t)) + \mathcal{O}(\varepsilon), \tag{1.24}$$

$$g_2(x_\varepsilon^{u,s}(t), y_\varepsilon^{u,s}(t), \tau) = g_2(x_0(t), y_0(t), \tau_0) + \mathcal{O}(\varepsilon), \tag{1.25}$$

then equating the coefficient of equal ε gives

$$\begin{cases} \dot{x}_1^{u,s}(t) = y_1^{u,s}(t) + g_1(x_0(t), y_0(t)), \\ \dot{y}_1^{u,s}(t) = f'(x_0(t))x_1^{u,s}(t) + g_2(x_0(t), y_0(t), \tau_0). \end{cases} \tag{1.26}$$

Substitute (1.26) into (1.22) to get

$$\frac{d}{dt}\Delta^{u,s}(t, \tau_0) = y_0(t)g_2(x_0(t), y_0(t), \tau_0) - f(x_0(t))g_1(x_0(t), y_0(t)),$$

or simply

$$\frac{d}{dt}\Delta^{u,s}(t, \tau_0) = (X_p h)|_{L_0(t)}.$$

Finally, we integrate from $-\infty$ to 0 and 0 to ∞ to obtain

$$\Delta^u(0, \tau_0) - \Delta^u(-\infty, \tau_0) = \int_{-\infty}^{0} (X_p h)|_{L_0(t)}\, dt,$$

$$\Delta^s(\infty, \tau_0) - \Delta^s(0, \tau_0) = \int_{0}^{\infty} (X_p h)|_{L_0(t)}\, dt.$$

Note that $\Delta^u(-\infty,\tau_0)=0$ and $\Delta^s(\infty,\tau_0)=0$ because $\lim_{t\to\pm\infty}(f(x_0(t)),y_0(t))=(0,0)$, and $x_1^{u,s}(t)$, $y_1^{u,s}(t)$ are bounded. Thus, the *Melnikov function* (1.20) becomes

$$M(\tau_0)=\Delta^u(0,\tau_0)-\Delta^s(0,\tau_0),$$

or

$$M(\tau_0)=\int_{-\infty}^{\infty}(X_p h)|_{L_0(t)}\,dt. \tag{1.27}$$

This function vanishes along the curve $M(\tau_0)=0$ which gives a zero-order asymptotic formula of the actual homoclinic bifurcation parameter $\tau=\tau_c(\varepsilon)$, *i.e.*, $\tau\approx\tau_c(0)$.

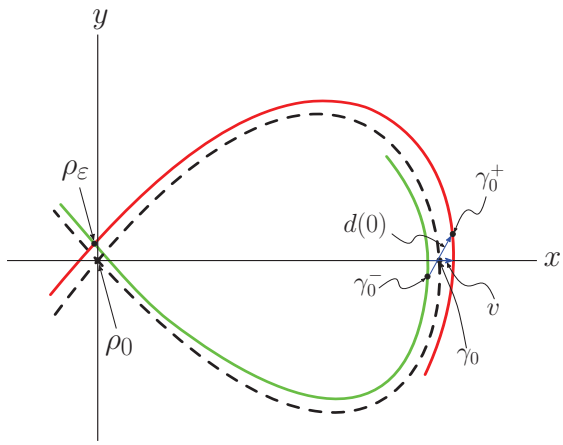

Figure 1.1: Construction of the distance function $d(0)$. The dashed curve is the unperturbed homoclinic orbit to ρ_0. The solid curves are the stable and unstable manifolds $W^s(\rho_\varepsilon)$, $W^u(\rho_\varepsilon)$ of the perturbation of the saddle ρ_0 (i.e., ρ_ε). The points γ_0^-, γ_0^+ represent the points on each of the stable and unstable manifolds, respectively, closest to the point $\gamma_0=L_0(0)$ on the unperturbed homoclinic orbit.

Example 1.1. Consider the following vector-field

$$V=V_1+V_2, \tag{1.28}$$

where $V_1=v\partial u+\left(-4+u^2\right)\partial v$ and $V_2=\left(\varepsilon\frac{b}{a}v\,(\tau+u)\right)\partial v$, which results from applying the singular rescaling (3.1) to the BT normal form (2.23). The vector-field V_1 is a Hamiltonian system with the first integral

$$h(u,v):=\frac{v^2}{2}+4u-\frac{u^3}{3}-k=0\quad k\in\mathbb{R}. \tag{1.29}$$

The phase portrait of (1.29) is presented in Figure 1.2. Every closed orbit of (1.29) surrounding $(-2,0)$ corresponds to a level curve: $\Gamma_h = \left\{ (u,v) \mid h(u,v) = 0,\ \frac{-16}{3} < k < \frac{16}{3} \right\}$, Γ_h shrinks to the equilibrium $(-2,0)$ as $k \to \frac{-16}{3}$ and tends to a homoclinic solution as $k \to \frac{16}{3}$. The Hamiltonian system has a well-known explicit homoclinic solution $L_0(s) = (u_0(s), v_0(s))$ given by (see for example [16, p.213]): $L_0(s) = \left(2 - 6\,\mathrm{sech}^2(s), 12\,\mathrm{sech}^2(s)\tanh(s)\right)$. The Melnikov integral (1.27) is given by

$$M(\tau_0) = \int_{\infty}^{-\infty} (V_2 h)|_{L_0(s)}\, ds = \varepsilon \frac{b}{a} \int_{-\infty}^{\infty} v_0^2(s)\,(\tau_0 + u_0(s))\, ds = \varepsilon \frac{192}{35} \frac{b}{a} (7\tau_0 - 10)\,.$$

This function vanishes when $\tau_0 = \frac{10}{7}$, and hence the homoclinicity of (1.28) occurs at

$$\tau = \frac{10}{7} + \mathcal{O}(\varepsilon). \tag{1.30}$$

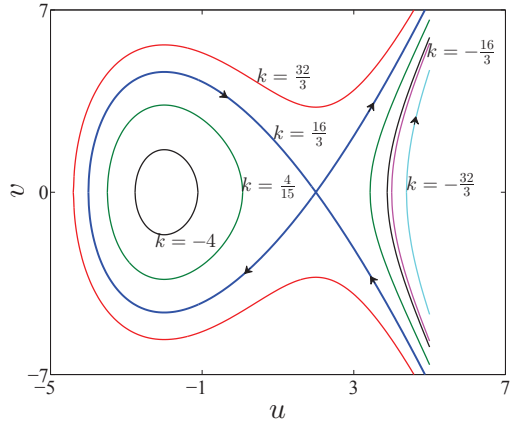

Figure 1.2: The phase curves of (1.29) for $k = \{\frac{-32}{3}, \frac{-16}{3}, -4, \frac{4}{15}, \frac{16}{3}, \frac{32}{3}\}$

A collision criterion of the limit cycle with a homoclinic orbit

Assume that at $\tau = \tau_c(\varepsilon)$ the homoclinic orbit of (1.14) exists by the (dis)appearance of an isolated periodic orbit (limit cycle) C. Suppose that for ε small, C survives in the neighborhood of the homoclinic orbit of the unperturbed vector-field X_h. Let c_0 be a point on C and the line that connects the perturbed hyperbolic saddle ρ_ε to the focus F, see Figure 1.3. It is clear that as $\tau \to \tau_c$ we have $c_0 \to \rho_\varepsilon$. Thus, the homoclinicity condition $\tau = \tau_c(\varepsilon)$ is satisfied if a collision occurs between the limit cycle and the saddle, i.e,:

$$c_0 = \rho_\varepsilon. \tag{1.31}$$

In [13, 14], it was shown that if the k^{th}-order approximation of the limit cycle $(\hat{x}, \hat{y})$,

$$\begin{pmatrix} \hat{x} \\ \hat{y} \end{pmatrix} = \begin{pmatrix} x_0 \\ y_0 \end{pmatrix} + \varepsilon \begin{pmatrix} \hat{x}_1 \\ \hat{y}_1 \end{pmatrix} + \ldots + \varepsilon^k \begin{pmatrix} \hat{x}_k \\ \hat{y}_k, \end{pmatrix}$$

that bifurcates near the unperturbed homoclinic orbit exists, then one can use condition (1.31) to derive a higher-order approximation for the homoclinicity condition

$$\tau_c(\varepsilon) = \sum_{n=0}^{k-1} \varepsilon^n \tau_n + \mathcal{O}(\varepsilon^k).$$

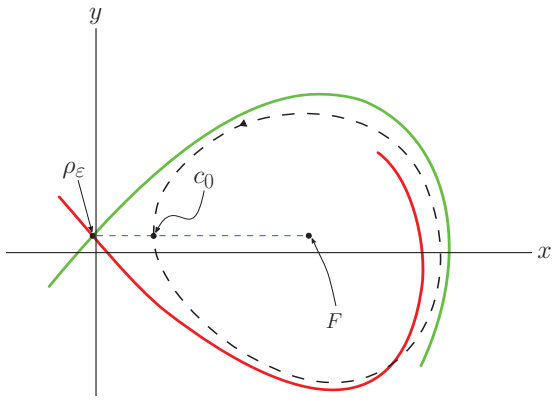

Figure 1.3: The collision of the periodic orbit C and the perturbation saddle ρ_ε.

In Chapter 3, we derive a second-order approximation for the homoclinic bifurcation parameter of (1.28) by using a generalization of the Lindstedt-Poincaré perturbation method based on the criterion (1.31) [†]. This parameter is

$$\tau = \frac{10}{7} + \varepsilon^2 \frac{288}{2401} \frac{b^2}{a^2} + \mathcal{O}(\varepsilon^3). \tag{1.32}$$

For $(a, b) = (-1, 1)$, we integrate (1.28) using the built-in MATLAB function `ode45`. The initial point is set to $(x, y) = (1.99999, 0)$. We use the homoclinic bifurcation parameter as given in (1.30) and (1.32) with different ε values. As a result, the Melnikov method fails in predicting the homoclinic orbits for ε moderate, see Figure 1.4a. On the other hand,

[†]In Chapter 3, we use hyperbolic functions rather than the Jacobian elliptic functions were used in [13]. This allows to approximate the actual homoclinic situation. In [13], the Jacobian elliptic functions was used to approximate the limit cycle of period T close to the homoclinicity. However, both functions lead to the same homoclinicity condition $\tau_c(\varepsilon)$.

the solution based on the collision criterion (1.31) leads to a good approximation to the bifurcation parameter τ even for ε small where the computed orbits always converge to the actual homoclinic situation, see Figure 1.4b.

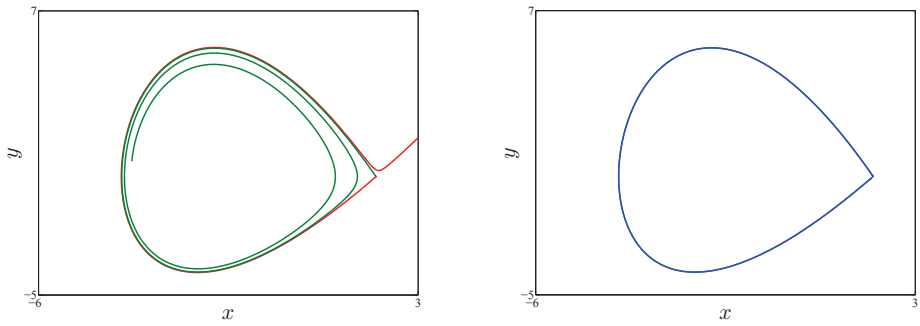

(a) (b)

Figure 1.4: Forward and backward numerical integration of (1.28) starting at $(x, y) = (1.99999, 0)$ for ε=0.3 and $(a, b) = (-1, 1)$. (a) $\tau = \frac{10}{7}$, (b) $\tau = \frac{10}{7} + \varepsilon^2 \frac{288}{2401}$.

Homoclinicity using Mathematica

This section discusses a numerical method to approximate the homoclinic bifurcation parameter $\tau = \tau_c(\varepsilon)$ in (1.28). The simple idea is based on using the interactive command *Manipulate* of the software package Mathematica. Consider again the vector-field (1.28). We can numerically integrate the invariant manifolds of the saddle point $(2, 0)$ for fixed values of ε and τ. However, to obtain the homoclinic solution, we need a suitable choice (*a homoclinic choice*) of these variables[†]. In fact, we can use the command *Manipulate* to control these variables via an interactive interface and then to handle them until the homoclinicity occurs. To do so, we assume that $\tau \in [\frac{10}{7}, 1.55]$ (where τ steps through this interval with step 10^{-6}) and $\varepsilon \in [0, 1]$ (with step equal to 0.05). Evaluating the following command

```
Clear[u, s, tau, T, eps]
Manipulate[Module[{sol=NDSolve[{u''[s]+4-u[s]^2==eps*u'[s]*(tau+u[s]),
u[0]==p[[1]], u'[0]==p[[2]]},u,{s,0,T}]},
ParametricPlot[Evaluate[{u[s],u'[s]}/.sol],{s,0,T},
PlotRange->{{-5,3},{-10, 5}}]],{{p,{1.9999999,0.0000001}},Locator},
{{T,-20},-500,500},{{tau,10/7},10/7,1.55,1*10^-6},{{eps,0},0,1,0.05}]
```

returns the interactive window presented in Figure 1.5. We gradually increase ε with step size 0.05. At each ε we find the corresponding value of τ where the homoclinicity occurs, i.e., the stable and unstable manifolds connect again at the saddle point $(2, 0)$. Figure 1.6a

[†]One option is to use (1.32). However, here we do not assume any information about the homoclinicity in (1.28).

shows the situation when $\varepsilon = 0.6$ and $\tau = \frac{10}{7}$, it is clear that there is no homoclinic orbit. We increase τ until the homoclinicity occurs which happens at $\tau = \frac{10296541}{7000000}$, see Figure 1.6b. By computing the value of τ at each ε, we obtain the following list of homoclinic sets $\{\varepsilon, \tau\}$:

```
hom = {{0,10/7},                {0.05,5001057/3500000}, {0.1,10009429/7000000},
       {0.15,10018879/7000000},{0.2,10033607/7000000}, {0.25,2010507/1400000},
       {0.3,2015113/1400000},  {0.35,315699/218750},   {0.4,101337/70000},
       {0.45,635521/437500},   {0.5, 10207277/7000000},{0.55, 256251/175000},
       {0.6, 10296541/7000000},{0.65,5173341/3500000}, {0.7, 10400323/7000000},
       {0.75,5228669/3500000}, {0.8, 10517573/7000000},{0.85,10580867/7000000},
       {0.9, 5323519/3500000}, {0.95,1071589/700000},  {1,10787213/7000000}}
```

Next, we fit these pairs with a curve:

```
tau=Rationalize[Fit[hom,{1,eps^2,eps^4},eps],10^-4]
```

The result of this is

$$\tau = \frac{10}{7} + \frac{7}{58}\varepsilon^2 - \frac{1}{122}\varepsilon^4. \tag{1.33}$$

Compared to the homoclinicity condition (1.32), equation (1.33) gives a better prediction to the actual homoclinic situation for large ε. This can be easily checked by plugging (1.32) and (1.33) back into the first Mathematica command. For $\varepsilon = 1.4$, Figure 1.7 plots the solution of (1.28) based on (1.32) (Figure 1.7a) and based on (1.33) (Figure 1.7b).

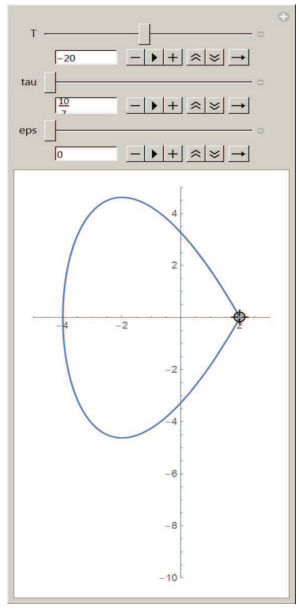

Figure 1.5: Mathematica interactive window of the command *Manipulate*. The unperturbed homoclinic orbit of (1.28) is shown. Note that the unperturbed part is independent of the choice of τ.

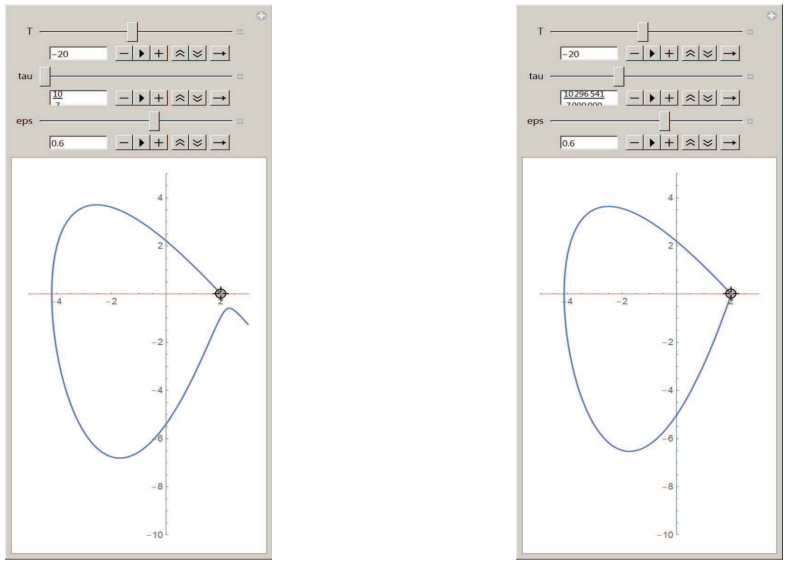

(a) (b)

Figure 1.6: Mathematica interactive window of the command *Manipulate*. For $\varepsilon = 0.6$, (a) the invariant manifolds of the saddle $(2, 0)$ for $\tau = \frac{10}{7}$, (b) homoclinic orbit to the saddle $(2, 0)$ for $\tau = \frac{10296541}{7000000}$.

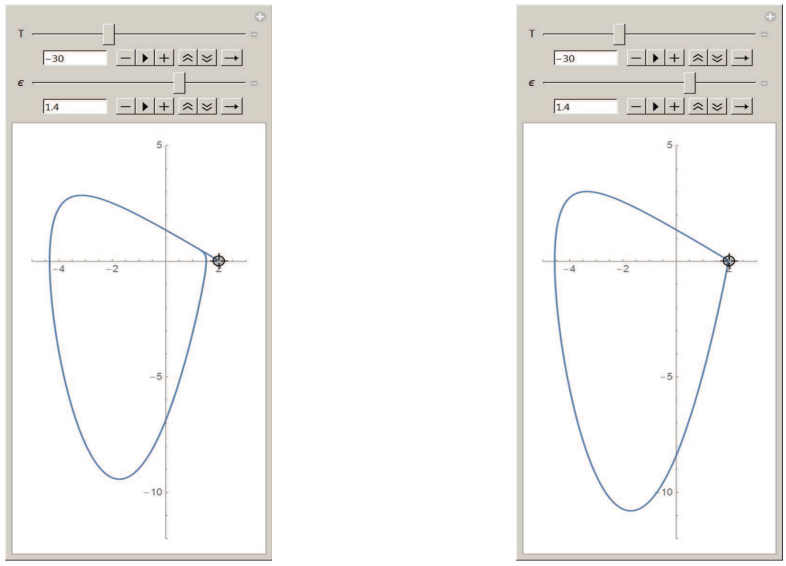

(a) (b)

Figure 1.7: Mathematica interactive window of the command *Manipulate*. For $\varepsilon = 1.4$, (a) the invariant manifolds of the saddle point $(2, 0)$ based on (1.32), (b) homoclinic orbit to the saddle $(2, 0)$ based on (1.33).

1.6 Chaos and the logistic map

In this section we introduce some concepts and lemmas, which will be used in Chapter 6. As an illustration, we briefly study the logistic map. The standard form of this map is

$$x_{n+1} = f(x_n), \quad n = 1, 2, 3, \dots \tag{1.34}$$

where $f(x) := \mu x(1-x)$ and $\mu > 0$ is a parameter. The logistic map was first introduced by the Belgian sociologist and mathematician, Pierre-François Verhulst (1804-1849), see [129], to describe the population growth with limited resource from time n to $n+1$. The variable x represents the population and μ represents the growth rate. For all $x > 1$ and $x < 0$, $f^n(x) \to -\infty$ as $n \to \infty$ [50, **Proposition 5.2**]. So the interesting behaviors occur in the unit interval $[0, 1]$.

Existence and stability of 2-,3-cycles

Definition 1.14. *Consider the map (1.4). For a fixed value of α, $\alpha = \alpha_0$, a point x_0 is said to be a period-k point of f if $f^k(x_0, \alpha_0) = x_0$ and $f^j(x_0, \alpha_0) \neq x_0$ for $1 \leq j \leq k-1$. The k-tuple $\{x_j\}_{j=0}^{k-1}$ is then said to be a k-cycle or cycle of period k, where $x_{j+1} = f(x_j, \alpha_0)$ for $0 \leq j \leq k-2$.*

A point $x \in [0, 1]$ is a period-1 point (a fixed point) of (1.34) if $f(x) = x$. This occurs for $x = 1 - \frac{1}{\mu}$ and $x = 0$. The first point $x = 1 - \frac{1}{\mu} \in [0, 1)$ is asymptotically stable if $\mu \in [1, 3)$ and unstable if $\mu > 3$. On the other hand, the point $x = 0$ is unstable for all $\mu > 1$. If $f^2(x) = x$ and $f(x) \neq x$ then $x \in [0, 1]$ is a period-2 point. Thus, the points of period-2 can be found by computing the discriminant of $\dfrac{f^2(x) - x}{f(x) - x} = 0$, which is $\dfrac{(1+\mu)(3-\mu)}{\mu^2}$. So, at $\mu = 3$, a 2-cycle emerges (i.e., μ is a *period-doubling* bifurcation[†]). The stability of this 2-cycle is given by the following Lemma.

Lemma 1.7. *Let x_0 be a k-periodic point of f. Assume that λ_i are the eigenvalues of the Jacobian matrix $Df^k(x_0)$. Then the following statements holds*

(1) x_0 is asymptotically stable if $|\lambda_i| < 1$ for all i,

(2) x_0 is unstable if $|\lambda_i| > 1$ for some i.

[†]A period-doubling bifurcation occurs when the Jacobian has only one eigenvalue λ for which $|\lambda| = 1$, namely $\lambda = -1$, and some non-degeneracy conditions are satisfied, see [88].

Note that, if $\{x_0, x_1, \ldots, x_{k-1}\}$ denotes a cycle of period k. Then by the chain rule, the stability of x_0 can be obtained from

$$Df^k(x_0) = Df(x_{k-1})Df(x_{k-2})\ldots Df(x_0). \tag{1.35}$$

In general, the stability at any point x_r, $r = 0, 1, \ldots, k-1$, in the cycle can be defined from

$$Df^k(x_r) = Df(x_{r-1})Df(x_{r-2})\ldots Df(x_0)Df(x_{k-1})\ldots Df(x_r). \tag{1.36}$$

Remark 1.1. *The eigenvalues of (1.35) and (1.36) are identical.*

Definition 1.15. *A cycle Γ of period k, $\Gamma := \{x_0, x_1, \ldots, x_{k-1}\}$, is stable if x_0 is a stable fixed point of f^k.*

By Lemma 1.7, the 2-cycles of (1.34) are asymptotically stable for $\mu \in (\mu_2, \mu_4]$, $\mu_2 := 3$, $\mu_4 := 1 + \sqrt{6}$, and unstable for $\mu > \mu_4$. Further, at $\mu = \mu_4$ a stable 2^2-cycle emerges (μ_4 is a period-doubling bifurcation point). The process of period-doubling bifurcations continue which indicates the existence of cycles of period 2^3, 2^4, $\ldots$, 2^n, $\ldots$.

Similarly, a 3-cycle can be computed by solving $\dfrac{f^3(x) - x}{f(x) - x} = 0$. This equation has six roots which may be complex. Myrberg [103] proved that $\mu = \mu_3$, $\mu_3 = 1 + \sqrt{8}$ allows a real solution. Saha and Strotgatz [115] simplified the proof by expressing the solution in terms of three points (see also [12, 69]),

$$x \to y \to z \to x.$$

So the value of μ corresponding to the 3-cycle satisfies

$$\frac{df(z)}{dz}\frac{df(y)}{dy}\frac{df(x)}{dx} = 1 \Rightarrow \mu^3 (1 - 2z)(1 - 2y)(1 - 2x) = 1.$$

Therefore, the 3-cycle is given by a system of four equations with four unknowns (x, y, z, μ):

$$y = f(x), \quad z = f(y), \quad x = f(z), \quad \mu^3 (1 - 2z)(1 - 2y)(1 - 2x) = 1.$$

They solved this system to obtain the solution $\mu = \mu_3$. Later, Shi and Yu [120] proved that there exist two 3-cycles when $\mu > \mu_3$.

Bifurcation diagram

The bifurcation diagram of (1.34) is presented in Figure 1.8. The period-doubling cascade starting at $\mu = \mu_2$ coexists with other "windows" of periodic cycles even in the chaotic region, see Figure 1.8a. The largest region starts at $\mu = \mu_3$ where we have a window of 3-cycles, which undergoes period-doubling with periods 6, 12, 24, ... until one enters again into the chaotic regime, see Figure 1.8b. The most important parts of the bifurcation diagram are as follows (for computational background see [12, 50, 57, 115, 120, 124]):

(1) Cycles of period 2 emerge at $\mu = \mu_2$ (μ_2 is a period-doubling bifurcation point).

(2) 2^2-cycles emerge at $\mu = \mu_4$ (μ_4 is a period-doubling bifurcation point) and are asymptotically stable for $\mu \in (\mu_4, \mu_8)$, $\mu_8 \approx 3.54409$, but unstable for $\mu > \mu_8$.

(3) The process of period-doubling bifurcation continues to period 2^3, 2^4, ... (*period-doubling cascade*) and finally gives rise to *chaos* at $\mu_\infty \approx 3.569946$. This is the famous period-doubling scenario leading to chaos. This is only confirmed by numerical simulation and not proved yet.

(4) For $\mu \in (\mu_\infty, \mu_3)$, the system alternates between periodic and chaotic behavior.

(5) For $\mu \in (\mu_3, \mu_6)$, $\mu_6 \approx 3.8415$, cycles of period 3 appear.

(6) For $\mu \in (\mu_6, 4]$, the system exhibits only chaotic behavior.

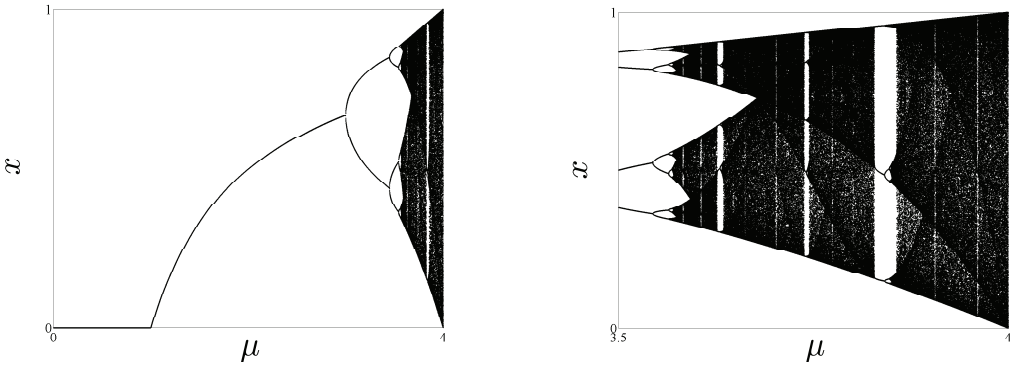

Figure 1.8: Bifurcation diagram of the logistic map with (a) $0 \le \mu \le 4$, (b) $3.5 \le \mu \le 4$ (5,000 points, uniformly distributed). For each μ the initial points were reset to $x_0 = 0.01$, $10,000$ map iterations were performed and $9,900$ iterations were discarded.

Chaos and Lyapunov exponents

There is no universal mathematical definition of "chaos" in dynamical systems. The use of the word "chaos" was introduced by Li and Yorke in [95]. Brown and Chua [28] review the different mathematical definitions of chaos. Many authors call the system chaotic when, for example:

- It has a positive Lyapunov exponent [79].
- It has a Smale horseshoe [43].
- It has sensitive dependence on initial conditions and is topologically transitive[†] [130].
- It has sensitive dependence on the initial conditions, has a dense set of periodic orbits and is topologically transitive [50].

The "sensitive dependence on initial conditions" plays a central role in the idea of chaos; it is simply the classical notion of Lyapunov instability [50]. The quantitative measure of sensitive dependence on initial conditions is the Lyapunov exponent, which measures the exponential separation of nearby orbits. A positive Lyapunov exponent can be considered as an indicator of chaos. Since the sign of the Lyapunov exponent of maps can be computed numerically, we will use in this thesis the following notion of chaos that mainly depends on the Lyapunov exponents:

Definition 1.16. *[122] Chaos is aperiodic long-term behavior[‡] in a deterministic system[§] that exhibits sensitive dependence on initial conditions.*

Now consider a one-dimensional map. Also, consider a small displacement Δ_0 applied to the initial point x_0 and let Δ_n be the resulting displacement from $f^n(x_0)$ after n iterations. If this displacement evolves approximately as

$$|\Delta_n| \approx |\Delta_0| e^{n\sigma}, \tag{1.37}$$

then σ is the Lyapunov exponent.

[†]There are two definitions of topological transitivity which are the following (see [86]): Consider the metric space X and the continuous map $f : X \to X$. We say that f is topologically transitive if:

- for every pair of non-empty open (nopen) sets U and V in X there exists a positive integer k such that $f^k(U) \cap V \neq \emptyset$.
- there exists $x \in X$ such that its orbit $\{ f^n(x) \mid n \geq 0\}$ is dense in X (i.e., $\overline{\{ f^n(x) \mid n \geq 0\}} = X$).

Note that these definitions are not equivalent.

[‡]Aperiodic long-term behavior means that there are orbits which do not settle down to fixed points, periodic orbits, or quasi-periodic orbits as $n \to \infty$.

[§]A system is deterministic if for each state in the phase space there is a unique future.

Taking logarithms of both sides of (1.37) and noticing that

$$\Delta_n = f^n(x_0 + \Delta_0) - f^n(x_0),$$

we obtain

$$\sigma \approx \frac{1}{n} \ln \frac{|\Delta_n|}{|\Delta_0|} = \frac{1}{n} \ln \frac{|f^n(x_0 + \Delta_0) - f^n(x_0)|}{|\Delta_0|}. \tag{1.38}$$

Taking the limit $\Delta_0 \to 0$ for (1.38) gives

$$\sigma = \frac{1}{n} \ln \left| (f^n)' (x_0) \right|.$$

Then using (1.35) in the term inside the logarithm leads to

$$\sigma = \frac{1}{n} \ln |\prod_{i=0}^{n-1} f'(x_i)| = \frac{1}{n} \sum_{i=0}^{n-1} \ln |f'(x_i)|. \tag{1.39}$$

Figure 1.9 shows the Lyapunov exponent of (1.34). A negative Lyapunov exponent indicates a stable periodic solution. The Lyapunov exponents approach zero at the points where stable fixed points or cycles are born (at $\mu = 1$ the stable fixed point emerges, at $\mu = \mu_2$ the stable 2-cycle emerges, ...). The first rise for σ is around μ_∞ due to the chaotic behavior which is clear in Figure 1.8b. The dips for $\mu > \mu_\infty$ are caused by stable periodic cycles (at $\mu = \mu_3$ a stable 3-cycle emerges, ...).

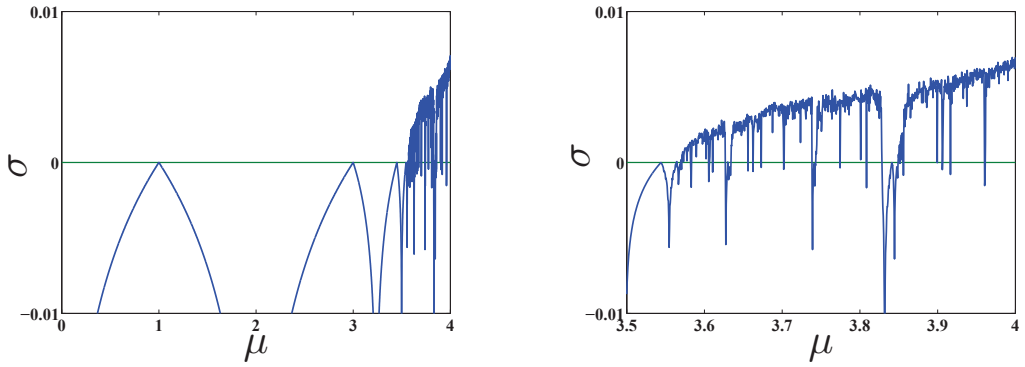

(a) (b)

Figure 1.9: Lyapunov exponents for the logistic map when (a) $0 \leq \mu \leq 4$, (b) $3.5 \leq \mu \leq 4$. Note that there are intervals of stability in the chaotic region corresponding to periodic cycles.

1.7 MatCont

MatCont is a MATLAB interactive toolbox for the numerical study of continuous-time dynamical systems [†]. The software development started in 2000 [100, 113] and the first publication appeared in 2003 [51]. For a historical overview and recent development of MatCont, see [45, 52, 72]. The numerical analysis of equilibria, cycles and connecting orbits as well as their stability and bifurcations can partly be reduced to the continuation of curves parametrized by parameter(s) in some space $\mathbb{R}^m$, for background information, see [16, 88]. The aim of MatCont is to provide a continuation toolbox which is compatible with the standard MATLAB ODE representation of differential equations. In MatCont, most curves are computed with the same prediction-correction continuation algorithm based on the *Moore-Penrose matrix pseudo-inverse*, see [16, 70, 82, 88]. The continuation of bifurcation points of equilibria and limit cycles, in one and two parameters, is based on *bordering methods* [73, 82] and *minimally extended systems* [16]. The limit cycles are computed by an approach based on the discretization via piecewise polynomial approximation with orthogonal collocation of the corresponding boundary value problems. The sparsity of the discretized systems for the computation of limit cycles and their bifurcation points is exploited by using the standard MATLAB sparse matrix methods. The same approach is applied for homoclinic orbits, in combination with the continuation of invariant subspaces for the equilibrium end point of the homoclinic orbit, see [49, 61]. MatCont uses test functions that have regular zeroes at the bifurcation points to detect and accurately locate bifurcations along the computed curve; for details see for example [88, Chapter 10] or [70]. Moreover, MatCont provides the normal form coefficients for all codim-1 and -2 bifurcations of equilibria as well as periodic normal-form coefficients for all codim-1 and 2 bifurcations of limit cycles. The necessary expansions of the unfolding parameters to switch to (some) limit cycle and (some) homoclinic bifurcation curves rooted there are also obtained. See [2, 46, 88, 90] for further details and notation used. The relationships between objects of codim-0, 1 and 2 computed by MatCont are presented in Figure 1.10. The symbols and their meaning are summarized in the Table below the figure, where the labels based on standard terminology are given in [88]. An arrow in the figures from an object of type A to an object of type B means that the object of type B can be detected (either automatically or by inspecting the output during the computation of a curve of objects of type A). Each object of codim-0 and 1 can be continued in one or two system parameters, respectively. We note that generically a curve of HHS emanates from a BT point, as well as (under some conditions on the normal form coefficients) two such curves from a Zero-Hopf bifurcation point (ZH). The current version of MatCont fully supports, however, only one such connection: BT to HHS, which is not presented in Figure 1.10.

[†]The computational core of MatCont is called CL_MatCont. It can be used independently as a general-purpose non-interactive continuation toolbox in MATLAB.

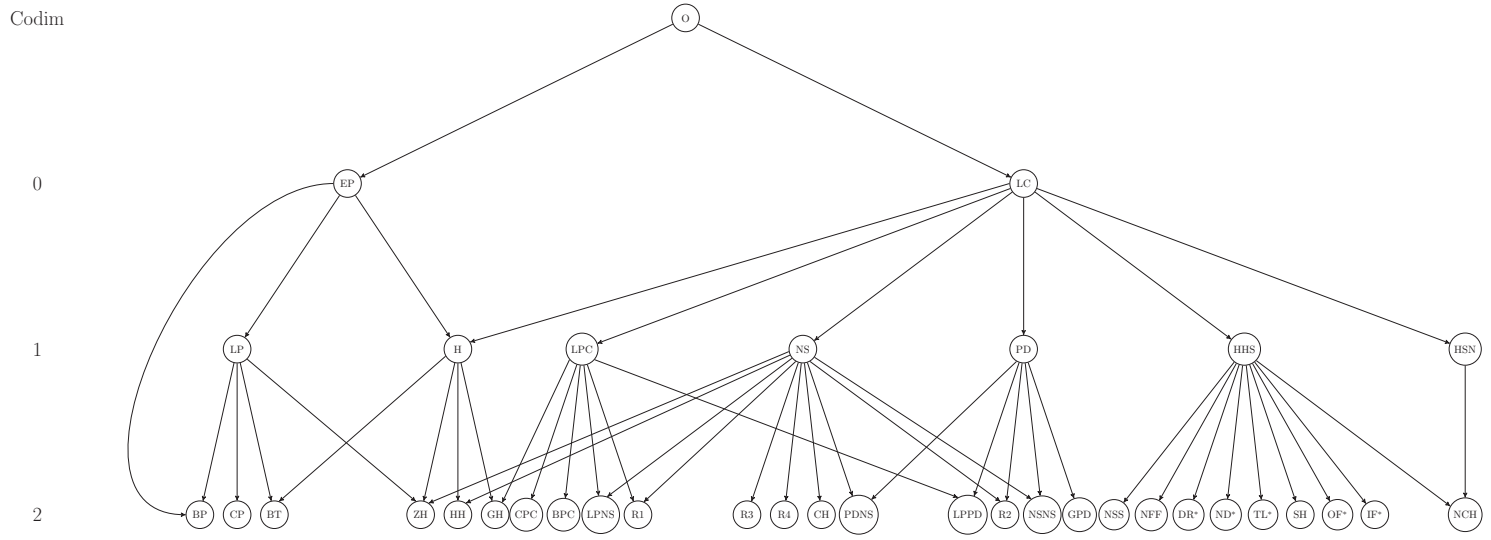

Figure 1.10: Relationships between objects of codim-0, 1 and 2 computed by MatCont. The symbols and their meaning are summarized in the Table below, where the labels are based on standard terminology given in [88]. An arrow in the figures from an object of type A to an object of type B means that that object of type B can be detected during the computation of a curve of objects of type A. Each object of codim-0 and 1 can be continued in one or two system parameters, respectively.

Label	Type of object	Label	Type of object	Label	Type of object	Label	Type of object
O	Orbit	**EP**	Equilibrium	**LC**	Limit cycle	**LP**	Limit point
H	Andronov-Hopf	**LPC**	LP bifurcation of cycles	**NS**	Neimark-Sacker	**PD**	Period-doubling (flip)
HHS	Homoclinic to Hyperbolic Saddle	**HSN**	Homoclinic to Saddle-Node	**BP**	Branch point	**CP**	Cusp point
BT	Bogdanov-Takens	**ZH**	Zero-Hopf	**HH**	Double Hopf	**GH**	Generalized Hopf (Bautin)
CPC	Cusp bifurcation of cycles	**BPC**	Branch Point of Cycles	**LPNC**	LP-NS	**R1**	1:1 Resonance
R3	1:3 Resonance	**R4**	1:4 Resonance	**PDNS**	PD-NS	**CH**	Chenciner
LPPD	Fold-Flip	**R2**	1:2 Resonance	**NSNS**	Double NS	**GPD**	Generalized Period-doubling
NSS	Neutral saddle	**NSF**	Neutral saddle-focus	**NFF**	Neutral Bi-Focus	**DR***†	Double Real S/U leading eigenvalue
ND*	Neutrally-Divergent saddle-focus S/U	**TL***	Three Leading eigenvalues S/U	**SH**	Shilnikov-Hopf	**OF***	Orbit-Flip with respect to the S/U manifold
IF*	Inclination-Flip with respect to the S/U manifold	**NCH**	Non-Central Homoclinic to saddle-node				

†The symbol "$*$" stands for either S or U, depending on whether a Stable or an Unstable invariant manifold is involved.

CHAPTER 2

The Bogdanov-Takens bifurcation

In this chapter we introduce the smooth BT normal form and the complete bifurcation diagram near the BT point. We compute the critical normal form on the two-dimensional center manifold of a generic n-dimensional system that has a BT point at its equilibrium. Using the homological equation technique, we derive a quantitative relation between orbits of the smooth BT normal form and of the generic n-dimensional system. By solving all linear systems appearing from the homological equation, we correct the parameter transformation exiting in the literature. Finally, we discuss the existence of the BT bifurcation in the Gray-Scott model.

2.1 The smooth normal form

Consider the continuous-time dynamical system

$$\dot{x} = f(x, \alpha), \tag{2.1}$$

where $f : \mathbb{R}^n \times \mathbb{R}^2 \to \mathbb{R}^n$ is generic and sufficiently smooth. The BT bifurcation occurs in the two-parameter system (2.1) when for some parameter values, the equilibrium of (2.1) has a

double-zero eigenvalue with the Jordan block

$$J = \begin{pmatrix} 0 & 1 \\ 0 & 0 \end{pmatrix}.$$

Assume that (2.1) has a BT point at $(0,0)$. Then the Taylor expansion of (2.1) at the fixed $\alpha = 0$ can be written as

$$\dot{x} = Ax + \frac{1}{2}B(x,x) + \mathcal{O}(\|x\|^3), \tag{2.2}$$

where A and B are given as in (1.5). The matrix A has a double (but not semi-simple) zero eigenvalue. Then there exist two real linearly independent (generalized) eigenvectors $q_{0,1} \in \mathbb{R}^n$, of A, and two adjoint eigenvectors $p_{0,1} \in \mathbb{R}^n$, of A^T, such that

$$\begin{pmatrix} A & 0 \\ -I_n & A \end{pmatrix} \begin{pmatrix} q_0 \\ q_1 \end{pmatrix} = 0, \quad \begin{pmatrix} A^{\mathrm{T}} & 0 \\ -I_n & A^{\mathrm{T}} \end{pmatrix} \begin{pmatrix} p_1 \\ p_0 \end{pmatrix} = 0, \tag{2.3}$$

where I_n is the $n \times n$ unit matrix. We can assume that these vectors satisfy

$$p_0^{\mathrm{T}} q_0 = p_1^{\mathrm{T}} q_1 = 1, \quad p_0^{\mathrm{T}} q_1 = p_1^{\mathrm{T}} q_0 = 0, \quad q_0^{\mathrm{T}} q_0 = 1, \quad q_1^{\mathrm{T}} q_0 = 0, \tag{2.4}$$

and this defines them uniquely up to a common $\pm$ signs. Define the center eigenspace (E^c) of A as the space spanned by q_0 and q_1; and the stable eigenspace (E^s) as the space spanned by the eigenvectors corresponding to the eigenvalues with negative real part. So for any $y_1 \in E^c$ there is $(u_1, u_2) \in \mathbb{R}^2$ so that

$$y_1 = u_1 q_0 + u_2 q_1.$$

Assume that $\mathbb{R}^n$ is spanned by E^s and E^c only (i.e., there are no eigenvalues with positive real part). Then any vector $x \in \mathbb{R}^n$ can be written in a unique way as

$$x = y_1 + y_2, \quad y_2 \in E^s, \tag{2.5}$$

By (2.4) the new coordinates (u_1, u_2) are given by

$$\begin{cases} u_1 = p_0^{\mathrm{T}} x, \\ u_2 = p_1^{\mathrm{T}} x, \end{cases} \tag{2.6}$$

The vectors (y_1, y_2) can be represented as

$$\begin{cases} y_1 = \pi_c x, \\ y_2 = (I_n - \pi_c)\, x, \end{cases} \tag{2.7}$$

where π_c is a projection of $\mathbb{R}^n$ onto E^c. Substituting (2.6) and (2.7) into (2.2) together with (2.5), we obtain the following system

$$\dot{u} = Ju + \begin{pmatrix} \frac{1}{2}p_0^{\mathrm{T}} R_2(u, y_2) \\ \\ \frac{1}{2}p_1^{\mathrm{T}} R_2(u, y_2) \end{pmatrix} + \mathcal{O}(\|(u, y_2)\|^3), \tag{2.8a}$$

$$\dot{y_2} = Ay_2 + \frac{1}{2}(I - \pi_c)R_2(u, y_2) + \mathcal{O}(\|(u, y_2)\|^3), \tag{2.8b}$$

where $u = (u_1, u_2)$ and

$$\begin{aligned} R_2(u, y_2) = {} & u_1^2 B(q_0, q_0) + 2u_1 u_2 B(q_0, q_1) + u_2^2 B(q_1, q_1) \\ & + 2B(u_1 q_0, y_2) + 2B(u_2 q_1, y_2) + B(y_2, y_2). \end{aligned}$$

On the center manifold $W^c(0)$ we have (see Theorem 1.6),

$$y_2 = H_2(u) + \mathcal{O}(\|u\|^3), \quad H_2 : E^c \to E^s, \tag{2.9}$$

where the component $H_2(u)$ takes the form

$$H_2(u) = \frac{1}{2}H_{20}u_1^2 + H_{11}u_1 u_2 + \frac{1}{2}H_{02}u_2^2, \tag{2.10}$$

and $H_{ij} \subset E^c \in \mathbb{R}^n$ are unknown vectors to be determined. This allows us to write system (2.8a), on the center manifold, for the center eigenspace variables (u_1, u_2) only,

$$\dot{u} = Ju + \begin{pmatrix} \frac{1}{2}p_0^{\mathrm{T}} \Big(u_1^2 B(q_0, q_0) + 2u_1 u_2 B(q_0, q_1) + u_2^2 B(q_1, q_1) \Big) \\ \\ \frac{1}{2}p_1^{\mathrm{T}} \Big(u_1^2 B(q_0, q_0) + 2u_1 u_2 B(q_0, q_1) + u_2^2 B(q_1, q_1) \Big) \end{pmatrix} + \mathcal{O}(\|u\|^3). \tag{2.11}$$

Differentiating both sides of (2.9) gives

$$\dot{y_2} = \frac{\partial H_2}{\partial u_1}\dot{u}_1 + \frac{\partial H_2}{\partial u_2}\dot{u}_2. \tag{2.12}$$

Then by substituting (2.11) and (2.10) into (2.12), we obtain

$$\dot{y_2} = H_{20}u_1 u_2 + H_{11}u_2^2 + \mathcal{O}(\|u\|^3). \tag{2.13}$$

Since the center manifold $W^c(0)$ is invariant, equation (2.9) should satisfy (2.8b), and hence $\dot{y}_2$ can be expressed as

$$\begin{aligned}\dot{y}_2 = &\frac{1}{2}(AH_{20} + (I-\pi_c)B(q_0,q_0))u_1^2 + (AH_{11} + (I-\pi_c)B(q_0,q_1))u_1u_2 \\ &+ \frac{1}{2}(AH_{02} + (I-\pi_c)B(q_1,q_1))u_2^2 + \mathcal{O}(\|u\|^3).\end{aligned} \tag{2.14}$$

Comparing the coefficients of corresponding terms of (2.14) and (2.13), we obtain

$$\begin{cases} H_{20} = -A^{\mathrm{INV}}((I-\pi_c)B(q_0,q_0)), \\ H_{11} = -A^{\mathrm{INV}}((I-\pi_c)B(q_0,q_1) - H_{20}), \\ H_{02} = -A^{\mathrm{INV}}((I-\pi_c)B(q_1,q_1) - 2H_{11}), \end{cases} \tag{2.15}$$

where the expression $h = A^{\mathrm{INV}}r$ is defined as solving the non-singular border system

$$\begin{pmatrix} A & p_1 \\ q_0^T & 0 \end{pmatrix}\begin{pmatrix} h \\ s \end{pmatrix} = \begin{pmatrix} r \\ 0 \end{pmatrix},$$

where r is in the range of A. This uniquely defines the local center manifold system (2.9) up to quadratic terms.

As in Section 1.3, the two-dimensional center manifold system (2.11) can be simplified by introducing a near-identity coordinate transformation of the form

$$u = w + z_2(w), \quad z_2(w) \in \mathcal{H}^2, \tag{2.16}$$

whose coefficients are to be determined, i.e,

$$z_2(w) = \begin{pmatrix} a_{20}w_0^2 + a_{11}w_0w_1 + a_{02}w_1^2 \\ \\ b_{20}w_0^2 + b_{11}w_0w_1 + b_{02}w_1^2 \end{pmatrix}.$$

Substituting (2.16) into (2.11) gives

$$\left(I + \frac{\partial}{\partial w}z_2(w)\right)\dot{w} = Jw + Jz_2(w) + g_1^2(w) + \mathcal{O}(\|w\|^3), \tag{2.17}$$

where

$$g_1^2(w) = \begin{pmatrix} \frac{1}{2}p_0^{\mathrm{T}}B(q_0,q_0)w_0^2 + p_0^{\mathrm{T}}B(q_0,q_1)w_0w_1 + \frac{1}{2}p_0^{\mathrm{T}}B(q_1,q_1)w_1^2 \\ \\ \frac{1}{2}p_1^{\mathrm{T}}B(q_0,q_0)w_0^2 + p_1^{\mathrm{T}}B(q_0,q_1)w_0w_1 + \frac{1}{2}p_1^{\mathrm{T}}B(q_1,q_1)w_1^2 \end{pmatrix}$$

Therefore, after the change of variables (2.16) system (2.11) takes the form (see also system (1.12))

$$\dot{w} = Jw + Jz_2(w) - \left(\frac{\partial}{\partial w} z_2(w)\right) Jw + g_1^2(w) + \mathcal{O}(\|w\|^3) = Jw + \mu_2(w) + \mathcal{O}(\|w\|^3), \quad (2.18)$$

where

$$\mu_2(w) = \begin{pmatrix} \frac{1}{2} p_0^{\mathrm{T}} B(q_0, q_0) + b_{20} \\ \frac{1}{2} p_1^{\mathrm{T}} B(q_0, q_0) \end{pmatrix} w_0^2 + \begin{pmatrix} p_0^{\mathrm{T}} B(q_0, q_1) - 2a_{20} + b_{11} \\ p_1^{\mathrm{T}} B(q_0, q_1) - 2b_{20} \end{pmatrix} w_0 w_1 + \begin{pmatrix} \frac{1}{2} p_0^{\mathrm{T}} B(q_1, q_1) - a_{11} + b_{02} \\ \frac{1}{2} p_1^{\mathrm{T}} B(q_1, q_1) - b_{11} \end{pmatrix} w_1^2.$$

Substituting

$$b_{11} = \tfrac{1}{2} p_1^{\mathrm{T}} B(q_1, q_1), \quad a_{20} = \tfrac{1}{2} p_0^{\mathrm{T}} B(q_0, q_1) + \tfrac{1}{4} p_1^{\mathrm{T}} B(q_1, q_1),$$

$$b_{20} = -\tfrac{1}{2} p_0^{\mathrm{T}} B(q_0, q_0), \quad a_{11} - b_{02} := \tfrac{1}{2} p_0^{\mathrm{T}} B(q_1, q_1),$$

into (2.18) gives[†]

$$\dot{w} = Jw + \begin{pmatrix} 0 \\ a w_0^2 + b w_0 w_1 \end{pmatrix} + \mathcal{O}(\|w\|^3), \quad (2.19)$$

where

$$\begin{cases} a = \frac{1}{2} p_1^{\mathrm{T}} B(q_0, q_0), \\ b = p_1^{\mathrm{T}} B(q_0, q_1) + p_0^{\mathrm{T}} B(q_0, q_0). \end{cases} \quad (2.20)$$

It is clear that the term w_0^2 is a resonance term where we cannot eliminate it by the nonlinear transformation (2.16). Further, by a change of coordinates

$$\begin{cases} w_0 \to w_0, \\ w_1 \to w_1 + \mathcal{O}(\|w\|^3), \end{cases}$$

system (2.19) transforms to

$$\begin{cases} \dot{w}_0 = w_1, \\ \dot{w}_1 = a w_0^2 + b w_0 w_1 + \mathcal{O}(\|w\|^3), \end{cases} \quad (2.21)$$

The following theorem is a direct consequence of the previous computations

[†]It is clear that the choice of b_{20} is not unique. By the choice of $b_{20} = \frac{1}{2} p_1^{\mathrm{T}} B(q_0, q_1)$ we obtain the critical normal form $\dot{w} = Jw + \begin{pmatrix} \frac{1}{2} b w_0^2 \\ a w_0^2 \end{pmatrix} + \mathcal{O}(\|w\|^3)$. However this form and (2.19) are completely equivalent, see [7, **Proposition** 2.4.3].

Theorem 2.1. *At the critical parameter value $\alpha = 0$, system (2.2) is locally C^k-equivalent near $x = 0$ to a parameter-independent system given by*

$$\dot{w} = \begin{pmatrix} w_1 \\ aw_0^2 + bw_0w_1 \end{pmatrix} + \mathcal{O}(\|w\|^3). \tag{2.22}$$

The normal form (2.22) is called the critical normal form because it is computed by substituting the critical parameter value, $\alpha = 0$, into the original system (2.2). However, the interesting dynamical behaviors of (2.2) happen in a neighborhood of the critical parameter value, i.e., when $\alpha \neq 0$, $|\alpha| \ll 1$. In order to study these behaviors, we need to re-construct the parameter-dependence in the normal form (2.22). Theoretically, this is done by constructing a *versal deformation* (also called unfolding) of the linear part of (2.22). A universal unfolding of the critical BT normal form, *i.e.*, the topological normal form, is (see, *e.g.* [6, 78])

$$\dot{w} = \begin{pmatrix} w_1 \\ \beta_1 + \beta_2 w_1 + aw_0^2 + bw_0w_1 \end{pmatrix}, \tag{2.23}$$

where $\beta = (\beta_1, \beta_2) \in \mathbb{R}^2$ are the unfolding parameters. This was proved independently by Takens [123] and Bogdanov [20]†. System (2.23) contains all possible qualitative dynamics behavior that occurs near the critical parameter value of the original system (2.1).

The present thesis uses the smooth BT normal form

$$\begin{aligned} \dot{w} = G(w, \beta) = &\begin{pmatrix} w_1 \\ \beta_1 + \beta_2 w_1 + aw_0^2 + bw_0w_1 + g(w, \beta_2) \end{pmatrix} \\ &+ \mathcal{O}\left(|\beta_1|\|w\|^2 + |\beta_2|w_1^2\right) + \mathcal{O}\left(\|\beta\|^2\|w\|^2 + \|\beta\|\|w\|^3 + \|w\|^4\right), \end{aligned} \tag{2.24}$$

where $g(w, \beta_2) := a_1\beta_2w_0^2 + b_1\beta_2w_0w_1 + dw_0^3 + ew_0^2w_1$. Truncating the $\mathcal{O}$-terms and omitting $g(w, \beta_2)$ gives the topological normal form for the BT bifurcation. We emphasize that it is essential to include the term $g(w, \beta_2)$ in addition to the topological normal form to achieve an accurate second-order approximation for the homoclinic solution of (2.1) which depends on the term $g(w, \beta_2)$ [92]. This term was ignored in earlier studies [15, 91]. Details of the effect of this term on the second-order correction to the homoclinic solution near a generic BT point will be presented in Chapter 3.

†This normal form is slightly but equivalent to that used in [20, 123], where the second unfolding term was β_2w_0.

2.2 The bifurcation diagram near a BT point

In this section, we study the bifurcation diagram of the topological normal form system (2.23). Assume that $a > 0$ [†], then the system (2.23) has two hyperbolic equilibrium points which are given by

$$\left(s^{\pm}, 0\right) = \left(\pm\sqrt{-\frac{\beta_1}{a}}, 0\right), \quad \beta_1 < 0$$

and there are no equilibria if $\beta_1 > 0$. The Jacobian evaluated at these equilibria is

$$A = \begin{pmatrix} 0 & 1 \\ 2as^{\pm} & \beta_2 + bs^{\pm} \end{pmatrix}.$$

The eigenvalues associated with these equilibria therefore are given by

$$\lambda_{1,2} = \frac{1}{2}\left(\left(\beta_2 + bs^{\pm}\right) \pm \sqrt{\left(\beta_2 + bs^{\pm}\right)^2 + 8as^{\pm}}\right).$$

(1) For $\beta_1 < 0$, $\beta_2 \neq 0$, the quantity under the square root for s^+ is greater (in absolute value) than $(\beta_2 + bs^+)^2$. So the eigenvalues have opposite signs, and hence $(s^+, 0)$ is a saddle for all β_2. On the other hand, the second equilibrium point $(s^-, 0)$ has purely imaginary eigenvalues for $\beta_2 = b\sqrt{-\frac{\beta_1}{a}}$. This point is a source for $\beta_2 > b\sqrt{-\frac{\beta_1}{a}}$ and a sink for $\beta_2 < b\sqrt{-\frac{\beta_1}{a}}$. The generic phase portrait for $\beta_1 < 0$, $\beta_2 \neq 0$ is presented in Figure 2.1.

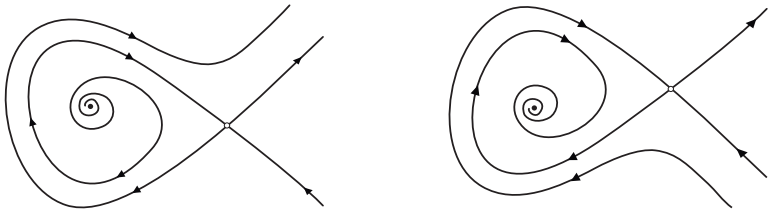

(a) (b)

Figure 2.1: Generic phase portrait of (2.23) for $a > 0$, β_1 slightly negative and (a) $\beta_2 > b\sqrt{-\frac{\beta_1}{a}}$ (b) $\beta_2 < b\sqrt{-\frac{\beta_1}{a}}$.

[†]A similar analysis can be carried out for $a < 0$.

(2) For $\beta_1 = \beta_2 = 0$, the system (2.23) has a nonhyperbolic equilibrium point at the origin. It follows from [5, **Theorem 67**, p.362] that system (2.23) has a "cusp" at the origin, see Figure 2.2.

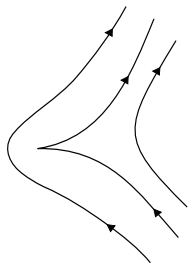

Figure 2.2: Generic phase portrait of (2.23) for $\beta_1 = \beta_2 = 0$.

(3) For $\beta_1 = 0$, $\beta_2 \neq 0$, the system (2.23) has a nonhyperbolic equilibrium at $(0, 0)$ with the eigenvalues

$$\lambda_{0,1} = 0,\ \beta_2. \tag{2.25}$$

The eigenvectors $\{q_0, q_1\}$ corresponding to the eigenvalues (2.25), respectively, are given by $q_0 = (1, 0)$, $q_1 = (1, \beta_2)$. To investigate the nature of the flow on the one-dimensional center manifold system, we apply the linear transformation

$$w = [q_0, q_1]\, v, \quad v = (v_1, v_2) \in \mathbb{R}^2,$$

which transforms (2.23) into

$$\begin{aligned}
\dot{v}_1 &= -\frac{\beta_1}{\beta_2} - \frac{a}{\beta_2} v_1^2 - \left(b + \frac{2a}{\beta_2}\right) v_1 v_2 - \left(b + \frac{a}{\beta_2}\right) v_2^2, \\
\dot{v}_2 &= \frac{\beta_1}{\beta_2} + \beta_2 v_2 + \frac{a}{\beta_2} v_1^2 + \left(b + \frac{2a}{\beta_2}\right) v_1 v_2 + \left(b + \frac{a}{\beta_2}\right) v_2^2.
\end{aligned}$$

The center manifold can be approximated by considering the tangent plane approximation, i.e., $v_2 = 0$,

$$\dot{v}_1 = -\frac{1}{\beta_2}\left(\beta_1 + a v_1^2\right). \tag{2.26}$$

For $\beta_2 < 0$, the flow on the center manifold system (2.26) is given in Figure 2.3. Notice that the position of the stable and unstable manifolds of the saddle will be reversed for $\beta_2 > 0$. It is clear that system (2.26) exhibits a limit point bifurcation, see Figure 2.4.

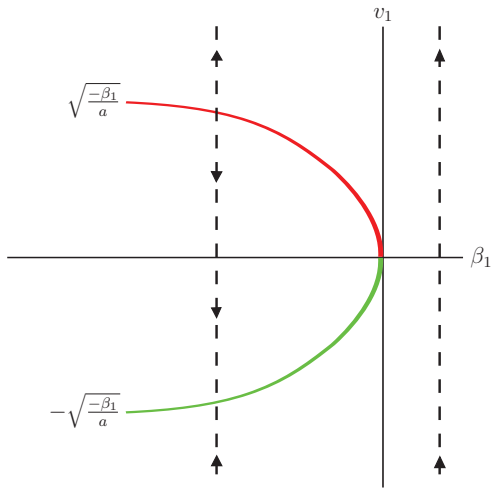

Figure 2.3: The bifurcation diagram of (2.26) for $a > 0$ and $\beta_2 < 0$.

Given the information we have collected, we conclude that limit point bifurcations occur on the line

$$\text{LP:} \quad \beta_1 = 0, \quad \beta_2 \neq 0, \tag{2.27}$$

while

$$\text{H:} \quad \beta_2(\beta_1) = b\sqrt{-\frac{\beta_1}{a}}, \quad \beta_1 < 0, \tag{2.28}$$

is a bifurcation curve on which $(s^-, 0)$ undergoes a (nondegenerate) Andronov-Hopf bifurcation, i.e., the equilibrium $(s^-, 0)$ has a pair of eigenvalues with zero sum. Along the Andronov-Hopf curve, the eigenvalues are given by

$$\left(\lambda(\beta_1), \overline{\lambda(\beta_1)}\right) = (i\omega, -i\omega), \tag{2.29}$$

where $\omega = \sqrt{2\sqrt{-a\beta_1}}$. If $b > 0$ then the Andronov-Hopf curve is located in the second quadrant of the (β_1, β_2)-plane; this curve is located in the third quadrant if $b < 0$. To study the stability of the Andronov-Hopf bifurcation and the existence of the limit cycle bifurcation, we use a method described in [88, Section 3.5]. Firstly, we fix $\beta_2 = b\sqrt{-\frac{\beta_1}{a}}$ and then we apply the following linear change of the coordinates

$$\begin{pmatrix} w_0 \\ w_1 \end{pmatrix} \to \begin{pmatrix} w_0 - s^- \\ w_1 \end{pmatrix},$$

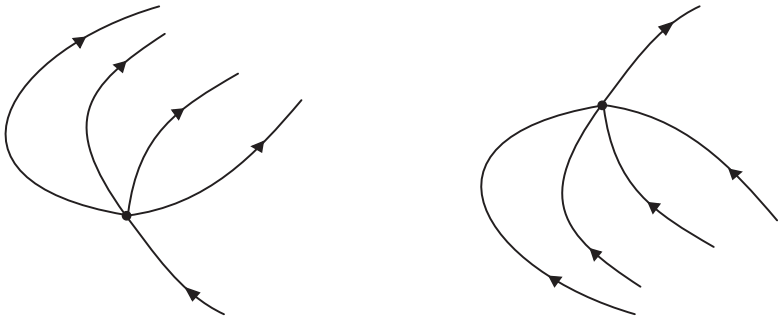

(a) (b)

Figure 2.4: Generic phase portrait of (2.23) for $a > 0$, $\beta_1 = 0$ and (a) $\beta_2 > 0$. (b) $\beta_2 < 0$.

which places the equilibrium at the origin. This transforms (2.23) into

$$\dot{w} = A(\beta_1)\, w + F(w, \beta_1), \tag{2.30}$$

where

$$A(\beta_1) = \begin{pmatrix} 0 & 1 \\ -\omega^2 & 0 \end{pmatrix}, \quad F(w, \beta_1) = \begin{pmatrix} 0 \\ a w_0^2 + b w_0 w_1 \end{pmatrix}.$$

For small $|\beta_1|$, the matrix $A(\beta_1)$ has the eigenvalues (2.29). Then there exist an eigenvector $q(\beta_1) \in \mathbb{C}^2$, of $A(\beta_1)$, and an eigenvector $p(\beta_1) \in \mathbb{C}^2$, of $A^{\mathrm{T}}(\beta_1)$, corresponding to the eigenvalues $\lambda(\beta_1)$ and $\overline{\lambda(\beta_1)}$, respectively, such that

$$A(\beta_1)\, q(\beta_1) = \lambda(\beta_1)\, q(\beta_1), \quad A^{\mathrm{T}}(\beta_1)\, p(\beta_1) = \overline{\lambda(\beta_1)}\, p(\beta_1), \quad \langle p(\beta_1), q(\beta_1) \rangle = 1, \tag{2.31}$$

where $\langle p, q \rangle = \overline{p}^{\mathrm{T}} q$. The vectors

$$q(\beta_1) = \begin{pmatrix} 1 \\ i\omega \end{pmatrix}, \quad p(\beta_1) = \frac{1}{2\omega} \begin{pmatrix} \omega \\ i \end{pmatrix},$$

satisfy (2.31). Using these vectors we can uniquely represent w for small $|\beta_1|$ as

$$w = z q(\beta_1) + \overline{z}\, \overline{q(\beta_1)} = \big(z + \overline{z}\,,\, i\omega (z - \overline{z}) \big), \tag{2.32}$$

for some complex z. Taking the scalar product with $p(\beta_1)$ of both side of (2.32) and using the fact that $\left\langle p(\beta_1), \overline{q(\beta_1)} \right\rangle = 0$, we obtain

$$\dot{z} = \langle p\left(\beta_1\right), \dot{w}\rangle = \lambda\left(\beta_1\right) z + \overline{p\left(\beta_1\right)} F\big(\left(z+\overline{z},\, i\omega\left(z-\overline{z}\right)\right), \beta_1\big), \tag{2.33}$$

or

$$\dot{z} = 2i\omega z + g_{11}\left(\beta_1\right) z\overline{z} + \frac{1}{2} g_{20}\left(\beta_1\right) z^2 + \frac{1}{2} g_{02}\left(\beta_1\right) \overline{z}^2,$$

where

$$g_{11}\left(\beta_1\right) = -i\,\frac{a}{\omega}, \quad g_{20}\left(\beta_1\right) = -i\,\frac{a}{\omega} + b, \quad g_{02}\left(\beta_1\right) = -i\,\frac{a}{\omega} - b.$$

Hence the first Lyapunov coefficient ℓ_1 along the Andronov-Hopf curve in the BT normal form (2.23) is given by

$$\ell_1\left(\beta_1\right) = \frac{1}{2\omega^2}\,\mathrm{Re}\big(i\, g_{20} g_{11}\big) = -\left(\frac{b}{8\beta_1}\right)\omega, \quad \beta_1 < 0.$$

It is clear that $\ell_1(\beta_1) < 0$ for all $b < 0$. This indicates a *supercritical* Andronov-Hopf bifurcation. This bifurcation gives rise to a unique stable limit cycle (LC) as β_2 increases from $\beta_2 = \sqrt{-\frac{\beta_1}{a}}$ (the uniqueness of the limit cycle was proved for instant in [94]). On the other hand, for $b > 0$ we have a *subcritical* Andronov-Hopf bifurcation in which an unstable limit cycle bifurcates from s^- as β_2 decreases from $\beta_2 = \sqrt{-\frac{\beta_1}{a}}$ for each $\beta_1 < 0$. The generic unstable limit cycle is presented in Figure 2.5a. The unstable (stable) limit cycle generated in the Andronov-Hopf bifurcation expands monotonically as β_2 decreases (increases) from $\sqrt{-\frac{\beta_1}{a}}$ until it intersects the saddle at s^+ and forms a homoclinic loop at some parameter value $\beta_2(\beta_1)$ [21], see Figure 2.5b. It follows from Chapter 3 (see also [91]) that this homoclinic loop bifurcation curve in (β_1, β_2)-plane is given by

$$\text{HHS:}\quad \beta_2 = -\frac{72b^3}{2401a^2}\beta_1 + \frac{5b}{7a}\sqrt{-a\beta_1} + \mathcal{O}\left(|\beta_1|^{\frac{5}{4}}\right) \tag{2.34}$$

As conclusion, for system (2.23) we have the following theorem

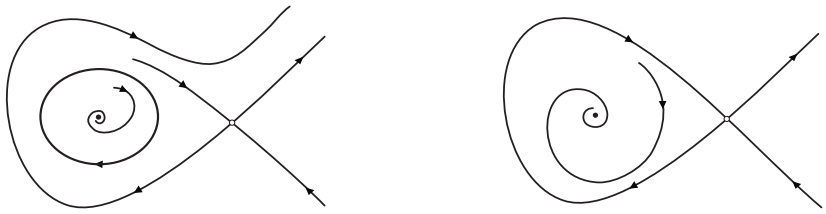

(a) (b)

Figure 2.5: Generic phase portrait of (2.23) (a) For $b > 0$, a unique unstable limit cycle emerges from the Andronov-Hopf curve (2.28) as β_2 decreases from $\beta_2 = \sqrt{-\frac{\beta_1}{a}}$. (b) The homoclinic orbits corresponding to the parameter value (2.34).

Theorem 2.2. *For $a > 0$, $b > 0$ the five bifurcations occur near the BT point of (2.23) are*

(1) $LP^{+} = \{ (\beta_1, \beta_2) \mid \beta_2 > 0,\ \beta_1 = 0 \}$,

(2) $LP^{-} = \{ (\beta_1, \beta_2) \mid \beta_2 < 0,\ \beta_1 = 0 \}$,

(3) $H = \left\{ (\beta_1, \beta_2) \mid \beta_2 = b\sqrt{-\dfrac{\beta_1}{a}},\ \beta_1 < 0 \right\}$,

(4) $HHS = \left\{ (\beta_1, \beta_2) \mid \beta_2 = -\dfrac{72b^3}{2401a^2}\beta_1 + \dfrac{5b}{7a}\sqrt{-a\beta_1} + \mathcal{O}\left(|\beta_1|^{\frac{5}{4}}\right),\ \beta_1 < 0 \right\}$,

(5) a unique LC when β_2 lies between H and HHS for $\beta_1 < 0$.

To summarize we plot the full bifurcation diagram of system (2.23) for $a > 0$, $b > 0$, see Figure 2.6.

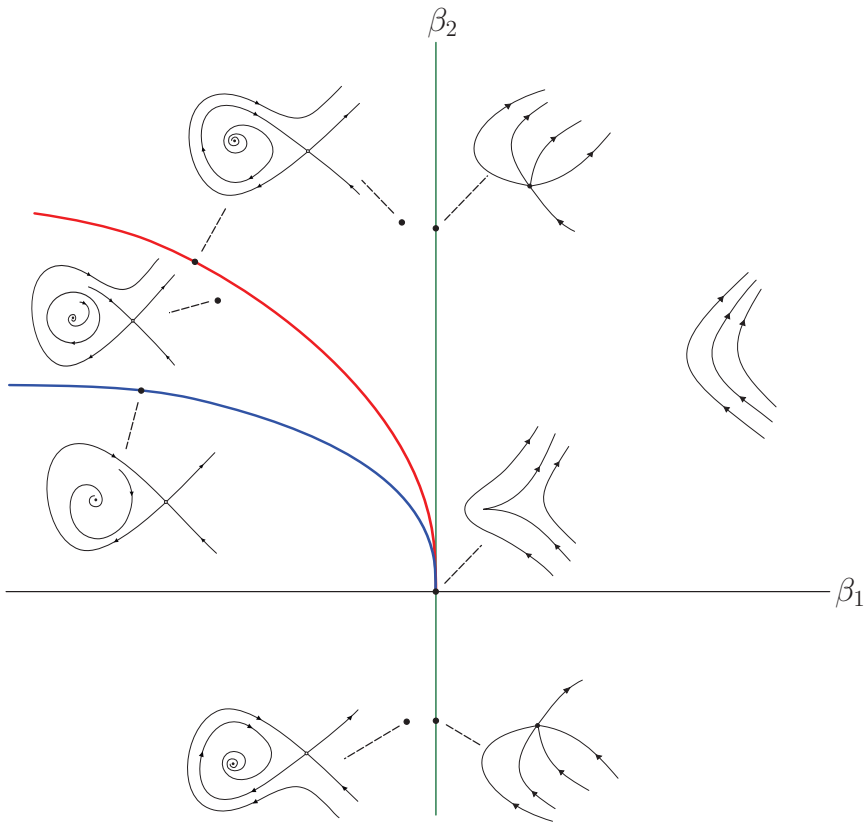

Figure 2.6: The bifurcation diagram of (2.23) for $a > 0$ and $b > 0$.

2.3 Smooth normal form in the parameter-dependent center manifold

Suppose that an explicit formula giving an emanating codim-1 bifurcation for the normal form (2.24) is available. In order to transfer this back to the original system (2.1) we need a relation

$$\alpha = K(\beta), \quad K : \mathbb{R}^2 \to \mathbb{R}^2 \tag{2.35}$$

between the unfolding parameters β and the system parameter α. Moreover, we need to parametrize the center manifold of (2.1) with respect to (w, β),

$$x = H(w, \beta), \quad H : \mathbb{R}^2 \times \mathbb{R}^2 \to \mathbb{R}^n. \tag{2.36}$$

Taking (2.36) and (2.35) together as $(x, \alpha) = (H(w, \beta), K(\beta))$ yields the center manifold for the suspended system

$$\begin{cases} \dot{x} = f(x, \alpha), \\ \dot{\alpha} = 0. \end{cases} \tag{2.37}$$

The invariance of the center manifold implies *the homological equation* [42, 58, 87]:

$$H_w(w, \beta)\, G(w, \beta) = f(H(w, \beta), K(\beta)). \tag{2.38}$$

We write the Taylor expansions of K, H and f as

$$\begin{aligned} f(x, \alpha) &= Ax + J_1\alpha + \frac{1}{2}B(x, x) + A_1(x, \alpha) + \frac{1}{2}J_2(\alpha, \alpha) + \frac{1}{6}C(x, x, x) + \frac{1}{2}B_1(x, x, \alpha) \\ &\quad + \mathcal{O}\left(\|x\|\|\alpha\|^2 + \|\alpha\|^3\right) + \mathcal{O}\left(\|(x, \alpha)\|^4\right), \end{aligned} \tag{2.39a}$$

$$\begin{aligned} H(w, \beta) &= q_0 w_0 + q_1 w_1 + H_{0010}\beta_1 + H_{0001}\beta_2 + \frac{1}{2}H_{2000}w_0^2 + H_{1100}w_0 w_1 + \frac{1}{2}H_{0200}w_1^2 \\ &\quad + H_{1010}\beta_1 w_0 + H_{1001}\beta_2 w_0 + H_{0110}\beta_1 w_1 + H_{0101}\beta_2 w_1 + \frac{1}{2}H_{0002}\beta_2^2 + \frac{1}{6}H_{3000}w_0^3 \\ &\quad + \frac{1}{2}H_{2100}w_0^2 w_1 + \frac{1}{2}H_{2001}\beta_2 w_0^2 + H_{1101}\beta_2 w_0 w_1 \; + \; \mathcal{O}\left(\beta_1^2 + |\beta_1\beta_2|\right) + \; \mathcal{O}\Big(|w_1|^3 \\ &\quad + |w_0 w_1^2| + |\beta_2 w_1^2| + |\beta_1|\|w\|^2 + \|\beta\|^2\|w\| + \|\beta\|^3\Big) + \mathcal{O}\left(\|(w, \beta)\|^4\right), \end{aligned} \tag{2.39b}$$

$$K(\beta) = K_{1,0}\beta_1 + K_{1,1}\beta_2 + \frac{1}{2}K_2\beta_2^2 + \mathcal{O}\left(\beta_1^2 + |\beta_1\beta_2|\right) + \mathcal{O}(\|\beta\|^3), \tag{2.39c}$$

where A, J_1, B, A_1, J_2, C, B_1 are given as in (1.5). We insert the expansions (2.39a)-(2.39c) into (2.38) together with the smooth normal form (2.24). Then the resulting equations for terms of the same order in w and β can be solved by a recursive procedure based on

Fredholm's solvability condition that gives the Taylor coefficients of H and K. Collecting the terms with equal components in w and β up to the second order in the *homological equation* leads to the following systems†

$$w_0 : Aq_0 = 0, \tag{2.40a}$$

$$w_1 : Aq_1 = q_0, \tag{2.40b}$$

$$\beta_1 : AH_{0010} + J_1 K_{1,0} = q_1, \tag{2.40c}$$

$$\beta_2 : AH_{0001} + J_1 K_{1,1} = 0, \tag{2.40d}$$

$$w_0^2 : AH_{2000} + B(q_0, q_0) = 2aq_1, \tag{2.40e}$$

$$w_0 w_1 : AH_{1100} + B(q_0, q_1) = H_{2000} + bq_1, \tag{2.40f}$$

$$w_1^2 : AH_{0200} + B(q_1, q_1) = 2H_{1100}, \tag{2.40g}$$

$$w_0\beta_1 : AH_{1010} + B(q_0, H_{0010}) + A_1(q_0, K_{1,0}) = H_{1100}, \tag{2.40h}$$

$$w_0\beta_2 : AH_{1001} + B(q_0, H_{0001}) + A_1(q_0, K_{1,1}) = 0, \tag{2.40i}$$

$$w_1\beta_1 : AH_{0110} + B(q_1, H_{0010}) + A_1(q_1, K_{1,0}) = H_{0200} + H_{1010}, \tag{2.40j}$$

$$w_1\beta_2 : AH_{0101} + B(q_1, H_{0001}) + A_1(q_1, K_{1,1}) = H_{1001} + q_1, \tag{2.40k}$$

$$\beta_2^2 : AH_{0002} + J_1 K_2 + B(H_{0001}, H_{0001}) + 2A_1(H_{0001}, K_{1,1}) + J_2(K_{1,1}, K_{1,1}) = 0. \tag{2.40l}$$

The solvability condition for (2.40e),

$$\underbrace{p_1^{\mathrm{T}} A}_{0} H_{2000} + p_1^{\mathrm{T}} B(q_0, q_0) = 2a \underbrace{p_1^{\mathrm{T}} q_1}_{1},$$

gives

$$a = \frac{1}{2} p_1^{\mathrm{T}} B(q_0, q_0). \tag{2.41}$$

Taking the scalar product of both sides of (2.40e) with p_0^{T} yields

$$p_1^{\mathrm{T}} H_{2000} = -p_0^{\mathrm{T}} B(q_0, q_0). \tag{2.42}$$

The solvability condition for (2.40f) gives

$$b = p_1^{\mathrm{T}} B(q_0, q_1) - p_1^{\mathrm{T}} H_{2000}. \tag{2.43}$$

†The systems are computed with Maple, see Appendix A.1.

Taking into account (2.42), we get

$$b = p_1^{\mathrm{T}} B(q_0, q_1) + p_0^{\mathrm{T}} B(q_0, q_0). \tag{2.44}$$

The coefficients (a, b) are known and given in (2.20). However, given a and b, the solutions to the singular linear systems (2.40e)-(2.40g) are not unique. The uniqueness of the solutions can be guaranteed by requiring that (2.40g) is solvable for H_{0200} (see [88, Section 8.7]). The solvability condition for (2.40g) requires that

$$2p_1^{\mathrm{T}} H_{1100} - p_1^{\mathrm{T}} B(q_1, q_1) = 0 \tag{2.45}$$

Multiplying both sides of (2.40f) by p_0^{T} gives

$$p_1^{\mathrm{T}} H_{1100} = p_0^{\mathrm{T}} H_{2000} - p_0^{\mathrm{T}} B(q_0, q_1).$$

Substituting this into (2.45) yields

$$2p_0^{\mathrm{T}} H_{2000} - 2p_0^{\mathrm{T}} B(q_0, q_1) - p_1^{\mathrm{T}} B(q_1, q_1) = 0. \tag{2.46}$$

Using the substitution $H_{2000} \mapsto H_{2000} + rq_0$, with

$$r := \frac{1}{2}\left(-2p_0^{\mathrm{T}} H_{2000} + 2p_0^{\mathrm{T}} B(q_0, q_1) + p_1^{\mathrm{T}} B(q_1, q_1)\right), \tag{2.47}$$

makes the L.H.S of (2.46) equal to zero. So this substitution implies that (2.40g) is solvable for H_{0200}. Thus, from (2.40e), (2.40f) and (2.40g) the vectors H_{2000}, H_{1100} and H_{0200} can be uniquely determined by solving the non-singular $(n+1)-$dimensional systems,

$$\begin{cases} H_{2000} = A^{\mathrm{INV}}\left(2aq_1 - B(q_0, q_0)\right), \quad H_{2000} \mapsto H_{2000} + rq_0 \\ H_{1100} = A^{\mathrm{INV}}\left(bq_1 - B(q_0, q_1) + H_{2000}\right), \\ H_{0200} = A^{\mathrm{INV}}\left(2H_{1100} - B(q_1, q_1)\right). \end{cases} \tag{2.48}$$

Rewrite system (2.40c) and (2.40d) into the following vector form

$$AH_{01} + J_1 K_1 = [q_1, 0], \tag{2.49}$$

where $H_{01} = [H_{0010}, H_{0001}]$, $K_1 = [K_{1,0}, K_{1,1}]$. The solvability condition for (2.40h) and (2.40i) gives

$$p_1^{\mathrm{T}} B(q_0, H_{01}) + p_1^{\mathrm{T}} A_1(q_0, K_1) = [p_1^{\mathrm{T}} H_{1100}, 0]. \tag{2.50}$$

The solvability condition for (2.40g) gives

$$p_1^{\mathrm{T}} H_{1100} = \frac{1}{2} p_1^{\mathrm{T}} B(q_1, q_1), \tag{2.51}$$

while the scalar product of both sides with p_0^{T} gives

$$p_1^{\mathrm{T}} H_{0200} = -p_0^{\mathrm{T}} B(q_1, q_1) + 2 p_0^{\mathrm{T}} H_{1100}. \tag{2.52}$$

Substituting (2.51) into (2.50) then yields

$$p_1^{\mathrm{T}} B(q_0, H_{01}) + p_1^{\mathrm{T}} A_1(q_0, K_1) = \frac{1}{2}[p_1^{\mathrm{T}} B(q_1, q_1), 0]. \tag{2.53}$$

The solvability conditions for (2.40j) and (2.40k) yield the following equations

$$\begin{cases} p_1^{\mathrm{T}} B(q_0, H_{0010}) + p_1^{\mathrm{T}} A_1(q_1, K_{1,0}) = p_1^{\mathrm{T}} H_{1010} + p_1^{\mathrm{T}} H_{0200}, \\ \\ p_1^{\mathrm{T}} B(q_0, H_{0001}) + p_1^{\mathrm{T}} A_1(q_1, K_{1,1}) = p_1^{\mathrm{T}} H_{1001} + 1. \end{cases} \tag{2.54}$$

On the other hand, taking the scalar product of both sides of system (2.40h) and (2.40i) with p_0^{T} gives

$$\begin{cases} p_1^{\mathrm{T}} H_{1010} = -(p_0^{\mathrm{T}} B(q_0, H_{0010}) + p_0^{\mathrm{T}} A_1(q_1, K_{1,0})) + p_0^{\mathrm{T}} H_{1100}, \\ \\ p_1^{\mathrm{T}} H_{1001} = -(p_0^{\mathrm{T}} B(q_0, H_{0001}) + p_0^{\mathrm{T}} A_1(q_1, K_{1,1})). \end{cases} \tag{2.55}$$

Substituting the formula of $p_1^{\mathrm{T}} H_{1010}$ and $p_1^{\mathrm{T}} H_{1001}$ into (2.54) gives

$$\begin{cases} p_1^{\mathrm{T}} B(q_0, H_{0010}) + p_1^{\mathrm{T}} A_1(q_1, K_{1,0}) = \\ \qquad -(p_0^{\mathrm{T}} B(q_0, H_{0010}) + p_0^{\mathrm{T}} A_1(q_1, K_{1,0})) + p_0^{\mathrm{T}} H_{1100} + p_1^{\mathrm{T}} H_{0200}, \\ \\ p_1^{\mathrm{T}} B(q_0, H_{0001}) + p_1^{\mathrm{T}} A_1(q_1, K_{1,1}) = -(p_0^{\mathrm{T}} B(q_0, H_{0001}) + p_0^{\mathrm{T}} A_1(q_1, K_{1,1})) + 1, \end{cases} \tag{2.56}$$

or in vector form

$$p_0^{\mathrm{T}} B(q_0, H_{01}) + p_0^{\mathrm{T}} A_1(q_1, K_1) + p_1^{\mathrm{T}} B(q_0, H_{01}) + p_1^{\mathrm{T}} A_1(q_1, K_1) = \left[p_0^{\mathrm{T}} H_{1100} + p_1^{\mathrm{T}} H_{0200}, 1\right]. \tag{2.57}$$

With additional information from (2.52) about $p_1^{\mathrm{T}} H_{0200}$, (2.57) becomes

$$p_0^{\mathrm{T}} B(q_0, H_{01}) + p_0^{\mathrm{T}} A_1(q_1, K_1) + p_1^{\mathrm{T}} B(q_0, H_{01}) + p_1^{\mathrm{T}} A_1(q_1, K_1) = \left[-p_0^{\mathrm{T}} B(q_1, q_1) + 3 p_0^{\mathrm{T}} H_{1100}, 1\right]. \tag{2.58}$$

Taking (2.49), (2.53) and (2.58) together, one computes K_1 and H_{01} by solving the $(n+2)$-dimensional system

$$\begin{pmatrix} A & J_1 \\ p_1^{\mathrm{T}}\mathrm{B}q_0 & p_1^{\mathrm{T}}\mathrm{A}_1 q_0 \\ p_0^{\mathrm{T}}\mathrm{B}q_0 + p_1^{\mathrm{T}}\mathrm{B}q_1 & p_0^{\mathrm{T}}\mathrm{A}_1 q_0 + p_1^{\mathrm{T}}\mathrm{A}_1 q_1 \end{pmatrix} \begin{pmatrix} H_{01} \\ K_1 \end{pmatrix} = \begin{pmatrix} q_1 & 0 \\ \frac{1}{2}p_1^{\mathrm{T}}B(q_1,q_1) & 0 \\ c & 1 \end{pmatrix}, \tag{2.59}$$

where $c := 3p_0^{\mathrm{T}}H_{1100} - p_0^{\mathrm{T}}B(q_1,q_1)$ and the expressions with matrix B, A_1 have natural interpretations. We note that the existence and uniqueness of the solution to (2.59) requires that the $(n+2)\times(n+2)$ matrix

$$M = \begin{pmatrix} A & J_1 \\ p_1^{\mathrm{T}}\mathrm{B}q_0 & p_1^{\mathrm{T}}\mathrm{A}_1 q_0 \\ p_0^{\mathrm{T}}\mathrm{B}q_0 + p_1^{\mathrm{T}}\mathrm{B}q_1 & p_0^{\mathrm{T}}\mathrm{A}_1 q_0 + p_1^{\mathrm{T}}\mathrm{A}_1 q_1 \end{pmatrix} \tag{2.60}$$

is non-singular. The left $(n+2)\times n$ block has full rank n since the null vector q_0 of A is not orthogonal to the row vectors in the $(2,1)$ and $(3,1)$ block entries of M if $a \neq 0$ and $b \neq 0$. Since the right block column of M contains parameter derivatives in all entries, the non-singularity of M is the transversality condition for the BT point.

To prove that K_1 is non-singular we proceed by contradiction. Suppose that there exist real variables γ and η not both zero, such that $K_1(\gamma,\eta) = 0$. Then

$$M \begin{pmatrix} \xi \\ 0 \\ 0 \end{pmatrix} = \begin{pmatrix} \gamma q_1 \\ \frac{\gamma}{2}p_1^{\mathrm{T}}B(q_1,q_1) \\ -\gamma p_0^{\mathrm{T}}B(q_1,q_1) + 3\gamma p_0^{\mathrm{T}}H_{1100} + \eta \end{pmatrix}$$

with $\xi \in \mathbb{R}^n$. This implies that $A\xi = \gamma q_1$, hence $0 = p_1^{\mathrm{T}}A\xi = \gamma p_1^{\mathrm{T}}q_1 = \gamma$. Hence

$$M(\xi,0,0) = (0,0,\eta),$$

with $\eta \neq 0$. This, in turn, implies that $\xi = \mu q_0$ for a scalar $\mu \neq 0$. From the second block row in M we then have $\mu p_1^{\mathrm{T}}B(q_0,q_0) = 0$, which contradicts $a \neq 0$. The system (2.59) above corrects [15, 16], where a wrong formula to compute K_1 is suggested based on the assumption that K_1 satisfies the equation (2.49) only. The terms K_2 is immediately obtained from (2.40l)

$$K_2 = -p_1^{\mathrm{T}}\left(B(H_{0001},H_{0001}) + 2A_1(H_{0001},K_{1,1}) + J_2(K_{1,1},K_{1,1})\right)K_{1,0}. \tag{2.61}$$

Using (2.40l), (2.40i) and (2.40k), one obtains

$$\begin{cases} H_{0002} = -A^{\mathrm{INV}}\left(B(H_{0001}, H_{0001}) + 2A_1(H_{0001}, K_{1,1}) + J_2(K_{1,1}, K_{1,1}) + A_1K_2\right), \\ H_{1001} = -A^{\mathrm{INV}}\left(B(q_0, H_{0001}) + B(q_0, K_{1,1})\right), \\ H_{0101} = -A^{\mathrm{INV}}\left(B(q_1, H_{0001}) + B(q_1, K_{1,1}) - H_{1001} - q_1\right). \end{cases} \tag{2.62}$$

Collecting the terms with equal components in w and β of order three at *the homological equation* lead to

$$w_0^3 : AH_{3000} + C(q_0, q_0, q_0) + 3B(q_0, H_{2000}) = 6aH_{1100} + 6dq_1, \tag{2.63a}$$

$$\begin{aligned} w_0^2 w_1 : {} & AH_{2100} + C(q_0, q_0, q_1) + 2B(q_0, H_{1100}) + B(q_1, H_{2000}) \\ & = 2bH_{1100} + 2aH_{0200} + H_{3000} + 2eq_1 \end{aligned} \tag{2.63b}$$

$$\begin{aligned} w_0^2 \beta_2 : {} & AH_{2001} + C(q_0, q_0, H_{0001}) + B_1(q_0, q_0, K_{1,1}) + 2B(q_0, H_{1001}) \\ & + B(H_{0001}, H_{2000}) + A_1(H_{2000}, K_{1,1}) = 2aH_{0101} + 2a_1q_1, \end{aligned} \tag{2.63c}$$

$$\begin{aligned} w_0 w_1 \beta_2 : {} & AH_{1101} + C(q_0, q_1, H_{0001}) + B_1(q_0, q_1, K_{1,1}) + B(q_1, H_{1001}) + B(H_{0001}, H_{1100}) \\ & + B(q_0, H_{0101}) + A_1(H_{1100}, K_{1,1}) = bH_{0101} + H_{1100} + H_{2001} + b_1q_1. \end{aligned} \tag{2.63d}$$

The solvability condition gives the following expressions for the cubic coefficients:

$$d = \frac{1}{6}p_1^{\mathrm{T}}\left(C(q_0, q_0, q_0) + 3B(q_0, H_{2000}) - 6aH_{1100}\right), \tag{2.64}$$

$$H_{3000} = -A^{\mathrm{INV}}\left(C(q_0, q_0, q_0) + 3B(q_0, H_{2000}) - 6aH_{1100} - 6dq_1\right), \tag{2.65}$$

$$\begin{aligned} e = \frac{1}{2}p_1^{\mathrm{T}} & \left(C(q_0, q_0, q_1) + 2B(q_0, H_{1100}) + B(q_1, H_{2000})\right. \\ & \left. - 2bH_{1100} - 2aH_{0200} - H_{3000}\right), \end{aligned} \tag{2.66}$$

$$\begin{aligned} a_1 = \frac{1}{2}p_1^{\mathrm{T}} & \left(C(q_0, q_0, H_{0001}) + B_1(q_0, q_0, K_{1,1}) + 2B(q_0, H_{1001}) + B(H_{0001}, H_{2000})\right. \\ & \left. + A_1(H_{2000}, K_{1,1}) - 2aH_{0101}\right), \end{aligned} \tag{2.67}$$

$$\begin{aligned} H_{2001} = -A^{\mathrm{INV}} & \left(C(q_0, q_0, H_{0001}) + B_1(q_0, q_0, K_{1,1}) + 2B(q_0, H_{1001})\right. \\ & \left. + B(H_{0001}, H_{2000}) + A_1(H_{2000}, K_{1,1}) - 2aH_{0101} - 2a_1q_1\right). \end{aligned} \tag{2.68}$$

$$\begin{aligned} b_1 = p_1^{\mathrm{T}} & \left(C(q_0, q_1, H_{0001}) + B_1(q_0, q_1, K_{1,1}) + B(q_1, H_{1001}) + B(H_{0001}, H_{1100})\right. \\ & \left. + B(q_0, H_{0101}) + A_1(H_{1100}, K_{1,1}) - bH_{0101} - H_{1100} - H_{2001}\right). \end{aligned} \tag{2.69}$$

In formulas (2.48), (2.62), (2.65) and (2.68), we define the expression $x = A^{\mathrm{INV}}y$ as solving the non-singular border system

$$\begin{pmatrix} A & p_1 \\ q_0^{\mathrm{T}} & 0 \end{pmatrix} \begin{pmatrix} x \\ s \end{pmatrix} = \begin{pmatrix} y \\ 0 \end{pmatrix},$$

where y is in the range of A.

2.4 Bogdanov-Takens point in the Gray-Scott model

In this section, we study the BT bifurcation of the Gray-Scott kinetic model

$$\begin{cases} \dfrac{dU}{dt} = -UV^2 + F(1-U), \\ \dfrac{dV}{dt} = UV^2 - (F+k)V, \end{cases} \tag{2.70}$$

(see [99, 125]). The model (2.70) describes cubic *autocatalytic* chemical or biochemical reactions. This model serves as a reaction part of the reaction diffusion system describing various pattern formation phenomena [75–77]. The analysis of (2.70) shows that points $(1,0)$ and

$$\left(\frac{2(k+F)^2}{F \pm \rho}, \frac{(F \pm \rho)}{2\,(k+F)}\right),$$

where

$$\rho = \sqrt{F^2\,(1-4F) - 4Fk\,(k+2F)},$$

are the equilibria. The trivial point $(1,0)$ always exists and it is stable for all k and F. The Jacobian matrix of (2.70) at an equilibrium point (U_c, V_c) is

$$A = \begin{pmatrix} -V_c^2 - F & -2U_cV_c \\ V_c^2 & 2U_cV_c - F - k \end{pmatrix}. \tag{2.71}$$

The BT bifurcation conditions, i.e., Determinate(A)=Trace(A)=0, imply that

$$\begin{aligned} -2FU_cV_c + FV_c^2 + kV_c^2 + F^2 + Fk = 0, \\ 2U_cV_c - V_c^2 - 2F - k = 0. \end{aligned} \tag{2.72}$$

Substituting any of the nontrivial steady states into (2.72), and then solving this system for (k, F) gives the critical parameter value $(k_c, F_c) = (\frac{1}{16}, \frac{1}{16})$ with $(U_c, V_c) = (\frac{1}{2}, \frac{1}{4})$. Therefore, system (2.70) exhibits a BT bifurcation at (k_c, F_c).

Theorem 2.3. *At the parameter values* (k_c, F_c)*, system* (2.70) *is locally* C^∞*- equivalent near* (U_c, V_c) *to*

$$\begin{cases} \dot{w_0} = w_1, \\ \dot{w_1} = \dfrac{1}{16} w_0^2 + w_0 w_1 + \mathcal{O}(\|w\|^3). \end{cases} \tag{2.73}$$

Proof. Under the change of variables

$$(U, V) = (U_c + x_1, V_c + x_2)\,, \quad (F, k) = (F_c + \alpha_1, k_c + \alpha_2)\,, \tag{2.74}$$

the system (2.70) takes the form

$$\begin{cases} \dot{x}_1 = -\dfrac{1}{8}x_1 - \dfrac{1}{4}x_2 + \dfrac{1}{2}\alpha_2 - \dfrac{1}{2}(x_1 x_2 + x_2^2) - x_1\alpha_2 - x_1 x_2^2, \\ \dot{x}_2 = \dfrac{1}{16}x_1 + \dfrac{1}{8}x_2 - \dfrac{1}{4}(\alpha_1 + \alpha_2) + \dfrac{1}{2}(x_1 x_2 + x_2^2) - x_2(\alpha_1 + \alpha_2) + x_1 x_2^2, \end{cases} \tag{2.75}$$

which has the BT-equilibrium $x = (x_1, x_2) = (0, 0)$ at $\alpha = (\alpha_1, \alpha_2) = (0, 0)$. The system (2.75) can be represented at $\alpha = (0, 0)$ as (2.2) where

$$A = \begin{pmatrix} -\dfrac{1}{8} & -\dfrac{1}{4} \\ \dfrac{1}{16} & \dfrac{1}{8} \end{pmatrix}, \quad B(x, y) = \begin{pmatrix} -\dfrac{1}{2}(x_1 y_2 + x_2 y_1) - x_2 y_2 \\ \dfrac{1}{2}(x_1 y_2 + x_2 y_1) - x_2 y_2 \end{pmatrix}, \tag{2.76}$$

The normal form coefficients a, b can be computed using *the homological equation* technique as we described in Section 2.3. The vectors

$$q_0 = \frac{1}{2} m\,(2, -1)\,, \quad q_1 = -\frac{1}{2} m\,(-2n, n + 8m)\,, \quad p_1 = r\,(1, 2)\,, \quad p_0 = (s, 16r + 2s)\,,$$

where $\{m, n, r, s\} \in \mathbb{R}$, satisfy (2.3). We can select these vectors to satisfy (2.4) so that we obtain the following numerical value for the vectors $q_{0,1}$, $p_{0,1}$

$$q_0 = \pm\frac{\sqrt{5}}{5}\,(-2, 1)\,, \quad q_1 = \pm\frac{16\sqrt{5}}{25}\,(1, 2)\,, \quad p_0 = q_0, \quad p_1 = \pm\frac{\sqrt{5}}{16}\,(1, 2)\,.$$

Using these vectors with B as we defined in (2.76), we can compute a, b as

$$(a, b) = \mp\frac{\sqrt{5}}{10}\left(\frac{1}{16}, 1\right). \tag{2.77}$$

Since the critical normal form coefficients (a, b) can be simultaneously divided by $\mp\frac{\sqrt{5}}{10}$ by applying an appropriate scaling of the phase coordinates (w_0, w_1) in (2.22), we arrive at (2.73). □

CHAPTER 3

Homoclinic orbits near a Bogdanov-Takens point of a vector-field

With a regular perturbation (R-P) method and a generalization of the Lindstedt-Poincaré (L-P) perturbation method, we derive the explicit computational formulas for the second-order homoclinic predictor to a generic n-dimensional ODE. The generic homoclinic predictors are applied to explicitly compute the homoclinic solutions in the Gray-Scott kinetic model.

3.1 Blowing-up the smooth normal form

To construct an approximation for the homoclinic solution of (2.24), one first performs a blow-up transformation. We take the normal form (2.24) and apply the rescaling

$$\beta_1 = -\frac{4}{a}\varepsilon^4 \ ^\dagger, \quad \beta_2 = \frac{b}{a}\varepsilon^2\tau, \quad w_0 = \frac{\varepsilon^2}{a}u, \quad w_1 = \frac{\varepsilon^3}{a}v, \quad \varepsilon t = s. \tag{3.1}$$

†We use $-\frac{4}{a}\varepsilon^4$ rather than $-\frac{1}{a}\varepsilon^4$ as used in [78]. This simplifies the final result. The minus sign in the expression of β_1 comes from the fact that the equilibria are $\left(\pm\sqrt{\frac{-\beta_1}{a}}, 0\right)$. This requires $\text{sign}(\beta_1) = -\text{sign}(a)$.

This gives

$$\begin{cases} \dot{u} = v \\ \\ \dot{v} = -4 + u^2 + \varepsilon \frac{b}{a} v\,(\tau + u) + \varepsilon^2 \frac{1}{a^2} u^2\,(\tau b a_1 + du) + \varepsilon^3 \frac{1}{a^2} uv\,(\tau b b_1 + eu) + \mathcal{O}(\varepsilon^4), \end{cases}$$

or

$$\ddot{u} - u^2 + 4 = \varepsilon \frac{b}{a} \dot{u}\,(\tau + u) + \varepsilon^2 \frac{1}{a^2} u^2\,(\tau b a_1 + du) + \varepsilon^3 \frac{1}{a^2} u\dot{u}\,(\tau b b_1 + eu) + \mathcal{O}(\varepsilon^4), \tag{3.2}$$

where $0 < \varepsilon \ll 1$ and τ are the new parameters. The dot now indicates the derivative with respect to s. For $\varepsilon = 0$, (3.2) is a Hamiltonian system with the homoclinic solution (see, for example, [16])

$$\begin{cases} u_0(s) = 2\left(1 - 3\mathrm{sech}^2(s)\right), \\ \\ v_0(s) = 12\mathrm{sech}^2(s)\tanh(s). \end{cases} \tag{3.3}$$

3.2 The regular perturbation method

The regular perturbation method can be used to compute the homoclinic orbits to (3.2), **cf.** [91, 92]. Assume that the homoclinic solution of (3.2) is parametrized by ε and approximated by

$$\begin{pmatrix} u(s) \\ \\ v(s) \\ \\ \tau \end{pmatrix} = \begin{pmatrix} u_0(s) \\ \\ v_0(s) \\ \\ \tau_0 \end{pmatrix} + \varepsilon \begin{pmatrix} u_1(s) \\ \\ v_1(s) \\ \\ \tau_1 \end{pmatrix} + \varepsilon^2 \begin{pmatrix} u_2(s) \\ \\ v_2(s) \\ \\ \tau_2 \end{pmatrix} + \varepsilon^3 \begin{pmatrix} u_3(s) \\ \\ v_3(s) \\ \\ \tau_3 \end{pmatrix} + \mathcal{O}\left(\varepsilon^4\right). \tag{3.4}$$

Inserting (3.4) into (3.2) and equating equal powers of ε leads to the following systems

$$\text{Order}\left(\varepsilon^0\right) : \ \ddot{u}_0 - u_0^2 + 4 = 0, \tag{3.5}$$

$$\text{Order}\left(\varepsilon^i\right) : \ \ddot{u}_i - 2u_0 u_i = z_i(u, v, \tau), \quad i = 1, 2, 3, \ldots \tag{3.6}$$

where

$$z_1(u,v,\tau) = \frac{b}{a}\dot{u}_0\left(\tau_0+u_0\right),$$

$$z_2(u,v,\tau) = \frac{b}{a}\dot{u}_0\left(\tau_1+u_1\right) + \frac{b}{a}\dot{u}_1\left(\tau_0+u_0\right) + \frac{1}{a^2}u_0^2\left(a_1b\tau_0+du_0\right) + u_1^2,$$

$$\begin{aligned} z_3(u,v,\tau) = {} & \frac{b}{a}\dot{u}_0\left(\tau_2+u_2\right) + \frac{b}{a}\dot{u}_1\left(\tau_1+u_1\right) + \frac{b}{a}\dot{u}_2\left(\tau_0+u_0\right) + 2u_1u_2 \\ & + \frac{2}{a^2}u_0u_1\left(a_1b\tau_0+du_0\right) + \frac{1}{a^2}u_0\dot{u}_0\left(bb_1\tau_0+eu_0\right) + \frac{1}{a^2}u_0^2\left(a_1b\tau_1+du_1\right), \\ & \vdots \end{aligned}$$

The ε^0-terms yield the Hamiltonian system with solution (3.3). Differentiating (3.5) with respect to s we find that $\varphi_1(s) = \dot{u}_0(s)$ solves the homogeneous problem of (3.6), i.e.,

$$\ddot{\varphi} - 2u_0\varphi = 0. \tag{3.7}$$

Then there exists a second solution to (3.7) in the form

$$\varphi_2 = \varphi_1\theta, \tag{3.8}$$

for some differentiable function θ. Substituting (3.8) into (3.7) gives

$$\cancel{\ddot{\varphi}_1\theta} + 2\dot{\varphi}_1\dot{\theta} + \varphi_1\ddot{\theta} - \cancel{2u_0\varphi_1\theta} = 0. \tag{3.9}$$

If we define $\rho = \dot{\theta}$, (3.9) becomes

$$2\dot{\varphi}_1\rho + \varphi_1\dot{\rho} = 0 \tag{3.10}$$

with solution $\rho = \dfrac{2\cosh^6(s)}{3\sinh^2(s)}$. Therefore, a second solution for the homogeneous problem (3.7) is

$$\varphi_2 = \varphi_1\int \rho\,\mathrm{d}s = 2\cosh^2(s) + 15\,\mathrm{sech}^2(s)\left(s\tanh(s)-1\right) + 5. \tag{3.11}$$

As we have two linearly independent solutions $\{\varphi_1, \varphi_2\}$ for the homogeneous problem (3.7), it is straightforward to solve the inhomogeneous problems of (3.6). The general solution for these problems can be written as

$$u_i(s) = \left(C_{2(i-1)+1} - \overbrace{\int \frac{\varphi_2 z_i}{W\left(\varphi_1,\varphi_2\right)}\,\mathrm{d}x}^{g_i}\right)\varphi_1 + \left(C_{2(i-1)+2} + \overbrace{\int \frac{\varphi_1 z_i}{W\left(\varphi_1,\varphi_2\right)}\,\mathrm{d}x}^{f_i}\right)\varphi_2, \tag{3.12}$$

$i = 1, 2, 3, \ldots$, where $W(\varphi_1, \varphi_2)$ is the *Wronskian* of $\{\varphi_1, \varphi_2\}$, $C_{2(i-1)+1}$, $C_{2(i-1)+2}$ are undetermined integration constants and $f_i(0) = g_i(0) = 0$ must hold. The description of the homoclinic solution (3.4) to the saddle of (3.2) requires that u and v are bounded, i.e., $\lim_{s\to\pm\infty} |u(s)| \neq \infty$ and $\lim_{s\to\pm\infty} |v(s)| \neq \infty$, and as $s \to \pm\infty$ the solution must approach the saddle. This implies

$$\lim_{s\to\pm\infty} |u_l(s)| \neq \infty, \quad \text{for} \quad l \geq 1.$$

Thus, the first-order correction to the Hamiltonian homoclinic solution can be written as

$$u_1(s) = (C_1 - g_1(s))\,\varphi_1(s) + (C_2 + f_1(s))\,\varphi_2(s),$$

where

$$\begin{aligned}
f_1(s) &= \frac{b}{35a}\frac{\sinh^3(s)(7\tau_0 - 10)}{\cosh^3(s)} + \frac{3b}{70a}\frac{\sinh^3(s)(7\tau_0 - 10)}{\cosh^5(s)} - \frac{9b}{7a}\frac{\sinh^3(s)}{\cosh^7(s)},\\
g_1(s) &= \frac{6b}{7a}\log(2\cosh(s)) + s\frac{b}{28a}\frac{\sinh(s)(7\tau_0 - 10)}{\cosh(s)} + \frac{b}{28a}\frac{(-7\tau_0 + 1)}{\cosh^2(s)}\\
&\quad + s\frac{b}{56a}\frac{\sinh(s)(7\tau_0 - 10)}{\cosh^3(s)} + \frac{3b}{56a}\frac{(7\tau_0 + 30)}{\cosh^4(s)} + s\frac{3b}{56a}\frac{\sinh(s)(-7\tau_0 - 20)}{\cosh^5(s)}\\
&\quad - \frac{45b}{28a}\left(\frac{1}{\cosh^6(s)} - s\frac{\sinh(s)}{\cosh^7(s)}\right) - \frac{b}{a}\left(\frac{\tau_0}{8} + \frac{1}{28} + \frac{6}{7}\log(2)\right).
\end{aligned}$$

Now we check the limits of $u_1(s)$ for $s \to \pm\infty$. First we see that

$$\lim_{s\to\pm\infty} g_1(s)\varphi_1(s) = \lim_{s\to\pm\infty} \varphi_1(s) = 0.$$

So we focus on the other terms. We find

$$\lim_{s\to\pm\infty} (C_2 + f(s)) = C_2 \pm \frac{b}{a}\frac{7\tau_0 - 10}{35}.$$

Thus we recover

$$\tau_0 = \frac{10}{7} \tag{3.13}$$

together with $C_2 = 0$. We point out that (3.13) coincides with the result of the Melnikov method in (1.30). Therefore, we obtain the following first-order correction to the Hamiltonian homoclinic solution

$$\begin{cases} u_1(s) = -\dfrac{72}{7}\dfrac{b}{a}\dfrac{\sinh(s)\log(\cosh(s))}{\cosh^3(s)} + C_1\varphi_1(s), \\ v_1(s) = \dot{u}_1(s). \end{cases} \tag{3.14}$$

The constant C_1 can be determined by adding an extra condition that fixes the solution phase. This condition can be used to determine all $C_{2(i-1)+1},\ i = 2, 3, ...$ and hence to obtain a unique description for the homoclinic solution (3.4). Next we discuss two approaches to define such a unique solution.

3.2.1 A point phase condition

By fixing the solution phase by requiring that [15]:

$$v_i(0) = \dot{u}_i(0) = 0, \quad i = 1, 2, 3, \dots \tag{3.15}$$

one can obtain a (unique) i^{th}-order correction for the homoclinic solution $(u(s),\ v(s),\ \tau)$. The condition (3.15) requires that $C_1 = 0$. Thus, we get

$$\begin{cases} u_1(s) = -\dfrac{72}{7}\dfrac{b}{a}\dfrac{\sinh(s)\log(\cosh(s))}{\cosh^3(s)}, \\ \\ v_1(s) = -\dfrac{72b}{7a}\dfrac{\sinh^2(s) + \left(1 - 2\sinh^2(s)\right)\log(\cosh(s))}{\cosh^4(s)}, \end{cases} \tag{3.16}$$

as first reported in [91]. Applying the previous procedure to (3.6) for $i = 2$ gives

$$\tau_1 = 0, \quad C_3 = 0, \quad C_4 = \frac{18b^2 - 140a_1 b + 245d}{392a^2},$$

and hence

$$\begin{cases} u_2(s) = -\dfrac{216}{49}\dfrac{b^2}{a^2}\dfrac{\log^2(\cosh(s))(\cosh(2s) - 2)}{\cosh^4(s)} - \dfrac{216}{49}\dfrac{b^2}{a^2}\dfrac{\log(\cosh(s))(1 - \cosh(2s))}{\cosh^4(s)} \\ \qquad + \dfrac{\left(\frac{30}{7}ba_1 - 30d\right)}{\cosh^2(s)a^2} - \dfrac{18}{49}\dfrac{b^2}{a^2}\dfrac{(6s\sinh(2s) - 7\cosh(2s) + 8)}{\cosh^4(s)} - \dfrac{2\left(5ba_1 + 7d\right)}{7a^2} \\ \qquad + \dfrac{s\left(\frac{30}{7}ba_1 + 12d\right)\sinh(s)}{\cosh^3(s)a^2} + \dfrac{27d}{\cosh^4(s)a^2}, \\ v_2(s) = \dot{u}_2(s). \end{cases} \tag{3.17}$$

We notice that the same value of the homoclinic parameter τ_1 was derived in [15, 16] using different methods. By solving equation (3.6) for $i = 3$, we obtain

$$\begin{cases} \tau_2 = \dfrac{4}{a}\left(\dfrac{25}{49}b_1 - \dfrac{e}{b}\right) + \dfrac{2}{49a^2}\left(\dfrac{144}{49}b^2 - 25ba_1 + 73d\right), \\ C_5 = C_6 = 0, \end{cases} \tag{3.18}$$

with the third-order correction $(u_3(s), v_3(s))$ to the Hamiltonian homoclinic solution explicitly given by

$$\begin{cases} u_3(s) = \left(\left(\dfrac{3}{\cosh^2(s)} - 2\right)\log(\cosh(s)) + \tanh^2(s)\right)\dfrac{sc_1}{\cosh^2(s)} + \dfrac{c_2\tanh^3(s)}{\cosh^2(s)} \\ \qquad - \left(\dfrac{1728b^3}{343a^3}\left(\ \log(\cosh(s))^2 - 3\log(\cosh(s))\right) + c_3\right)\dfrac{\sinh(s)\log(\cosh(s))}{\cosh^3(s)} \\ \qquad + \left(\dfrac{1296b^3}{343a^3}\left(4\log(\cosh(s))^2 - 7\log(\cosh(s))\right) + c_4\right)\dfrac{\sinh(s)\log(\cosh(s))}{\cosh^5(s)}, \\ v_3(s) = \dot{u}_3(s). \end{cases} \tag{3.19}$$

where

$$c_1 = \frac{36}{343a^3}\left(36b^3 - 35a_1b^2 - 98bd\right), \quad c_2 = -\frac{6}{7a^3}\left(\frac{234}{49}b^3 - 28ae + 3bd\right),$$
$$c_3 = \frac{36b}{49a^3}\left(20b_1a - 25a_1b + 60d - \frac{312}{49}b^2\right), \quad c_4 = \frac{648}{7a^3}\left(bd - \frac{6}{49}b^3\right).$$

Note that we will use $\{u_i, v_i, \tau_i\}$, $i = 0, 1, 2$ to derive a second-order homoclinic predictor for the n-dimensional system (2.1) (See Section 3.5). However, as shown above, we need to compute u_3, v_3 to obtain the value of τ_2. Since the actual homoclinic curve in the two parameter space of (2.1) could be nonlinear, deriving (at least) a second-order predictor arises naturally. Also, it is clear that the above $\{u_2, v_2, \tau_2\}$ depend on the terms $g(w, \beta_2)$ in the smooth normal form (2.24). So a wrong second-order homoclinic solution will be derived if we use the topological normal form (2.23). The correct second-order solution was presented in [2, 92], while the third-order approximation (3.19) was reported in [2]. A part of the Maple commands that we have used to make the previous explicit computations is shown in Appendix A.2.

Substituting $\{u_0, v_0, u_i, v_i, \tau_{i-1}\}$, $i = 1, 2, 3$ into (3.4) and then plugging the substitution back into (3.1), we obtain the third-order approximation for the homoclinic solution of the BT normal form system (2.24):

$$\begin{cases} w_0(t) = \dfrac{\varepsilon^2}{a}\left(\displaystyle\sum_{i=0}^{3}\varepsilon^i u_i(\varepsilon t)\right) + \mathcal{O}(\varepsilon^6), \\ w_1(t) = \dfrac{\varepsilon^3}{a}\left(\displaystyle\sum_{i=0}^{3}\varepsilon^i v_i(\varepsilon t)\right) + \mathcal{O}(\varepsilon^7), \\ \beta_1 = -\dfrac{4}{a}\varepsilon^4, \\ \beta_2 = \dfrac{b}{a}\varepsilon^2\left(\tau_0 + \varepsilon^2\tau_2\right) + \mathcal{O}(\varepsilon^5). \end{cases} \tag{3.20}$$

3.2.2 An integral phase condition

The phase condition (3.15) can be replaced by a different one that uses an integral phase condition as in [33, 47, 55]. The expansion of $u(s)$ in (3.4) can be grouped as

$$u(s) - u_0(s) = \sum_{i=1}^{3} \varepsilon^i u_i(s) + \mathcal{O}\left(\varepsilon^4\right). \tag{3.21}$$

Then we can fix the phase of $u(s)$ by requiring its minimal L_2-distance to the Hamiltonian solution $u_0(s)$, i.e.,

$$\int_{-\infty}^{+\infty} \tilde{u}(s)\, ds = \int_{-\infty}^{+\infty} \Big(\sum_{i=1}^{3} \varepsilon^i \tilde{u}_i(s) + \mathcal{O}\left(\varepsilon^4\right) \Big)\, ds = 0. \tag{3.22}$$

where

$$\begin{cases} \tilde{u}(s) = \langle u(s) - u_0(s), \dot{u}_0(s) \rangle, \\ \tilde{u}_i(s) = \langle u_i(s), \dot{u}_0(s) \rangle, \quad i = 1, 2, 3. \end{cases}$$

Dividing both sides in (3.22) by ε, we get

$$\frac{\cancelto{0}{\int_{-\infty}^{+\infty} \tilde{u}(s) ds}}{\varepsilon} = \int_{-\infty}^{+\infty} \tilde{u}_1(s) ds + \varepsilon \int_{-\infty}^{+\infty} \tilde{u}_2(s) ds + \varepsilon^2 \int_{-\infty}^{+\infty} \tilde{u}_3(s) ds + \mathcal{O}\left(\varepsilon^3\right). \tag{3.23}$$

For $\varepsilon \to 0$, the following phase condition

$$\int_{-\infty}^{+\infty} \tilde{u}_1(s) ds = \int_{-\infty}^{+\infty} \langle u_1(s), \dot{u}_0(s) \rangle ds = 0 \tag{3.24}$$

holds for (3.14) if

$$C_1 = \frac{11b}{10a} - \frac{3b}{14a}(1 + 4\log(2)).$$

This implies

$$\begin{cases} \tilde{u}_1(s) = -\dfrac{12b}{35a} \dfrac{\sinh(s)(-31 + 30\log(2\cosh(s)))}{\cosh^3(s)}, \\ \tilde{v}_1(s) = \dot{\tilde{u}}_1(s). \end{cases} \tag{3.25}$$

Similarly, if we divide both sides of (3.22) by ε^2 and take (3.24) into account, we obtain

$$\int_{-\infty}^{+\infty} \tilde{u}_2(s) ds = \int_{-\infty}^{+\infty} \langle u_2(s), \dot{u}_0(s) \rangle ds = 0. \tag{3.26}$$

The phase condition (3.26) with (3.25) leads to

$$\begin{cases} \tau_1 = 0, \quad C_3 = 0, \\ C_4 = -\dfrac{b^2}{a^2}\left(\dfrac{9\log(2)\,(15\log(2)+31)}{245} - \dfrac{1329}{2450}\right) - \dfrac{1}{a^2}\left(\dfrac{5ba_1}{14a^2} - \dfrac{5d}{8}\right), \end{cases} \tag{3.27}$$

and hence we get the following second-order correction for the Hamiltonian homoclinic solution

$$\begin{cases} \tilde{u}_2(s) = \left(35ba_1 \; - \; 36b^2 + 98d\right)\dfrac{6s\sinh(s)}{49a^2\cosh^3(s)} \; + \; \dfrac{27\left(804b^2+1225d\right)}{1225a^2\cosh^4(s)} \\ \qquad + 216\left(\dfrac{3}{\cosh^2(s)} - 2\right)\dfrac{b^2\log(2\cosh(s))^2}{49a^2\cosh^2(s)} - \dfrac{6\left(2732b^2+6125d\right)}{1225a^2\cosh^2(s)} \\ \qquad - \dfrac{72}{5}\left(\dfrac{123}{\cosh^2(s)} - 92\right)\dfrac{b^2\log(2\cosh(s))}{49a^2\cosh^2(s)} + \dfrac{30ba_1}{7a^2\cosh^4(s)} - \dfrac{2\,(5a_1b+7d)}{7a^2}, \\ \tilde{v}_2(s) = \dot{\tilde{u}}_2(s). \end{cases} \tag{3.28}$$

3.2.3 Analysis of the homoclinic asymptotics

In Figure 3.1a–Figure 3.1d, we plot the homoclinic solution[†]

$$\begin{cases} u(s) = u_0(s) + \varepsilon\tilde{u}_1(s) + \varepsilon^2\tilde{u}_2(s), \\ v(s) = v_0(s) + \varepsilon\tilde{v}_1(s) + \varepsilon^2\tilde{v}_2(s), \end{cases}$$

for several values of ε and with $a = -1$, $b = 1$, $a_1 = b_1 = e = d = 0$. It is remarkable, see also the close-up, that the orbits for $\varepsilon \neq 0$ approach the saddle along the "wrong" direction, making a "parasitic turn" when $s \to +\infty$ or $s \to -\infty$. Indeed, the difference

$$2 - (u_0(s) + \varepsilon\tilde{u}_1(s))$$

asymptotically behaves for $s \to \pm\infty$ as

$$\frac{288}{7}\frac{b}{a}\varepsilon s e^{\mp 2s},$$

[†]Similar results were obtained in [91] by using (3.16) and (3.17).

and, therefore, is negative for $s \to -\infty$ if $ab > 0$ or for $s \to +\infty$ if $ab < 0$ (provided that $\varepsilon > 0$). On any finite time interval $[-T, T]$ the tangent predictor, i.e., $u(s) = u_0(s) + \varepsilon\tilde{u}_1(s)$, with sufficiently small ε does approximate the "true" homoclinic solution better than the Hamiltonian predictor with $\varepsilon = 0$. In particular, while the Hamiltonian homoclinic orbit (3.3) is symmetric w.r.t. the u-axis, the tangent predictor defines a non-symmetric approximate orbit, better corresponding to the non-symmetric true homoclinic orbit in (3.2) and in the normal form (2.24) (see Figure (3.2b) for a graphical illustration). Figure 3.1e and Figure 3.1f show a comparison between the different solutions using (3.16), (3.17) and (3.25), (3.28). It is clear that the second-order predictor with (3.25) and (3.28) has a smaller "parasitic loop".

3.2.4 A comparison in the topological normal form

Consider the topological BT normal form, i.e., the system (2.23). We want to compare the predicted homoclinic solutions with those obtained via the high-accuracy numerical continuation in MatCont [47]. From (3.20) we obtain that $\varepsilon = \sqrt[4]{-\frac{a}{4}\beta_1}$. Substituting this into the expression of β_2 in (3.20), we obtain the following second-order approximation for the homoclinic bifurcation curve in the parameter plane (β_1, β_2) of (2.23):

$$\beta_2 = -\frac{72b^3}{2401a^2}\beta_1 + \frac{5b}{7a}\sqrt{-a\beta_1} + \mathcal{O}\left(|\beta_1|^{\frac{5}{4}}\right), \quad \text{sign}(\beta_1) = -\text{sign}(a). \tag{3.29}$$

For $a = -1$ and $b = 1$, this approximation is shown as the red curve Hom^{Pred} in Figure 3.2a. We use MatCont to start a continuation of equilibria with initial parameter values $(\beta_1, \beta_2) = (1, -2)$ and the equilibrium point $(w_0, w_1) = (1, 0)$; β_2 is the free parameter. We find two bifurcation points along the curve of equilibria, limit point and Andronov-Hopf. The limit point continuation is now carried out to detect the BT-bifurcation point at $(\beta_1, \beta_2) = (0, 0)$. We start the homoclinic continuation with $\varepsilon = 0.08$. This yields the dashed blue curve Hom^{Com} in Figure 3.2a and the blue orbits in Figure 3.2b. The predicted orbits (red orbits in Figure 3.2b) are computed by taking the computed homoclinic orbits from the numerical continuation. This gives the values of β_1 which yield the values for ε in the predictor. The predictors are then compared with the computed solution using the time points of the fine mesh in the numerical continuation, after a time shift so that the computed and predicted curves coincide for $t = 0$. We see that the improved predictors perform better than the one based on the Hamiltonian solution since the homoclinic orbit is indeed non-symmetric w.r.t. w_0 (as is correctly predicted by (3.20)).

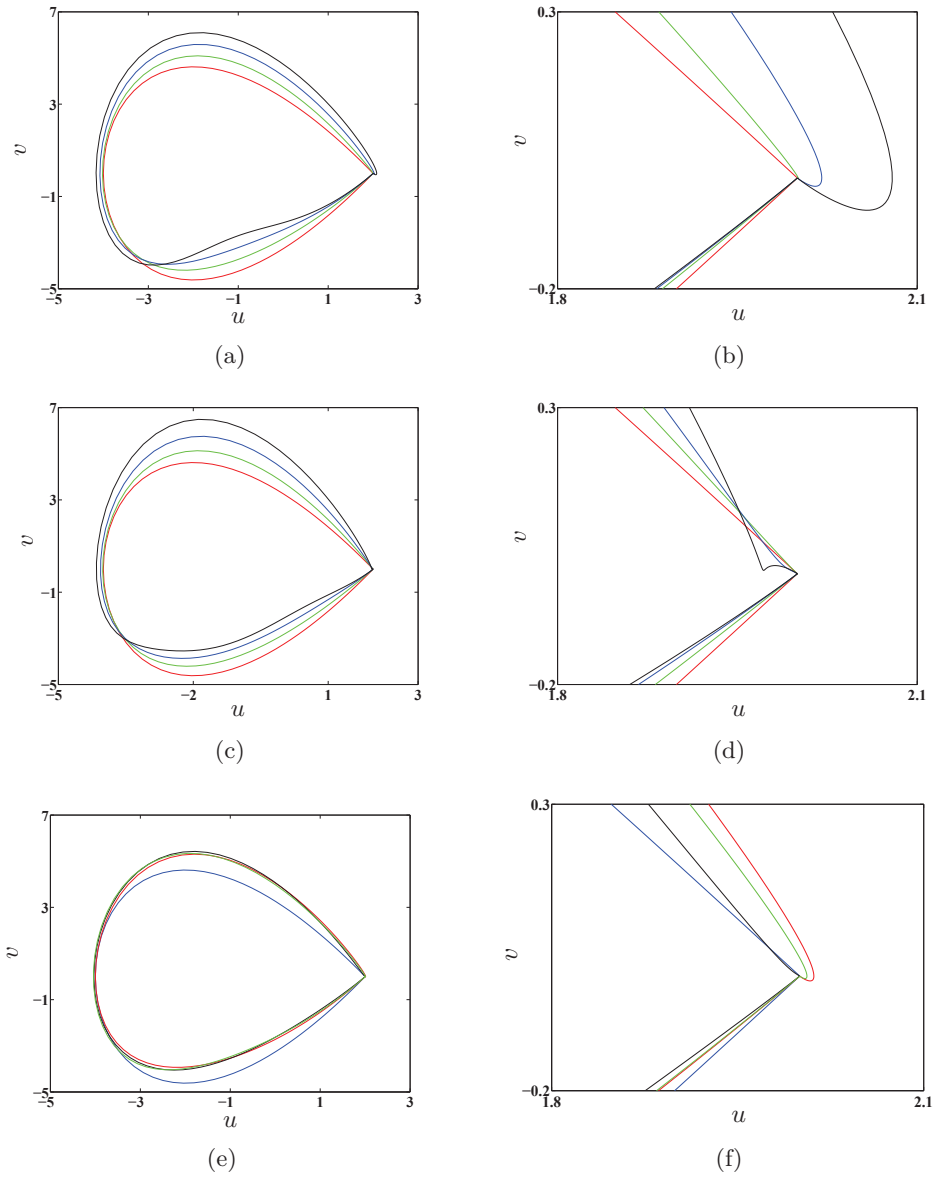

Figure 3.1: Homoclinic solution for $a = -1$, $b = 1$, $a_1 = b_1 = e = d = 0$ and $\varepsilon = 0$ (red), 0.2 (green), 0.4 (blue), 0.6 (black). (a) Tangent predictors using (3.25); (b) Zoom of the tangent predictors near the saddle: the "parasitic turn" is clearly visible; (c) The second-order predictors using (3.25) and (3.28); (d) Zoom of the second-order predictors near the saddle: the "parasitic loop" is not clear but will appear for large ε, (e) Homoclinic solution for $a = -1$, $b = 1$, $a_1 = b_1 = e = d = 0$ and $\varepsilon = 0$ (blue), 0.3 tangent predictors (red using (3.16), green using (3.25)) and second-order predictors (black using (3.16) and (3.17) , brown using (3.25) and (3.28)). (f) Zoom of the same curves near the saddle: the second-order predictor where we fix the solution phase by requiring the "minimal distance" is the best one approaching the zero order predictor near the saddle.

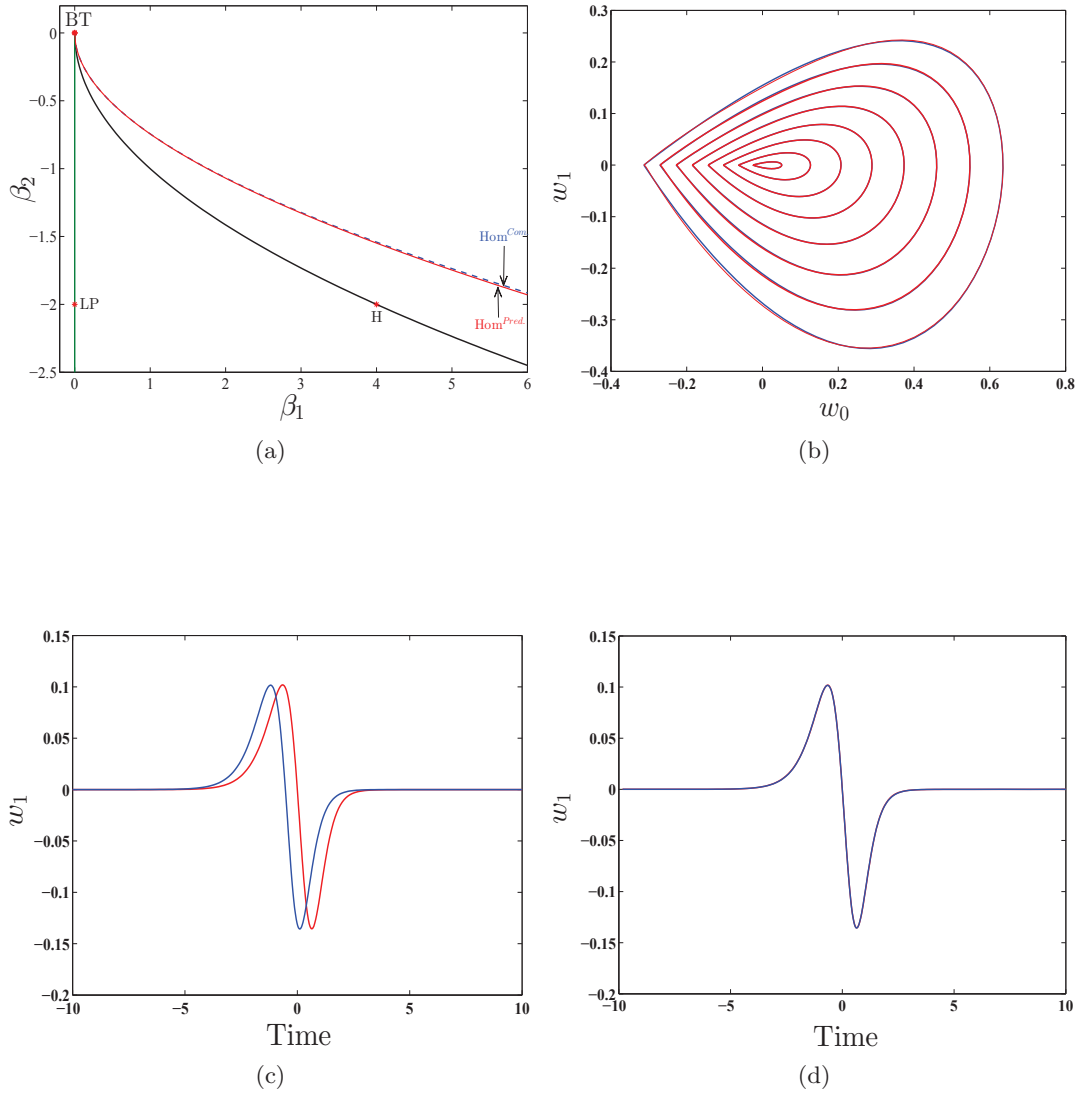

Figure 3.2: (a) Predicted using (3.29) (red) and computed (dashed blue) homoclinic bifurcation curves in parameter space, (b) The comparison of homoclinic orbits in phase space between computed (blue) and predicted (red) using the second-order correction with (3.16), (3.17) for $^{10}\log(\beta_1) = -3.755, -2.313, -1.647, -1.267, -1.005, -0.801, -0.638$. (c) and (d) The time shift so that the predicted (red) and computed (blue) curves consider at $t = 0$ for $^{10}\log(\beta_1) = -1.005$.

3.3 The Lindstedt-Poincaré method

In this section, we apply a generalization of the Lindstedt-Poincaré (L-P) method combined with hyperbolic functions instead of the Jacobian elliptic functions used in [13, 37]. We prove that this method gives the same homoclinicity conditions and the same predictor in the parameter space. Chen et. al. [35, 36, 38–40] used the L-P method to study the homoclinic solution to a family of nonlinear oscillators. They applied a non-linear transformation of time instead of the linear one used in the original L-P method for periodic solutions (see, *e.g.* [105]). Belhaq *et al.* [13] proved that the generalized L-P method combined with a special criterion leads to the same results as the classical Melnikov method. This criterion is based on a collision between the bifurcating limit cycle near the homoclinic orbits with a saddle equilibrium point. We should also point out that yet another approach based on periodic time transformations exists in the literature [30]. However, the L-P method has a clear advantage since it provides an explicit time-parametrization which is necessary for numerical continuation.

First, we introduce the non-linear transformation of time,

$$\frac{d\xi}{ds} = \omega(\xi), \tag{3.30}$$

where $\omega(\xi)$ is a bounded positive function for all ξ. Then

$$\begin{cases} \dfrac{d}{ds} = \dfrac{d\xi}{ds}\dfrac{d}{d\xi} = \omega(\xi)\dfrac{d}{d\xi}, \\ \dfrac{d^2}{ds^2} = \omega(\xi)\dfrac{d}{d\xi}\left(\omega(\xi)\dfrac{d}{d\xi}\right). \end{cases}$$

The new parametrization of time transforms (3.2) into

$$\omega\frac{d}{d\xi}\left(\omega\hat{u}'\right) - \hat{u}^2 + 4 = \varepsilon\,\frac{b}{a}\omega\hat{u}'\left(\tau + \hat{u}\right) + \varepsilon^2\,\frac{1}{a^2}\hat{u}^2\left(\tau b a_1 + d\hat{u}\right) + \varepsilon^3\,\frac{1}{a^2}\,\hat{u}\,\omega\hat{u}'\left(\tau b b_1 + e\hat{u}\right) + \mathcal{O}\left(\varepsilon^4\right). \tag{3.31}$$

The *hat* is used to distinguish the solution of the L-P method from the R-P solution while the prime denotes the derivative of $\hat{u}$ with respect to the new independent variable ξ. As before, we assume that the homoclinic solution of (3.31) is parametrized by ε and approximated by

$$\begin{pmatrix} \hat{u}(\xi) \\ \hat{v}(\xi) \\ \omega(\xi) \\ \tau \end{pmatrix} = \begin{pmatrix} \hat{u}_0(\xi) \\ \hat{v}_0(\xi) \\ \omega_0(\xi) \\ \tau_0 \end{pmatrix} + \varepsilon \begin{pmatrix} \hat{u}_1(\xi) \\ \hat{v}_1(\xi) \\ \omega_1(\xi) \\ \tau_1 \end{pmatrix} + \varepsilon^2 \begin{pmatrix} \hat{u}_2(\xi) \\ \hat{v}_2(\xi) \\ \omega_2(\xi) \\ \tau_2 \end{pmatrix} + \varepsilon^3 \begin{pmatrix} \hat{u}_3(\xi) \\ \hat{v}_3(\xi) \\ \omega_3(\xi) \\ \tau_3 \end{pmatrix} + \mathcal{O}\left(\varepsilon^4\right). \tag{3.32}$$

Substituting the series expansions (3.32) into equation (3.31) with $\omega_0(\xi) = 1$ [†]; and then successively collecting the terms with equal power in ε leads to the following systems:

$$\text{Order}\left(\varepsilon^0\right):\ \hat{u}_0'' - \hat{u}_0^2 + 4 = 0, \tag{3.33}$$

$$\text{Order}\left(\varepsilon^1\right):\ \hat{\Phi}_1^1 = \frac{b}{a}\hat{u}_0'\left(\tau_0 + \hat{u}_0\right), \tag{3.34}$$

$$\text{Order}\left(\varepsilon^2\right):\ \hat{\Phi}_2^2 + \hat{\Psi}_1^1 - \hat{u}_1^2 = \frac{b}{a}\hat{u}_0'\left(\tau_1 + \hat{u}_1\right) + \hat{\Gamma}_1, \tag{3.35}$$

$$\text{Order}\left(\varepsilon^3\right):\ \hat{\Phi}_3^3 + \hat{\Psi}_1^2 + \hat{\Psi}_2^1 - 2\hat{u}_2\hat{u}_1 + \omega_2\frac{d}{d\xi}\left(\omega_1\hat{u}_0'\right) = \frac{b}{a}\hat{u}_0'\left(\hat{u}_2 + \tau_2\right) + \hat{\Gamma}_2 + \hat{\Omega}, \tag{3.36}$$

where

$$\begin{aligned}
\hat{\Phi}_i^j &= \frac{d}{d\xi}\left(\omega_j\hat{u}_0'\right) + \omega_j\hat{u}_0'' + \hat{u}_i'' - 2\hat{u}_0\hat{u}_i,\\
\hat{\Psi}_i^j &= \frac{d}{d\xi}\left(\omega_j\hat{u}_i'\right) + \omega_j\hat{u}_i'' + \omega_1\frac{d}{d\xi}\left(\omega_j\hat{u}_{i-1}'\right),\\
\hat{\Gamma}_i &= \frac{b}{a}\left(\omega_1\hat{u}_0' + \hat{u}_1'\right)\left(\tau_{i-1} + \hat{u}_{i-1}\right) + \frac{1}{a^2}\hat{u}_0^2\left(ba_1\tau_{i-1} + \hat{u}_{i-1}d\right),\\
\hat{\Omega} &= \frac{2}{a^2}\hat{u}_0\hat{u}_1\left(ba_1\tau_0 + d\hat{u}_0\right) + \frac{1}{a^2}\hat{u}_0'\hat{u}_0\left(bb_1\tau_0 + e\hat{u}_0\right) + \frac{b}{a}\left(\omega_2\hat{u}_0' + \omega_1\hat{u}_1' + \hat{u}_2'\right)\left(\tau_0 + \hat{u}_0\right).
\end{aligned}$$

Equation (3.33) is identical to (3.2) with $\varepsilon = 0$. So it has the exact homoclinic solution

$$\begin{cases}
\hat{u}_0(\xi) = -6\text{sech}^2(\xi) + 2,\\
\\
\hat{v}_0(\xi) = 12\text{sech}^2(\xi)\tanh(\xi).
\end{cases} \tag{3.37}$$

For $\varepsilon \neq 0$, we assume that the homoclinic solution of (3.31) is still given by (see, for example [37]):

$$\begin{cases}
\hat{u}(\xi) = \sigma\text{sech}^2(\xi) + \delta,\\
\\
\hat{v}(\xi) = \hat{u}'(\xi) = -\dfrac{1}{6}\sigma\omega(\xi)\hat{v}_0(\xi),
\end{cases} \tag{3.38}$$

where σ and δ are parameters that depend on ε,

$$\begin{cases}
\sigma = \sigma_0 + \varepsilon\sigma_1 + \varepsilon^2\sigma_2 + \varepsilon^3\sigma_3 + \mathcal{O}\left(\varepsilon^4\right),\\
\\
\delta = \delta_0 + \varepsilon\delta_1 + \varepsilon^2\delta_2 + \varepsilon^3\delta_3 + \mathcal{O}\left(\varepsilon^4\right).
\end{cases} \tag{3.39}$$

[†]If we keep $\omega_0(\xi)$ free then the homoclinic solution to (3.33) requires that $\omega_0(\xi) = 1$.

Substituting (3.39) into (3.38) and then equating each of the coefficients of ε^i to (3.32) yields that $\sigma_0 = -6$, $\delta_0 = 2$ and

$$\hat{u}_i(\xi) = \sigma_i \mathrm{sech}^2(\xi) + \delta_i, \quad i = 1, 2, 3, \tag{3.40}$$

$$\hat{v}_1(\xi) = \left(\omega_1(\xi) - \frac{\sigma_1}{6}\right)\hat{v}_0(\xi), \tag{3.41}$$

$$\hat{v}_2(\xi) = \left(\omega_2(\xi) - \frac{\sigma_1}{6}\omega_1(\xi) - \frac{\sigma_2}{6}\right)\hat{v}_0(\xi), \tag{3.42}$$

$$\hat{v}_3(\xi) = \left(\omega_3(\xi) - \frac{\sigma_1}{6}\omega_2(\xi) - \frac{\sigma_2}{6}\omega_1(\xi) - \frac{\sigma_3}{6}\right)\hat{v}_0(\xi). \tag{3.43}$$

Using the assumptions (3.40)-(3.43), we solve the linear equations (3.34)-(3.36) for $\hat{u}_i(\xi)$, one by one to determine τ_{i-1}, δ_i, σ_i and $\omega_i(\xi)$ for $i = 1, 2, 3$.

We multiply both sides of (3.34) by $\hat{u}_0'$ and then integrate both sides from ξ_0 to ξ, and get

$$\underbrace{\int_{\xi_0}^{\xi} \hat{u}_0' \frac{d}{dx}\left(\omega_1 \hat{u}_0'\right) dx + \int_{\xi_0}^{\xi} \hat{u}_0' \omega_1 \hat{u}_0'' \, dx}_{\text{I}} + \underbrace{\int_{\xi_0}^{\xi} \hat{u}_0' \hat{u}_1'' \, dx - 2\int_{\xi_0}^{\xi} \hat{u}_0' \hat{u}_0 \hat{u}_1 \, dx}_{\text{II}} = \frac{b}{a}\int_{\xi_0}^{\xi} \hat{u}_0'^2 \left(\tau_0 + \hat{u}_0\right) dx \tag{3.44}$$

Differentiating (3.33) with respect to ξ, we obtain

$$\hat{u}_0''' = 2\hat{u}_0\hat{u}_0' \Rightarrow \int_{\xi_0}^{\xi} \hat{u}_1 \hat{u}_0''' \, dx = 2\int_{\xi_0}^{\xi} \hat{u}_1 \hat{u}_0 \hat{u}_0' \, dx. \tag{3.45}$$

The terms I and II of (3.44) can be simplified by

$$\text{I} = \omega_1 \hat{u}_0'^2\big|_{\xi_0}^{\xi} - \cancel{\int_{\xi_0}^{\xi} \omega_1 \hat{u}_0' \hat{u}_0'' \, dx} + \cancel{\int_{\xi_0}^{\xi} \omega_1 \hat{u}_0' \hat{u}_0'' \, dx} \;=\; \omega_1 \hat{u}_0'^2\big|_{\xi_0}^{\xi},$$

$$\text{II} = (\hat{u}_0'\hat{u}_1' - \hat{u}_1\hat{u}_0'')\big|_{\xi_0}^{\xi} + \underbrace{\cancel{\int_{\xi_0}^{\xi} \hat{u}_1 \hat{u}_0''' \, dx} - 2\cancel{\int_{\xi_0}^{\xi} \hat{u}_0' \hat{u}_0 \hat{u}_1 \, dx}}_{\text{Using (3.45)}} \;=\; (\hat{u}_0'\hat{u}_1' - \hat{u}_1\hat{u}_0'')\big|_{\xi_0}^{\xi}.$$

Therefore, (3.44) can be written as

$$\left(\omega_1 \hat{u}_0'^2 + \hat{u}_0'\hat{u}_1' - \hat{u}_1\hat{u}_0''\right)\Big|_{\xi_0}^{\xi} = \frac{b}{a}\int_{\xi_0}^{\xi} \hat{u}_0'^2 \left(\tau_0 + \hat{u}_0\right) dx. \tag{3.46}$$

Setting $\xi_0 = -\infty$ and $\xi = \infty$ in (3.46) yields the following condition for the bifurcation of homoclinic orbit:

$$\frac{b}{a}\int_{-\infty}^{\infty} \hat{u}_0'^2\,(\tau_0 + \hat{u}_0)\,dx = 0. \tag{3.47}$$

and hence

$$\frac{b}{a}\frac{192\,(7\tau_0 - 10)}{35} = 0 \Rightarrow \tau_0 = \frac{10}{7}. \tag{3.48}$$

Note that the same condition was derived using the classical Melnikov technique (see (1.30)). By setting $\xi_0 = 0$, $\xi = \infty$, we find that

$$\sigma_1 = -\delta_1. \tag{3.49}$$

We change the integration boundaries to 0 and ξ, and get

$$12\omega_1(\xi) + \delta_1 \cosh(2\xi) = -\frac{72b}{7a}\tanh(\xi). \tag{3.50}$$

Since $\omega(\xi)$ is bounded function, we can choose the parameter δ_1 such that

$$\lim_{\xi\to\pm\infty} |\omega_1(\xi)| \neq \infty.$$

This condition implies that

$$\delta_1 = 0.$$

Thus, $\omega_1(\xi)$ is given by

$$\omega_1(\xi) = -\frac{6b}{7a}\tanh(\xi). \tag{3.51}$$

Substituting the values of δ_1, σ_1, $\omega_1(\xi)$ into (3.40) and (3.41) gives the first-order correction to the initial homoclinic solution $(\hat{u}_0(\xi), \hat{v}_0(\xi))$

$$\begin{cases} \hat{u}_1(\xi) = 0, \\ \hat{v}_1(\xi) = -\dfrac{6b}{7a}\tanh(\xi)\hat{v}_0(\xi). \end{cases} \tag{3.52}$$

We multiply both sides of (3.35) by $\hat{u}_0'$ and then integrate both sides from ξ_0 to ξ. Then we simplify to

$$\left(\omega_2\hat{u}_0'^2 + \omega_1\hat{u}_1'^2 + \hat{u}_0'\hat{u}_2' - \hat{u}_2\hat{u}_0''\right)\Big|_{\xi_0}^{\xi} + \frac{2592b^2}{49a^2}\frac{\sinh^4(x)}{\cosh^8(x)}\Big|_{\xi_0}^{\xi} = \int_{\xi_0}^{\xi} \hat{u}_0'\,\Big(\text{ R.H.S. of (3.35) }\Big)\,dx \tag{3.53}$$

We repeat the last procedure of changing the integration variables to equation (3.53) and get

$$\begin{cases} \tau_1 = 0, \\ \delta_2 = -\dfrac{2\,(5a_1b + 7d)}{7a^2}, \\ \sigma_2 = -\dfrac{3}{49a^2}\left(6b^2 - 70ba_1 + 49d\right), \\ \omega_2(\xi) = \dfrac{1}{7a^2}\left(\dfrac{18}{7}b^2 + \dfrac{5}{2}ba_1 + 7d\right) - \dfrac{9}{4a^2}\left(\dfrac{6}{49}b^2 + d\right)\operatorname{sech}^2(\xi), \end{cases} \tag{3.54}$$

with

$$\begin{cases} \hat{u}_2(\xi) = -\dfrac{3}{49a^2}\left(6b^2 - 70ba_1 + 49d\right)\operatorname{sech}^2(\xi) - \dfrac{2\,(5a_1b + 7d)}{7a^2}, \\ \hat{v}_2(\xi) = \dfrac{1}{a^2}\left(\left(\dfrac{3}{7}b^2 - \dfrac{5}{14}ba_1 + \dfrac{3}{2}d\right) - \dfrac{9}{4}\left(\dfrac{6}{49}b^2 + d\right)\operatorname{sech}^2(\xi)\right)\hat{v}_0(\xi). \end{cases} \tag{3.55}$$

Similarly, we multiply both sides of (3.36) by $\hat{u}_0'$ and then integrate both sides from ξ_0 to ξ. Then we simplify to

$$\begin{aligned} &\left(\omega_3\hat{u}_0'^2 + \omega_2\hat{u}_1'^2 + \omega_1\hat{u}_2'^2 + \hat{u}_0'\hat{u}_3' - \hat{u}_3\hat{u}_0''\right)\Big|_{\xi_0}^{\xi} + \frac{1944b}{7a^3}\left(\frac{6}{49}b^2 + d\right)\frac{\sinh^3(x)}{\cosh^9(x)}\Big|_{\xi_0}^{\xi} \\ &- \frac{432b}{7a^3}\left(2d + \frac{5}{7}ba_1 + \frac{36}{49}b^2\right)\frac{\sinh^3(x)}{\cosh^7(x)}\Big|_{\xi_0}^{\xi} = \int_{\xi_0}^{\xi}\hat{u}_0'\left(\text{ R.H.S. of (3.36) }\right)dx \end{aligned} \tag{3.56}$$

The last procedure of changing the integration variables is used to obtain

$$\begin{cases} \tau_2 = \dfrac{4}{a}\left(\dfrac{25}{49}b_1 - \dfrac{e}{b}\right) + \dfrac{2}{49a^2}\left(\dfrac{144}{49}b^2 - 25ba_1 + 73d\right), \\ \delta_3 = 0, \\ \sigma_3 = 0, \\ \omega_3(\xi) = \left(c_5\operatorname{sech}^2(\xi) - \dfrac{3}{49a^3}\left(\dfrac{66}{49}b^3 - 20b^2a_1 + 11bd\right) + c_6\right)\tanh(\xi), \end{cases} \tag{3.57}$$

where

$$c_5 = \frac{4}{a^2}e - \frac{3}{7a^3}\left(bd + \frac{6}{49}b^3\right),$$

$$c_6 = -\frac{60}{49a^2}bb_1 + \frac{3}{7a^5}\left(\frac{1}{2}bd^2 - \frac{10}{7}b^2a_1d + \frac{50}{49}b^3a_1^2 + \frac{6}{49}b^3d - \frac{60}{343}b^4a_1 + \frac{18}{2401}b^5\right),$$

with

$$\begin{cases} \hat{u}_3(\xi) = 0, \\ \hat{v}_3(\xi) = \left(c_5 \mathrm{sech}^2(\xi) - \dfrac{18}{49a^3} \left(\dfrac{18}{49} b^3 - 5b^2 a_1 + 3bd \right) + c_6 \right) \tanh(\xi) \hat{v}_0(\xi). \end{cases} \tag{3.58}$$

We notice that the same values of the homoclinic bifurcation parameters $\{\tau_0, \tau_1, \tau_2\}$ were derived in Section 3.1 using the regular perturbation method. A part of the Maple commands that we have used to perform the previous explicit computations is shown in Appendix A.3.

Finally, the third-order approximation to the homoclinic orbit of the smooth BT normal form system (2.24) is given by

$$\begin{cases} w_0(t) = \dfrac{\varepsilon^2}{a} \left(\displaystyle\sum_{i=0}^{3} \varepsilon^i \hat{u}_i(\xi) \right) + \mathcal{O}(\varepsilon^6), \\ w_1(t) = \dfrac{\varepsilon^3}{a} \left(\displaystyle\sum_{i=0}^{3} \varepsilon^i \hat{v}_i(\xi) \right) + \mathcal{O}(\varepsilon^7), \end{cases} \tag{3.59}$$

where β_1, β_2 are the unfolding parameter as in (3.20).

Notice that the small displacement $\varepsilon^2 \delta_2$ in the saddle point $(2, 0)$ can be determined just using the boundedness assumption and the equation (3.31). Indeed, the saddle point is given by

$$\lim_{\xi \to \pm\infty} (\hat{u}(\xi), \hat{v}(\xi)) = (\delta, 0).$$

Since $\hat{u}'(\xi) = v(\xi)$ and $\omega(\xi)$ is a bounded function, taking the limit of both sides in equation (3.31) leads to

$$-\delta^2 + 4 = \varepsilon^2 \frac{1}{a^2} \delta^2 \left(\tau b a_1 + d\delta \right).$$

Substituting the expansions for τ and δ in this and collecting powers of ε, we get

$$\begin{aligned} &\text{Order } \left(\varepsilon^0\right) : \ -\delta_0^2 + 4 = 0 \\ &\text{Order } \left(\varepsilon^1\right) : \ -2\delta_0 \delta_1 = 0 \\ &\text{Order } \left(\varepsilon^2\right) : \ -2\delta_0 \delta_2 - \delta_1^2 = \frac{\delta_0^2 \left(a_1 b \tau_0 + d\delta_0 \right)}{a^2}. \end{aligned}$$

We then solve at each order to get

$$\delta_0 = 2, \quad \delta_1 = 0, \quad \delta_2 = -\frac{(a_1 b \tau_0 + 2d)}{a^2}.$$

Note that it is only necessary to compute τ_0 to determine the ε^2-shift of the saddle.

3.4 A comparison in the topological normal form

Consider again the topological normal form (2.24). It is required that the homoclinic orbits of (2.24) satisfy $w_1(0) = 0$ and approach the w_0-axis at the saddle from both sides as $t \to \pm\infty$. Before we proceed, we check if the solutions (3.4) and (3.32) satisfy these requirements. Consider the point $c = (u(s_0), v(s_0))$, $s_0 \in (-\infty, +\infty)$ on the homoclinic orbit (replace s by ξ and (u, v) by $(\hat{u}, \hat{v})$ when we consider the homoclinic solution (3.32)), see Figure 3.3. The slope of the homoclinic orbit at a time $s = s_0$ is given by $S(s_0) = \dfrac{\dot{v}(s_0)}{\dot{u}(s_0)}$. The correct homoclinic orbit (the blue curve in Figure 3.3) can only have one *vertical* asymptote at time $s_0 = 0$ (*i.e.*, where $v(0) = 0$ or equivalently, the denominator of $S(0)$ vanishes). We can use this criterion to check whether the homoclinic solutions (3.4) and (3.32) approach the saddle along the correct direction. Since we discuss the normal form system (2.24), we set $a_1 = b_1 = e = d = 0$. The homoclinic solution (3.32) has only one *vertical* asymptote because

$$\hat{u}'(\xi_0) = \cosh^4(\xi_0)\sinh(\xi_0)\left(3b^2a^3\varepsilon^2 + 49a^5\right) = 0,$$

has only the trivial solution $\xi_0 = 0$ for all $\varepsilon > 0$. Moreover, the component $\hat{v}(\xi) = \sum_{i=0}^{3} \varepsilon^i \hat{v}_i(\xi)$ of (3.32) can be written as $\hat{v}(\xi) = l(\xi)\hat{v}_0(\xi)$, where

$$l(\xi) = 1 - \varepsilon\frac{6b}{7a}\tanh(\xi) + \varepsilon^2\frac{3b^2}{7a^2}\left(1 - \frac{9}{14}\mathrm{sech}^2(\xi)\right) - \varepsilon^3\frac{18b^3}{343a^3}\left(\frac{3\left(42a^2 - b^2\right)}{49a^2} + \mathrm{sech}^2(\xi)\right)\tanh(\xi).$$

Then for a given (a, b), we can always define an ε-interval such that $l(\xi) > 0$. This interval can be found by solving the inequalities $\lim_{\xi\to\pm\infty} l(\xi) > 0$ for ε (*e.g.*, for $a = b = 1$, the function $l(\xi)$ is positive for all $\varepsilon \in [0, 1.9927)$). Thus for this ε-interval the homoclinic solution $(\hat{u}(\xi), \hat{v}(\xi))$ intersects the $\hat{u}$-axis only once at $\xi = 0$ and approaches the saddle point $(-2, 0)$ from both sides as $\xi \to \pm\infty$ along the correct direction. On the other hand, for the first-order solution of (3.4), *i.e.*, $u(s) = u_0(s) + \varepsilon u_1(s)$, the homoclinic orbit has two *vertical* asymptotes, at $s_0 = 0$ and at the solution s_0 to

$$\frac{7}{6}\sinh(s_0)\cosh(s_0)a + \varepsilon\Big(\left(2\cosh^2(s_0)b - 3b\right)\log(\cosh(s_0)) - \cosh^2(s_0) + b\Big) = 0. \qquad (3.60)$$

Figure 3.4a plots the left-hand side of (3.60) as a function of time s_0 for $a = b = 1$ and $\varepsilon = 0.01$. It is clear that this function has a nontrivial solution at $s_0 \approx -59.52285$. This solution corresponds to the appearance of the "parasitic turn" near the saddle (as "globally" presented in the red curve in Figure 3.3). Figures 3.4b plots (3.60) for $\varepsilon = 0.1$. We notice

that as ε increases, the "parasitic turn" is expanding away from the saddle and the nontrivial zero of (3.60) gets closer to 0 (In general, as $\varepsilon \to 0$, the nontrivial zero of (3.60) $\to -\infty$ and the "parasitic turn" shrinks to the saddle point. On the other hand, as $\varepsilon \to 1$, the nontrivial zero of (3.60) $\to 0$ and the "parasitic turn" grows till the homoclinic orbit breaks down). The corresponding "parasitic turn" to the numerically computed $s_0 \neq 0$ in Figure 3.4b is presented in Figure 3.5a. This Figure plots (3.4) for $s \in [-16, -12.5]$ and 100,000 points, uniformly distributed. Figure 3.5a and 3.5b show the "parasitic turn" in the first- and third-order solution of (3.4), respectively. Note that, the visualization of the "parasitic turn" for both solutions requires a different scale. This indicates that the third-order solution provides a much more accurate solution in comparison to the first-order one. To summarize, we plot Figure 3.5c.

We switch back to the original problem of finding the homoclinic solution to (2.24). Figure 3.6 plots the homoclinic orbits of (2.24) computed with a continuation method (blue) for $a = b = 1$ and (β_1, β_2) free. At each orbit, a value of ε can be computed by taking the computed β_1 from the numerical continuation data and then solving the third equation of (3.20) for ε. This gives: $\varepsilon = 0.139, 0.230, 0.326, 0.401, 0.470, 0.531, 0.589, 0.647, 0.707, 0.767$. Using these values of ε, we plot the corresponding homoclinic orbits obtained by (3.20) (red), (3.59) (green). Since the bounded $\mathcal{O}(\varepsilon)$-terms in $\omega(\xi)$ are small, see Figure 3.7, we approximate $\omega(\xi)$ by 1. This allows to approximate ξ by εt. It is clear that, the L-P solution (*i.e.*, (3.59)) has accurate orbits which nearly coincide with the computed orbits. These orbits approach the saddle along the correct direction as $t \to \pm\infty$, *i.e.*, near the saddle the strange "parasitic turn" does not appear, see Figure 3.6b.

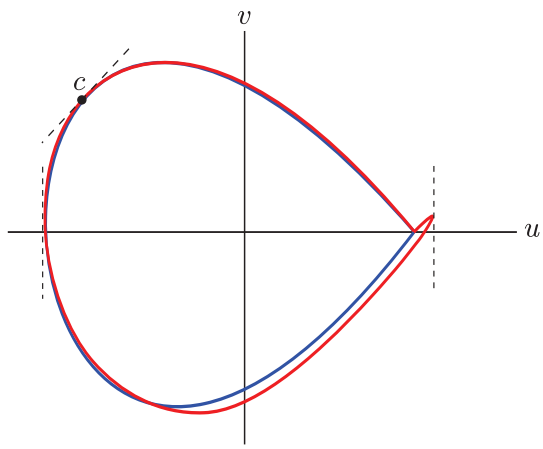

Figure 3.3: The "parasitic turn" near the saddle of the homoclinic orbit (red) predicted by (3.4).

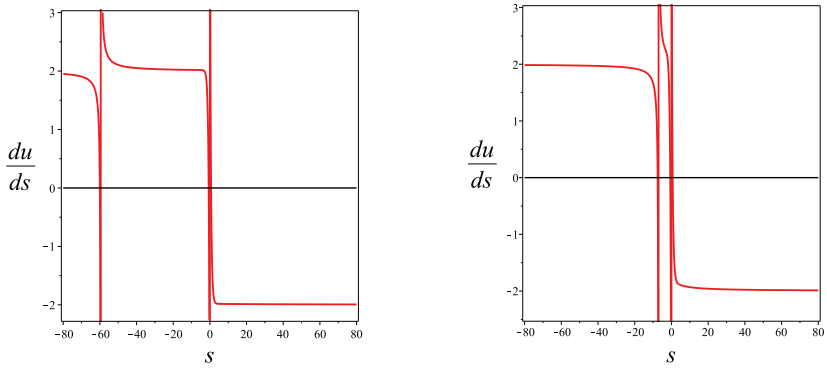

(a) (b)

Figure 3.4: The asymptotes of equation (3.60) for $a = b = 1$ and (a) $\varepsilon = 0.01$, (b) $\varepsilon = 0.1$.

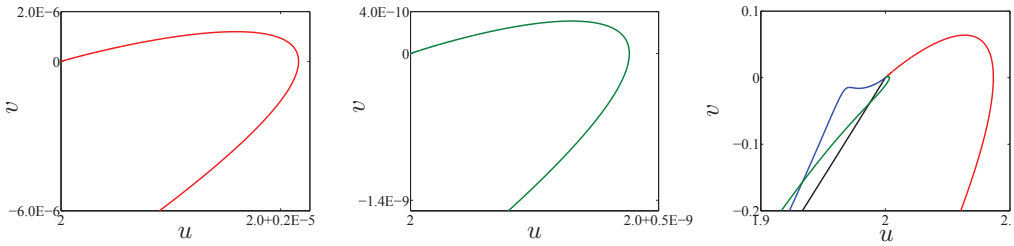

(a) (b) (c)

Figure 3.5: The "parasitic turn" for $\varepsilon = 0.1$. (a) The first-order solution of (3.4), (b) The third-order solution of (3.4). The "parasitic turn" of the third-order solution is very small so that we cannot compare it with the one of the first-order solution. (c) For $\varepsilon = 0.3$, the "parasitic turn" in the first-order (red), the second-order (blue) and the third-order (green) solutions of (3.4). The black curve denotes the third-order solution of (3.32)

3.5 Homoclinic asymptotics in n-dimensional systems

In this section, we provide two explicit asymptotics for the bifurcating homoclinic orbits of (2.1). Following the procedure described in Section 2.3, we transfer the smooth BT normal form (2.24) with the homoclinic approximation (3.20), and (3.59) back to the original system (2.1).

With data collected in (2.41), (2.44), (2.48), (2.59), (2.61), (2.62), (2.64)-(2.69), we get two second-order homoclinic predictors x_{R} (*i.e.*, *the regular homoclinic asymptotic*) and x_{L} (*i.e.*, *Lindstedt-Poincaré homoclinic asymptotic*) for the original system (2.1). Thus, we obtain the following second-order homoclinic predictions in phase space for the the original system (2.1) (see also Appendix A.4):

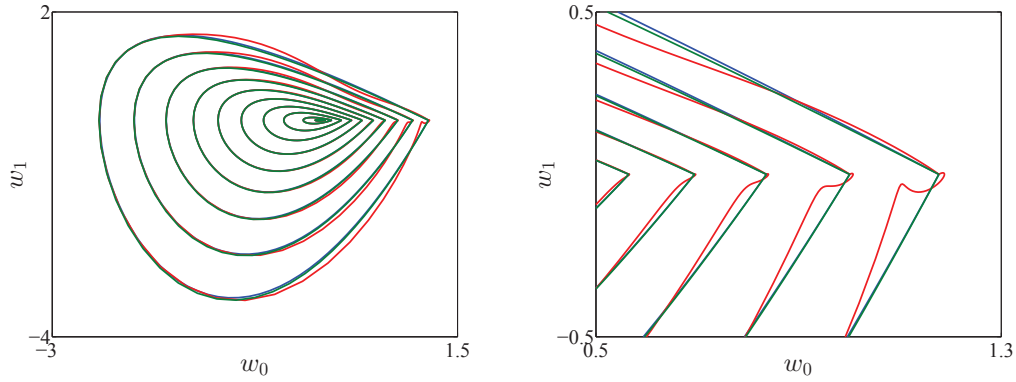

(a) (b)

Figure 3.6: (a) Homoclinic orbits in phase space of (2.24) for $a = b = 1$ and ε= 0.139, 0.230, 0.326, 0.401, 0.470, 0.531, 0.589, 0.647, 0.707, 0.767. Blue orbits are computed with a continuation method, red orbits denote the homoclinic orbits obtained by (3.20), while the green orbits denote the homoclinic orbits obtained by (3.59). (b) Zoom of Figure 3.6a. For $\varepsilon \neq 0$, the approximate orbits obtained by (3.20) approach the saddle along the "wrong" direction making a "parasitic turn". This turn does not appear in the orbits obtained by (3.59).

$$\alpha = \frac{\varepsilon^2}{a}\frac{10b}{7}K_{1,1} + \frac{\varepsilon^4}{a}\left(-4K_{1,0} + \frac{50b^2}{49a}K_2 + b\tau_2 K_{1,1}\right) + \mathcal{O}(\varepsilon^5), \tag{3.61}$$

$$\begin{aligned} x_{\mathrm{R}}(t) = \frac{\varepsilon^2}{a}\left(\frac{10b}{7}H_{0001} + u_0(s)q_0\right) + \frac{\varepsilon^3}{a}\Big(v_0(s)q_1 + u_1(s)q_0\Big) + \frac{\varepsilon^4}{a}\left(-4H_{0010} + \frac{50b^2}{49a}H_{0002}\right. \\ \left. + b\tau_2 H_{0001} + u_2(s)q_0 + v_1(s)q_1 + \frac{1}{2a}u_0^2(s)H_{2000} + \frac{10b}{7a}u_0(s)H_{1001}\right) + \mathcal{O}(\varepsilon^5), \end{aligned} \tag{3.62}$$

$$\begin{aligned} x_{\mathrm{L}}(t) = \frac{\varepsilon^2}{a}\left(\frac{10b}{7}H_{0001} + \hat{u}_0(\xi)q_0\right) + \frac{\varepsilon^3}{a}\Big(\hat{v}_0(\xi)q_1 + \hat{u}_1(\xi)q_0\Big) + \frac{\varepsilon^4}{a}\left(-4H_{0010} + \frac{50b^2}{49a}H_{0002}\right. \\ \left. + b\tau_2 H_{0001} + \hat{u}_2(\xi)q_0 + \hat{v}_1(\xi)q_1 + \frac{1}{2a}\hat{u}_0^2(\xi)H_{2000} + \frac{10b}{7a}\hat{u}_0(\xi)H_{1001}\right) + \mathcal{O}(\varepsilon^5), \end{aligned} \tag{3.63}$$

where τ_2 is given in (3.18); (u_0, v_0), (u_1, v_1) and u_2 are specified by (3.3), (3.16) and (3.17), respectively; and $(\hat{u}_0, \hat{v}_0)$, $(\hat{u}_1, \hat{v}_1)$ and $\hat{u}_2$ are specified by (3.37), (3.52), and (3.55), respectively. Notice that ξ in (3.63) is related to $s = \varepsilon t$ by the differential equation (3.30). However, as explained before, we can approximate $\omega(\xi)$ by 1 and replace ξ by εt.

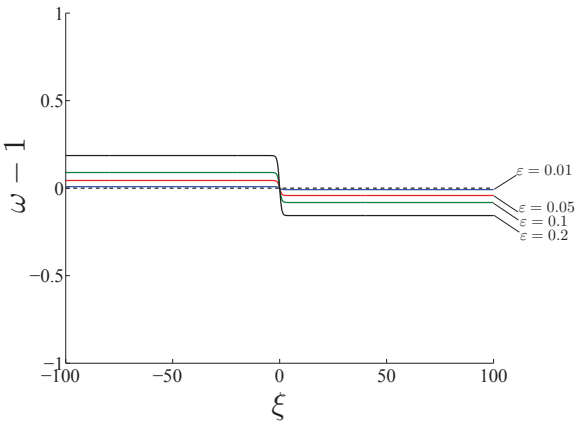

Figure 3.7: The bounded function $\omega(\xi) - 1$ for $(a, b) = (1, 1)$ and ε=0.01, 0.05, 0.1, 0.2.

3.6 The homoclinic solutions of the Gray-Scott model

In this section, we use the second-order predictors (3.61) and (3.63) to explicitly derive an accurate approximation for the homoclinic solution in the Gray-Scott kinetic model (2.70). We compare these solutions with the homoclinic solutions computed by a numerical continuation method to illustrate the accuracy.

Theorem 3.1. *The parameters (F, k) unfold the BT singularity generically and for parameter values near (F_c, k_c) system (2.70) has a homoclinic orbit, provided $k < k_c$ and*

$$F - F_c = -\frac{5}{148}\sqrt{-74(k - k_c)} + \frac{8952}{9065}(k - k_c) + \mathcal{O}(|k - k_c|^{\frac{5}{4}}). \tag{3.64}$$

Proof. As discussed in Section 2.4, the change of variables (2.74) transforms the system (2.70) into (2.75). This system has a BT-equilibrium $x = (x_1, x_2) = (0, 0)$ and $\alpha = (\alpha_1, \alpha_2) = (0, 0)$. Therefore, the system (2.75) can be recast as system (2.1) with $f(x, \alpha)$ as in (2.39a) where

$$A = \begin{pmatrix} -\frac{1}{8} & -\frac{1}{4} \\ \frac{1}{16} & \frac{1}{8} \end{pmatrix}, \quad J_1 = \begin{pmatrix} \frac{1}{2} & 0 \\ -\frac{1}{4} & -\frac{1}{4} \end{pmatrix}, \quad B(x, y) = \begin{pmatrix} -\frac{1}{2}(x_1y_2 + x_2y_1) - x_2y_2 \\ \frac{1}{2}(x_1y_2 + x_2y_1) + x_2y_2 \end{pmatrix},$$

$$A_1(x, \alpha) = \begin{pmatrix} -x_1\alpha_2 \\ -x_2\alpha_1 - x_2\alpha_2 \end{pmatrix}, \quad C(x, y, z) = \begin{pmatrix} -2(x_1y_2z_2 + x_2y_1z_2 + x_2y_2z_1) \\ 2(x_1y_2z_2 + x_2y_1z_2 + x_2y_2z_1) \end{pmatrix},$$

and $J_2 = B_1 = (0, 0)$. The vectors

$$q_0 = \frac{\sqrt{5}}{5}\Big(-2, 1\Big), \qquad q_1 = \frac{16\sqrt{5}}{25}\Big(1, 2\Big), \qquad p_0 = \frac{\sqrt{5}}{5}\Big(-2, 1\Big), \qquad p_1 = \frac{\sqrt{5}}{16}\Big(1, 2\Big),$$

satisfy (2.3) and (2.4). The normal form coefficients a and b are given in (2.77), i.e.,

$$a = -\frac{\sqrt{5}}{160}, \quad b = -\frac{\sqrt{5}}{10}.$$

To find an explicit formula for the homoclinic solutions of (2.70), we compute the coefficients of (2.48), (2.59), (2.61), (2.62) and (2.64)-(2.69) to get

$$\begin{cases} H_{2000} = \frac{96}{125}\begin{pmatrix}-1\\2\end{pmatrix}, & H_{1100} = \frac{768}{625}\begin{pmatrix}1\\2\end{pmatrix}, & H_{0200} = -\frac{73728}{3125}\begin{pmatrix}1\\2\end{pmatrix}, \\ H_{0010} = \frac{64\sqrt{5}}{125}\begin{pmatrix}-26\\\frac{219}{5}\end{pmatrix}, & H_{0001} = \begin{pmatrix}0\\-2\end{pmatrix}, & K_{1,0} = \frac{32\sqrt{5}}{5}\begin{pmatrix}\frac{179}{125}\\-1\end{pmatrix}, \\ K_{1,1} = \begin{pmatrix}-1\\0\end{pmatrix}, & K_2 = 8\begin{pmatrix}\frac{179}{125}\\-1\end{pmatrix}, & H_{0002} = \frac{1728}{625}\begin{pmatrix}1\\2\end{pmatrix}, \\ H_{1001} = -\frac{16\sqrt{5}}{25}\begin{pmatrix}1\\2\end{pmatrix}, & H_{0101} = \frac{768\sqrt{5}}{125}\begin{pmatrix}1\\2\end{pmatrix}, & d = -\frac{1}{40}, \\ H_{3000} = \frac{21312\sqrt{5}}{15625}\begin{pmatrix}1\\2\end{pmatrix}, & e = -\frac{679}{625}, & a_1 = \frac{7\sqrt{5}}{50}, \\ H_{2001} = -\frac{384}{125}\begin{pmatrix}1\\2\end{pmatrix}, & b_1 = \frac{36\sqrt{5}}{25}. & \end{cases} \tag{3.65}$$

Substituting these values into (3.61) and (3.63) gives the following second-order predictor for the homoclinic solution of (2.75),

$$\begin{pmatrix}\alpha_1\\\alpha_2\end{pmatrix} = -\varepsilon^2\begin{pmatrix}\frac{160}{7}\\0\end{pmatrix} - \varepsilon^4\begin{pmatrix}\frac{73334784}{12005}\\\frac{303104}{49}\end{pmatrix} + \mathcal{O}\left(\varepsilon^5\right), \tag{3.66}$$

$$\begin{aligned}\begin{pmatrix}x_1\\x_2\end{pmatrix} &= \varepsilon^2\begin{pmatrix}64\hat{u}_0\\-32\hat{u}_0 - \frac{320}{7}\end{pmatrix} + \varepsilon^3\begin{pmatrix}64\hat{u}_1 - \frac{512}{5}\hat{v}_0\\-32\hat{u}_1 - \frac{1024}{5}\hat{v}_0\end{pmatrix} \\ &\quad + \varepsilon^4\begin{pmatrix}\frac{16384}{7}\hat{u}_0 - \frac{49152}{25}\hat{u}_0^2 - \frac{512}{5}\hat{v}_1 + 64\hat{u}_2 - \frac{9551872}{1225}\\\frac{32768}{7}\hat{u}_0 + \frac{86016}{25}\hat{u}_0^2 - \frac{1024}{5}\hat{v}_1 - 32\hat{u}_2 - \frac{848551936}{60025}\end{pmatrix} + \mathcal{O}\left(\varepsilon^5\right),\end{aligned} \tag{3.67}$$

where $\hat{u}_0, \hat{v}_0, \hat{u}_1, \hat{v}_1$ and $\hat{u}_2$ are explicit functions of εt given by (3.37), (3.52), and (3.55), respectively. Using

$$\varepsilon \approx \sqrt[4]{-\frac{49}{303104}\alpha_2},$$

we obtain the second-order approximation for the homoclinic bifurcation curve of (2.75) in the (α_1, α_2)-space that implies (3.64). The formulas (3.66)-(3.67) are computed using Maple. The full commands can be found in Appendix A.5. □

The homoclinic curve and the corresponding orbits are shown in Figure 3.8. The BT point is $(\frac{1}{2}, \frac{1}{4})$ in the phase space and $(\frac{1}{16}, \frac{1}{16})$ in the parameter space. In Figure 3.8a, the dashed black curve is obtained by predictor (3.64). The blue curve is obtained by a continuation method [47, 51, 52]. It is clear that the predictor (3.64) gives a good approximation to the computed homoclinic curve based on a continuation method for the saddle point as well as for the homoclinic curve, see Figures 3.8a and 3.8b. The normal form (2.73) predicts the birth of an *unstable* limit cycle via a *subcritical* Andronov-Hopf bifurcation near the BT point. However, this bifurcation becomes *supercritical* away from the BT point at the Generalized Hopf point at $(k, F) \approx (0.0352, 0.0117)$. Here a curve of limit points of cycles emerges. This curve (solid black) and the homoclinic seem to extend to the origin, see Figure 3.8c.

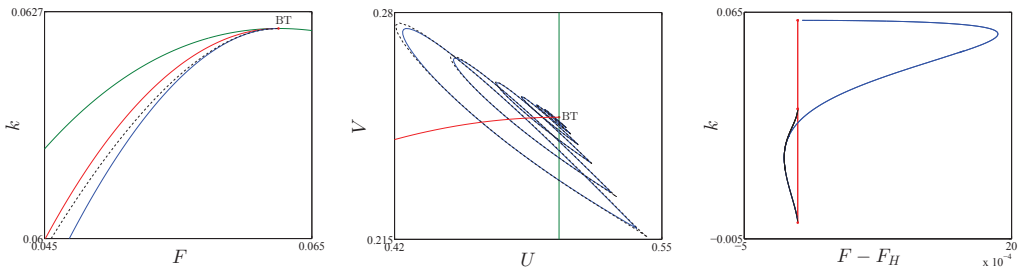

(a) (b) (c)

Figure 3.8: (a) Bifurcation diagram of (2.70) near the BT point: The blue curve is the saddle homoclinic curve computed by a continuation method, the dashed black curve corresponds to the predictor (3.64), the limit point and Andronov-Hopf bifurcation curves are green and red, respectively; (b) The predicted homoclinic orbits using the predictor (3.67) in the phase space for ε=0.0052, 0.0066, 0.0084, 0.0109, 0.0142, 0.0173 and the numerical solutions (blue) obtained for the corresponding values of k; (c) Andronov-Hopf (red), homoclinic (blue), and limit points of cycles (black) bifurcation curves in the $(F-F_H, k)$-plane, where $F_H = \frac{1}{2}\sqrt{k}(1-\sqrt{1-4\sqrt{k}}-2\sqrt{k})$ is the Andronov-Hopf bifurcation value of parameter F at a given k.

CHAPTER 4

Initialization of a homoclinic solution

In this chapter we discuss the implementation of the derived homoclinic asymptotics in the MATLAB continuation package MatCont. Five numerical examples illustrating its efficiency are presented.

4.1 Initialization issue

From a numerical point of view, the continuation problem of homoclinic orbits is well defined near but not at the BT point. So, a small nonzero step away form the BT point (essentially determined by the perturbation parameter ε) should be chosen so that the initial prediction is sufficiently close to the actual homoclinic solution. The continuation problem itself should be defined in a finite time interval instead of an infinite one. In the present chapter, we derive an important relation between the geometric amplitude of the homoclinic orbit and the initial perturbation parameter ε, see **Step 2** in Section 4.1.1. We also present an extra parameter that can be used by the user to find a suitable finite time interval where the continuation problem will converge, see Figure 4.1 and **Step 3** in Section 4.1.1.

In general, to continue the homoclinic orbits in two free parameters, MatCont uses an extended defining system that consists of several components (see [47, 61]).

First, the infinite time interval $[-\infty, \infty]$ is truncated to a finite interval with suitable boundary conditions, say $[-T, +T]$, where T is the half-return time. So, after applying this truncation of time, system (2.1) becomes

$$\dot{x} - 2Tf(x(t), \alpha) = 0. \tag{4.1}$$

The interval $[-T, +T]$ is rescaled to $[0, 1]$ and divided into mesh intervals where the solution is approximated by a vector polynomial of degree m (typically, $m = 4$), a linear combination of the rescaled Lagrange basis polynomials. The mesh is non-uniform and adaptive. Each mesh interval is further subdivided by $(m + 1)$ equidistant fine mesh points and contains m collocation (Gauss) points. These points are the rescaled roots of the $m^{\text{th}}-$degree Legendre polynomials [44, 88]. The numbers `ntst` of mesh intervals and `ncol` $= m$ of collocation points are part of the continuation data chosen by the user. Equation (4.1) must be satisfied at each collocation point.

The second part is the equilibrium condition

$$f(x_0, \alpha) = 0. \tag{4.2}$$

Third, if two homoclinic parameters are free, then the following integral phase condition is added

$$\int_0^1 \left\langle x(t) - \tilde{x}(t), \dot{\tilde{x}}(t) \right\rangle \, \mathrm{d}t = 1, \tag{4.3}$$

where $\tilde{x}$ is the homoclinic solution obtained at previously found point on the curve.

Fourth, the equations (4.1), (4.2) and (4.3) must be complemented with projection boundary conditions at 0 and 1:

$$\begin{cases} Q_S(x(0) - x_0) = 0, \\ \\ Q_U(x(1) - x_0) = 0, \end{cases} \tag{4.4}$$

where Q_S and Q_U are matrices whose rows form a basis for the stable (S) and unstable (U) eigenspaces respectively of $A^{\mathrm{T}}(x_0, \alpha)$. The projection boundary conditions place the solution at the two end points in the unstable and stable eigenspaces of $A(x_0, \alpha)$ respectively [33]. MatCont uses a specific algorithm that depends on the real Schur factorization and a Riccati equation to construct and update Q_S, Q_U, for more details see [19, 47, 49, 53, 54, 61].

Finally, the distance between $x(0)$ (respectively, $x(1)$) and x_0 must be small enough, *i.e.*

$$\begin{cases} \varepsilon_0 = \|x(0) - x_0\|, \\ \varepsilon_1 = \|x(1) - x_0\|. \end{cases} \tag{4.5}$$

The half-return time T, ε_0 and ε_1 are called *the homoclinic parameters*. We note that either one or two homoclinic parameters can be free.

MatCont calculates the initial homoclinic solution, the initial T, ε_0 and ε_1 by the homoclinic predictor (3.63) (or (3.62) in MatCont 6.2 and older earlier versions). This is done by calling the initializer `init_BT_Hom.m` that implements *the Lindstedt-Poincaré predictor* (3.63); then MatCont uses the initial data to start up the homoclinic continuation by calling the continuer `cont.m` which itself calls `homoclinic.m`.

4.1.1 The initializer `init_BT_Hom.m`

The algorithm to initialize the homoclinic continuation data proceeds as follows:

Assume that system (2.1) has a BT point at (x_0, α_0).

Step 0. Introduce new variables, $(x, \alpha) \to (x - x_0, \alpha - \alpha_0)$, that move the BT point of (2.1) to the origin, $(0, 0)$.

Step 1. Compute the matrices and multilinear forms A, J_1, B, A_1, J_2, C and B_1. Then define the non-singular bordered system (BS) by

$$\mathtt{BS} = \begin{pmatrix} A & w \\ v^{\mathrm{T}} & 0 \end{pmatrix} \in \mathbb{R}^{(n+1)\times(n+1)}.$$

The vectors w, $v \in \mathbb{R}^n$ are chosen such that BS is non-singular. To compute the eigenvectors

$$\{q_0, q_1, p_1, p_0\} \in \mathbb{R}^n$$

one starts by solving

$$\mathtt{BS}\,(q_0, s) = (0, 1)\,, \quad \mathtt{BS}\,(q_1, s) = (q_0, 0)\,, \quad \mathtt{BS}^{\mathrm{T}}\,(p_1, s) = (0, 1)\,, \quad \mathtt{BS}^{\mathrm{T}}\,(p_0, s) = (p_1, 0)\,.$$

Following [89], these vectors are normalized by

$$\mu = \sqrt{|q_0^{\mathrm{T}} q_0|}, \quad q_0 := \frac{1}{\mu} q_0, \quad q_1 := \frac{1}{\mu} q_1, \quad q_1 := q_1 - (q_0^{\mathrm{T}} q_1) q_0,$$
$$\nu = q_0^{\mathrm{T}} p_0, \quad p_1 := \frac{1}{\nu} p_1, \quad p_0 := p_0 - (p_0^{\mathrm{T}} q_1) p_1, \qquad p_0 := \frac{1}{\nu} p_0,$$

and hence BS can be redefined as

$$\mathtt{BS} = \begin{pmatrix} A & p_1 \\ q_0^{\mathrm{T}} & 0 \end{pmatrix} \in \mathbb{R}^{(n+1)\times(n+1)},$$

Step 2. Compute a,b, H_{2000}, H_{1100}, H_{0200}, $K_{1,0}$, $K_{1,1}$, H_{0010}, H_{0001}, K_2, H_{0002}, H_{1001}, H_{0101}, d, H_{3000}, e, a_1, H_{2001}, b_1.

Step 3. Substituting these values into (3.61) and (3.63) gives an approximation of the homoclinic solution $(x(t,\varepsilon), \alpha(\varepsilon))$. Therefore the asymptotic homoclinic of the solution in the parameter and state space of (2.1) is given by $(x(t,\varepsilon), \alpha(\varepsilon)) \to (x(t,\varepsilon) + x_0, \alpha(\varepsilon) + \alpha_0)$.

Step 4. Let

$$A_0 := \|x(\pm\infty, \varepsilon) - x(0, \varepsilon)\|$$

be the size of the initial homoclinic orbit (see Figure 4.1). Using (3.63) we approximate A_0 for small ε by

$$A_0 = \left\| \varepsilon^2 \left(\frac{2}{a} \right) q_0 - \varepsilon^2 \left(\frac{-4}{a} \right) q_0 \right\| = \varepsilon^2 \left(\frac{6}{|a|} \right).$$

The amplitude A_0 is chosen by the user, so we get

$$\varepsilon = \sqrt{A_0 \frac{|a|}{6}}. \tag{4.6}$$

This defines the initial perturbation parameter ε.

Step 5. We choose the initial T such that, at the end points, the distance

$$k := \|x(\pm\infty, \varepsilon) - x(\pm T, \varepsilon)\| \tag{4.7}$$

is sufficiently small [15], see Figure 4.1. For small ε, we approximate k using (3.63) as

$$k = \varepsilon^2 \left(\frac{6\|q_0\|}{|a|} \right) \operatorname{sech}^2(\pm\varepsilon T). \tag{4.8}$$

Hence, the half-return time T can be estimated by solving

$$\operatorname{sech}(\varepsilon T) = \frac{1}{\varepsilon}\sqrt{\frac{k|a|}{6}},$$

or, equivalently,

$$\operatorname{sech}(\varepsilon T) = \sqrt{\frac{k}{A_0}}. \tag{4.9}$$

The tolerance k should be small; by default it is set to 1×10^{-5}. However, in the case where a is small, we sometimes need to adjust k to find a suitable T to initialize the continuation of homoclinic orbits. This takes some trial-and-error to set k, as well as A_0. It is possible for users to change the default values if needed in the GUI input window of MatCont (i.e., in the **Starter** window, see Figure 4.2), where the parameters k and A_0 are denoted by `Tolerance` and `Amplitude`, respectively. Examples will be discussed in Section 4.2.

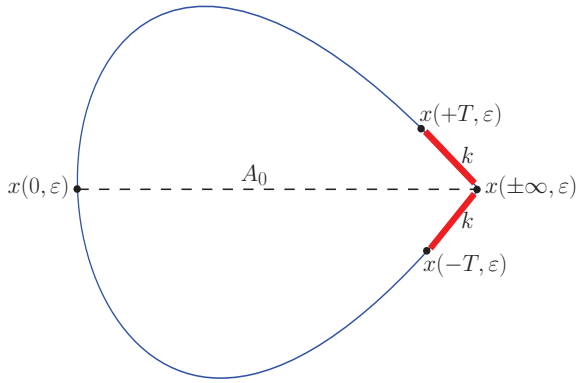

Figure 4.1: The initial homoclinic solution.

Step 6. Compute the initial cycle by discretizing the interval $[0,1]$ into equidistant points f_i (*the fine mesh*) and then evaluate (3.63) at each t where t is given by

$$t = (2f_i - 1)T, \quad f_i \in [0,1].$$

The initial saddle point x^* (*i.e.*, $x(\pm\infty,\varepsilon)$) is approximated by

$$x^* = x_0 + \varepsilon^2\left(\frac{10b}{7a}H_{0001} + \frac{2}{a}q_0\right).$$

Step 7. From data collected in **Step 3**, it is now easy to compute the initial values of ε_0 and ε_1. It is worth pointing out that $\varepsilon_{0,1}$ are computed from (3.63) with terms up to ε^3. On the other hand, the value of k is computed by truncating the $\mathcal{O}(\varepsilon^3)$ form (3.63). So, in general k is greater than $\varepsilon_{0,1}$.

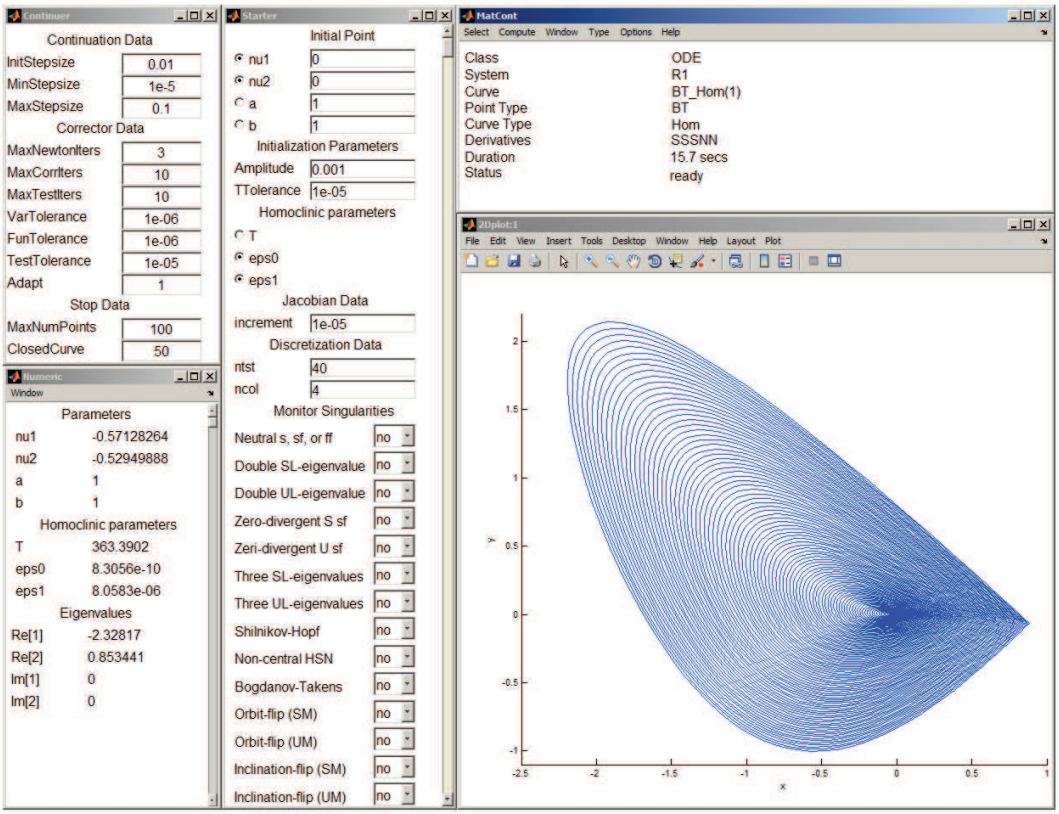

Figure 4.2: MatCont window during the homoclinic orbits continuation from a BT point.

Step 8. Since all curves in MatCont are computed by a prediction-correction continuation method applied to a defining system in an appropriate discretization space $\mathbb{R}^{N+1}$ [51], the homoclinic orbits continuation involves a calculation of the tangent vector to predict and correct the next point. If the initial point $X^i \in \mathbb{R}^{N+1}$ is sufficiently close to the homoclinic curve, then the next point in the homoclinic curve can be predicted using the initial tangent prediction

$$X^{i+1} = X^i + h_i V^i, \tag{4.10}$$

where h_i is the current step size and $V^i \in \mathbb{R}^{N+1}$ is the normalized tangent vector at the homoclinic curve at point X^i. The tangent vector at X^i is computed by solving

$$J(X^i)V^i = 0, \tag{4.11}$$

where $J(X^i) \in \mathbb{R}^{N\times(N+1)}$ is the Jacobian matrix of the defining system evaluated at X^i. The initial point can be obtained from predictor (3.63). **Compute**|**Forward** and **Compute**|**Backward** select the appropriate sign of V^0 without any additional computation.

4.2 Examples

In this section we use MatCont to start homoclinic orbits that emanate from BT points in several models[†]. Recall that in the GUI of MatCont k is denoted as `TTolerance`. In all examples, we will set `TTolerance`=10^{-5}. As a rule, the `Amplitude` should always be larger than `TTolerance` given the geometric meaning of both variables, *cf.* Figure 4.1. In all cases, ε_0 and ε_1 are the free homoclinic parameters since this appears to be the most stable choice. As another rule, the BT point itself should be computed to a geometric precision significantly smaller than `TTolerance`. This can be achieved in MatCont by decreasing the tolerances `VarTolerance` and `TestTolerance` for the curve on which the BT points are detected.

4.2.1 Morris-Lecar model

Every cell in our body has a membrane that controls the movement of ions in and out of the cell. Cell membranes have specific channels that allow ions to move across the membrane. In the Morris-Lecar model (see [102]) we have calcium (Ca^{2+}) and potassium (K^{1+}) voltage channels and a leak (L) channel. The resulting system is

$$\begin{cases} C\dot{V} = I_{app} - I_{ion}, \\ \\ \dot{w} = \dfrac{\phi(w_\infty - w)}{\tau}, \end{cases} \tag{4.12}$$

[†]The examples require MatCont 6.2 or higher

where

$$I_{ion} = g_{Ca} m_\infty (V - V_{Ca}) + g_K w (V - V_K) + g_L (V - V_L),$$

$$m_\infty = 0.5 \left(1 + \tanh(\frac{V - v_1}{v_2})\right),$$

$$w_\infty = 0.5 \left(1 + \tanh(\frac{V - v_3}{v_4})\right),$$

and

$$\tau = \frac{1}{\cosh(\frac{V - v_3}{2v_4})}.$$

In these equations, C is the membrane capacitance; I_{app} is the applied current; I_{ion} collects the Ca^{2+}, K^{1+} and L currents; g_L, g_{Ca} and g_K are the maximal conductance's for L, Ca^{2+} and K^{1+} channels, respectively. V is the membrane potential; V_L, V_{Ca} and V_K are the equilibrium potentials corresponding to L,Ca^{2+} and K^{1+} conductance's, respectively; w is the fraction of open K^{1+} channels; m_∞ and w_∞ are the fractions of open Ca^{2+} and K^{1+} channels at steady state respectively; $\frac{\tau}{\phi}$ determines the activation time for the K^{1+} current. Note that v_1,v_2,v_3 and v_4 are parameters chosen to fit the model data.

We fix the parameter values as follows, $C = 20$, $V_L = -60$, $V_{Ca} = 120$, $V_K = -84$, $g_L = 2$, $g_{Ca} = 4.4$, $g_K = 8$, $v_1 = -1.2$, $v_2 = 18$, $v_3 = 2$, $v_4 = 30$, $\phi = \frac{1}{25}$. Then we compute the equilibrium curve with free parameter I_{app}, starting with initial values $I_{app} = 0$, $V = -60.854568$ and $w = 0.014914$. Two Andronov-Hopf points are detected. In the **Continuer** window we set `MaxStepSize` $= 1$. We start from any Andronov-Hopf point and compute the Andronov-Hopf curve passing through it with (I_{app}, v_3) free parameters. Four BT points are detected, see Table 4.1 and 4.2. We compute the homoclinic to saddle curve from each BT point with: (I_{app}, v_3) free system parameters, (`eps0`,`eps1`) as free homoclinic parameters, `TTolerance` $= 1 \times 10^{-5}$, `ntst` $= 80$, `Adapt` $= 1$ and initial numerical data as in Table 4.3, see Figure 4.3 and Figure 4.4.

Label	I_{app}	v_3	**State variables**
$\mathbf{BT}_1$	519.625363	−63.401900	(−11.152829, 0.970208)
$\mathbf{BT}_2$	487.997701	−51.777427	(2.815616, 0.974408)
$\mathbf{BT}_3$	−227.131893	69.755741	(13.611167, 0.023136)
$\mathbf{BT}_4$	48.225883	21.734195	(−27.149905, 0.037007)

Table 4.1: Parameter, state values at the bifurcation points in Figure 4.3.

Label	a	b	d	e	a_1	b_1
$\mathbf{BT}_1$	0.000738	0.022894	−0.000007	−0.000837	−0.002540	−0.053071
$\mathbf{BT}_2$	−0.000749	−0.029614	−0.000040	−0.001595	0.005192	0.070564
$\mathbf{BT}_3$	−0.001120	−0.033012	0.000026	0.000779	−0.000223	−0.058309
$\mathbf{BT}_4$	0.000277	0.015131	0.000004	0.000602	−0.000554	0.065855

Table 4.2: BT normal form coefficient $\{a, b, d, e, a_1, b_1\}$ values at the bifurcation points in Figure 4.3.

Label	`Amplitude`	Initial T	Initial ε	Compute|
$\mathbf{BT}_1$	3.2×10^{-5}	22046.73	6.28×10^{-5}	**Backward**
$\mathbf{BT}_2$	1.5×10^{-5}	12599.94	4.33×10^{-5}	**Forward**
$\mathbf{BT}_3$	1.5×10^{-5}	10301.45	5.29×10^{-5}	**Backward**
$\mathbf{BT}_4$	1.5×10^{-5}	20727.74	2.63×10^{-5}	**Forward**

Table 4.3: The initial continuation data at each BT point defined as in Table.4.1.

4.2.2 Predator-prey model with constant rate harvesting

Consider the following predator-prey system with constant rate predator harvesting (see [24]):

$$\begin{cases} \dot{x} = rx(1 - \dfrac{x}{k}) - y\dfrac{x}{e+x}, \\ \\ \dot{y} = y(-d + \dfrac{x}{e+x}) - h, \end{cases} \tag{4.13}$$

where k is the carrying capacity of the prey population, d is the death rate of the predator, r is the intrinsic growth rate of the prey population, and h is the harvesting rate. The function $\frac{x}{e+x}$ is often called the functional response of Holling type II. Xiao and Ruan [133] show the existence of a BT bifurcation in (4.13) and sketch the global bifurcation diagram including the homoclinic curve which emanates from the BT point. We study the occurrence of homoclinic orbits that emanate from the computed BT point using MatCont. We fix the parameter values as follows: $r = 1$, $e = 1$, $k = 2$, $h = 0.5$, then we compute the equilibria with free parameter d (initially $d = 0$) and initial value for state variables $x = 1$ and $y = 1$. A limit point is detected. We compute the limit point curve passing through it with (d, h) as free parameters. One BT point is detected (see Table 4.4). The smooth BT normal form coefficients at the BT point are shown in Table 4.5. To initialize the homoclinic orbit from the BT point with (d, h) as free system parameters, we input the following numerical data in the MatCont **Starter** window: `Amplitude` $= 10^{-3}$, `TTolerance` $= 10^{-5}$ and `ntst` $= 40$.

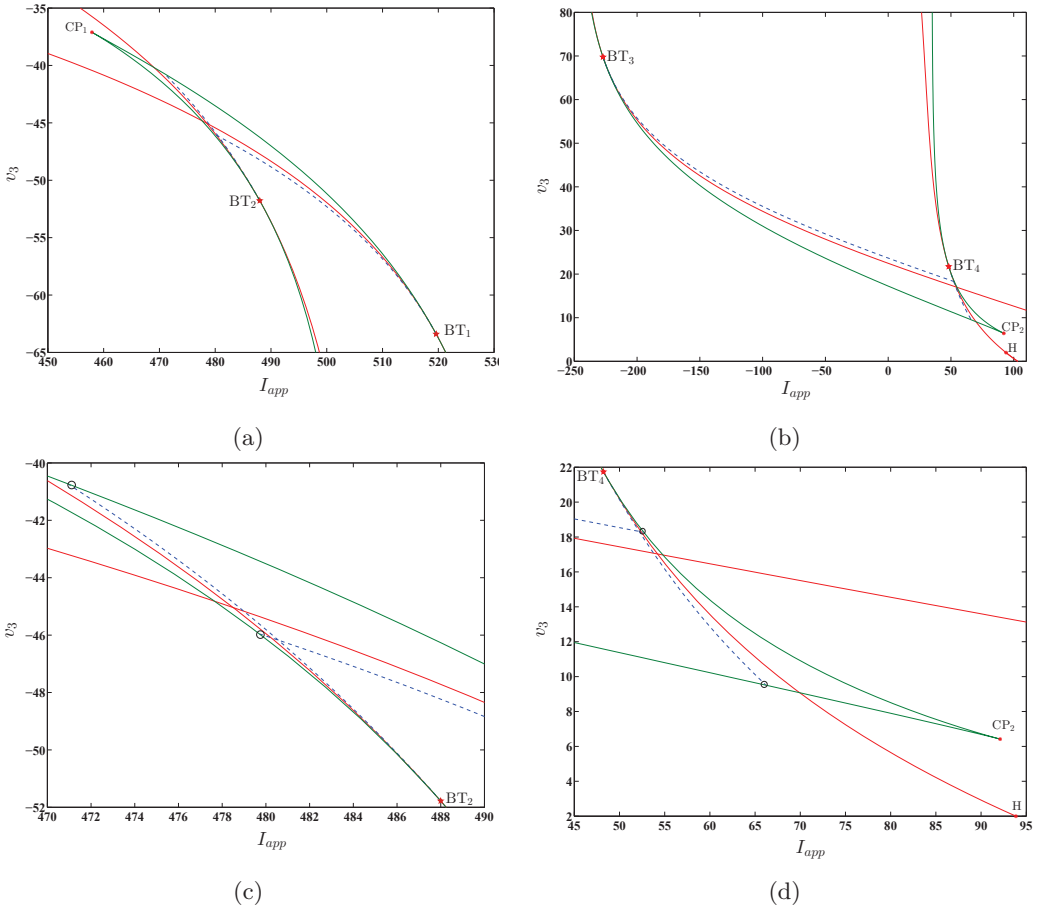

Figure 4.3: (a) and (b) Homoclinic orbits in parameter space (I_{app}, v_3). The dashed blue curves are homoclinic curves. The green line is the limit point curve. The red line is the Andronov-Hopf curve. (c) and (d) The same curves as in Figure 4.3a and Figure 4.3b, respectively, zoomed near the $BT_{2,4}$ points. The non-central-homoclinic-to-saddle-node orbit on the limit point curve is circled, where the homoclinic curve ends.

In the **Continuer** window we set `Adapt` $= 1$. Activate `eps0` and `eps1` as free homoclinic parameters and then **Compute**|**Backward**. The result is shown in Figure 4.5. The initial ε is 5.475×10^{-3} and during continuation $T = 856.934$. Note that by computing the Hopf curve passing through the BT point, a *degenerate BT point*[†] is detected. This point is labeled by BT_0 in Figure 4.5. The critical BT normal form coefficients, the state and parameter values at this BT point are: $(a, b) = (0, -1)$, $(x, y, d, h) = (0, 1, 0, 0)$. Recall that the homoclinic asymptotics (3.61)-(3.63) can be used only in the case of the nondegenerat BT points.

[†]Degenerate because the critical normal form coefficients (a, b) satisfies $ab = 0$.

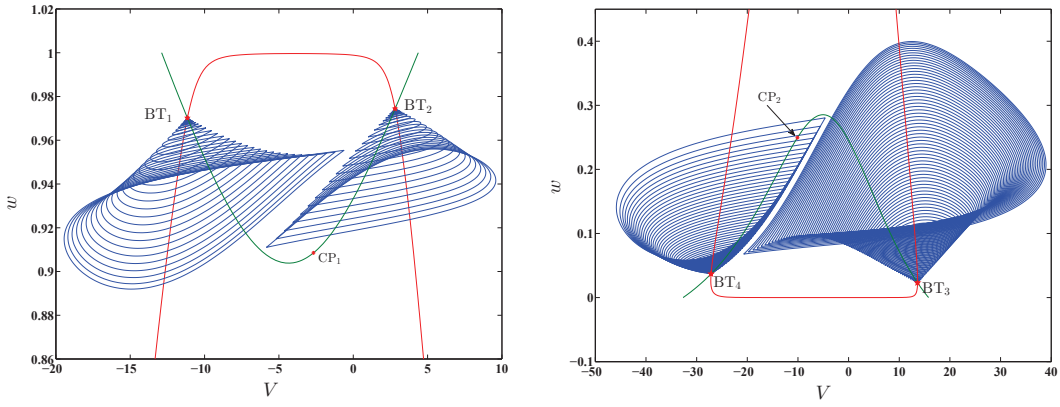

(a) (b)

Figure 4.4: Homoclinic orbits (blue curves) in the Morris-Lecar model in state space (V, w). The green line is the limit point curve; the red line is the Andronov-Hopf curve.

Label	d	h	State variables
BT	0.198909	0.307265	(1.124149, 0.930219)

Table 4.4: Parameter and state values at the bifurcation point in Figure 4.5.

Label	a	b	d	e	a_1	b_1
BT	−0.179826	0.378287	0.063886	-0.479004	−0.169755	−0.157654

Table 4.5: BT normal form coefficient $\{a, b, d, e, a_1, b_1\}$ values at the bifurcation point in Figure 4.5.

4.2.3 CO-oxidation in a platinum model.

Consider the following chemical model which describes CO-oxidation in platinum (see [15, 29, 83])

$$\begin{cases} \dot{x} = 2k_1 z^2 - 2k_{-1}x^2 - k_3 xy, \\ \dot{y} = k_2 z - k_{-2} y - k_3 xy, \\ \dot{s} = k_4(z - \lambda s). \end{cases} \tag{4.14}$$

where $z := 1 - x - y - s$ and $\lambda = \frac{k_{-4}}{k_4}$. The underlying reaction scheme is studied in [29] and we notice that a factor 2 is missing in front of $k_1 z^2$ in [83].

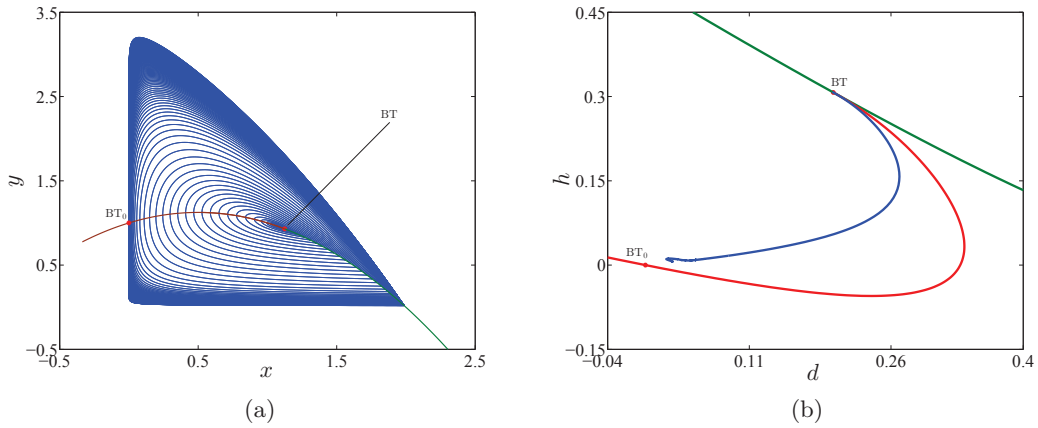

(a) (b)

Figure 4.5: (a) The homoclinic orbits in state space for system (4.13), (b) The homoclinic orbits in parameter space. The dashed blue curve is the homoclinic curve. The red is the Andronov-Hopf curve and the green is the limit point curve.

We fix the reaction rates (constants) above as follows $k_1 = 2.5$, $k_{-1} = 1$, $k_3 = 10$, $k_{-2} = 0.1$, $k_4 = 0.0675$, $k_2 = 1.4707$, $\lambda = 0.4$. We compute the equilibria curve with free k_2 and initial state variables $x = 0.002954$, $y = 0.762104$, $s = 0.167816$. Two limit points are detected. We start the limit point continuation from the first computed limit point-point with (λ, k_2) free system parameters. Two BT points are detected, see Table 4.6. The smooth BT normal form coefficients at the BT points are listed in Table 4.7.

From BT_1 and with $(k_2,\ \lambda)$ as free system parameters we start the homoclinic curve continuation using `Amplitude` $= 2 \times 10^{-5}$, `TTolerance` $= 1 \times 10^{-5}$ and `ntst` $=$ 40. In the **Continuer** window we set `InitStepsize` $= 1 \times 10^{-3}$, `Adapt` $= 1$. Then **Compute**|**Backward** with (`eps0`,`eps1`) as free homoclinic parameters. It turns out that the initial ε is 5.28×10^{-4} and $T = 1667.78$. For BT_2 we set `InitStepsize` $= 1 \times 10^{-2}$, `Amplitude` $= 1.2 \times 10^{-6}$, `TTolerance` $= 1 \times 10^{-8}$, `ntst` $= 40$, `Adapt` $= 1$ then we use **Compute**|**Backward**. Notice that the initial ε is 9.821×10^{-5} and during continuation $T = 49559.486$. The results are presented in Figure 4.6

Label	k_2	λ	**State variables**
$\mathbf{BT}_1$	1.417629	0.971400	$(0.115909, 0.315467, 0.288436)$
$\mathbf{BT}_2$	1.161198	0.722334	$(0.016337, 0.638408, 0.200457)$

Table 4.6: Parameter and state values at the BT points in Figure 4.6.

Label	a	b	d	e	a_1	b_1
$\mathbf{BT}_1$	−0.083785	−2.136283	−0.177758	−7.142211	0.861775	7.117579
$\mathbf{BT}_2$	−0.048225	−1.937610	−0.074466	9.236539	0.660272	13.446324

Table 4.7: BT normal form coefficient $\{a, b, d, e, a_1, b_1\}$ values at the BT points in Figure 4.6.

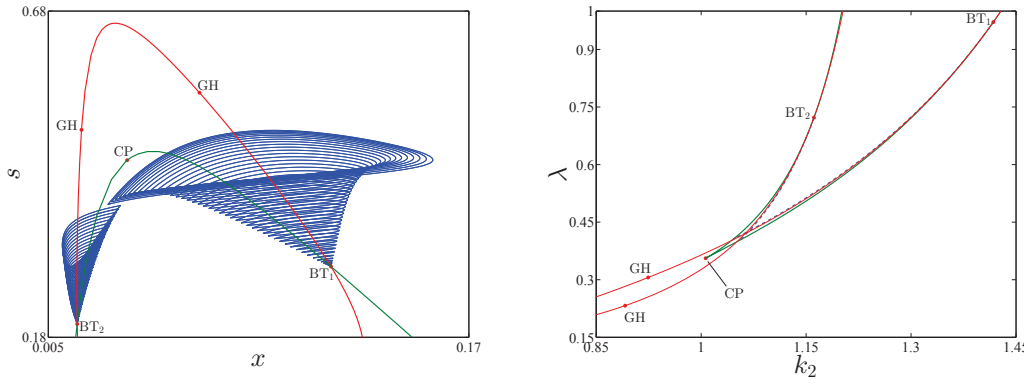

(a) (b)

Figure 4.6: (a) Homoclinic orbits in (x, s)-space for the CO−oxidation model, (c) Homoclinic orbits in parameter space. The dashed blue curve is the homoclinic curve. The green curve is the limit point curve and the red is the Andronov-Hopf curve.

4.2.4 Indirect field oriented control model

The indirect field oriented control (IFOC) system of an induction motor can be mathematically described as in [10, 116] by the following ODEs:

$$\begin{cases} \dot{x}_1 = -c_1 x_1 + c_2 x_4 - \dfrac{k c_1}{u_2^0} x_2 x_4, \\ \dot{x}_2 = -c_1 x_2 + c_2 u_2^0 + \dfrac{k c_1}{u_2^0} x_1 x_4, \\ \dot{x}_3 = -c_3 x_3 - c_4 c_5 \left(x_2 x_4 - u_2^0 x_1\right) + \left(c_4 T_m + c_3 w_{ref}\right), \\ \dot{x}_4 = -(k_i - k_p c_3) x_3 - k_p c_4 c_5 \left(x_2 x_4 - u_2^0 x_1\right) + k_p \left(c_4 T_m + c_3 w_{ref}\right). \end{cases} \tag{4.15}$$

Here x_1, x_2, x_3 and x_4 are the state variables, where x_1 and x_2 denote direct and quadrature components of the rotor flux; x_3 is the rotor speed error (i.e., the difference between the

reference and the real mechanical speeds of the rotor); and x_4 denotes the quadrature axis component of the stator current. We also define the following constants and parameters: u_2^0 is a constant reference for the rotor flux magnitude; c_1 to c_5 are machine parameters; k_p and k_i are the proportional (P) and the integral (I) control gains, respectively; w_{ref} is the speed reference; T_m the load torque; k the measure of rotor time constant mismatches. The occurrence of limit points and Andronov-Hopf points in IFOC has been characterized as a result of rotor time constant mismatches (see, for example, [11, 68] and [101]). The first results on the occurrence of a BT bifurcation in the IFOC model were presented in [117]. A detailed analytical study for the codim-2 bifurcations of (4.15) can be found in [116].

By continuation of equilibria with free k (initially $k = 17$) and fixed parameters $T_m = 5$, $c_1 = 4.4868$, $c_2 = 0.3567$, $c_3 = 0$, $c_4 = 9.743$, $c_5 = 1.911$, $u_2^0 = 11.3$, $k_p = 4.5$, $k_i = 500$, $w_{ref} = 0$, and initial point $(x_1, x_2, x_3, x_4) = (-0.207486, 0.107263, 0.0, 2.534337)$, MatCont detects a limit point and an Andronov-Hopf point. Further, we continue of the limit point with (k, T_m) free, a BT point is detected (in Table 4.8 this point is labeled by BT_1). We select BT_1 and we compute the the Andronov-Hopf curve passing through it with (k, T_m) free, an extra BT point is detected (labeled by BT_2). The smooth BT normal form at the BT points are listed in Table 4.9. From the BT_2 point we start the continuation of the homoclinic curve, using k and T_m as free system parameters, (`eps0`,`eps1`) as free homoclinic parameters, initial `Amplitude` $= 2 \times 10^{-5}$, `TTolerance` $= 1 \times 10^{-5}$, `ntst` $= 40$, `Adapt` $= 1$. Then **Compute**|**Forward**, noticing that during continuation $T = 91.221$. For BT_1 we use the same procedure then **Compute**|**Backward**, noticing that during continuation $T = 91.221$. In both cases, the initial ε is 0.01, see Figure 4.7.

Label	k	T_m	**State variables**
$\mathbf{BT}_1$	4.538573	8.109670	$(-0.163289, 0.238334, 0.0, \quad 10.063675)$
$\mathbf{BT}_2$	4.538585	−8.109652	$(\ 0.163288, 0.238333, 0.0, -10.063682)$

Table 4.8: Parameter and state values at the bifurcation points in Figure 4.7.

Label	a	b	d	e	a_1	b_1
$\mathbf{BT}_1$	28.005817	−0.911013	−4.468334	−0.435057	4.388082	0.066363
$\mathbf{BT}_2$	28.006045	−0.911099	−4.468354	−0.435062	4.388129	0.066366

Table 4.9: BT normal form coefficient $\{a, b, d, e, a_1, b_1\}$ values at the bifurcation points in Figure 4.7.

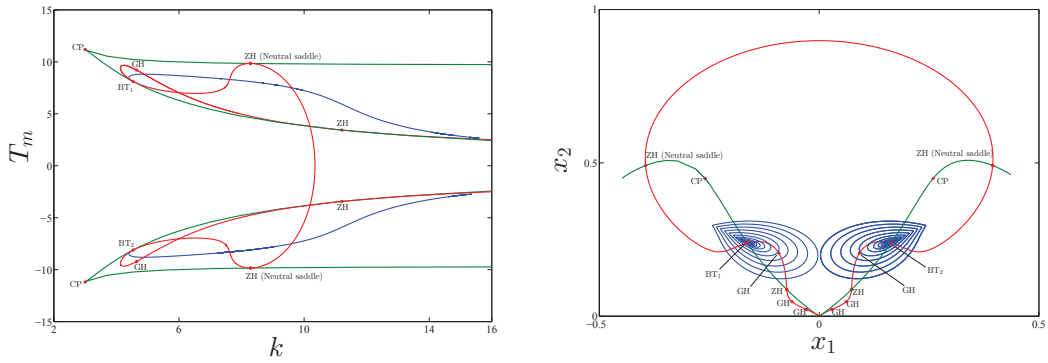

Figure 4.7: (a) Homoclinic orbits emanating from the BT points of the IFOC model in parameter space (k, T_m). The blue dashed curve is the homoclinic orbit. The green is the limit point curve and the red is the Andronov-Hopf curve. (b) The homoclinic orbits in state space (x_1, x_2).

4.2.5 The extended Lorenz-84 model

This example is an extended version of the Lorenz-84 model. In this model we can find all codim-2 points of equilibria (i.e., BT, CP, GH, ZH and HH) [93, 121, 127]. Here, we discuss the switching from the BT points to the homoclinic branches.

The extended Lorenz-84 model has the form

$$\begin{cases} \dot{X} = -Y^2 - Z^2 - \alpha X + \alpha F - \xi U^2, \\ \dot{Y} = XY - \beta XZ - Y + G, \\ \dot{Z} = \beta XY + XZ - Z, \\ \dot{U} = -\delta U + \xi UX + S. \end{cases} \tag{4.16}$$

In this system, X models the intensity of a baroclinic wave, Y and Z the sin and cos coefficients of the wave respectively, the variable U is added to study the influence of external parameters such as temperature.

We fix the parameters as follows $\alpha = 0.25$, $\beta = 1$, $G = 0.25$, $\delta = 1.04$, $\xi = 0.987$ and $F = 2.61$. We start the equilibria continuation with free S (initially $S = 0$) and with initial state variable values $X = 1.053698$, $Y = -0.012060$, $Z = 0.236645$, $U = -0.580787$. Two

limit points are detected. From any limit point we can compute the limit point curve passing through it with (F, S) as free system parameters to find two BT points (see Table 4.10). The smooth BT points are listed in Table 4.11. From BT_1 we start the homoclinic continuation with (F, S) free, `Amplitude` $= 4 \times 10^{-5}$, `TTolerance` $= 1 \times 10^{-5}$, `ntst` $= 40$, `Adapt` $= 3$ and we choose (`eps0`, `eps1`) as the free homoclinic parameters then **Compute**|**Forward**. In the resulting continuation $T = 1346.112$ is fixed and the initial ε is 1.2×10^{-3}. The obtained homoclinic orbits are as in Figure 4.8. For BT_2 the same procedure works with `Amplitude` $= 4 \times 10^{-5}$ and then **Compute**|**Backward** leads to a continuation with $T = 1346.112$ as well. The initial ε is 1.2×10^{-3}.

Label	F	S	State variables
$\mathbf{BT}_1$	1.446717	0.020940	$(1.225641, -0.036321, 0.197288, -0.123390)$
$\mathbf{BT}_2$	1.446722	-0.020941	$(1.225646, -0.036321, 0.197287, \ 0.123392)$

Table 4.10: Parameter and state values at the bifurcation points in Figure 4.8.

Label	a	b	d	e	a_1	b_1
$\mathbf{BT}_1$	0.214424	0.606515	-0.2381464	-2.815244	0.588486	1.238143
$\mathbf{BT}_2$	0.214426	0.606525	-0.2381432	-2.815177	0.588481	1.238118

Table 4.11: BT normal form coefficient $\{a, b, d, e, a_1, b_1\}$ values at the bifurcation points in Figure 4.8.

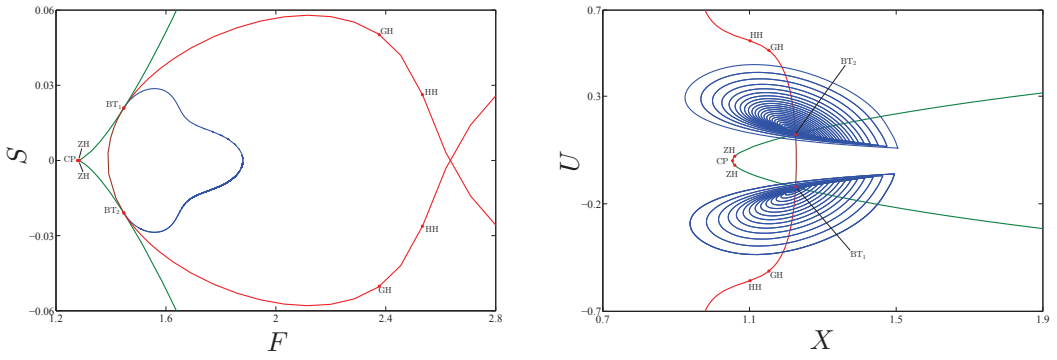

(a) (b)

Figure 4.8: (a) Homoclinic orbits in parameter space for the Lorenz-84 model. The blue curve is the homoclinic curve. The red is the Andronov-Hopf curve and the green is the limit point curve, (b) Homoclinic orbits in $(X, U)-$space.

CHAPTER 5

Homoclinic structure in the Bogdanov-Takens map

In this chapter we derive an accurate asymptotic expression for the homoclinic parameter of the BT map. We show how to use the derived homoclinic parameter to continue branches of homoclinic tangencies in the BT map. By a reduction to the parameter-dependent center manifold at the BT point, we derive an asymptotic expression for the homoclinic parameter at a generic BT point of maps.

5.1 Bogdanov-Takens map

A fixed point of an n-dimensional smooth map

$$x \mapsto f(x, \alpha), \quad f : \mathbb{R}^n \times \mathbb{R}^2 \longrightarrow \mathbb{R}^n, \tag{5.1}$$

with double-unit eigenvalue is said to be a fixed point of BT type[†] if the only Jordan block of the Jacobian matrix of (5.1) corresponding to the unit eigenvalue is

$$\begin{pmatrix} 1 & 1 \\ 0 & 1 \end{pmatrix}.$$

[†]also known as 1:1 resonance point, see [88].

Similar to the theory of the BT bifurcation of ODEs (see Chapter 2), there is a change of coordinates and parameters that transforms such map into a two-parameter normal form family,

$$\begin{pmatrix} u_0 \\ u_1 \end{pmatrix} \to \begin{pmatrix} 1 & 1 \\ 0 & 1 \end{pmatrix} \begin{pmatrix} u_0 \\ u_1 \end{pmatrix} + \begin{pmatrix} 0 \\ \nu_1 + \nu_2 u_1 + \tilde{a} u_0^2 + \tilde{b} u_0 u_1 \end{pmatrix} + \mathcal{O}(\|(u,\nu)\|^3),$$

where $(\tilde{a}, \tilde{b}) \in \mathbb{R}^2$ are the normal form coefficients, $u = (u_0, u_1) \in \mathbb{R}^2$ parametrizes the two-dimensional parameter-dependent center manifold of (5.1) and $\nu = (\nu_1, \nu_2) \in \mathbb{R}^2$ are the unfolding parameters. The truncated map,

$$G : \begin{pmatrix} u_0 \\ u_1 \end{pmatrix} \to \begin{pmatrix} 1 & 1 \\ 0 & 1 \end{pmatrix} \begin{pmatrix} u_0 \\ u_1 \end{pmatrix} + \begin{pmatrix} 0 \\ \nu_1 + \nu_2 u_1 + \tilde{a} u_0^2 + \tilde{b} u_0 u_1 \end{pmatrix}, \tag{5.2}$$

(or simply *the BT map*) coincides with the time-1 flow (up to a certain order of terms) of a system of ODEs which exhibits a BT point at its equilibrium (the same fixed point of the map (5.2)). This system is called *the approximating system*[†]. The dynamic behavior of (5.2) is different form the approximating system. In the approximating system, the parameters that correspond to the homoclinic bifurcation form a curve in the plane, while a homoclinic region bounded by two curves corresponding to homoclinic tangencies is possible in system (5.2), see Figure 5.1. If a parameter (ν_1, ν_2) is located in the homoclinic region, then the BT map possesses transverse homoclinic trajectories. On the curves of the tangencies, the homoclinic trajectories become nontransverse.

Definition 5.1. *For a fixed value of α, let x^* be a hyperbolic saddle fixed point of (5.1). Suppose that the stable and unstable manifolds $W^s(x^*)$, $W^u(x^*)$ of x^* intersect transversally at a point $x_0 \neq x^*$. Let $\{x_k\}_{k=-\infty}^{\infty}$ be the orbit through x_0. $\{x_k\}$ is called a transversal homoclinic orbit (or simply homoclinic orbit) and each x_k is called a homoclinic point. Since x_0 lies in both the stable and unstable manifolds, so does the homoclinic orbit $\{x_k\}$. The homoclinic orbit $\{x_k\}$ is referred to as tangential if $W^s(x^*)$ and $W^u(x^*)$ intersect tangentially at $\{x_k\}$.*

Although the exact bifurcation structure is different for the map (5.2) and the approximating ODE, the usage of the ODE provides information that is hardly available by the analysis of the map alone. The approximating system allows to predict the homoclinic structure that appears in the map. This structure occurs near the homoclinic bifurcation of the

[†]By the theory presented in Chapter 2, we can further express the approximating system near the BT point as the normal form (2.24).

approximating system. Our main concern throughout this chapter is to present an accurate asymptotic of the homoclinic solution of the BT map in order to continue the branches of homoclinic tangencies. Then we can transfer this asymptotic into the parameter space of the generic n-dimensional map (5.1). It is worth noting that J. Chávez [34] attempted to construct an asymptotic for the homoclinic orbits near a generic BT point of (5.1). However, neither the asymptotic of the homoclinic solution nor the parameter transformation is correct since it is based on flawed assumptions inherited from earlier studies.

In this chapter, we improve the asymptotics of the homoclinic parameter that are presented in [26, 34, 64, 66] by

(a) considering all the second-order terms of the coordinates and parameters in the approximating system that results from the method of Picard iteration.

(b) using the accurate homoclinic asymptotic derived in Chapter 3 to derive an asymptotic of the homoclinic parameter in the approximating system.

Moreover, by systemically solving all linear systems appearing from the homological equation, we correct the parameter transformation presented in [34].

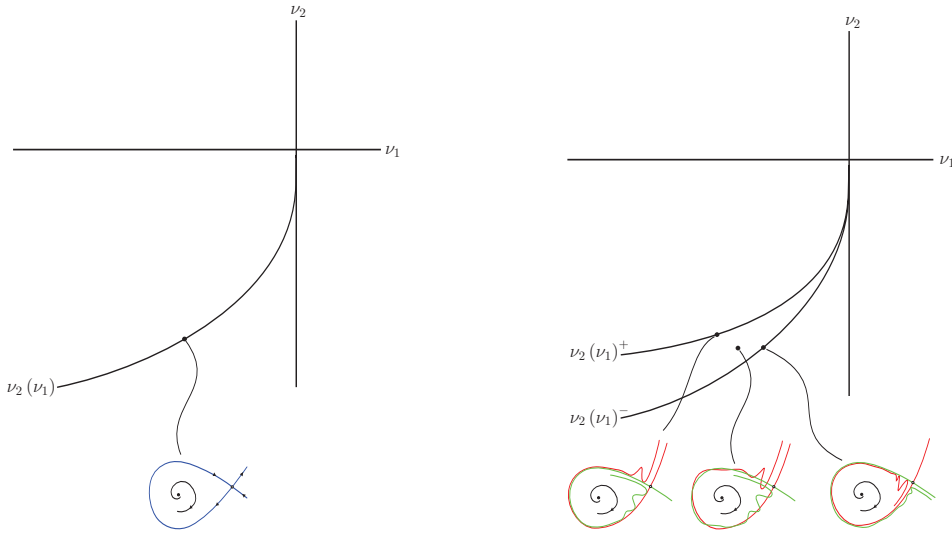

(a) (b)

Figure 5.1: The bifurcation diagram in the unfolding parameter space of the BT map. (a) The homoclinic curve $\nu_2(\nu_1)$ of the approximating ODE. (b) The homoclinic structure of the BT map. The points (ν_1, ν_2) situated between the lower and upper curves (i.e., $\nu_2(\nu_1)^+$ and $\nu_2(\nu_1)^-$) are the (transverse) homoclinic points. These points collide on the curves of tangencies $\nu_2(\nu_1)^+$, $\nu_2(\nu_1)^-$.

5.2 The parameter-dependent center manifold

We use the *homological equation* technique described in Section 2.3 to obtain the coefficients $(\tilde{a}, \tilde{b})$ of (5.2) on the parameter-dependent center manifold of (5.1), as well as to derive an explicit relation between the orbits of (5.2) and those of the original system (5.1). Since the Jacobian matrix, A, of (5.1) at the BT point has a double unit eigenvalue, there exist two real independent eigenvectors $q_{0,1} \in \mathbb{R}^n$, of A, and two adjoint eigenvectors $p_{0,1} \in \mathbb{R}^n$, of A^{T}, such that

$$\begin{pmatrix} A - I_n & 0 \\ -I_n & A - I_n \end{pmatrix} \begin{pmatrix} q_0 \\ q_1 \end{pmatrix} = \begin{pmatrix} 0 \\ 0 \end{pmatrix}, \quad \begin{pmatrix} A^{\mathrm{T}} - I_n & 0 \\ -I_n & A^{\mathrm{T}} - I_n \end{pmatrix} \begin{pmatrix} p_1 \\ p_0 \end{pmatrix} = \begin{pmatrix} 0 \\ 0 \end{pmatrix}.$$

We assume that the vectors satisfy

$$p_0^{\mathrm{T}} q_0 = p_1^{\mathrm{T}} q_1 = 1, \quad p_0^{\mathrm{T}} q_1 = p_1^{\mathrm{T}} q_0 = 0, \quad q_0^{\mathrm{T}} q_0 = 1, \quad q_1^{\mathrm{T}} q_0 = 0.$$

Further, we define a relation

$$\alpha = K(\nu), \quad K : \mathbb{R}^2 \to \mathbb{R}^2, \tag{5.3}$$

between the unfolding parameter ν and the original system parameter α. The local parameter -dependent center manifold for (5.1) can be parametrized by (u, ν),

$$x = H(u, \nu), \quad H : \mathbb{R}^2 \times \mathbb{R}^2 \to \mathbb{R}^n. \tag{5.4}$$

Since the center manifold is invariant, we obtain the following homological equation:

$$H(G(u, \nu), \nu) = f(H(u, \nu), K(\nu)). \tag{5.5}$$

We can solve the homological equation by the same recursive procedure based on Fredholm's solvability condition that we have described in Section 2.3. We insert the Taylor expansions of K, H and f

$$f(x, \alpha) = Ax + J_1\alpha + \frac{1}{2}B(x, x) + A_1(x, \alpha) + \mathcal{O}\left(\|\alpha\|^2 + \|\,(x, \alpha)\,\|^3\right), \tag{5.6}$$

$$K(\nu) = K_{1,0}\nu_1 + K_{1,1}\nu_2 + \frac{1}{2}K_2\nu_2^2 + \mathcal{O}\left(\nu_1^2 + |\nu_1\nu_2|\right) + \mathcal{O}\left(\|\nu\|^3\right), \tag{5.7}$$

$$\begin{aligned} H(u, \nu) = {} & H_{0010}\nu_1 + H_{0001}\nu_2 + q_0u_0 + q_1u_1 + H_{1010}\nu_1u_0 + H_{1001}\nu_2u_0 + H_{0110}\nu_1u_1 \\ & + H_{0101}\nu_2u_1 + \frac{1}{2}H_{2000}u_0^2 + H_{1100}u_0u_1 + \mathcal{O}\left(u_1^2 + \|\nu\|^2 + \|\,(u, \nu)\,\|^3\right). \end{aligned} \tag{5.8}$$

into (5.5) together with the BT map (5.2).

From linear and quadratic u-terms in the homological equation, we obtain

$$\tilde{a} = \frac{1}{2} p_1^T B(q_0, q_0), \tag{5.9}$$

$$\tilde{b} = p_1^T B(q_0, q_1) + p_0^T B(q_0, q_0), \tag{5.10}$$

$$H_{2000} = (A - I_n)^{\mathrm{INV}}(2\tilde{a} q_1 - B(q_0, q_0)) \quad H_{2000} \mapsto H_{2000} + r q_0, \tag{5.11}$$

$$H_{1100} = (A - I_n)^{\mathrm{INV}}(\tilde{b} q_1 - B(q_0, q_1) + H_{2000}). \tag{5.12}$$

where r is given in (2.47). Moreover, the vectors $K_{1,0}$, $K_{1,1}$, H_{0010} and H_{0001} can be computed by solving the $(n+2)$-dimensional system

$$\begin{pmatrix} A - I_n & J_1 \\ p_1^{\mathrm{T}} \mathrm{B} q_0 & p_1^{\mathrm{T}} \mathrm{A}_1 q_0 \\ p_0^{\mathrm{T}} \mathrm{B} q_0 + p_1^{\mathrm{T}} \mathrm{B} q_1 & p_0^{\mathrm{T}} \mathrm{A}_1 q_0 + p_1^{\mathrm{T}} \mathrm{B}_1 q_1 \end{pmatrix} \begin{pmatrix} H_{0010} & H_{0001} \\ K_{1,0} & K_{1,1} \end{pmatrix} = \begin{pmatrix} q_1 & 0 \\ p_1^T H_{1100} & 0 \\ c & 1 \end{pmatrix}, \tag{5.13}$$

where $c := 3p_0^T H_{1100} + p_0^T H_{2000} + p_1^T H_{1100} - p_0^T B(q_1, q_1)$. We define $x = (A - I_n)^{\mathrm{INV}} y$ by solving the $(n+1) \times (n+1)$ non-singular bordered system

$$\begin{pmatrix} A - I_n & p_1 \\ q_0^{\mathrm{T}} & 0 \end{pmatrix} \begin{pmatrix} x \\ s \end{pmatrix} = \begin{pmatrix} y \\ 0 \end{pmatrix},$$

where y is in the range of $A - I_n$. As soon as $K_{1,0}$, $K_{1,1}$, H_{0010} and H_{0001} are determined, we can compute the quadratic term

$$K_2 = (-p_1^{\mathrm{T}} z) K_{1,0}, \tag{5.14}$$

where

$$z := B(H_{0001}, H_{0001}) + 2A_1(H_{0001}, K_{1,1}) + J_2(K_{1,1}, K_{1,1}).$$

5.3 Approximation by a flow

In this section we describe two methods known in the literature to approximate the map (5.2) by a system of ODEs, namely, the interpolating technique and the method of Picard iteration. For each system we derive an asymptotic of the homoclinic orbits. In Section 5.4, we will compare these asymptotics with the homoclinic structure of (5.2) to show the accuracy.

5.3.1 Interpolation by a flow

It is possible to formally interpolate the map G by an autonomous system of ODEs

$$\begin{aligned}\dot{u}_0 &= P(u,\nu),\\ \dot{u}_1 &= Q(u,\nu),\end{aligned}$$

or in the vector-field form:

$$U_\nu = P\partial u_0 + Q\partial u_1, \tag{5.15}$$

where P and Q are formal power series in u_0, u_1, ν_1 and ν_2. Generally speaking, we say that U_ν is the approximating vector-field of the map

$$G = e^{U_\nu}\,(u_0, u_1)\,,$$

if the series $e^{U_\nu}\,(u_0, u_1)$ coincides with the time-1 shift along trajectories of U_ν. Following [64], we say that the order of the monomial $u_0^k\,u_1^l\,\nu_1^m\,\nu_2^n$ is given by[†]

$$\delta(u_0^k\,u_1^l\,\nu_1^m\,\nu_2^n) = 2k + 3l + 4m + 2n. \tag{5.16}$$

Thus the formal series P and Q can be expressed as

$$\begin{cases} P = \displaystyle\sum_{i\geq 3} p_i(u_0, u_1, \nu_1, \nu_2),\\ Q = \displaystyle\sum_{j\geq 4} q_j(u_0, u_1, \nu_1, \nu_2),\end{cases} \tag{5.17}$$

where p_i and q_j are δ-homogenous polynomials of order i and j respectively, i.e.,

$$\begin{cases} p_i = \displaystyle\sum_{2k+3l+4m+2n=i} c_{klmn}\;u_0^k\;u_1^l\;\nu_1^m\;\nu_2^n,\\ q_j = \displaystyle\sum_{2k+3l+4m+2n=j} d_{klmn}\;u_0^k\;u_1^l\;\nu_1^m\;\nu_2^n.\end{cases} \tag{5.18}$$

with coefficients c_{klmn}, $d_{klmn} \in \mathbb{R}$ to be determined. We ignore the convergence question. Then the vector-field U_ν can be expanded into a sum of δ-homogenous polynomial vector-fields,

$$U_\nu = \sum_{i\geq 1} U_i, \quad U_i = p_{i+2}\partial u_0 + q_{i+3}\partial u_1. \tag{5.19}$$

[†]The idea of ordering the terms this way is to arrive at a vector-field with terms ordered according to (3.1).

We note that when we apply U_i to a δ-homogenous polynomial of δ-order n we obtain a δ-homogenous polynomial of δ-order $n+i$. Using the assumptions above, we are ready to prove the following proposition (**cf.** [65]):

Lemma 5.1. *For all sufficiently small $\|\nu\|$, there is a unique formal vector-field Z such that*

$$(G,\,\nu)^T = e^Z\,(u,\,\nu)^T. \tag{5.20}$$

Proof. Assume that the vector-field Z can be expressed as

$$Z = P\partial u_0 + Q\partial u_1 + R\partial\nu_1 + S\partial\nu_2,$$

where P, Q, R and S are formal power series in u_0, u_1, ν_1, ν_2. Expand the vector-field Z into a sum of δ-homogenous polynomial vector-fields

$$Z = \sum_{i\geq 1} Z_i.$$

Let π_i denote the projection of a formal series onto the subspace of δ-homogenous polynomials of δ-order i and assume that

$$\begin{cases} p_{i+2} = \pi_{i+2}\left(u_0 + u_1 - e^Z u_0\right), \\ q_{i+3} = \pi_{i+3}\left(u_1 + g(u,\nu) - e^Z u_1\right), \\ r_{i+4} = \pi_{i+4}\left(\nu_1 - e^Z \nu_1\right), \\ s_{i+2} = \pi_{i+2}\left(\nu_2 - e^Z \nu_2\right). \quad i \geq 1, \end{cases} \tag{5.21}$$

where $g(u,\nu) := \nu_1 + \nu_2 u_1 + \tilde{a}u_0^2 + \tilde{b}u_0 u_1$. The right hand side of (5.21) are finite sums and depend on p_{n_1} with $3 \leq n_1 \leq i-2$, q_{n_2} with $4 \leq n_2 \leq i-1$, r_{n_3} with $5 \leq n_3 \leq i$ and s_{n_4} with $3 \leq n_4 \leq i-2$ as well as on the coefficients of the terms of $(G,\,\nu)$. Define the exponent,

$$e^Z = I + \sum_{n\geq 1} \frac{1}{n!} Z^n, \tag{5.22}$$

where Z^n stands for the vector-field Z applied n-times, and the equality

$$Zu_0 = \sum_{i\geq 3} p_i, \quad Zu_1 = \sum_{i\geq 4} q_i, \quad Z\nu_1 = \sum_{i\geq 5} r_i, \quad Z\nu_2 = \sum_{i\geq 3} s_i. \tag{5.23}$$

Then by taking the leading order in (5.21), we obtain

$$Z_1\,(u,\,\nu)^{\mathrm{T}} = (p_3,\ q_4,\ r_5,\ s_3) = \left(u_1,\ \nu_1 + \tilde{a}_h u_0^2,\ 0,\ 0\right). \tag{5.24}$$

The polynomials p_3, q_4, r_5 and s_3 are uniquely defined and hence the recurrent polynomials p_{i+2}, q_{i+3}, r_{i+4} and s_{i+2}, $i \geq 2$ are also uniquely defined. Also, it is clear that the polynomials r_{i+4}, s_{i+2} are equal to zero for all $i \geq 2$. Thus we can write the δ-homogenous polynomials vector-field Z_i, $i \geq 2$ found in the form

$$Z_i = (U_i,\,0)\,,$$

where

$$U_i = p_{i+2}\partial u_0 + q_{i+3}\partial u_1, \quad i \geq 2. \tag{5.25}$$

□

With a suitable number of terms in (5.22) and solving (5.21) for $i \geq 2$, we obtain

$$U_1 = u_1\partial u_0 + \left(\nu_1 + \tilde{a}u_0^2\right)\partial u_1,$$

$$U_2 = -\frac{1}{2}\left(\nu_1 + \tilde{a}u_0^2\right)\partial u_0 + \left(\nu_2 u_1 + \left(\tilde{b} - \tilde{a}\right)u_0 u_1\right)\partial u_1,$$

$$\begin{aligned} U_3 = &\left(-\frac{1}{2}\nu_2 u_1 + \left(\frac{2}{3}\tilde{a} - \frac{1}{2}\tilde{b}\right)u_0 u_1\right)\partial u_0 + \\ &\left(-\frac{1}{2}\left(\nu_1\nu_2 + \tilde{a}\nu_2 u_0^2\right) + \frac{1}{2}\left(\frac{1}{3}\tilde{a} - \tilde{b}\right)u_1^2 + \left(\frac{2}{3}\tilde{a} - \frac{1}{2}\tilde{b}\right)\nu_1 u_0 + \left(\frac{2}{3}\tilde{a}^2 - \frac{1}{2}\tilde{a}\tilde{b}\right)u_0^3\right)\partial u_1, \\ &\vdots \end{aligned}$$

It follows from Lemma 5.1 that the map (5.2) can be formally interpolated by the autonomous vector-field

$$U_\nu \,=\, U_1 \,+\, U_2 \,+\, U_3 \,+\, \ldots. \tag{5.26}$$

The first order vector-field U_1 defines a Hamiltonian system with

$$h := \frac{1}{2}\dot{u}_0^2 + V(u_0, \nu_1) - k = 0, \quad k \in \mathbb{R}, \tag{5.27}$$

where $\dot{u}_0 = u_1$ and the function $V(u_0, \nu_1)$ is given by

$$V(u_0, \nu_1) = -\int_0^{u_0}\left(\nu_1 + \tilde{a}u^2\right)\,du = -\left(\nu_1 u_0 + \frac{\tilde{a}u_0^3}{3}\right).$$

If $\frac{-\nu_1}{\tilde{a}} \geq 0$ then equation (5.27) has a homoclinic loop defined by $k = \frac{2}{3}\sqrt{\frac{(-\nu_1)^3}{\tilde{a}}}$. The function $V(u_0, \nu_1)$ and the phase portrait of the homoclinic solution of (5.27) are shown in Figure 5.2. The solution curve in the (u_0, u_1)-plane satisfies the homoclinic condition i.e., the phase point (u_0, u_1) approaches the saddle point

$$(u_0^s, u_1^s) = \left(\sqrt{\frac{-\nu_1}{\tilde{a}}}, 0\right), \quad \operatorname{sign}(\nu_1) = -\operatorname{sign}(\tilde{a}), \tag{5.28}$$

as $t \to \pm\infty$. The related homoclinic solution can be found explicitly

$$L_0(t) = (u_0(t), u_1(t)) = \left(\sqrt{\frac{-\nu_1}{\tilde{a}}}\left(1 - 3\operatorname{sech}^2\left(t\frac{\sqrt[4]{-\tilde{a}\nu_1}}{\sqrt{2}}\right)\right), \frac{d}{dt}u_0(t)\right). \tag{5.29}$$

This solution persists for $U_\nu \approx U_1 + U_2 + U_3$ if the Melnikov integral (1.27) vanishes:

$$\begin{aligned} M(\nu) &= \int_{-\infty}^{\infty} \Big(U_2 h + U_3 h\Big)\Big|_{L_0(t)}\, dt \\ &= \frac{24}{35}\nu_1\left(5\nu_1 - 5\sqrt[4]{-\nu_1}\right) + \frac{24}{7}\frac{(-\nu_1)^{\frac{5}{4}}}{\tilde{a}} + \frac{24}{5}\frac{(-\nu_1)^{\frac{3}{2}}\nu_2}{\sqrt{\tilde{a}}}. \end{aligned} \tag{5.30}$$

The function $M(\nu)$ vanishes along the curve

$$\nu_2^0 = \frac{5}{7}\frac{\nu_1\tilde{a} - \sqrt[4]{-\nu_1}\left(\tilde{a} - \tilde{b}\right)}{\sqrt{-\nu_1\tilde{a}}} \tag{5.31}$$

which gives an asymptotic for the homoclinic curve in the parameter space.

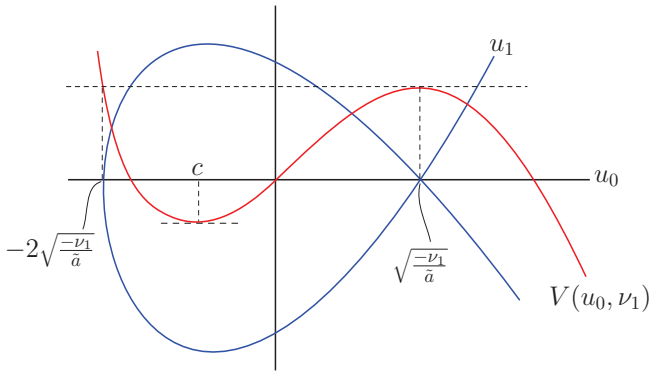

Figure 5.2: The function $V(u_0, \nu_1)$ and the phase portrait of equation (5.27).

5.3.2 The method of Picard iteration

Following [88], we start with writing system (5.2) at the fixed point as a 4-dimensional system

$$(G,\nu):(u,\nu)^{\mathrm{T}}\mapsto A\,(u,\nu)^{\mathrm{T}}+\left(F_{\nu}^{2},0\right)^{\mathrm{T}}, \tag{5.32}$$

where

$$A=\begin{pmatrix}1&1&0&0\\0&1&1&0\\0&0&1&0\\0&0&0&1\end{pmatrix},\quad F_{\nu}^{2}:=\begin{pmatrix}0\\ \nu_2u_1+\tilde{a}u_0^2+bu_0u_1\end{pmatrix}.$$

Assume that the approximating system to (5.32) having the same equilibrium (i.e., the fixed point of (5.2)) can be written as

$$(\dot{u},\dot{\nu})^{\mathrm{T}}=\Lambda\,(u,\nu)^{\mathrm{T}}+\left(f_{\nu}^{2}(u),0\right)^{\mathrm{T}}, \tag{5.33}$$

where Λ is a 4×4 matrix and the components of the two-dimensional vector $f_{\nu}^{2}(u)$ are smooth polynomials of order 2 in u_0, u_1, ν_1 and ν_2 with coefficients to be determined, i.e.,

$$\begin{aligned}f_{\nu}^{2}(u)=&\begin{pmatrix}\frac{1}{2}f_{2000}u_0^2+f_{1100}u_0u_1+\frac{1}{2}f_{0200}u_1^2\\ \frac{1}{2}g_{2000}u_0^2+g_{1100}u_0u_1+\frac{1}{2}g_{0200}u_1^2\end{pmatrix}+\begin{pmatrix}\frac{1}{2}f_{0020}\nu_1^2+f_{0011}\nu_1\nu_2+\frac{1}{2}f_{0002}\nu_2^2\\ \frac{1}{2}g_{0020}\nu_1^2+g_{0011}\nu_1\nu_0+\frac{1}{2}g_{0002}\nu_2^2\end{pmatrix}\\&+\begin{pmatrix}f_{1010}u_0\nu_1+f_{1001}u_0\nu_2+f_{0110}u_1\nu_1+f_{0101}u_1\nu_2\\ g_{1010}u_0\nu_1+g_{1001}u_0\nu_2+g_{0110}u_1\nu_1+g_{0101}u_1\nu_2\end{pmatrix}.\end{aligned} \tag{5.34}$$

The flow $\varphi_{\nu}^{t}(u)$ generated from the component $(\dot{u}_0,\dot{u}_1)$ in (5.33) can be seen as the first two components of the generalized flow

$$(u,\nu)^{\mathrm{T}}\mapsto\phi_{\nu}^{t}(u) \tag{5.35}$$

generated by (5.33), *i.e.*, $\phi_{\nu}^{t}(u):=(\varphi_{\nu}^{t}(u),\nu)^{\mathrm{T}}$. The method of Picard iteration can be used to generate the flow map (5.35). If the corresponding terms in the generated time-1 flow (i.e., $\phi_{\nu}^{1}(u)$) and (5.32) coincide then system (5.33) is said to be the approximating system of the map (5.32). The solution of the linear part of (5.33) can be used as initial data to generate the Picard iterate. Therefore, we set

$$U^{0}(t)=e^{\Lambda t}\,(u,\nu)^{\mathrm{T}}. \tag{5.36}$$

Since we seek a flow whose time-1 orbits coincide with (5.32), we have

$$e^{\Lambda} = A.$$

Solving for Λ gives

$$\Lambda = \begin{pmatrix} 0 & 1 & \frac{-1}{2} & 0 \\ 0 & 0 & 1 & 0 \\ 0 & 0 & 0 & 0 \\ 0 & 0 & 0 & 0 \end{pmatrix}.$$

Now, we perform a Picard iteration to compute the second order terms to ϕ^1:

$$U^1(t) = e^{\Lambda t}\,(u,\nu)^{\mathrm{T}} + \int_0^t e^{\Lambda(t-\tau)}\left(f_\nu^2\left(U^1(\tau)\right)\right)\,d\tau. \tag{5.37}$$

By comparing the coefficients of the similar terms in (5.37) for $t = 1$ and (5.32), we arrive at the following systems

$$u_0^2 : \begin{cases} \frac{1}{2}f_{2000} + \frac{1}{4}g_{2000} = 0, \\ \frac{1}{2}g_{2000} = \tilde{a}, \end{cases}, \qquad u_0u_1 : \begin{cases} \frac{1}{2}f_{2000} + f_{1100} + \frac{1}{6}g_{2000} + \frac{1}{2}g_{1100} = 0, \\ g_{1100} + \frac{1}{2}g_{2000} = \tilde{b}, \end{cases}$$

$$u_1^2 : \begin{cases} \frac{1}{2}f_{1100} + \frac{1}{6}g_{1100} + \frac{1}{24}g_{2000} + \frac{1}{6}f_{2000} + \frac{1}{2}f_{0200} + \frac{1}{4}g_{0200} = 0, \\ \frac{1}{2}g_{1100} + \frac{1}{6}g_{2000} + \frac{1}{2}g_{0200} = 0, \end{cases}$$

$$u_0\nu_1 : \begin{cases} \frac{1}{2}f_{1100} - \frac{1}{12}f_{2000} + f_{1010} - \frac{1}{24}g_{2000} + \frac{1}{2}g_{1010} + \frac{1}{6}g_{1100} = 0, \\ \frac{1}{2}g_{1100} - \frac{1}{12}g_{2000} + g_{1010} = 0, \end{cases}$$

$$u_0\nu_2 : \begin{cases} f_{1001} + \frac{1}{2}g_{1001} = 0, \\ g_{1001} = 0, \end{cases}$$

$$u_1\nu_1 : \begin{cases} \frac{1}{4}f_{1100} + \frac{1}{24}g_{1100} + \frac{1}{2}f_{1010} + f_{0110} + \frac{1}{2}f_{0200} + \\ \qquad\qquad \frac{1}{6}g_{0200} + \frac{1}{6}g_{1010} - \frac{1}{24}f_{2000} - \frac{1}{60}g_{2000} + \frac{1}{2}g_{0110} = 0, \\ \frac{1}{2}g_{0200} - \frac{1}{24}g_{2000} + g_{0110} + \frac{1}{4}g_{1100} + \frac{1}{2}g_{1010} = 0, \end{cases}$$

$$u_1\nu_2 : \begin{cases} \frac{1}{2}g_{0101} + f_{0101} + \frac{1}{2}f_{1001} + \frac{1}{6}g_{1001} = 0, \\ \frac{1}{2}g_{1001} + g_{0101} = 1, \end{cases}$$

$$\nu_1^2 : \begin{cases} \frac{1}{480}g_{2000} + \frac{1}{24}g_{0200} - \frac{1}{12}f_{1010} - \frac{1}{60}g_{1100} + \frac{1}{6}g_{0110} + \\ \quad \frac{1}{240}f_{2000} - \frac{1}{24}f_{1100} + \frac{1}{2}f_{0110} - \frac{1}{24}g_{1010} + \frac{1}{6}f_{0200} + \frac{1}{2}f_{0020} + \frac{1}{4}g_{0020} = 0, \\ \frac{1}{2}g_{0110} + \frac{1}{6}g_{0200} + \frac{1}{240}g_{2000} - \frac{1}{24}g_{1100} - \frac{1}{12}g_{1010} + \frac{1}{2}g_{0020} = 0, \end{cases}$$

$$\nu_1\nu_2 : \begin{cases} \frac{1}{2}f_{0101} + \frac{1}{6}g_{0101} + f_{0011} + \frac{1}{2}g_{0011} = 0, \\ \frac{1}{2}g_{0101} + g_{0011} = 0, \end{cases}, \qquad \nu_2^2 : \begin{cases} \frac{1}{2}g_{0002} + \frac{1}{2}f_{0002} = 0, \\ \frac{1}{2}g_{0002} = 0. \end{cases}$$

Solving for these systems will specify the components of (5.34). The unique solution for these systems is given as follows

$$\begin{aligned}
&g_{1001} = 0, \quad f_{1001} = 0, \quad g_{0002} = 0, \\
&f_{0002} = 0, \quad g_{2000} = 2\tilde{a}, \\
&f_{2000} = -\frac{1}{2}g_{2000}, \quad g_{1100} = -\frac{1}{2}g_{2000} + \tilde{b}, \\
&g_{0200} = -\left(g_{1100} + \frac{1}{3}g_{2000}\right), \quad f_{1100} = -\left(\frac{1}{6}g_{2000} + \frac{1}{2}g_{1100} + \frac{1}{2}f_{2000}\right), \\
&f_{0200} = -\left(\frac{1}{3}f_{2000} + \frac{1}{3}g_{1100} + f_{1100} + \frac{1}{2}g_{0200} + \frac{1}{12}g_{2000}\right), \\
&g_{1010} = -\left(\frac{1}{2}g_{1100} - \frac{1}{6}g_{2000}\right), \\
&f_{1010} = -\left(-\frac{1}{6}f_{2000} + \frac{1}{2}g_{1010} + \frac{1}{2}f_{1100} - \frac{1}{24}g_{2000} + \frac{1}{6}g_{1100}\right), \\
&g_{0101} = 1, \quad f_{0101} = -\frac{1}{2}g_{0101}, \quad g_{0110} = -\left(\frac{1}{4}g_{1100} + \frac{1}{2}g_{0200} - \frac{1}{24}g_{2000} + \frac{1}{2}g_{1010}\right), \\
&f_{0110} = -\left(\frac{1}{2}f_{1010} + \frac{1}{6}g_{0200} - \frac{1}{24}f_{2000} - \frac{1}{60}g_{2000} + \frac{1}{6}g_{1010}\right. \\
&\qquad \left. + \frac{1}{24}g_{1100} + \frac{1}{2}g_{0110} + \frac{1}{4}f_{1100} + \frac{1}{2}f_{0200}\right), \\
&g_{0020} = -\left(\frac{1}{3}g_{0200} - \frac{1}{3}g_{1010} + g_{0110} - \frac{1}{12}g_{1100} + \frac{1}{120}g_{2000}\right), \\
&f_{0020} = -\left(f_{0110} - \frac{1}{12}f_{1100} + \frac{1}{240}g_{2000} - \frac{1}{12}g_{1010} + \frac{1}{3}g_{0110}\right. \\
&\qquad \left. - \frac{1}{30}g_{1100} + \frac{1}{2}g_{0020} + \frac{1}{120}f_{2000} + \frac{1}{3}f_{0200} - \frac{1}{3}f_{1010} + \frac{1}{12}g_{0200}\right), \\
&g_{0011} = -\frac{1}{2}g_{0101}, \quad f_{0011} = -\left(\frac{1}{2}f_{0101} + \frac{1}{6}g_{0101} + \frac{1}{2}g_{0011}\right).
\end{aligned}$$

Thus, we have the following Lemma (**cf.** [126],[88, Sec.9.5.2]):

Lemma 5.2. *For all sufficiently small $\|\nu\|$, the map (5.2) can be represented as*

$$u^T \mapsto \varphi_\nu^1(u) + \mathcal{O}\left(\|(u,\nu)\|^3\right), \tag{5.38}$$

where $\varphi_\nu^t(u)$ is the flow of a planer system

$$\dot{u}^T = \begin{pmatrix} 0 & 1 \\ 0 & 0 \end{pmatrix} u^T + \begin{pmatrix} -\frac{1}{2}\nu_1 \\ \nu_1 \end{pmatrix} + f_\nu^2(u), \tag{5.39}$$

where

$$f_\nu^2(u) = \begin{pmatrix} \xi_{00}(\nu) \\ \zeta_{00}(\nu) \end{pmatrix} + \begin{pmatrix} \xi_{10}(\nu)u_0 + \xi_{01}(\nu)u_1 \\ \zeta_{10}(\nu)u_0 + \zeta_{01}(\nu)u_1 \end{pmatrix} + \begin{pmatrix} \frac{1}{2}\xi_{20}u_0^2 + \xi_{11}u_0u_1 + \frac{1}{2}\xi_{02}u_1^2 \\ \frac{1}{2}\zeta_{20}u_0^2 + \zeta_{11}u_0u_1 + \frac{1}{2}\zeta_{02}u_1^2 \end{pmatrix}$$

and

$$\begin{aligned}
&\xi_{00}(\nu) = \frac{1}{20}\left(2\tilde{b} - \tilde{a}\right)\nu_1^2 + \frac{1}{3}\nu_1\nu_2, && \zeta_{00}(\nu) = \left(\frac{1}{30}\tilde{a} - \frac{1}{12}\tilde{b}\right)\nu_1^2 - \frac{1}{2}\nu_1\nu_2,\\
&\xi_{10}(\nu) = \left(\frac{1}{3}\tilde{b} - \frac{1}{2}\tilde{a}\right)\nu_1, && \zeta_{10}(\nu) = \left(\frac{2}{3}\tilde{a} - \frac{1}{2}\tilde{b}\right)\nu_1\\
&\xi_{01}(\nu) = \left(\frac{1}{5}\tilde{a} - \frac{5}{12}\tilde{b}\right)\nu_1 - \frac{1}{2}\nu_2, && \zeta_{01}(\nu) = \left(\frac{1}{2}\tilde{b} - \frac{1}{6}\tilde{a}\right)\nu_1 + \nu_2,\\
&\xi_{20} = -\tilde{a}, && \zeta_{20} = 2\tilde{a},\\
&\xi_{11} = \left(\frac{2}{3}\tilde{a} - \frac{1}{2}\tilde{b}\right), && \zeta_{11} = \left(\tilde{b} - \tilde{a}\right),\\
&\xi_{02} = \left(\frac{2}{3}\tilde{b} - \frac{1}{3}\tilde{a}\right), && \zeta_{02} = \frac{1}{3}\tilde{a} - \tilde{b},
\end{aligned}$$

Note that, if we reorder the terms of (5.39) according to (5.16), then up to the quadratic terms in (u,ν), the similar terms of the systems (5.26) and (5.39) are equivalent. On the other hand, the cubic term $\left(\frac{2}{3}\tilde{a}^2 - \frac{1}{2}\tilde{a}\tilde{b}\right)u_0^3$ in U_3 will be present in (5.39) if we perform two Picard's iterations to (5.32) and add the polynomial vector $\left(f_\nu^3(u), 0\right)^{\mathrm{T}}$ to (5.33). Also solving (5.25) for U_4 will give the terms for $u_0\nu_2$, $u_1\nu_2$ and $\nu_1\nu_2$ exactly as in (5.39). Thus the interpolating technique and the method of Picard iteration are equivalent, *i.e.*,

$$\sum_{i=1}^{\infty} U_i \equiv \begin{pmatrix} 0 & 1 \\ 0 & 0 \end{pmatrix} u^{\mathrm{T}} + \begin{pmatrix} -\frac{1}{2}\nu_1 \\ \nu_1 \end{pmatrix} + \sum_{i=2}^{\infty} f_\nu^i(u).$$

Next we compute the homoclinic solution of (5.39) following the procedure described in Section 2.3 and 3.5 (see also Section 3.6). It is clear that system (5.39) has a BT point $u = 0$ at $\nu = 0$. The Jacobian matrix of (5.39) evaluated at the BT point is

$$A = \begin{pmatrix} 0 & 1 \\ 0 & 0 \end{pmatrix}.$$

This matrix has a double-zero eigenvalue with the generalized eigenvectors $q_0 = (1, 0)$, $q_1 = (0, 1)$ and $p_1 = (0, 1)$, $p_0 = (1, 0)$ which satisfy (2.3) and (2.4). At the BT point, the R.H.S. of (5.39) can be expressed as (2.39a),

$$\dot{u}^{\mathrm{T}} = Au + J_1\nu + \frac{1}{2}B(u,u) + A_1(u,\nu) + \frac{1}{2}J_2(\nu,\nu) + \frac{1}{6}C(u,u,u) + \frac{1}{2}B_1(u,u,\nu) + \dots .$$

where

$$J_1 = \begin{pmatrix} -\frac{1}{2} & 0 \\ 1 & 0 \end{pmatrix}, \quad B(u,v) = \begin{pmatrix} \left(\frac{2}{3}\tilde{a} - \frac{1}{2}\tilde{b}\right)(u_1v_0 + u_0v_1) + \left(\frac{2}{3}\tilde{b} - \frac{1}{3}\tilde{a}\right)u_1v_1 - \tilde{a}u_0v_0 \\ \left(\tilde{b} - \tilde{a}\right)(u_1v_0 + u_0v_1) + \left(\frac{1}{3}\tilde{a} - \tilde{b}\right)u_1v_1 + 2\tilde{a}u_0v_0 \end{pmatrix},$$

$$A_1(u,\nu) = \begin{pmatrix} \left(\frac{1}{3}\tilde{b} - \frac{1}{2}\tilde{a}\right)u_0\nu_1 + \left(\frac{1}{5}\tilde{a} - \frac{5}{12}\tilde{b}\right)u_1\nu_1 - \frac{1}{2}u_1\nu_2 \\ \left(\frac{2}{3}\tilde{a} - \frac{1}{2}\tilde{b}\right)u_0\nu_1 + \left(\frac{1}{2}\tilde{b} - \frac{1}{6}\tilde{a}\right)u_1\nu_1 + u_1\nu_2 \end{pmatrix},$$

$$J_2(\nu,\mu) = \begin{pmatrix} \left(\frac{1}{5}\tilde{b} - \frac{1}{10}\tilde{a}\right)\nu_1\mu_1 + \frac{1}{3}\nu_2\mu_1 + \frac{1}{3}\nu_1\mu_2 \\ \left(\frac{1}{15}\tilde{a} - \frac{1}{6}\tilde{b}\right)\nu_1\mu_1 - \frac{1}{2}\nu_2\mu_1 - \frac{1}{2}\nu_1\mu_2 \end{pmatrix}, \quad B_1 = C = \begin{pmatrix} 0 \\ 0 \end{pmatrix}.$$

We compute the coefficients of (2.41), (2.43), (2.48), (2.59), (2.61), (2.62) and (2.64)-(2.69) using the MAPLE commands in Appendix A.5. These coefficients are found as follows

$$a = \tilde{a}, \qquad b = \tilde{b} - 2\tilde{a}, \qquad H_{2000} = \begin{pmatrix} \frac{5}{6}\tilde{a} - \tilde{b} \\ \tilde{a} \end{pmatrix}, \qquad H_{1100} = \frac{1}{2}\begin{pmatrix} 0 \\ \frac{1}{3}\tilde{a} - \tilde{b} \end{pmatrix},$$

$$H_{0200} = \frac{1}{3}\begin{pmatrix} 0 \\ \tilde{a} - 2\tilde{b} \end{pmatrix} \qquad H_{0010} = \frac{1}{2}\begin{pmatrix} -\dfrac{\tilde{b}}{2\tilde{a}} \\ 1 \end{pmatrix}, \qquad H_{0001} = \begin{pmatrix} 0 \\ 0 \end{pmatrix},$$

$$K_{1,0} = \begin{pmatrix} 1 \\ \dfrac{2\tilde{a}^2 - 5\tilde{a}\tilde{b} + \tilde{b}^2}{4\tilde{a}} \end{pmatrix}, \qquad K_{1,1} = \begin{pmatrix} 0 \\ 1 \end{pmatrix}, \quad K_2 = \begin{pmatrix} 0 \\ 0 \end{pmatrix}, \qquad H_{0002} = \begin{pmatrix} 0 \\ 0 \end{pmatrix},$$

$$H_{1001} = \begin{pmatrix} 0 \\ 0 \end{pmatrix}, \qquad H_{0101} = \begin{pmatrix} 0 \\ \frac{1}{2} \end{pmatrix}, \qquad d = \frac{1}{6}\tilde{a}^2, \qquad H_{3000} = \frac{1}{2}\begin{pmatrix} 0 \\ \tilde{a}^2 - 3\tilde{a}\tilde{b} \end{pmatrix},$$

$$e = \frac{4}{3}\tilde{a}\tilde{b} - \frac{2}{3}\tilde{a}^2 - \frac{1}{2}\tilde{b}^2, \qquad a_1 = 0, \qquad H_{2001} = \frac{1}{2}\begin{pmatrix} 0 \\ \tilde{a} \end{pmatrix}, \qquad b_1 = 0.$$

Substituting these values into (3.61) and (3.63) gives the following asymptotic for the homoclinic solution of (5.39),

$$\begin{pmatrix} u_0(t) \\ u_1(t) \end{pmatrix} = \begin{pmatrix} \frac{\varepsilon^2}{\tilde{a}} \left(2 - 6\,\mathrm{sech}^2(\varepsilon t)\right) \\ \frac{\varepsilon^3}{\tilde{a}} \left(12 \tanh(\varepsilon t)\,\mathrm{sech}^2(\varepsilon t)\right) \end{pmatrix} + \frac{\varepsilon^4}{\tilde{a}} H(t,\varepsilon) + \mathcal{O}\left(\varepsilon^5\right), \tag{5.40}$$

$$\begin{pmatrix} \nu_1 \\ \nu_2 \end{pmatrix} = \frac{\varepsilon^2}{\tilde{a}} \begin{pmatrix} 0 \\ \frac{10}{7}\left(\tilde{b} - 2\tilde{a}\right) \end{pmatrix} - \frac{\varepsilon^4}{\tilde{a}} \begin{pmatrix} 4 \\ \delta \end{pmatrix} + \mathcal{O}\left(\varepsilon^5\right), \tag{5.41}$$

where

$$H(t,\varepsilon) = \begin{pmatrix} \left(5 - \frac{6\tilde{b}}{\tilde{a}}\right) \frac{3}{\cosh^4(\varepsilon t)} + \left(\frac{220\tilde{b}}{\tilde{a}} - \frac{6\tilde{b}^2}{\tilde{a}^2} - \frac{391}{2}\right) \frac{3}{49\cosh^2(\varepsilon t)} - \frac{\tilde{b}}{\tilde{a}} + \frac{4}{3} \\ 2\left(1 - 3\,\mathrm{sech}^2(\varepsilon t)\right)^2 - \frac{72}{7\tilde{a}}\left(\tilde{b} - 2\tilde{a}\right) \tanh^2(\varepsilon t)\,\mathrm{sech}^2(\varepsilon t) - 2 \end{pmatrix} \tag{5.42}$$

and

$$\delta := \frac{1}{2401\tilde{a}^2}\left(\tilde{b} - 2\tilde{a}\right)\left(857\tilde{a}^2 - 3650\tilde{a}\tilde{b} - 288\tilde{b}^2\right) + \frac{2\tilde{a}^2 - 5\tilde{a}\tilde{b} + \tilde{b}^2}{\tilde{a}}. \tag{5.43}$$

Using $\varepsilon \approx \sqrt[4]{\frac{\tilde{a}(-\nu_1)}{4}}$, we obtain the following approximation for the homoclinic bifurcation curve of (5.39) in the parameter space (ν_1, ν_2):

$$\nu_2 = \frac{10\sqrt{-\nu_1}}{7\sqrt{2\tilde{a}}}\left(\tilde{b} - 2\tilde{a}\right) + \frac{1}{4}\delta\nu_1 + \mathcal{O}\left(|\nu_1|^{\frac{5}{4}}\right). \tag{5.44}$$

5.4 The homoclinic zone of the Bogdanov-Takens map

To check whether the homoclinic asymptotic parameters (5.31) and (5.44) are located inside the homoclinic zone of (5.2), we use the MATLAB interactive toolbox for numerical study of smooth maps MatContM to compute the stable and unstable manifolds of the saddle at the approximated homoclinic parameter. MatContM uses an algorithm originally adopted from [59] (for details on the algorithm used see [84]). We set $\tilde{a} = \tilde{b} = 1$ and $\nu_1 = -0.15$. Then we use the saddle point (5.28) and the asymptotics of the homoclinic parameter (5.31), (5.44) to obtain $(u_0^s, u_1^s) = (0.387298, 0)$ and $\nu_2 = -0.249762$, $\nu_2^0 = -0.276642$. The growing of the stable and unstable manifolds of the saddle (u_0^s, u_1^s) at (ν_1, ν_2^0) and (ν_1, ν_2) is shown in Figure 5.3a and Figure 5.3b, respectively. For $\nu_1 = -0.15$, it is clear that the predicted homoclinic parameter based on (5.31) is located outside the homoclinic zone of (5.2).

The result is not surprising because (5.31) is derived by the Melnikov method which gives the zero-order approximation for the homoclinic parameter. In Figure 5.3b the stable and unstable manifolds of the saddle (u_0^s, u_1^s) intersect transversally. This proves the usefulness of the new asymptotic (5.44).

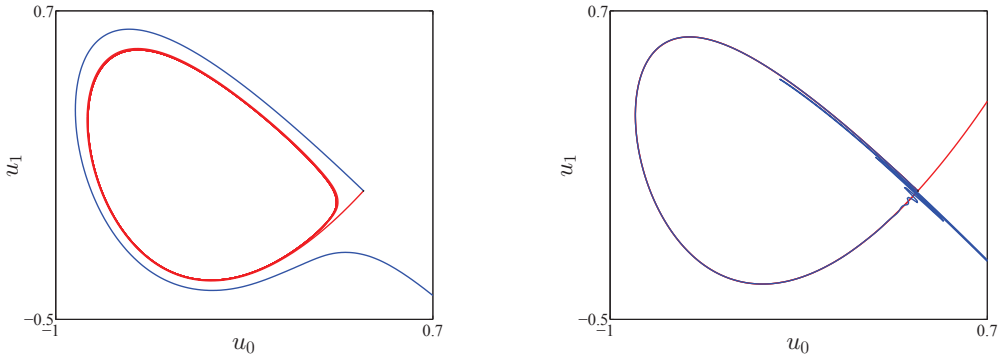

Figure 5.3: The growing of the stable and unstable manifolds of (5.1) for $\tilde{a} = \tilde{b} = 1$, $\nu_1 = -0.15$, $(u_0^s, u_1^s) = (0.387298, 0)$ and (a) $\nu_2^0 = -0.276642$, (b) $\nu_2 = -0.249762$.

The idea of continuing branches of homoclinic orbits and homoclinic tangencies, given a good starting point, was developed in [17, 18]. The algorithm implemented in MatContM can be used in the case of planar maps if an asymptotic of the homoclinic parameters exist. This algorithm is based on the existence of a finite number of intersection points of the stable and unstable manifolds of the saddle (i.e., the homoclinic points) (see [84]). Using MatContM we compute the intersection points of the manifolds presented in Figure 5.3b. These points are continued in one parameter (ν_1 freed while ν_2 is fixed) until two limit points are detected, which correspond to tangencies of the stable and unstable manifolds, see Figure 5.4a. Figure 5.4b and 5.4c show the corresponding tangential homoclinic orbit in the state space at the limit points LP_1 and LP_2 in Figure 5.4a, respectively. Continuation of such limit points in two parameters (ν_1, ν_2) gives the full homoclinic tangencies structure shown in Figure 5.4d.

Since we now have the whole homoclinic structure in the BT map, we can compare the numerically computed tangency branches with the asymptotic of the homoclinic curve (5.44) and the homoclinic curve obtained by (5.31) (see also [26, 66]), see Figure 5.5. This comparison demonstrates the accuracy of the present asymptotic (5.44). However the predicted curve is not always located in the homoclinic zone (i.e., between the homoclinic tangencies) so the homoclinic parameter should be carefully chosen.

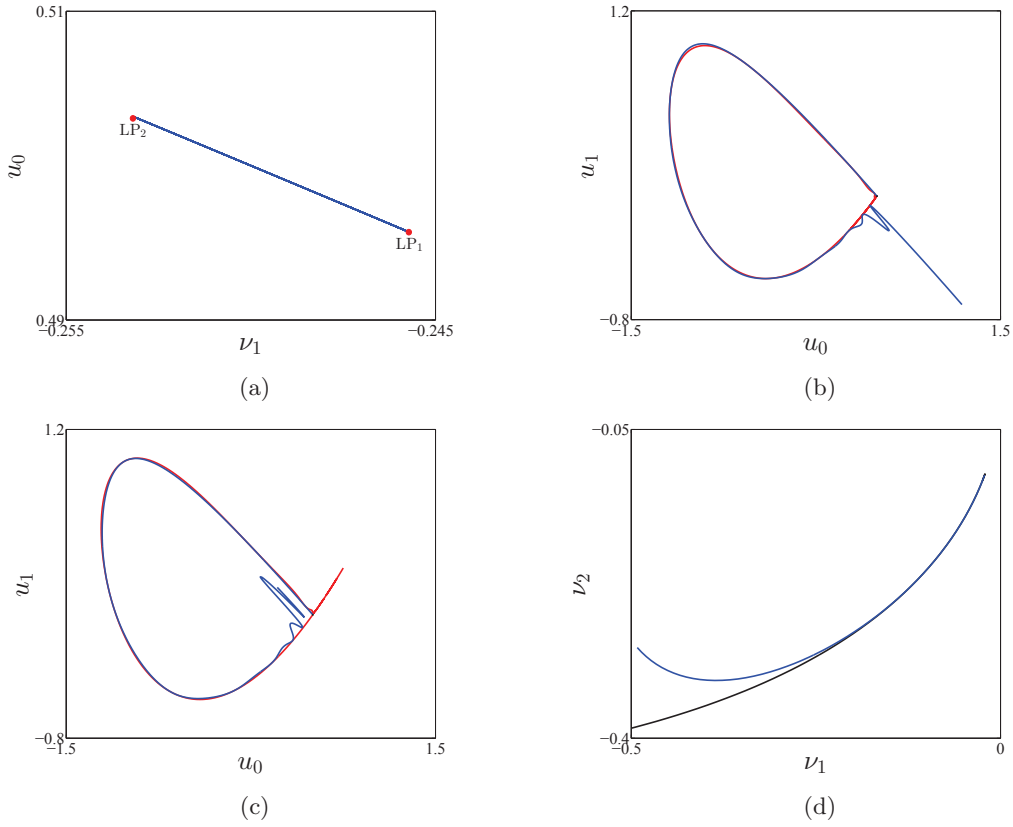

Figure 5.4: (a) The limit points are computed by continuing the homoclinic points in Figure 5.3b. During continuation, ν_1 is freed while ν_2 is fixed, (b) Stable and unstable manifolds along the first homoclinic tangential point (i.e., LP_1), (c) Stable and unstable manifolds along the second homoclinic tangential point (i.e., LP_2), (d) Two branches of the tangential homoclinic orbits are computed by continuing both of the LP's on Figure 5.4a with ν_1 and ν_2 free.

5.5 Homoclinic parameter in n-dimensional maps

For the BT map, we obtain an asymptotic for the homoclinic parameter at (ν_1, ν_2) which is given in (5.41). With the data collected in (5.7) and (5.9)-(5.14) we arrive at a generic asymptotic of the homoclinic parameter at the Bogdanov-Taken point of maps

$$\alpha(\varepsilon) = \frac{\varepsilon^2}{\tilde{a}} \frac{10}{7} \left(\tilde{b} - 2\tilde{a}\right) K_{1,1} - \frac{\varepsilon^4}{\tilde{a}} \left(4K_{1,0} + \delta K_{1,1} - \frac{50}{49} \frac{\left(\tilde{b} - 2\tilde{a}\right)^2}{\tilde{a}} K_2 \right) + \mathcal{O}(\varepsilon^5). \tag{5.45}$$

where δ is given in (5.43).

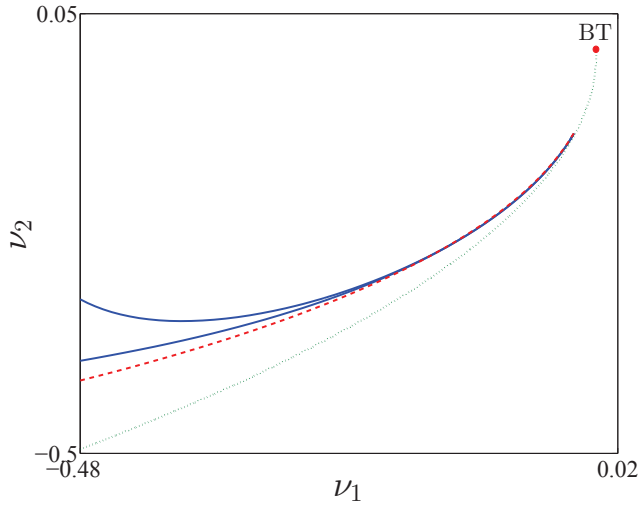

Figure 5.5: (a) The limit points are computed by continuing the homoclinic points in Figure 5.3b. During continuation, ν_1 is freed while ν_2 is fixed, (b) Stable and unstable manifolds along the first homoclinic tangential point (i.e., LP_1), (c) Stable and unstable manifolds along the second homoclinic tangential point (i.e., LP_2), (d) Two branches of the tangential homoclinic orbits are computed by continuing both of the LP's on Figure 5.4a with ν_1 and ν_2 free, (e) Branches of homoclinic tangencies (solid curves) of (5.2) are compared with: the asymptotic of the homoclinic curve (5.44) (dashed curve) and the homoclinic curve (5.31) (dotted curve) (see also [26, 64, 66]) to demonstrate the accuracy of the present asymptotic.

CHAPTER 6

The monopoly model

In this chapter we study the monopoly model with cubic price and quadratic marginal cost functions. A numerical continuation method is used to compute branches of solutions of period 5, 10, 13 and 17 and to determine the stability regions of these solutions. General formulas for solutions of period 4 are derived analytically. We show that the solutions of period 4 are never linearly asymptotically stable. A nonlinear stability criterion is combined with basin of attraction analysis and simulation to determine the stability region of the 4-cycles. This corrects the erroneous linear stability analysis in previous studies of the model. The chaotic and periodic behavior of the monopoly model is further analyzed by computing the largest Lyapunov exponents, and this confirms the above mentioned results.

6.1 Model description

During the last two decades increasing attention has been paid to the analysis of nonlinear dynamics of economic models using difference equations [74, 96, 112, 119, 134]. In particular, the monopoly model is well documented in [9, 111, 112]. Baumel and Quantdt [9] analyzed a cost-free monopoly model. They examined in both discrete and continuous systems the problem of maximizing the profit function.

T. Puu [111] assumes a cubic price and quadratic marginal cost function when the monopoly firm maximizes the profit using as strategic variable the produced quantity. In [111] the price p for a good is represented as a monotonically decreasing function

$$p(x) = A - Bx + Cx^2 - Dx^3, \tag{6.1}$$

of the produced quantity x. Decreasing is implied by requiring that $A, B, C, D > 0$ and $C^2 < 3BD$. The revenue of the monopolist is

$$R(x) = p(x)x. \tag{6.2}$$

The marginal revenue is then given by

$$MR := \frac{dR}{dx} = p + x\frac{dp}{dx}. \tag{6.3}$$

Also in [111], the marginal cost curve is assumed to be

$$MC = E - 2Fx + 3Gx^2, \tag{6.4}$$

where E, F and G are positive constants. A standard result of economic theory is that the profit is maximized at a point where $MR = MC$. The profit function is

$$\Pi(x) = (A - E)x - (B - F)x^2 + (C - G)x^3 - Dx^4 \tag{6.5}$$

up to a constant term. A simple algorithm to find the maximum of the not explicitly known function (6.5) is to evaluate (6.5) in the last two visited points x and y, and use a Newton-like iteration with step size δ. We get the next point as

$$\begin{aligned} y + \delta\frac{\Pi(y) - \Pi(x)}{y - x} = y + \delta\Big((A - E) - (B - F)(x + y) + (C - G)(x^2 + xy + y^2) \\ - D(x^3 + x^2y + xy^2 + y^3)\Big). \end{aligned} \tag{6.6}$$

The iteration of this procedure may lead to any of the profit maxima, to an oscillating process, or to chaos depending on the coefficients A through G and the step size δ. Following [111], we assume $A = 5.6$, $B = 2.7$, $C = 0.62$, $D = 0.05$, $E = 2$, $F = 0.3$ and $G = 0.02$. With these parameter values, the profit function (6.5) is symmetric about $(3, 3)$, i.e.,

$$\Pi(3 + x) = \Pi(3 - x), \tag{6.7}$$

for all x. The updating process (6.6) can be interpreted as the two-dimensional mapping

$$M : \begin{pmatrix} x_t \\ y_t \end{pmatrix} \mapsto \begin{pmatrix} x_{t+1} \\ y_{t+1} \end{pmatrix} = \begin{pmatrix} y_t \\ y_t + \delta P(x_t, y_t) \end{pmatrix}, \tag{6.8}$$

where

$$P(x, y) = 3.6 - 2.4(x + y) + 0.6(x^2 + xy + y^2) - 0.05(x^3 + x^2y + xy^2 + y^3). \tag{6.9}$$

The map has three steady states, which are extrema for the profit function, namely a local minimum and two local maxima. Puu [111, 112] provides incomplete information on the existence of cycles of period 4 and the chaotic behavior of (6.8). Most of the recent literature deals with simplified versions of the Puu model (6.8), cf. [1, 8, 98, 104], and none of them analyzes the dynamic behavior of the Puu model in detail. Naimzada and Ricchiuti [104] propose to use a demand function (6.1) without inflection point to achieve a one-dimensional map. Their model was generalized by Askar [8] and further by Matsumoto and Szidarovszky [98]. In these models the chaotic dynamic arises via a cascade of period-doubling bifurcations.

6.2 Dynamic analysis by simulation

A fixed point of (6.8) satisfies the equations

$$x = y, \tag{6.10}$$

$$y = y + \delta P(x, y). \tag{6.11}$$

Substituting (6.10) into (6.11), we find that

$$P(x, x) = 3.6 - 4.8x + 1.8x^2 - 0.2x^3 = 0, \tag{6.12}$$

with solutions $x = 3 \pm \sqrt{3}$ and $x = 3$. In fact, $\Pi(3 \pm \sqrt{3})$ are the maxima of $\Pi(x)$ and $\Pi(3)$ is the local minimum. To determine the stability of these points, we calculate the Jacobian matrix of (6.8)

$$J = \begin{pmatrix} 0 & 1 \\ \delta \frac{\partial P}{\partial x} & 1 + \delta \frac{\partial P}{\partial y} \end{pmatrix}. \tag{6.13}$$

The characteristic equation is

$$\rho(\lambda) = \lambda^2 - (1 + \delta \frac{\partial P}{\partial y})\lambda + \left(-\delta \frac{\partial P}{\partial x}\right) = 0. \tag{6.14}$$

We use the Jury test [81] to determine whether all roots of (6.14) lie in the open unit disk (i.e., $|\lambda| < 1$). The three conditions (Jury's stability criterion) are given by

$$\rho(1) = -\delta\frac{\partial P}{\partial y} - \delta\frac{\partial P}{\partial x} > 0, \tag{6.15}$$

$$\rho(-1) = 2 + \delta\frac{\partial P}{\partial y} - \delta\frac{\partial P}{\partial x} > 0, \tag{6.16}$$

$$-\delta\frac{\partial P}{\partial x} < 1. \tag{6.17}$$

The first condition is not satisfied for $x = 3$ since $\delta\frac{\partial P}{\partial x}|_{(3,3)} = \delta\frac{\partial P}{\partial y}|_{(3,3)} = 0.3\delta$, hence $\rho(1) < 0$ for all $\delta > 0$. Both fixed points $x = 3 \pm \sqrt{3}$ satisfy (6.15) and (6.16) since

$$\delta\frac{\partial P}{\partial x}|_{(3\pm\sqrt{3},3\pm\sqrt{3})} = \delta\frac{\partial P}{\partial y}|_{(3\pm\sqrt{3},3\pm\sqrt{3})} = -0.6\delta.$$

The fixed points $x = 3 \pm \sqrt{3}$ are therefore asymptotically stable if (6.17) is satisfied. This is the case iff $\delta \in \left(0, \frac{5}{3}\right)$. For $\delta = \frac{5}{3}$ we have $\lambda_{1,2} = \mathrm{e}^{\pm i\frac{\pi}{2}}$. So we have a (non-generic) 1:4 resonant Neimark-Sacker (NS) bifurcation. The same results were derived in [111] using a different method.

Figure 6.1a plots the bifurcation diagram of (6.8) with $\delta \in [1.5, 4]$[†].. For each δ the initial points were reset to $(x_0, y_0) = \{(3 \pm \varepsilon, 3 \pm \varepsilon), (3, 3)\}$, $\varepsilon = \sqrt{3} - 10^{-5}$, 10^5 map iterations were performed and transients were discarded. This leads to a crude bifurcation diagram that will be refined by a continuation method in Section 6.3. It is remarkable that as we exceed the NS value $\delta = \frac{5}{3}$ a cycle of period-4 is born. The fixed point $x = 3$ forms the middle line.

We see that for $\delta \in]0, \frac{5}{3}[$, (x_n, y_n) converges to a nonzero steady state and for $\delta > \frac{5}{3}$ cycles of period 4 are born. These cycles are indicated by three upper branches and three lower branches in Figure 6.1a. The middle upper and lower branches in Figure 6.1a are visited twice. Two typical 4-cycles are presented in Figure 6.2 for $\delta = 2.44$. In Section 6.4.3 we will see that the 4-cycles lose stability only for $\delta > -\frac{5}{2} + \frac{25}{18}\sqrt{21} \approx 3.8647$ but for $\delta > 2.62$ the radius of attraction is very small.

For δ around 2.45 a stable cycle of period 17 exists, see Figure 6.3a and Figure 6.3b.

For $\delta = 2.62$, the radius of convergence of the stable 4-cycle is very small and there is a nearby chaotic attractor in which a "ghost of 4-cycle" is still present, see Figure 6.4a.

[†]The Figure was produced using the MATLAB code in Appendix B.1

For δ around 2.63, a stable cycle of period 5 exists, see Figure 6.5a. At δ around 2.7, a stable cycle of period-10 exists, see Figure 6.5b.

For δ around 2.83 we find a stable cycle of period 13, see Figure 6.6 and Figure 6.1c.

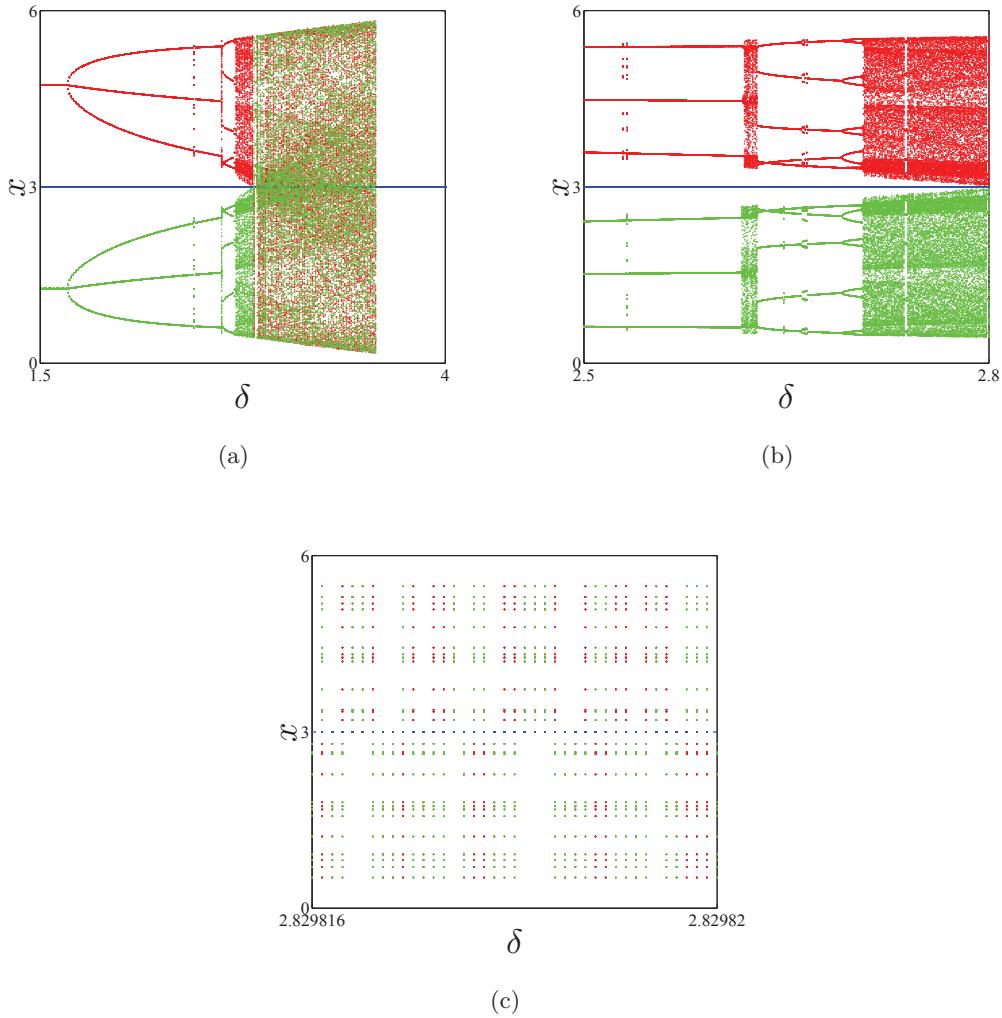

Figure 6.1: Bifurcation diagram of (6.8). For each δ the initial points were reset to $(x_0, y_0) = \{(3 \pm \varepsilon, 3 \pm \varepsilon), (3, 3)\}$, $\varepsilon = \sqrt{3} - 10^{-5}$ and transients were discarded. (a) $\delta \in [1.5, 2.8]$ with step size 1×10^{-2} and 1×10^5 map iterations were performed, (b) $\delta \in [2.5, 2.8]$ with step size 1×10^{-5} and 2×10^5 map iterations were performed, (c) $\delta \in [2.829816, 2.829820]$ with step size 1×10^{-7} and 5×10^5 map iterations were performed. The bifurcation diagrams show the existence of solutions of period 4, 5, 10, 13 and 17.

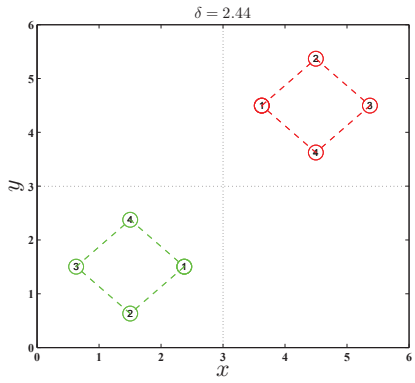

Figure 6.2: Two cycles of period-4 for $\delta = 2.44$. The cycles are point-symmetric around $(3, 3)$.

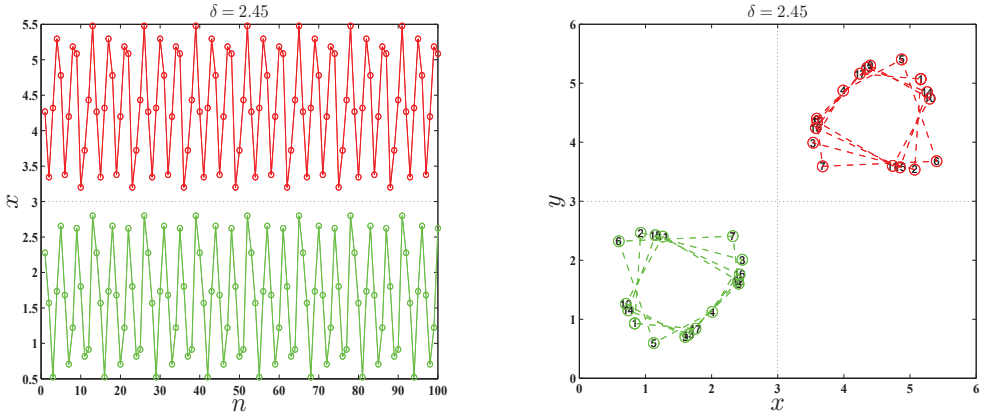

(a) (b)

Figure 6.3: (a) Two cycles of period-17 for $\delta = 2.45$ as a time series of x_n vs n. (b) The same cycles of period-17 in (x_n, y_n)-plane. The 5-cycles are point-symmetric around $(3, 3)$.

6.3 Analysis by numerical continuation

We perform a numerical stability analysis for the cycles of period 5, 10, 13 and 17 of (6.8). The stability analysis is based on a continuation method and uses the MATLAB package MatContM, see [71, 84]. For the cycles of period 5, 10, 13 and 17, and using the initial data in Table 6.1, we continue each cycle with free parameter δ. The continuation of each cycle leads to a closed curve of cycles. Limit point (LP), branch point (BP) and period-doubling (PD) bifurcations are found along these curves, see Figure 6.7.

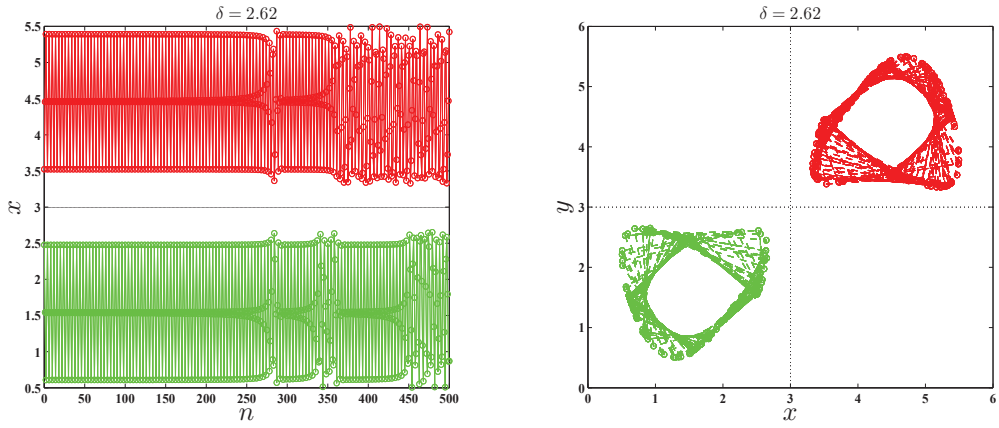

(a) (b)

Figure 6.4: (a) and (b) A chaotic attractor for $\delta = 2.62$. Note that this coexists with a 4 cycle.

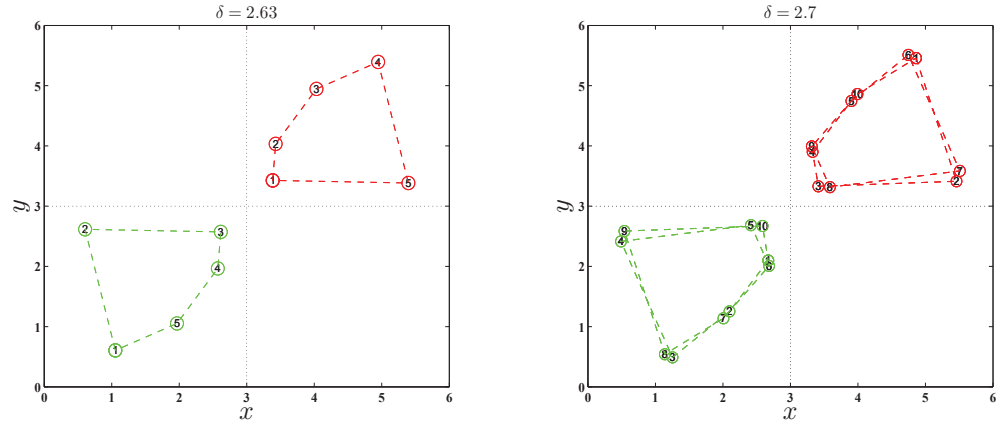

(a) (b)

Figure 6.5: (a) A cycle of period-5 for $\delta = 2.63$. (b) A cycle of period-10 for $\delta = 2.7$. It obviously arises from a period-doubling of a 5-cycle.

The computed bifurcation points on the computed curves are summarized in Table 6.2. The stability regions of the 5, 10, 13 and 17-cycles are bounded by the LP and PD points. The 10-cycles are stable in the regions bounded by the BP and PD points. The 5, 10, 13 and 17-cycles are unstable between two successive LP points or two successive PD points. Table 6.3 shows the stability regions for each cycle.

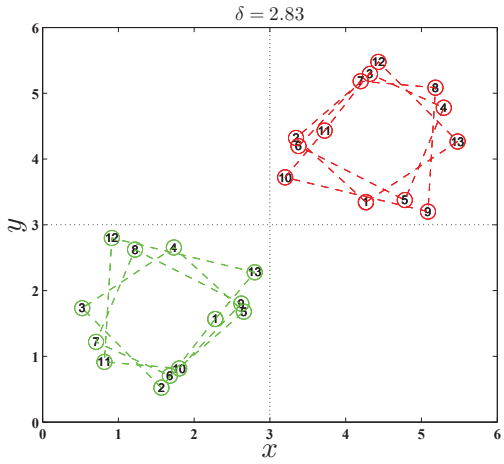

Figure 6.6: A cycle of period-13 for $\delta = 2.83$.

A branch point (BP2) on the 10-cycle curve is given by $(x, y) = (3.687975, 4.210773)$ and $\delta = 3.525215732$. Clearly the stable 10-cycles arise from a period-doubling of 5-cycles. The 10-cycle presented in Figure 6.7b arises from the PD2 point with $x = 3.687975$ on the 5-cycle curve. The same point is labeled as BP2 at the 10-cycle curve. The existence of PD bifurcations on the 10, 13, and 17-cycles indicates the existence of cycles of higher periods as well.

	5-Cycle	**10-Cycle**	**13-Cycle**	**17-Cycle**
$\boldsymbol{\delta}$	2.63	2.7	2.83	2.45
$\boldsymbol{x}$	5.39438	3.99216	5.47699	4.24294
$\boldsymbol{y}$	3.38445	4.86040	4.26739	5.16145

Table 6.1: One point on the 5,10,13,17-cycles.

	LP1	**BP1**	**PD1**	**PD2**	**PD3**	**LP2**	**PD4**	**BP2**
5-Cycle	2.62813		2.69111	3.52522		3.52573		
10-Cycle	2.80134	2.69111	2.70485	2.80214	3.12750	3.12753	3.52149	3.52522
13-Cycle	2.47864		2.48136	2.82987		2.83005		
17-Cycle	2.44977		2.45042	2.76425		2.76432		

Table 6.2: The bifurcation points on the continuation curves of the 5,10,13,17-cycles with the corresponding value of δ.

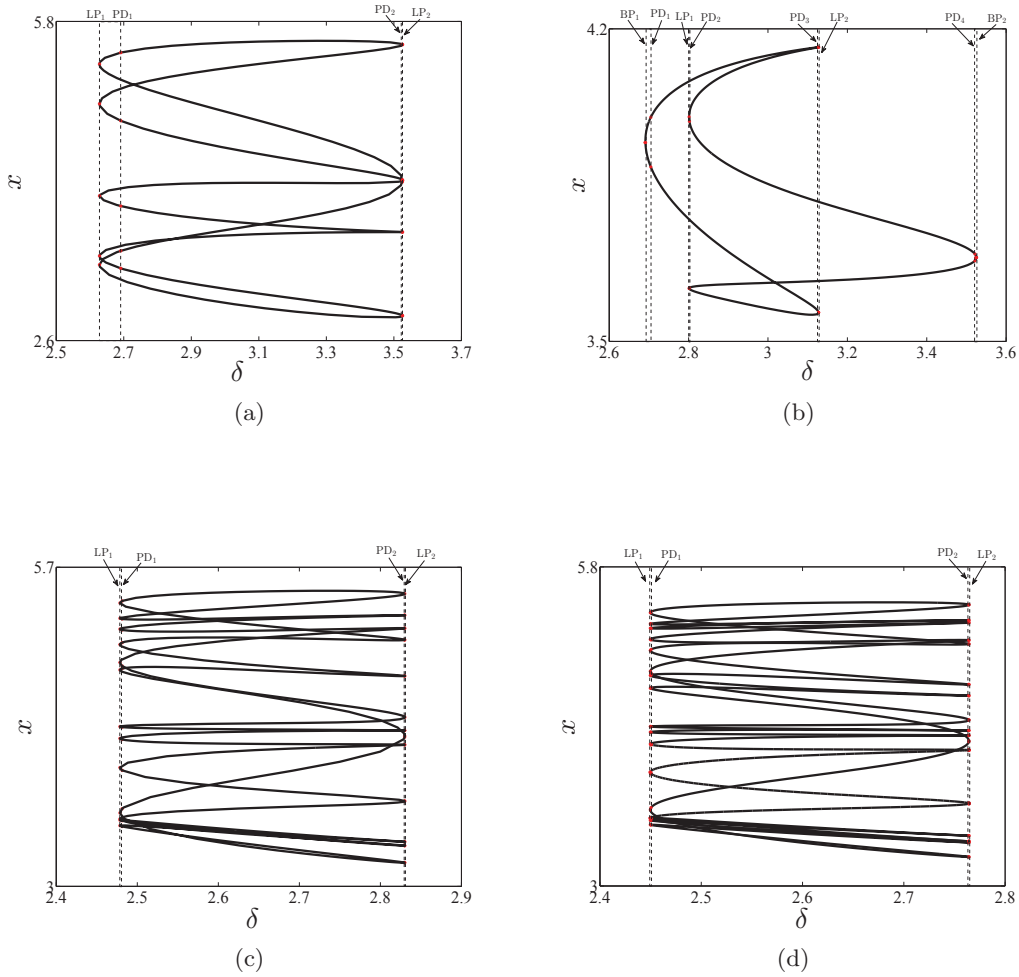

Figure 6.7: Bifurcation diagram in (δ, x)-plane of period-5 (a), period-10 (b), period-13 (c) and period-17 (d) cycles.

6.4 The existence of period-4 solutions

We now explore the existence of period-4 cycles in (6.8). We introduce the following general cycle notation

$$\begin{pmatrix} x \\ y \end{pmatrix} \to \begin{pmatrix} y \\ z \end{pmatrix} \to \begin{pmatrix} z \\ w \end{pmatrix} \to \begin{pmatrix} w \\ x \end{pmatrix} \to \begin{pmatrix} x \\ y \end{pmatrix}. \tag{6.18}$$

	Stable for δ in
5-Cycle	$(2.62813, 2.69111) \cup (3.52522, 3.52573)$
10-Cycle	$(2.69817, 2.70485) \cup (2.80134, 2.80214) \cup (3.12750, 3.12753) \cup (3.52149, 3.52522)$
13-Cycle	$(2.47864, 2.48136) \cup (2.82987, 2.83005)$
17-Cycle	$(2.44977, 2.45042) \cup (2.76425, 2.76432)$

Table 6.3: Stability regions of the 5,10,13 and 17-cycles of the monopoly model.

It follows from (6.10) and (6.11) that

$$z = y + \delta P(x, y), \tag{6.19}$$

$$w = z + \delta P(y, z), \tag{6.20}$$

$$x = w + \delta P(z, w), \tag{6.21}$$

$$y = x + \delta P(w, x). \tag{6.22}$$

6.4.1 The solutions

To investigate the case where one of the ordered pairs in (6.18) has two equal components, i.e., $x = y$ or $y = z$ or $z = w$ or $w = x$, we solve system (6.19) - (6.22) for $z = w$ (the other cases follow by cyclicity). Substituting $z = w$ into (6.19) - (6.22) gives

$$z - y = \delta P(x, y), \tag{6.23}$$

$$0 = \delta P(y, z), \tag{6.24}$$

$$x - z = \delta P(z, z), \tag{6.25}$$

$$y - x = \delta P(z, x). \tag{6.26}$$

or

$$(z - y)(y - x) = \delta(y - x)P(x, y), \tag{6.27}$$

$$0 = \delta(z - y)P(y, z), \tag{6.28}$$

$$(x - z) = \delta P(z, z), \tag{6.29}$$

$$(y - x)(x - z) = \delta(x - z)P(z, x). \tag{6.30}$$

Adding (6.27) to (6.28), we get

$$(z-y)(y-x) = -\delta(x-z)P(z,x). \tag{6.31}$$

From (6.30) it now follows that $x = y$. Plugging $x = y$ into (6.23)-(6.26), we obtain

$$z - y = \delta P(y,y), \tag{6.32}$$

$$y - z = \delta P(z,z), \tag{6.33}$$

$$0 = \delta P(y,z). \tag{6.34}$$

The set of equations (6.32)-(6.34) has the solutions

$$(y,z) = \begin{cases} (3,3), \left(3 \pm \sqrt{3}, 3 \pm \sqrt{3}\right) & \text{if} \quad \delta > 0, \\ \left(3 \pm \frac{\sqrt{3\delta^2+10\delta}}{\delta}, 3 \mp \frac{\sqrt{3\delta^2+10\delta}}{\delta}\right) & \text{if} \quad \delta \geq \frac{5}{3}. \end{cases} \tag{6.35}$$

The solutions for which $y = z$ are the fixed points of (6.8) and can be ignored. So, the general solution of period 4 for which two successive ordered pairs of cycle (6.18) have the same first component is given by

$$\begin{pmatrix} x \\ y \\ z \\ w \end{pmatrix} = \begin{pmatrix} 3 \pm \frac{\sqrt{3\delta^2+10\delta}}{\delta}, \\ x \\ 3 \mp \frac{\sqrt{3\delta^2+10\delta}}{\delta} \\ z \end{pmatrix}. \tag{6.36}$$

Figure 6.8 shows a plot of (6.36) for $\delta = 2$.

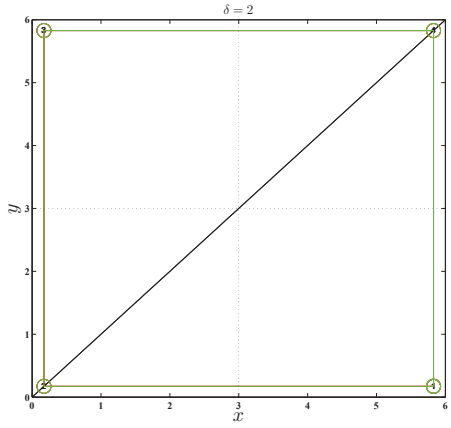

Figure 6.8: A cycle of period 4 for $\delta = 2$.

Now suppose that $x \neq y$, $y \neq z$, $z \neq w$ and $w \neq x$ in (6.18). Thus, system (6.19)-(6.22) is equivalent to

$$(z-y)(y-x) = \delta(y-x)P(x,y), \tag{6.37}$$

$$(w-z)(z-y) = \delta(z-y)P(y,z), \tag{6.38}$$

$$(x-w)(w-z) = \delta(w-z)P(z,w), \tag{6.39}$$

$$(y-x)(x-w) = \delta(x-w)P(w,x). \tag{6.40}$$

Adding (6.37) to (6.38), (6.38) to (6.39), (6.39) to (6.40), (6.40) to (6.37), we get

$$(z-y)(y-x+w-z) = \delta(z-x)P(x,z), \tag{6.41}$$

$$-(w-z)(y-x+w-z) = \delta(w-y)P(y,w), \tag{6.42}$$

$$(x-w)(y-x+w-z) = \delta(x-z)P(x,z), \tag{6.43}$$

$$-(y-x)(y-x+w-z) = \delta(y-w)P(y,w). \tag{6.44}$$

We now distinguish two cases:

6.4.1.1 Case 1: $x = z$

If $x = z$, we can solve system (6.41)-(6.44) for $\{y, z, w\}$ and obtain two solutions:

$$\begin{cases} \begin{pmatrix} x \\ y \\ z \\ w \end{pmatrix} = \begin{pmatrix} \frac{0.2(15\delta+r)}{\delta} \\ \frac{-0.2\left(15\delta+r+2\sqrt{15\delta^2-25\delta}\right)}{\delta} + \frac{0.4(15\delta+r)}{\delta} \\ x \\ \frac{0.2\left(15\delta+r+2\sqrt{15\delta^2-25\delta}\right)}{\delta} \end{pmatrix}, \\ \begin{pmatrix} x \\ y \\ z \\ w \end{pmatrix} = \begin{pmatrix} \frac{0.2(15\delta-r)}{\delta} \\ \frac{-0.2\left(15\delta-r-2\sqrt{15\delta^2-25\delta}\right)}{\delta} + \frac{0.4(15\delta-r)}{\delta} \\ x \\ \frac{0.2\left(15\delta-r-2\sqrt{15\delta^2-25\delta}\right)}{\delta} \end{pmatrix}, \end{cases} \tag{6.45}$$

where $r = \sqrt{15\delta^2 + 100\delta}$. This case has been studied by J. Vandenameele [128]. She derived the first 4-cycle in (6.45).

6.4.1.2 Case 2: $x \neq z$

If $x \neq z$, we have

$$\frac{(x-w)}{(x-z)} = \frac{(z-y)}{(z-x)}, \tag{6.46}$$

i.e.,

$$x = w - z + y. \tag{6.47}$$

Plugging (6.47) for x in (6.41)-(6.44) and solving this system for $\{y, z, w\}$, we get another formula for two-cycles of period-4:

$$\begin{cases} \begin{pmatrix} x \\ y \\ z \\ w \end{pmatrix} = \begin{pmatrix} \frac{27\delta^2-120\delta+\frac{4}{5}s\sqrt{\delta(20s+75\delta)}-3\sqrt{\delta(20s+75\delta)}\delta}{(9\delta-40)\delta} \\ \frac{27\delta^2-120\delta+\frac{2}{5}s\sqrt{\delta(20s+75\delta)}-\frac{3}{5}\sqrt{\delta(20s+75\delta)}\delta-4\sqrt{\delta(20s+75\delta)}}{(9\delta-40)\delta} \\ 3+\frac{1}{5}\frac{\sqrt{\delta(20s+75\delta)}}{\delta} \\ y \end{pmatrix}, \\ \begin{pmatrix} x \\ y \\ z \\ w \end{pmatrix} = \begin{pmatrix} \frac{27\delta^2-120\delta-\frac{4}{5}s\sqrt{\delta(20s+75\delta)}+3\sqrt{\delta(20s+75\delta)}\delta}{(9\delta-40)\delta} \\ \frac{27\delta^2-120\delta-\frac{2}{5}s\sqrt{\delta(20s+75\delta)}+\frac{3}{5}\sqrt{\delta(20s+75\delta)}\delta+4\sqrt{\delta(20s+75\delta)}}{(9\delta-40)\delta} \\ 3-\frac{1}{5}\frac{\sqrt{\delta(20s+75\delta)}}{\delta} \\ y \end{pmatrix}, \end{cases} \tag{6.48}$$

where $s = \sqrt{9\delta^2 + 45\delta - 100}$.

6.4.2 The symmetry property

The 4-cycles (6.36) (the stars), (6.45) (the black points) and (6.48) (the black points) are shown in Figure 6.9. The 4-cycles (6.45), (6.48) differ only in the choice of the first point of the cycle. Figure 6.9 possesses a point symmetry around $(3, 3)$ i.e., the upper 4-cycle is obtained by a rotation of the lower one over 180^o.

The vertices of each 4-cycle form a perfect square. The points $c_1 = \left(\frac{0.2(15\delta+r)}{\delta}, \frac{0.2(15\delta+r)}{\delta}\right)$ and $c_2 = \left(\frac{0.2(15\delta-r)}{\delta}, \frac{0.2(15\delta-r)}{\delta}\right)$ are the center points of the upper and lower square respectively; $c = (3, 3)$ is the center point for the big square.

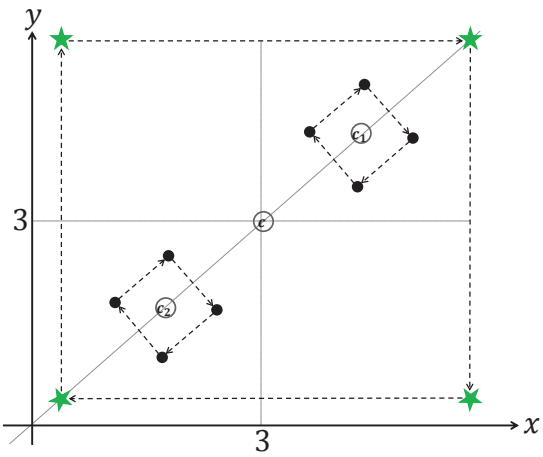

Figure 6.9: The general diagram for the 4-cycle (6.36) (the stars), (6.45) and (6.48) (the black points). The 4-cycles (6.45), (6.48) differ only in the choice of the first point of the cycle.

6.4.3 Stability analysis

The next step is to determine the stability of the cycles in Section 6.4.1.

Consider the 4-cycle (6.36). The Jacobian of the 4-cycle is the product of the Jacobians evaluated at each point of the cycle (6.36), i.e.,

$$J_{4,1} = J(w,x)J(z,w)J(y,z)J(x,y), \tag{6.49}$$

where

$$J(x,y) = \begin{pmatrix} 0 & 1 \\ \delta\frac{\partial}{\partial x}P(x,y) & 1+\delta\frac{\partial}{\partial y}P(x,y) \end{pmatrix}$$

and the other Jacobians follow by cyclicity.

After some computations we find

$$J_{4,1} = \begin{pmatrix} 0.36\delta^2+3.6\delta+9 & 0.36\delta^2+3.6\delta+8 \\ 0 & 1 \end{pmatrix}, \tag{6.50}$$

with eigenvalues

$$\lambda_{1,2} = \{1, 0.36\delta^2+3.6\delta+9\}. \tag{6.51}$$

The second eigenvalue is always greater than 1 for $\delta \geq \frac{5}{3}$. So the 4-cycle system (6.36) is unstable.

On the other hand, for the first 4-cycle in (6.45) (the same results hold for the second 4-cycle) the Jacobian matrix is given by

$$J_{4,2} = \begin{pmatrix} A & B \\ C & D \end{pmatrix}, \tag{6.52}$$

where

$$\begin{aligned}
A &= -\frac{144}{15625}\sigma\psi\delta + \frac{36}{3125}\delta^2 - \frac{216}{15625}\delta^3 + \frac{348}{625}\delta - \frac{84}{3125}\sigma\psi + \frac{13}{125} + \frac{44}{625}\frac{\sigma\psi}{\delta},\\
B &= -\frac{216}{15625}\sigma\psi\delta - \frac{36}{125}\delta^2 - \frac{276}{3125}\sigma\psi - \frac{36}{25}\delta + \frac{116}{625}\frac{\sigma\psi}{\delta} + \frac{16}{5},\\
C &= \frac{432}{390625}\sigma\psi\delta^2 + \frac{3024}{78125}\delta^3 + \frac{2592}{390625}\delta^4 - \frac{252}{15625}\delta^2 - \frac{792}{78125}\sigma\psi\delta\\
&\quad + \frac{276}{3125}\delta - \frac{1116}{15625}\sigma\psi - \frac{208}{625} + \frac{444}{3125}\frac{\sigma\psi}{\delta},\\
D &= \frac{3888}{390625}\delta^4 + \frac{8856}{78125}\delta^3 + \frac{144}{15625}\sigma\psi\delta - \frac{3348}{15625}\delta^2 + \frac{84}{3125}\sigma\psi - \frac{8796}{3125}\delta - \frac{44}{625}\frac{\sigma\psi}{\delta} + \frac{3553}{625},
\end{aligned}$$

and $\psi = \sqrt{3\delta^2 - 5\delta}$, $\sigma = \sqrt{3\delta^2 + 20\delta}$. The characteristic equation is

$$\rho_{4,2}(\lambda) = \lambda^2 - (k+1)\lambda + k = 0. \tag{6.53}$$

where

$$k = \frac{3888}{390625}\delta^4 + \frac{7776}{78125}\delta^3 - \frac{3168}{15625}\delta^2 - \frac{7056}{3125}\delta + \frac{2993}{625}.$$

At any point (ξ, η) of the 4-cycle (6.45), there are two eigenvalues

$$\lambda_{1,2} = \{1, k\}. \tag{6.54}$$

From (6.54) we infer the following results on the stability and bifurcations of the 4-cycle system (6.45):

- For $\frac{5}{3} < \delta < \frac{-5}{2} + \frac{25}{18}\sqrt{21}$, there are two eigenvalues $\lambda_1 = 1$ and $|\lambda_2| < 1$.
- At $\delta = \frac{-5}{2} + \frac{25}{18}\sqrt{21}$ a resonant 1:1 NS bifurcation occurs at

$$(x, y) = \left(3 + \frac{3\sqrt{26 + 2\sqrt{21}}}{-9 + 5\sqrt{21}}, 3 + \frac{3\sqrt{26 + 2\sqrt{21}} - 12\sqrt{11 - 2\sqrt{21}}}{-9 + 5\sqrt{21}}\right).$$

- For $\delta > \frac{-5}{2} + \frac{25}{18}\sqrt{21}$, there are two real eigenvalues $\lambda_1 = 1$ and $|\lambda_2| > 1$, and hence, the 4-cycle is unstable.

Since there is always an eigenvalue 1, the 4-cycle is never linearly asymptotically stable.The stability and the existence of bifurcation points for $\frac{5}{3} < \delta < \frac{-5}{2} + \frac{25}{18}\sqrt{21}$ are determined by the stability analysis in the direction of the eigenvector corresponding to $\lambda_1 = 1$. Let $(x, y)^{\mathrm{T}}$ be a fixed point of the fourth iterate of (6.8). For $0 < \varepsilon \ll 1$, let εv be a small perturbation of $(x, y)^{\mathrm{T}}$ where v is the unit right eigenvector corresponding to the eigenvalue one. We decompose

$$M^4\left((x,y)^{\mathrm{T}} + \varepsilon v\right) = \alpha_\varepsilon v + \beta_\varepsilon w + (x,y)^{\mathrm{T}}, \tag{6.55}$$

where α_ε, β_ε are scalars and w is an eigenvector corresponding to λ_2. Taking inner products of (6.55) with the left eigenvector v^l corresponding to the eigenvalue one, we get

$$\alpha_\varepsilon = \frac{(v^l)^{\mathrm{T}}\left[M^4\left((x,y)^{\mathrm{T}} + \varepsilon v\right) - (x,y)^{\mathrm{T}}\right]}{(v^l)^{\mathrm{T}} v}, \tag{6.56}$$

In the sense of the definition of the stability on a specific eigenvector of the linearized system at the fixed point (see for example [97, Chapter 2]), the 4-cycle at the fixed point $(x, y)^{\mathrm{T}}$ is stable in the direction v if $|\alpha_\varepsilon| < \varepsilon$ for all sufficiently small ε. Moreover, the fixed point $(x, y)^{\mathrm{T}}$ of the 4-cycle is unstable in the direction of v if $|\alpha_\varepsilon| > \varepsilon$ for all small enough values of ε. The vectors v and v^l are given by:

$$v = \begin{pmatrix} -\dfrac{375\delta^2 + 18\delta\sigma\psi + 2500\delta + 145\sigma\psi}{18\delta^3 + 15\delta^2 + 12\delta\sigma\psi - 700\delta + 55\sigma\psi} \\ 1 \end{pmatrix}, \tag{6.57}$$

$$v^l = \begin{pmatrix} \dfrac{\frac{36}{25}\sigma\psi\delta^2 + \frac{216}{25}\delta^4 - \frac{54}{5}\sigma\psi\delta + \frac{324}{5}\delta^3 - 111\sigma\psi + 87\delta^2 + 260\delta}{18\delta^3 + 15\delta^2 + 12\delta\sigma\psi - 700\delta + 55\sigma\psi} \\ 1 \end{pmatrix}. \tag{6.58}$$

Using MATLAB, we compute numerically the value α_ε for a large number of values of $\delta \in]\frac{5}{3}, 5[$ ($33,324$ points, uniformly distributed) for $\varepsilon = 10^{-2}$ and 10^{-6}. The results are presented in Figure 6.10. The 4-cycles where $|\alpha_\varepsilon| < \varepsilon$ are plotted in green. The 4-cycles where $|\alpha_\varepsilon| > \varepsilon$ are plotted in blue. The first labeled points are those where $|\alpha| - \varepsilon$ changes sign. The second labeled points indicate the resonant 1:1 NS point for which $\delta = \frac{-5}{2} + \frac{25}{18}\sqrt{21}$. We see that the change of sign happens for increasing values of δ if ε tends to zero. By numerical simulation for a large number of initial points computed by (6.45) for different values of δ in the range $[2.71, 3.9]$ we find that the 4-cycle is stable for all values of δ smaller than the value of the bifurcation point (i.e., the resonant 1:1 NS point) but with a very small domain of attraction. Figure 6.11b shows what happens if we round the initial point in Figure 6.11a to 8 digits: the initial point is no longer in the domain of attraction of the 4-cycle. For all δ greater than the value of the bifurcation point the 4-cycle is unstable, see Figure 6.11c.

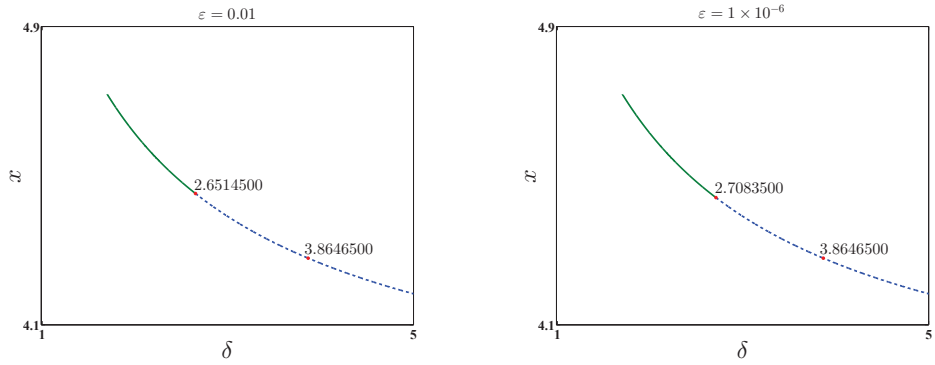

(a) (b)

Figure 6.10: (a) Stability analysis for the 4-cycle (6.45) using $\delta \in [1.7, 5]$ with step size 10^{-4}. Solid curve where points $|\alpha_\varepsilon| < \epsilon$; Dashed curve where points $|\alpha_\varepsilon| > \epsilon$. In the first labeled points $|\alpha_\varepsilon| - \epsilon$ changes sign.

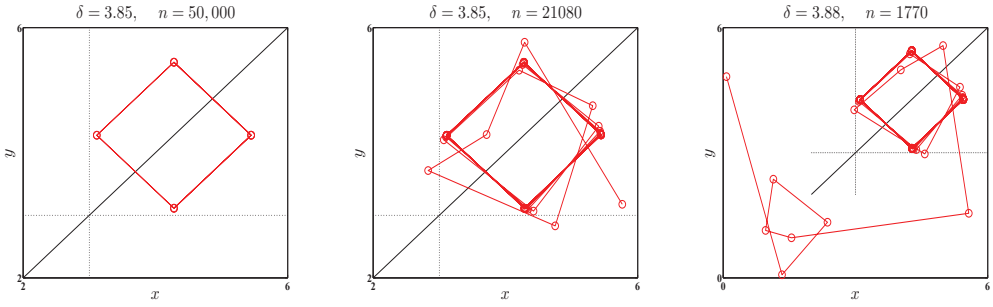

(a) (b) (c)

Figure 6.11: (a) Stable 4-cycle for $\delta = 3.85$ where the initial point is computed by (6.45), exact to machine precision. (b) Behavior if the initial point in (a) is rounded to 8 digits $[(x_0, y_0) = (4.28021914, 3.11358339)]$: the point is no longer in the domain of attraction of the 4-cycle, (c) Unstable 4-cycle for $\delta = 3.88$ with initial point exact to machine precision.

To further corroborate this result, we explore the "basin of attraction".

Definition 6.1. *[4] Let f be a smooth map on $\mathbb{R}^n$ and let x_i be a point or periodic orbit for f. Then basin of attraction of x_i, or just basin of x_i, is the set of points x such that*

$$|f^k(x) - f^k(x_i)| \to 0, \text{ as } k \to \infty.$$

The basin of attraction of the 4-cycles (6.45) is computed by performing 10^5 map iterations at 40,000 different initial points located in the range $[-1, 7] \times [-1, 7]$. Figure 6.12 shows the

basins of attraction of the 4-cycles (6.45) for four values of δ. The points in the attraction domain of the first 4-cycle in (6.45) are colored red, in the second 4-cycle green. The yellow points are these where no convergence was established after 10^5 iterations. For $\delta \leq 2.6$ the basin of attraction is connected, then it shrinks and contains holes. Already for $\delta = 2.615$ there are points very close to the 4-cycle which are not in its domain of attraction. However, numerical simulations show that even for values of δ slightly smaller than $\frac{-5}{2} + \frac{25}{18}\sqrt{21}$ the 4-cycle has a small radius of attraction, which is not the case for values slightly larger than $\frac{-5}{2} + \frac{25}{18}\sqrt{21}$. So the loss of stability of the 4-cycle is, in fact, caused by a 1:1 resonant Neimark-Sacker bifurcation.

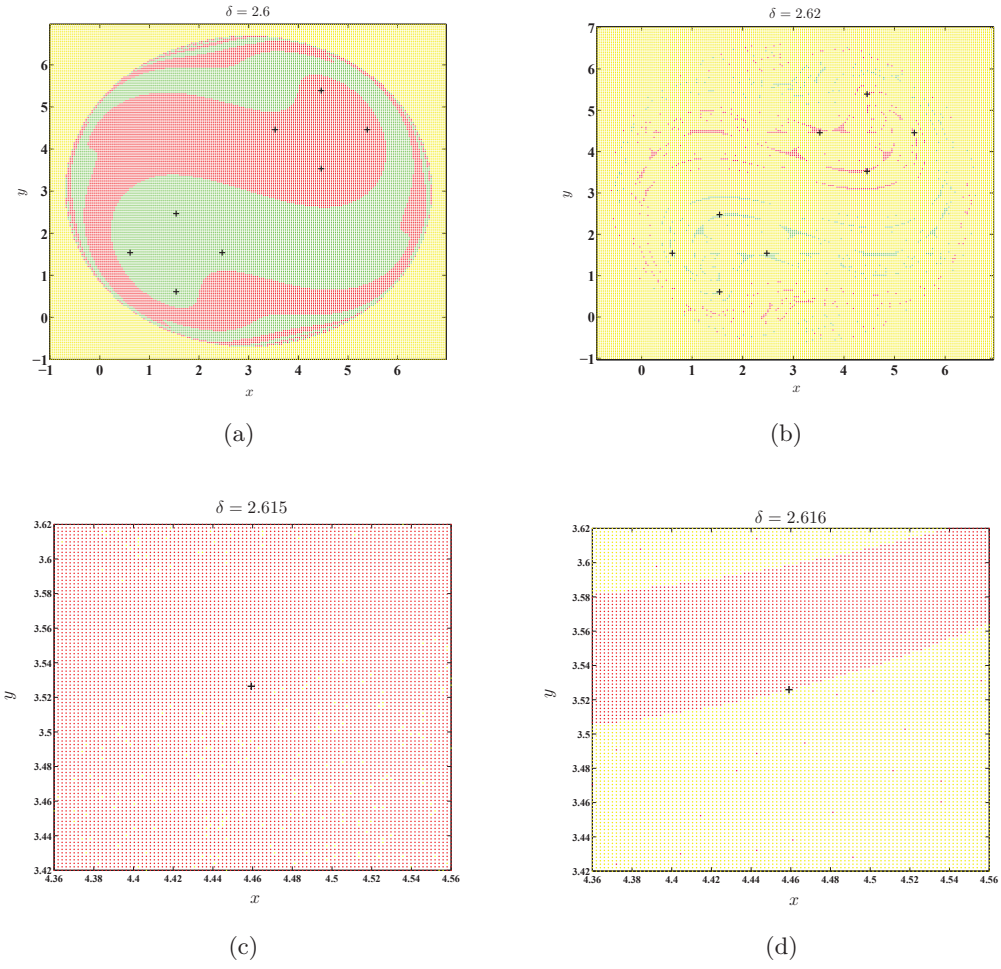

Figure 6.12: The basins of attraction of the 4-cycles (6.45) (a) for $\delta = 2.6$; (b) for $\delta = 2.62$; (c) for $\delta = 2.615$ and the initial points located in the range $[4.36, 4.56] \times [3.42, 3.62]$ and (d) for $\delta = 2.616$ and the initial points located in the same range as in (c).

6.5 Analysis by Lyapunov exponents

Consider the two-dimensional map

$$X_{n+1} = F(X_n), \quad X_n = (x_n, y_n), \quad n = 0, 1, 2, 3, \dots \ ,$$

where $F : \mathbb{R}^2 \to \mathbb{R}^2$. To monitor how a small error applied to the initial condition evolves after N iterations, we use the following algorithm:

Step 1. Iterate the initial point X_0, say, for k times[†] to obtain X_k. Initialize an accumulator to the value zero.

Step 2. For an arbitrary angle ϕ, we perturb X_k by a small finite displacement (*error*) $0 < \varepsilon_0 \ll 1$ in the direction $V = (\cos(\phi), \sin(\phi))$. Compute the perturbed point $\hat{X}_k = X_k + \varepsilon_0 V$.

Step 3. Iterate both points X_k , $\hat{X}_k$ and compute the distance ε_1 between them, *i.e.*, the new error.

Step 4. The error ε_0 increases by the factor $\left|\frac{\varepsilon_1}{\varepsilon_0}\right|$, we add the logarithm of this factor to the accumulator.

Step 5. Renormalize the distance between X_{k+1} and $\hat{X}_{k+1}$ so that the distance between them becomes equal to ε_0, see Figure 6.13. This is done by setting

$$\hat{X}^0_{k+1} = X_{k+1} + \frac{\varepsilon_0}{\varepsilon_1}\left(\hat{X}_{k+1} - X_{k+1}\right).$$

Step 6. Iterate steps 3-5 until N iterations have been performed.

Step 7. Divide the accumulator by N.

The average logarithmic growth of the relative error per iteration can be considered as the largest Lyapunov exponent [‡] in the direction V,

$$\sigma = \lim_{N\to\infty} \frac{1}{N} \sum_{i=1}^{N} \left|\frac{\varepsilon_i}{\varepsilon_0}\right|.$$

[†]To let the transient die out.

[‡]The formal definition of Lyapunov exponents is given in [78, Definition 5.8.2]. It is worth pointing out that, in the case of a two-dimensional map, there is a second Lyapunov exponent which indicates how much points near X_k are attracted after N iterations. See [22, 63, 108, 118, 132] for more details.

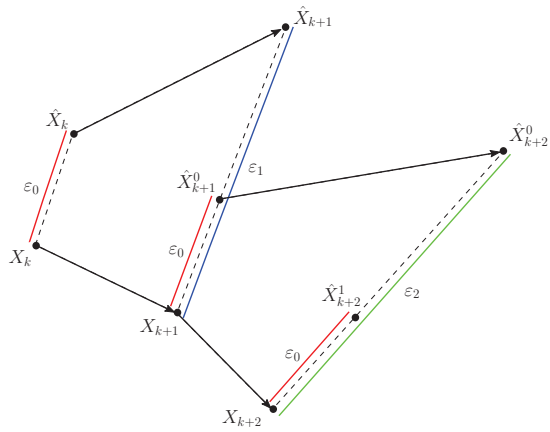

Figure 6.13: The renormalization step in the calculation of the largest Lyapunov exponent.

We apply this algorithm to calculate the largest Lyapunov exponent of the monopoly model (6.8) for $\delta \in [0.01, 4]$. For each δ we reset the initial data to $\varepsilon_0 = 0.00001$, $\phi = \frac{\pi}{2}$, $(x_0, y_0) = (3 + \sqrt{3} - 10^{-5}, 3 + \sqrt{3} - 10^{-5})$ and 10^5 map iterations are performed. This is done by evaluating the MATLAB code in Appendix B.2. The end result of this code is presented in Figure 6.14. The first problem with the preceding algorithm is that different error directions could produce different factors $\left\{ \left| \frac{\varepsilon_i}{\varepsilon_{i-1}} \right|, \ldots, \left| \frac{\varepsilon_1}{\varepsilon_0} \right| \right\}^{\dagger}$ and thus different Lyapunov exponents.

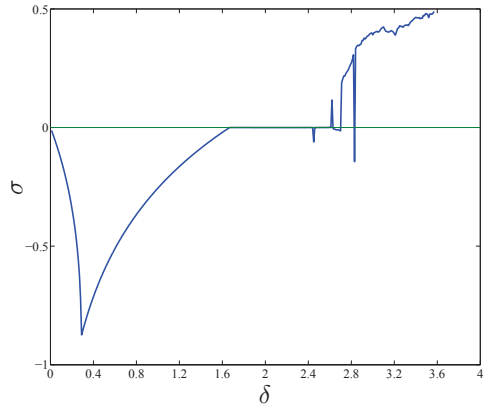

Figure 6.14: The largest Lyapunov exponent for $\delta \in [0.01, 4]$. Negative values correspond to stable cycles, zero corresponds to 4-cycles with one eigenvalue equal to one and positive values indicate chaotic behavior.

[†]To study how the error evolves after each iteration, we note that $\left| \frac{\varepsilon_i}{\varepsilon_0} \right| = \left| \frac{\varepsilon_i}{\varepsilon_{i-1}} \right| \left| \frac{\varepsilon_{i-1}}{\varepsilon_{i-2}} \right| \ldots \left| \frac{\varepsilon_1}{\varepsilon_0} \right|$.

For the monopoly model, we did the following numerical test. For a fixed value of δ, $\delta = 3$, we compute the largest Lyapunov exponent using four directions, namely $\phi_0 = 0,\ \frac{\pi}{2},\ \pi,\ \frac{3\pi}{2}$, with $\varepsilon_0 = 0.00001$. The numerical result is shown in Table 6.4. It is clear that as the number of iterations N increases, the computed exponents converge to the same value no matter what initial error direction is used. So the direction of the error is not really important in our model. However this is not the only problem since we still need to know how the Lyapunov exponent is affected by the choice of the initial error ε_0 to which we normalize after each iteration. To arrive at a well defined exponent we must let the size of the initial error to go to zero,

$$\sigma = \lim_{\varepsilon_0 \to 0} \lim_{N \to \infty} \frac{1}{N} \sum_{i=1}^{N} \left| \frac{\varepsilon_i}{\varepsilon_0} \right|,$$

which is not possible in the previous algorithm. To solve the limit problem, we can use the Jacobian matrix. This matrix can be used to project forward the initial displacement vector $V_0 = (\cos(\phi), \sin(\phi))$ to monitor the directions of stretching and shrinking at each iteration. To describe the new algorithm, let us consider the displacement from X_0 in the direction of the vector V_0, then the vector after N iterations given by

$$V_N = DF(X_{N-1})V_{N-1}, \tag{6.59}$$

will determine the displacement of the orbit for X_{N-1}, where $DF(X_{N-1})$ is the Jacobian matrix evaluated at X_{N-1}. Then the ratio

$$\frac{\|V_N\|}{\|V_0\|}, \quad \|V_0\| = 1$$

shows whether the displacement grows or shrinks. Therefor, the largest Lyapunov exponent

N	$\phi_0 = 0$	$\phi_0 = \frac{\pi}{2}$	$\phi_0 = \pi$	$\phi_0 = \frac{3\pi}{2}$
10	0.5806	0.6555	0.5806	0.6555
100	0.3914	0.3989	0.3914	0.3989
1000	0.3650	0.3658	0.3649	0.3657
10,000	0.3896	0.3897	0.3896	0.3897
100,000	0.3907	0.3907	0.3907	0.3907

Table 6.4: The largest Lyapunov exponent for $\delta = 3$ and using different error directions with $\varepsilon = 0.00001$ and increasing iteration numbers N. As the number of iterations increases, the computed exponents converge to the same value no matter what initial error direction is used.

for initial X_0 in the direction of the vector V_0 is given by

$$\sigma(X_0, V_0) = \lim_{N \longrightarrow \infty} \frac{1}{N} \ln (\|V_N\|). \tag{6.60}$$

From (6.59) we have

$$\begin{aligned} V_N &= DF(X_{N-1})DF(X_{N-2})V_{N-2} \\ &= DF(X_{N-1})DF(X_{N-2}) \dots DF(X_0)V_0 \\ &= DF^N(X_0)V_0. \end{aligned} \tag{6.61}$$

Hence, the Lyapunov exponent is given by

$$\sigma(X_0, V_0) = \lim_{N \longrightarrow \infty} \frac{1}{N} \ln \left(\|DF^N(X_0)V_0\|\right).$$

Using (6.59) and (6.60) the algorithm to estimate the Lyapunov exponents in this case is as follows [108]:

Step 1. Iterate the initial point X_0 k-times to arrive at X_k. Initialize an accumulator to zero.

Step 2. Chose an initial direction of error ϕ_0[†].

Step 3. Compute the direction vector of error E_{k+1} using the Jacobian matrix:

$$E_{k+1} = J(X_k) \left(\cos(\phi_0), \sin(\phi_0)\right).$$

Step 4. The error has increased (or decreased) by the factor $d = \|E_{k+1}\|$. Compute $\ln(d)$ and add it to the accumulator.

Step 5. Normalize the new error direction ($\hat{E}_{k+1} = \frac{E_{k+1}}{d}$) and then replace the error direction $(\cos(\phi_0), \sin(\phi_0))$ by the vector $\hat{E}_{k+1}$.

Step 6. Compute the next point of the map X_{k+1} and then go back to step (3) using X_{k+1} and the new error direction $\hat{E}_{k+1}$.

Step 7. After N iterations, divide the content of the accumulator by N.

The computed Lyapunov exponent of the monopoly model for $\delta \in [1.5, 4]$ using the second algorithm is shown in Figure 6.15a (see Appendix B.3 for the corresponding MATLAB code). The result looks exactly the same as in Figure 6.14. Table 6.5 shows the Lyapunov exponent

[†]This can be done by solving $(\cos(\phi_0), \sin(\phi_0)) = \frac{X_k}{\|X_k\|}$

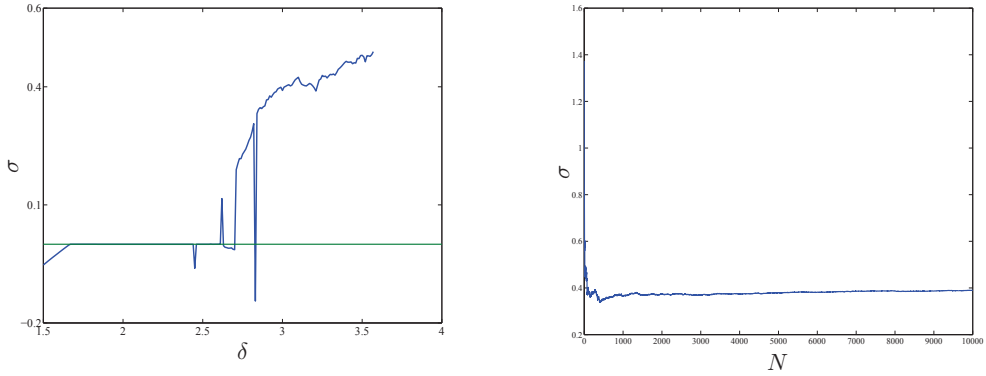

(a) (b)

Figure 6.15: (a) The largest Lyapunov exponents for $\delta \in [1.5, 4]$, (b) Convergence of the Lyapunov exponent for $\delta = 3$

of the monopoly model at $\delta = 3$ based on the first algorithm with different sizes of error (the first 3 columns) and base on the second algorithm (last column). It is clear that for $\varepsilon > 0$ the exponents of the first algorithm slowly converge to the actual exponent whose computed by the second algorithm.

N	$\varepsilon_0 = 0.1$	$\varepsilon_0 = 0.01$	$\varepsilon_0 = 0.001$	$\varepsilon_0 \to 0$
10	0.550702	0.578336	0.580343	0.592340
100	0.402211	0.385633	0.390898	0.393341
1000	0.374649	0.368181	0.366863	0.365137
10,000	0.384310	0.389172	0.389916	0.389626
100,000	0.388071	0.390482	0.390772	0.390703

Table 6.5: The largest Lyapunov exponent for $\delta = 3$ and using $\phi = \pi$ with different errors ε_0 for increasing number of iterations N.

6.6 Lyapunov exponents versus bifurcation diagram

Comparing the Lyapunov exponent diagram with the bifurcation diagram in Figure 6.16 and the cycle diagrams (Figure 6.3 - Figure 6.6), we notice that:

(1) For $\delta \in \left[0.01, \frac{5}{3}\right)$, σ is negative; it approaches zero at the 1:4 resonant NS bifurcation point $\delta = \frac{5}{3}$ where the cycles of period 4 are born. The Lyapunov exponent remains zero for $\frac{5}{3} < \delta < 2.615$ except for the dip around $\delta = 2.45$ caused by stable cycles of period 17.

(2) The first rise for σ is around $\delta = 2.62$ due to the chaotic behavior which is clear in Figure 6.4a and Figure 6.4b.

(3) The second dip between $\delta = 2.62$ and $\delta = 2.7$ is due to the stable period 5 cycles in Figure 6.5a. As δ touches zero around $\delta = 2.7$ a cycle of period 10 is born.

(4) For $\delta > 2.7$, the Lyapunov exponent increases and the system becomes more and more chaotic, except for the big dip caused by the stable period 13 cycles around $\delta = 2.83$, see Figure 6.6.

The chaotic behavior of the monopoly model can now be better understood with the help of the Lyapunov exponents analysis discussed above. Roughly speaking, the positive Lyapunov exponent for $\delta \in \{\approx 2.62\} \cup (2.7, \infty) \backslash \{\approx 2.83\}$ confirms the predominance of a chaotic attractor.

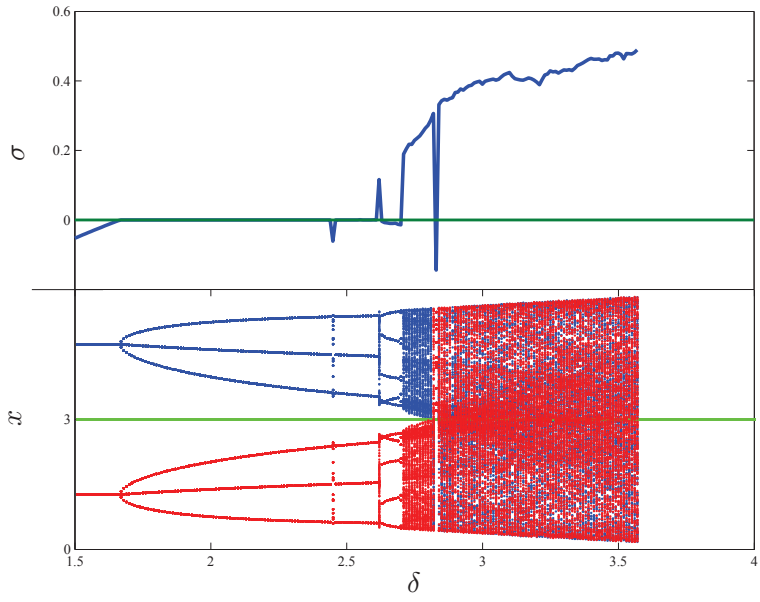

Figure 6.16: Plotting of Lyapunov exponents versus bifurcation diagram for $\delta \in [1.5, 4]$.

CHAPTER 7

Conclusions

In the first part of the thesis, accurate homoclinic predictors at a generic codim-2 BT bifurcation were derived. The procedure that we have used mainly consists of two steps:

(1) derive asymptotics of the homoclinic orbits and parameters of the two-dimensional BT normal form (the homoclinic predictor).

(2) transfer the derived predictors into the phase and parameter space of a given generic n-dimensional ODE.

For the first step we used an appropriate BT normal form (we called it the smooth BT normal form) to derive the explicit third-order homoclinic predictors by applying both the R-P and the L-P perturbation methods. Both methods give the same asymptotic for the homoclinic parameter values. However, the L-P predictor has a clear advantage, since it does not suffer from the "parasitic turn" in the asymptotic for the homoclinic orbit in the phase space. While doing so, we reported for the first time the explicit first-, second- and third-order homoclinic predictors for both R-P and L-P methods. We recall that the order of the predictor refers to the maximal order in the ε-expansion of the homoclinic solution in the perturbed Hamiltonian systems, and not the truncation ε-order in the final predictors. The L-P method for standard oscillators removes secular terms, *i.e.* a linear time-rescaling depending on the small parameter ε, yields a choice to eliminate unbounded terms and allows

to obtain a solution valid for all time. Then an expansion in ε recovers the unbounded term. Here we argue that our homoclinic predictor obtained from the L-P method is related in a similar way to the predictor from the R-P method. The difference though is that here we remove the parasitic turns rather than secular terms. Our claim is that if we expand the L-P predictor including the ε-dependent rescaled time, we recover the R-P predictor in the corresponding order. This implies that the geometry of the predictor is correct in phase space. We will restrict ourselves to first-order in ε. First of all, from (3.51) we have

$$\frac{d\xi}{ds} = 1 - \varepsilon\frac{6b}{7a}\tanh(\xi) + O(\varepsilon^2) \Longrightarrow \frac{ds}{d\xi} = 1 + \varepsilon\frac{6b}{7a}\tanh(\xi) + O(\varepsilon^2),$$

which can be integrated and inverted to yield

$$s = \xi + \varepsilon\frac{6b}{7a}\log(\cosh(\xi)) + O(\varepsilon^2) \Longrightarrow \xi = s - \varepsilon\frac{6b}{7a}\log(\cosh(s)) + O(\varepsilon^2).$$

Then it is easily checked that

$$u_{0,LP}(\xi(s)) = u_{0,RP}(s) + \varepsilon u_{1,RP}(s) + O(\varepsilon^2)$$

and that

$$v_{0,LP}(\xi(s)) + \varepsilon v_{1,LP}(\xi(s)) = v_{0,RP}(s) + \varepsilon v_{1,RP}(s) + O(\varepsilon^2).$$

The parasitic turn appears due to the log-term, so it is present in the R-P predictor. In the L-P predictor, this is removed by a nonlinear time reparametrization along the homoclinic orbit. We conjecture that this holds for higher order terms in ε as well. Note that for the L-P method we prescribe the u-solution restricting the homoclinic excursion to one side of the saddle. Then solvability requires additional freedom, provided by the time-rescaling. For the R-P method the solution satisfies $\dot{u} = v$, which by the time-rescaling does not hold in the L-P method. Also, for large values of ε, $\frac{d\xi}{ds}$ may become negative marking the end of the validity of the asymptotic.

The second step in the construction of generic homoclinic predictors was to obtain the smooth normal form on the center manifold. So we applied the standard parameter dependent center manifold reduction combined with the normalization, that is based on the Fredholm solvability of the homological equation. By systematically solving all linear systems appearing from the homological equation, we removed an ambiguity in the parameter transformation existing in the literature. Also, we reported for the first time the computational formulas of the coefficients (a_1, b_1, e, d) of the smooth BT normal form.

By collecting the results from both steps, we formulate an accurate homoclinic predictor at a generic codim-2 BT bifurcation. In Appendix A.5 we describe a sequence of Maple commands that can be used to explicitly compute the homoclinic solution rooted at a generic BT point of two-dimensional models. This solution is based on the L-P perturbation method. Using these commands we illustrate the homoclinic solution in the Gray-Scott model. We have also described an initializer implemented in MatCont to start homoclinic orbits from a generic BT point based on the L-P perturbation predictor. The initializer allows to compute the initial homoclinic solution and parameters so that the continuation of the homoclinic orbit can be started. Then we used MatCont to start the homoclinic orbits that emanate from BT points in several multidimensional models. In all examples, we set `TTolerance`$=10^{-5}$. As a rule, the `Amplitude` should always be larger than `TTolerance` given the geometric meaning of both variables. As another rule, the BT point itself should be computed to a geometric precision significantly smaller than `TTolerance`. This can be achieved in MatCont by decreasing the tolerances `VarTolerance` and `TestTolerance` for the curve on which the BT points are detected. We suggest to allow `eps0` and `eps1` to vary as homoclinic parameters. In the MatCont **continuer** window set **Adapt** $= 1$. Then start to increase/decrease the `Amplitude` value. This works for all studied models. However, this choice is not an absolute rule and it takes some trial-and-error to set all parameters (including `TTolerance`, continuation parameters and adaptation (`Adapt`)) for the successful continuation. Note that in each case both **Compute**|**Forward** and **Compute**|**Backward** should be tried. We recall that the idea of starting homoclinic orbit from BT point is based on applying a small nonzero step (ε) away from the BT point. However choosing a suitable ε such that the initial homoclinic prediction will be in the convergence domain of the homoclinic continuation problem is correlated, in some way, to the value of the BT normal form coefficient a. In general, cases where a has small (absolute) value are more difficult to handle than cases where a is moderate.

There is a similarity between the bifurcation structure in the BT normal form of an ODE and the BT map. We investigated the possibility of applying our asymptotic to predict the homoclinic parameter in the BT map with the aim to continue the branches of tangential homoclinic orbits. As a first step, we derived the homoclinic asymptotic for the ODE whose time-1 shift map coincides with orbits of the BT map. The result is a curve in the parameter space. We showed that for a suitable choice of the parameter value this curve is located inside the homoclinic zone in the BT map which means that the predicted homoclinic parameter can be used to approximate the homoclinic structure in the BT map. It is worth to point out that our predictor improves the existing one in the literature. Numerically, the derived asymptotic of the homoclinic parameter was sufficient to grow the stable and unstable manifolds of the saddle of the BT map. After numerically computing the (*transversal*) intersection points of

these manifolds we used these points as initial data to continue the homoclinic tangencies (the boundary of the homoclinic zone) so that we obtained the whole homoclinic structure in the BT map. However, we still believe that using the derived homoclinic asymptotic it could be possible to predict a finite number of intersection points of the stable and unstable manifolds and hence the tangential homoclinic orbits can be continued without growing and intersecting the stable and unstable manifolds which is time consuming.

In the second part of this thesis we studied the monopoly model. This study was motivated by the erroneous claims in the analysis of the model in the existing literature. Also because of the rich periodic behaviors, a part of this study was to apply the MATLAB interactive toolbox for numerical study of smooth maps (MatContM) in the analysis of these periodic behaviors and to study the stability regions. By numerical simulation, based on a crude bifurcation diagram, it was not difficult to find periodic points of period 4, 5, 10, 13 and 17. Computing these points for a specific value of the bifurcation parameter δ (with high accuracy) allows us to have good starting points to use MatContM to compute whole branches of solutions of period 5, 10, 13 and 17 (parametrized by δ) and to determine the stability regions of these solutions. The most interesting solutions were those of period 4. These solutions have always an eigenvalue equal to one which contradicts the claims in previous studies on the model where it is said this happens only for $\delta \approx 2.488$. We derived the explicit formula for solutions of period 4. Then we proved that these solutions are never linearly asymptotically stable. For $\delta > \frac{-5}{2} + \frac{25}{18}\sqrt{21}$ the second eigenvalue of the 4-cycles is always greater than one and hence the 4-cycles are unstable, so we focus our study in the interval $\frac{5}{3} < \delta < \frac{-5}{2} + \frac{25}{18}\sqrt{21}$. A nonlinear stability criterion is combined with basin of attraction analysis and simulation to show that the 4-cycles are stable in this interval. We also showed that the 4-cycles have a small radius of attraction for δ slightly smaller than $\frac{-5}{2} + \frac{25}{18}\sqrt{21}$. In agreement with the computed bifurcation points using MatContM, we exactly determined the value of δ for which two NS bifurcation occur. These values were $\delta = \frac{5}{3}$ where stable cycles of period 4 emerge and $\delta = \frac{-5}{2} + \frac{25}{18}\sqrt{21}$ where the 4-cycles lose their stability. Further, the chaotic and periodic behaviors of the monopoly model were analyzed by computing the largest Lyapunov exponents. The most interesting result was for $\delta > 2.7$ where the positive Lyapunov exponent increases and the system becomes more and more chaotic. The positive Lyapunov exponent for $\delta \in \{\approx 2.62\} \cup (2.7, \infty) \backslash \{\approx 2.83\}$ confirmed the predominance of a chaotic attractor. This corrects the previous literature where the chaotic behaviors was assumed to exist for $\delta > 2.48$.

CHAPTER 8

Future work

In the first part of the thesis we discussed the initialization of a branch of homoclinic orbits starting from a generic BT point in multidimensional ODEs. Homoclinic orbits are also known to emanate from Zero-Hopf (ZH) and Hopf-Hopf (HH) codim-2 bifurcation points. However, the initialization of these orbits starting from ZH and HH bifurcations is still an open problem. Some important results are obtained in [27, 31, 56, 62]. In the ZH case it is possible to derive an asymptotic of the homoclinic parameter and also the corresponding parameter-dependent center manifold reduction (see for example [93]). So a future research direction is to construct a suitable initial solution in the state space. Once the homoclinic asymptotics is derived, the next step should be to propose an initializer to start up homoclinic orbits from a generic ZH point and to introduce it into MatCont. The case of HH points is mathematically as well as computationally quite difficult.

In the map case, we derived a predictor for the homoclinic parameter at a generic BT point of maps. The problem of deriving such predictor in state space is first to construct an asymptotic of the homoclinic points in the BT map and then generalize the derived asymptotic. In general if a two-dimensional map consists of an area-preserving system (with explicitly known homoclinic solution) with a small perturbation part, then one can apply the Melnikov's method for maps to approximate the homoclinic points (see [48, 60, 67, 80]). In [67, 126], it was shown that the Melnikov method gives a fairly good approximation for the transverse intersection points of the homoclinic trajectories in the Hénon Map. However, the BT map neither possesses an area-preserving system with a known explicit homoclinic solution nor a perturbation part. In [126], it was claimed that it is possible to derive a small

perturbation part to the BT map by performing two Picard's iterations to the approximating system (the approximating system itself is constructed by performing one Picard's step), so that we get a map of the form $F = G + P$, where G is the BT map and P is the rest of the remaining higher-order terms. Thus $G = F - P$, meaning that P is a perturbation of the map F. If we assume that the orbits of F are close to those of G (for $\|P\|$ small), then at the derived homoclinic parameter of G, one can use the Melnikov method by considering F as "unperturbed map" and P as "perturbation" to find an approximation for the homoclinic points of the map G. However, using all quadratic and cubic terms in F and P does not lead us to the expected result. So more thinking on the construction of the perturbation part should be done. If the problem of constructing a suitable perturbation part such that the Melnikov method gives the desired result (i.e., an asymptotic to the homoclinic points) is solved, then because of the existence of the parameter dependent center manifold, the result should be extended to the n-dimensional case, and further an initializer to the tangential homoclinic orbit starting from a generic BT point of maps should be implemented into MatCont.

Another direction for further research is the stability of the 4-cycle in the monopoly model. In Section 6.4 we show (without rigorous proof) that the 4-cycle is stable for $\delta \in (\frac{5}{3}, \frac{-5}{2} + \frac{25}{18}\sqrt{21})$ and unstable otherwise. However there is a small region before the NS bifurcation point, i.e., $\delta = \frac{-5}{2} + \frac{25}{18}\sqrt{21}$, where the stability criterion indicates an unstable region. By simulations and basin of attraction analysis, we showed that the 4-cycle is still (locally) stable but coexists with other attractors in this region, so the real loss of the stability is caused by the NS bifurcation point. We recall that the idea of the stability criterion was based on studying a small displacement in the direction of the eigenvector corresponding to the eigenvalue located at the stability boundary. Since the basins of attraction are highly intermingled, even starting extremely close to the 4-cycle can lead to convergence to the coexisting attractor. So our stability criterion (6.56) is strongly affected by the choice of the size of the displacement ε (we clarified that in Figure 6.10). So for future research, the idea of the stability criterion should be reconsidered such that it becomes independent of the choice of ε. One idea is to expand $M^4\left((x,y)^{\mathrm{T}} + \varepsilon v\right)$ in (6.56) in terms of ε. The zero-order term will cancel and the first-order term will be equal to 1. So we would obtain a criterion of the form $\alpha_\varepsilon = \varepsilon(1 + A\varepsilon + B\varepsilon^2 + \ldots)$. Since ε should be allowed to be either positive or negative, the stability condition would require that $A = 0$ and $B < 0$. A symbolic computation of A and B looks challenging but some work in this direction is currently under development.

Besides the mathematical work, future directions of development of the MatCont software are in order. This work could include: (a) updating and improving the GUI of MatCont to make it more flexible; (b) introduce vector variables as MatCont input; (c) improve the graphical representation in two-dimensional and three-dimensional plots.

APPENDIX A

Homoclinic solutions using Maple

This appendix provides a part of the Maple commands that were used in our study of the homoclinic solution near a generic Bogdanov-Takens point.

A.1 The homological equation

The following sequence of MAPLE commands can be used to solve the *homological equation* (2.38):

```
>readlib(mtaylor):
>readlib(coeftayl):
```

The first two commands help us to compute the truncated multivariate Taylor series expansion and its individual coefficients.

```
>define(B,   'orderless',multilinear): define(A[1],'orderless',multilinear):
>define(J[2],'orderless',multilinear): define(C,   'orderless',multilinear):
>define(B1,  'orderless',multilinear):
```

Using these commands we define the multilinear forms B, A_1, J_2, C, B_1.

```
>CM:=mtaylor(sum(sum(sum(sum(H[i,j,k,l]*`w[0]`^i*`w[1]`^j*`beta[1]`^k*`beta[2]`^l/(
     factorial(i)*factorial(j)*factorial(k)*factorial(l)),i=0..4),j=0..4),k=0..4),l=0..4)
     ,[`w[0]`,`w[1]`,`beta[1]`, `beta[2]`],4):
>H[0,0,0,0]:= 0:    H[1,0,0,0]:= q[0]:       H[0,1,0,0]:= q[1]:
```

The above commands compose the Taylor series expansion of (2.39b).

```
>PS:=mtaylor(sum(sum(Kappa[n,m]*`beta[1]`^n*`beta[2]`^m/(factorial(m)*factorial(n)),n
    =0..4),m=0..4),[`beta[1]`, `beta[2]`],4):
>Kappa[0,0]:= 0:
>Kappa[1,0]:= Kappa[`1,0`]:  Kappa[0,1]:= Kappa[`1,1`]:  Kappa[0,2]:= Kappa[`2`]:
```

The above commands compose the Taylor series expansions of (2.39c).

```
>`g[1]`:=`w[1]`:
>`g[2]`:=`beta[1]`+`beta[2]`*`w[1]`+(`beta[2]`*a[1]+a)*`w[0]`^2+ (`beta[2]`*b[1]+b)*`w
    [0]`*`w[1]`+d*`w[0]`^3+e*`w[0]`^2*`w[1]`:
>LHS:=(diff(CM,`w[0]`))*`g[1]`+(diff(CM,`w[1]`))*`g[2]`:
```

By the commands above, we compute the LHS of (2.38).

```
>tmp:=constants:   constants:=constants,`w[0]`,`w[1]`,`beta[1]`,`beta[2]`:
>RHS:=simplify(A*CM+J[1]*PS+(1/2)*B(CM,CM)+A[1](CM,PS)+(1/2)*J[2](PS,PS)+(1/6)*C(CM,CM,CM
    )+(1/2)*B1(CM,CM,PS)):
>constants:=tmp:
```

The above commands compute the RHS of (2.38) where $f(.,.)$ is composed as in (2.39a).

```
>Hom:=RHS-LHS=0:
>sort(collect(Hom,{`beta[1]`,`beta[2]`,`w[0]`,`w[1]`},distributed)):
```

The above command is used to evaluate (2.38).

```
>coeftayl(Hom,[`w[0]`,`w[1]`,`beta[1]`,`beta[2]`]=[0,0,0,0],[i1,i2,i3,i4]);
```

The final command can be used to compute a particular equation for terms of the same order in w and β. For example, we set `i1=1`, `i2=i3=i4=0` to find (2.40a). In the same way, we can compute the equations (2.40b)-(2.40l) and (2.63a)-(2.63d).

A.2 R-P solution

The following sequence of MAPLE commands can be used to derive the first-order correction to the Hamiltonian homoclinic solution of (2.24). This solution is based on the R-P method, see Section 3.1.

```
>u0:=t->2-6/cosh(t)^2:
>v0:=t->12*tanh(t)/cosh(t)^2:
>phi1:=t->12*tanh(t)/cosh(t)^2:
>phi2:=t->2*cosh(t)^2+5+15*t*sinh(t)/cosh(t)^3-15/cosh(t)^2:
>w:=simplify(phi1(t)*(diff(phi2(t),t))-(diff(phi1(t),t))*phi2(t)):
>F1:=t->b*v0(t)*(tau0+u0(t))/a:
>g:=integrate(phi2(s)*F1(s)/w,s=0..t):
>f:=integrate(phi1(s)*F1(s)/w,s=0..t):
>tu1:=simplify(convert(phi1(t)*(c1-g)+phi2(t)*(c2+f),exp)):
```

By the commands above, we define $u_1(s)$ using to the formula of the general solution (3.12).

```
>limit(tu1,t=infinity):
>limit(tu1,t=-infinity):
```

The above commands are used to check the limits of $u_1(s)$. The results of these are

$$\frac{35ac2 + 7b\tau 0 - 10b}{a}, \quad \frac{35ac2 - 7b\tau 0 + 10b}{a}.$$

We solve these equations for $c2$ and $\tau 0$ by the following commands

```
>sol:= solve({(35*a*c2+7*b*tau0-10*b)/a, (35*a*c2-7*b*tau0+10*b)/a},{c2,tau0}):
>assign(sol):
```

This gives (3.13) with $C_2 = 0$.

```
>tu1:=collect(simplify(expand(convert(simplify(tu1),trigh))),{ln(cosh(2*t)+sinh(2*t)+1),t
    ,ln(2)}):
>tu1:=collect(expand(subs(ln(cosh(2*t)+sinh(2*t)+1)=(ln(2)+t+ln(cosh(t))),tu1)),{ln(cosh(
    t))}):
```

These commands are used to obtain (3.14).

```
>tv1:=diff(tu1,t):
>c1:=solve(eval(tv1,t=0),c1):
```

Using these commands we compute the value of C_1 based on condition (3.15).

```
>u1:=t->simplify(tu1):
>v1:=t->simplify(tv1):
>u1(t):
>collect(v1(t),{ln(cosh(t))});
```

The final commands are used to compute (3.16). The same procedure can be used to compute the second-order as well as the third-order solutions.

A.3 L-P solution

The following sequence of MAPLE commands can be used to derive the first-order correction to the Hamiltonian homoclinic solution of (2.24). This solution based on the L-P method, see Section 3.2.

```
>readlib(mtaylor);
>readlib(coeftayl);

>BTsys2:=omega(mu)*diff(omega(mu)*diff(u(mu),mu),mu)+4-u(mu)^2=epsilon*(omega(mu)*b*diff(
    u(mu),mu)*(Tau+u(mu))/a)+epsilon^2*u(mu)^2*(Tau*a1*b+u(mu)*d)/a^2+epsilon^3*u(mu)*
    omega(mu)*diff(u(mu),mu)*(Tau*b*b1+u(mu)*e)/a^2:
>u:='u':
>omega(mu):=1+sum(epsilon^i*omega[i](mu),i=1..5):
>Tau:=sum(epsilon^i*tau[i],i=0..5):
>u(mu):=sum(epsilon^i*u[i](mu),i=0..5):
>Sigma:=sum(epsilon^i*sigma[i],i=0..5):
>Temp:= BTsys2:
```

The above commands are used to compose (3.31) while taking (3.32) into account.

```
>EqEps0:=subs(epsilon = 0, Temp);
>EqEps1:=coeff(lhs(Temp),epsilon)=coeff(rhs(Temp),epsilon);
>EqEps2:=coeff(lhs(Temp),epsilon^2)=coeff(rhs(Temp),epsilon^2);
>EqEps3:=coeff(lhs(Temp),epsilon^3)=coeff(rhs(Temp),epsilon^3);

>u[0]:= mu->sigma[0]*sech(mu)^2+delta[0]:
>u[1]:= mu->sigma[1]*sech(mu)^2+delta[1]:
>u[2]:= mu->sigma[2]*sech(mu)^2+delta[2]:
>u[3]:= mu->sigma[3]*sech(mu)^2+delta[3]:
>v[0]:=diff(u[0](mu),mu):
>v[1]:=coeff(-1/6*Sigma*omega(mu),epsilon,1)*v[0]:
>v[2]:=coeff(-1/6*Sigma*omega(mu),epsilon,2)*v[0]:
>v[3]:=coeff(-1/6*Sigma*omega(mu),epsilon,3)*v[0]:
>delta[0]:= 2:
>sigma[0]:=-6:
>simplify(lhs(EqEps0));
                        0
>rhs(EqEps0);
                        0
```

By these commands we obtain (3.33)-(3.36) and (3.40)-(3.43). Also we set the initials `delta0=2`, `sigma[0]=-6` such that `u[0]` and `v[0]` are equivalent to (3.37).

```
>tau[0]:=solve(int(diff(u[0](mu),mu)*rhs(EqEps1),mu=-infinity..infinity),tau[0]);
```

The above command computes (3.47)-(3.48).

```
>lhs1:=omega[1](mu)*(diff(u[0](mu),mu))^2+diff(u[0](mu),mu)*diff(u[1](mu),mu)-u[1](mu)*
    diff(u[0](mu),mu,mu):
>L10:=simplify(subs(mu=infinity,lhs1)-subs(mu=0,lhs1)):
>L11:=simplify(int(diff(u[0](mu),mu)*rhs(EqEps1),mu=0..infinity)):
>sigma[1]:=solve(L10=L11,sigma[1]):
```

The above yields (3.49).

```
>L12:=simplify(subs(mu=x,lhs1)-subs(mu=0,lhs1)):
>L13:=int(diff(u[0](mu),mu)*rhs(EqEps1),mu = 0 .. x):
>omega[1]:=solve(L12=L13,omega[1]):
```

These commands compute the function $\omega_1(\xi)$. Since $\omega_1(\xi)$ should be bounded we compute the limits by the following commands

```
>limit(omega[1](t),t=+infinity);
>limit(omega[1](t),t=-infinity);
```

to get

```
                    -signnum(delta[1]) infinity
                    -signnum(delta[1]) infinity
```

So $\omega_1(\xi)$ is bounded iff $\delta_1 = 0$. So we set

```
>delta[1]:=0:
```

The following commands are used to check if $u_1(\xi)$ is a bounded function and also to get the simplified expressions (3.52):

```
>limit(u[1](t),t=infinity);
>limit(u[1](t),t=-infinity);
>simplify(u[1](t));
>simplify(v[1]);
>omega[1](t);
```

The same procedure can be used to compute the second-order as well as the third-order solutions.

A.4 Asymptotics in n-dimensional systems

The following commands are used to compute (3.61)-(3.62).

```
>readlib(mtaylor); readlib(coeftayl);
>X:=mtaylor(sum(sum(sum(sum(Eta[i,j,k,l]*w[0]^i*w[1]^j*beta[1]^k*beta[2]^l/(factorial(i)*
     factorial(j)*factorial(k)*factorial(l)),i=0..2),j=0..2),k=0..2),l=0..2),[w[0],w[1],
     beta[1],beta[2]],3);
>Eta[0,0,0,0]:=0;
>Eta[1,0,0,0]:=q[0];
>Eta[0,1,0,0]:=q[1];
>alpha:=mtaylor(sum(sum(Kappa[m,n]*beta[1]^m*beta[2]^n/(factorial(m)*factorial(n)),n
     =0..2),m=0..2),[beta[1],beta[2]],3);
>Kappa[0,0]:=0;
>Kappa[1,0]:= Kappa[‘1,0‘]:  Kappa[0,1]:= Kappa[‘1,1‘]:  Kappa[0,2]:= Kappa[‘2‘]:
```

The above commands compose the Taylor series expansions of (2.36) and (2.35).

```
>w[0]:=epsilon^2/a*(u[0]+epsilon*u[1]+epsilon^2*u[2]):
>w[1]:=epsilon^3/a*(v[0]+epsilon*v[1]+epsilon^2*v[2]):
>beta[1]:=-4*epsilon^4/a:
>beta[2]:=b*epsilon^2/a*(tau[0]+epsilon*tau[1]+epsilon^2*tau[2]):
```

The above commands define w_0, w_1, β_1, β_2 according to the singular rescaling (3.1).

```
>X:= mtaylor(X,[epsilon],5);
>alpha:=mtaylor(alpha,[epsilon],5);
```

The final commands are used to obtain (3.61)-(3.62).

A.5 Computing homoclinic solutions in two-dimensional systems

The following sequence of MAPLE commands can be used to compute the homoclinic solutions rooted at a BT point of two-dimensional ODEs. We note that this code can be used to explicitly derive the homoclinic expression of a two-dimensional system after replacing the BT point (in the parameter as well as in the state space) at $(0, 0)$ by an appropriate change

of coordinates. In the following commands, the free parameters are assumed to be (r_1, r_2) while the state parameters are (X_1, X_2)

```
> with(plots):
> with(LinearAlgebra):
> with(VectorCalculus):
```

The first command allows us to use the MAPLE linear algebra and vector calculus packages.

```
> f[1]:=-(1/4)*X[2]-(1/2)*X[2]^2-(1/8)*X[1]-(1/2)*X[1]*X[2]-X[1]*X[2]^2+(1/2)*r[1]-r[1]*X
    [1]:
> f[2]:=(1/8)*X[2]+(1/2)*X[2]^2+(1/16)*X[1]+(1/2)*X[1]*X[2]+X[1]*X[2]^2-(1/4)*r[1]-r[1]*X
    [2]-(1/4)*r[2]-r[2]*X[2]:
```

These commands define the system (2.75) which results after we apply the change of variables (2.74) to the Gray-Scott model (2.70).

```
>  A:=Jacobian([f[1],f[2]],[X[1],X[2]]):
> AT:=A^(%T):
> J1:=Jacobian([f[1],f[2]],[r[1],r[2]]):
>  B:=Matrix([[Hessian(f[1],[X[1],X[2]])],[Hessian(f[2],[X[1],X[2]])]]):
> J2:=Matrix([[Hessian(f[1],[r[1],r[2]])],[Hessian(f[2],[r[1],r[2]])]]):
> A1:=Matrix(2,4):
> for i from 1 to 2 do
>     column:=0:
>     for j from 1 to 2 do
>        for k from 1 to 2 do
>                column:=column+1;
>                A1[i,column]:=diff(f[j],r[i],X[k]);
>        end do:
>     end do:
> end do:
> C:=Matrix(2,8):
> for i from 1 to 2 do
>     column:=0:
>     for j from 1 to 2 do
>        for k from 1 to 2 do
>            for l from 1 to 2 do
>               column:=column+1;
>               C[i,column]:=diff(f[i],X[j],X[k],X[l]);
>            end do:
>        end do:
>     end do:
> end do:
> B1:=Matrix(2,8):
> for i from 1 to 2 do
>     column:=0:
>     for j from 1 to 2 do
>        for k from 1 to 2 do
>            for l from 1 to 2 do
>               column:=column+1;
>               B1[i,column]:=diff(f[i],X[j],X[k],r[l]);
>            end do:
>        end do:
>     end do:
> end do:
```

The above commands are used to compute the matrices and the multilinear forms A, A^T, J_1, B, A_1, J_2, C, B_1.

```
> r[1]:=0:
> r[2]:=0:
> X[1]:=0:
> X[2]:=0:
```

The above commands evaluate the previous and the next commands at the Bogdanov-Takens point, *i.e.*,, `(X[1],X[2])=(0,0)`, `(r[1],r[2])=(0,0)`.

```
Eg:=evalf(Eigenvectors(A)):
EgT:=evalf(Eigenvectors(AT)):
for i from 1 to 2 do
  if  (abs(Re(Eg[1][i]))<10^(-6)) and (not (Equal(Re(Vector(Eg[2][]..(),i])),<0,0>)))
     then c1:=i end if;
  if (abs(Re(EgT[1][i]))<10^(-6)) and (not (Equal(Re(Vector(EgT[2][]..(),i])),<0,0>)))
     then c2:=i end if;
end do:
v:=Re(Eg[2][]..(),c1]):
w:=Re(EgT[2][]..(),c2]):
Bd1:=Matrix([[A,w],[v^%T,0]]):
tq0:=LinearSolve(Bd1, <0,0,1>):
tq0:=simplify((Vector([tq0[1],tq0[2]]))):
tp1:=LinearSolve(Bd1^(%T), <0,0,1>):
tp1:=simplify((Vector([tp1[1],tp1[2]]))):
Bd2:=Matrix([[A,tp1],[tq0^%T,0]]):
tq1:=LinearSolve(Bd2, <tq0,0>):
tq1:=simplify((Vector([tq1[1],tq1[2]]))):
tp0:=LinearSolve(Bd2^(%T), <tp1,0>):
tp0:=simplify((Vector([tp0[1],tp0[2]]))):
N1:=sqrt(abs(tq0^(%T).tq0)):
q0:=1/N1*tq0:
q1:=1/N1*tq1:       q1:=q1-(q0^(%T).q1)*q0:
N2:=q0^(%T).tp0:
p1:=(1/N2)*tp1:
p0:=tp0-(tp0^(%T).q1)*p1:    p0:=(1/N2)*tp0:
A.q0;
          0e[x]+0e[y]
A.q1-q0;
          0e[x]+0e[y]
AT.p1;
          0e[x]+0e[y]
AT.p0-p1;
          0e[x]+0e[y]
```

The above commands are used to compute the vectors q_0, q_1, p_0, p_1. We note that these vectors are computed in such a way that (2.3) and (2.4) are satisfied (see also **Step 0** in Section 4.1).

```
> BQ00:=Vector([(B[1..2].q0).q0,(B[3..4].q0).q0]):
> BQ01:=Vector([(B[1..2].q0).q1,(B[3..4].q0).q1]):
> BQ11:=Vector([(B[1..2].q1).q1,(B[3..4].q1).q1]):
> a:=simplify(expand((1/2)*p1^%T.BQ00)):
> b:=simplify(p0^%T.BQ00+p1^%T.BQ01):
```

The above commands are used to compute the normal form coefficients a and b of the Bogdanov-Takens bifurcation.

```
> Bord:=Matrix([[A,p1],[q0^%T,0]]):
> RHS1:=simplify(Vector([2*a*q1-BQ00,0])):
> H2000:=LinearSolve(Bord, RHS1):
> H2000:=simplify((Vector([H2000[1],H2000[2]]))):
> H2000:=H2000+1/2*(-2*p0.H2000+2*p0.BQ01+p1.BQ11).q0;
> RHS2:=Vector([b*q1-BQ01+H2000,0]):
> H1100:=LinearSolve(Bord,RHS2):
> H1100:=simplify(Vector([H1100[1],H1100[2]])):
> RHS3:=Vector([2*H1100-BQ11,0]):
> H0200:=LinearSolve(Bord,RHS3):
> H0200:=simplify(Vector([H0200[1],H0200[2]])):

> p1.(2*H1100-BQ11);
                    0
```

The above commands are used to compute the vectors H_{2000}, H_{1100} and H_{0200}. See system (2.48).

```
> BQ0 :=Matrix([[B[1..2].q0,B[3..4].q0]])^(%T):
> BQ1 :=Matrix([[B[1..2].q1,B[3..4].q1]])^(%T):
> A1q0:=Matrix([A1[]..(),1..2].q0,A1[]..(),3..4].q0])^(%T):
> A1q1:=Matrix([A1[]..(),1..2].q1 ,A1[]..(),3..4].q1])^(%T):
> Blk1:=Matrix([[p1^%T.BQ0],[evalm(p0^%T.BQ0+p1^%T.BQ1)]]):
> Blk2:=Matrix([[p1^%T.A1q0],[evalm(p0^%T.A1q0+p1^%T.A1q1)]]):
> BigSys:=Matrix([[A,J1],[Blk1,Blk2]]):
> RHS4:=Vector([q1,(1/2)*(p1^%T.BQ11),3*(p0^%T.H1100)-p0^%T.BQ11]):
> RHS5:=Vector([0,0,0,1]):
> HK:=Matrix([[LinearSolve(BigSys,RHS4),LinearSolve(BigSys,RHS5)]]):
> H1:=HK[1..2]: H0010:=H1[]..(),1]: H0001:=H1[]..(),2]:
> K1:=HK[3..4]: K10:=K1[]..(),1]:   K11:=K1[]..(),2]:
```

By the above commands we solve (2.59) for H_{1000}, H_{0100}, $K_{1,0}$, $K_{1,1}$.

```
> z1:=Vector([(B[1..2] .H0001).H0001,(B[3..4] .H0001).H0001]):
> z2:=Vector([(A1[]..(),1..2].H0001).K11 ,(A1[]..(),3..4].H0001).K11] ):
> z3:=Vector([(J2[1..2].K11 ).K11 ,(J2[3..4].K11 ).K11] ):
>  z:=Vector([z1+2*z2+z3]):
> K2:=simplify(Vector([-(p1^(%T).z)*K10])):
> RHS6:=-Vector([z+Vector(J1.K2),0]):

> H0002:=LinearSolve(Bord,RHS6):
> H0002:=simplify(Vector([H0002[1],H0002[2]])):
> h1:=Vector([(B[1..2].q0).H0001,(B[3..4].q0).H0001]):
> h2:=Vector([(A1[]..(),1..2].q0).K11,(A1[]..(),3..4].q0).K11]):
> RHS7:=Vector([-h1-h2,0]):

> H1001:=LinearSolve(Bord,RHS7):
> H1001:=simplify(Vector([H1001[1],H1001[2]])):
> h3:=Vector([(B[1..2].q1).H0001,(B[3..4].q1).H0001]):
> h4:=Vector([(A1[]..(),1..2].q1).K11,(A1[]..(),3..4].q1).K11]):
> RHS8:=Vector([-h3-h4+H1001+q1,0]):
> H0101:=LinearSolve(Bord,RHS8):
> H0101:=simplify(Vector([H0101[1],H0101[2]])):
```

The above commands are used to compute the vectors (2.61)-(2.62). The following commands are used to compute the vectors (2.64)-(2.69).

```
> column:=0:

> V1:=Vector(8):  V2:=Vector(8):   V3:=Vector(8):
> V4:=Vector(8):   V5:=Vector(8):   V6:=Vector(8):

> for j from 1 to 2 do
>   for k from 1 to 2 do
>     for l from 1 to 2 do
>      column:=column+1;
>      V1[column]:=q0[j]*q0[k]*q0[l];
>      V2[column]:=q0[j]*q0[k]*q1[l];
>      V3[column]:=q0[j]*q0[k]*H0001[l];
>      V4[column]:=q0[j]*q1[k]*H0001[l];
>      V5[column]:=q0[j]*q0[k]*K11[l];
>      V6[column]:=q0[j]*q1[k]*K11[l];
>     end do:
>   end do:
> end do:

> Cq000:=Vector([C[1]^(%T).V1,C[2]^(%T).V1]):
> Cq001:=Vector([C[1]^(%T).V2,C[2]^(%T).V2]):
> Cq00H:=Vector([C[1]^(%T).V3,C[2]^(%T).V3]):
> Cq01H:=Vector([C[1]^(%T).V4,C[2]^(%T).V4]):
> Cq00K:=Vector([B1[1]^(%T).V5,B1[2]^(%T).V5]):
> Cq01K:=Vector([B1[1]^(%T).V6,B1[2]^(%T).V6]):

> h5:=Vector([(B[1..2].q0).H2000,(B[3..4].q0).H2000]):
> d:=simplify(p1^%T.(1/6*Cq000+1/2*h5-a*H1100)):
> RHS9:=6*Vector([-1/6*Cq000-1/2*h5+a*H1100+d*q1,0]):
> H3000:=LinearSolve(Bord,RHS9):
> H3000:=Vector([H3000[1],H3000[2]]):
> h6:=Vector([(B[1..2],q0).H1100,(B[3..4].q0).H1100]):
> h7:=Vector([(B[1..2],q1).H2000,(B[3..4].q1).H2000]):
>  e:=simplify(p1^%T.(1/2*Cq001+h6+1/2*h7-H1100*b-H0200*a-1/2*H3000)):
> h9:=Vector([(B[1..2].q0).H1001,(B[3..4].q0).H1001]):
> h10:=Vector([(B[1..2].H0001).H2000,(B[3..4].H0001).H2000]):
> h11:=Vector([(A1[]..(),1..2].H2000).K11,(A1[]..(),3..4].H2000).K11]):
> a1:=simplify(p1^%T.(1/2*Cq00H+1/2*Cq00K+h9+1/2*h10+1/2*h11-H0101*a)):
> RHS11:=2*Vector([-1/2*Cq00H-1/2*Cq00K-h9-1/2*h10-1/2*h11+H0101*a+q1*a1,0]):
> H2001:=LinearSolve(Bord,RHS11):
> H2001:=simplify(Vector([H2001[1],H2001[2]])):
> h12:=Vector([(B[1..2].q1).H1001,(B[3..4].q1).H1001]):
> h13:=Vector([(B[1..2].H0001).H1100,(B[3..4].H0001).H1100]):
> h14:=Vector([(B[1..2].q0).H0101,(B[3..4].q0).H0101]):
> h15:=Vector([(A1[]..(),1..2].H1100).K11,(A1[]..(),3..4].H1100).K11]):
> b1:=simplify(p1^%T.(Cq01H+Cq01K+h12+h13+h14+h15-H0101*b-H1100-H2001)):
```

To summarize, we use the following commands to obtain the concrete formulas (3.65).

```
> a;  b;  H2000;   H1100;   H0200;  H0010;
> H0001;    K10;     K11;      K2;  H0002;
> H1001;  H0101;       d;   H3000;  e; a1;
> H2001;     b1;
```

The following commands are used to obtain (3.66) and (3.66).

```
> t0:=10/7:
> t1:=0:
> t2:=simplify((2/2401)*(2450*a*b*b1-1225*a1*b^2+144*b^3-4802*a*e+3577*b*d)/(a^2*b)):
> ALPHA:=convert(K11*t0*b*epsilon^2/a+K11*t1*b*epsilon^3/a+(-4*K10/a+K11*t2*b/a+(1/2)*K2*
    t0^2*b^2/a^2)*epsilon^4, Vector):
> ALPHA[1]:
> ALPHA[2]:
> XS:=convert((u0*q0/a+t0*b*H0001/a)*epsilon^2+(u1*q0/a+v0*q1/a+t1*b*H0001/a)*epsilon^3+(
    t2*b*H0001/a+t0*b*u0*H1001/a^2+(1/2)*u0^2*H2000/a^2+(1/2)*t0^2*b^2*H0002/a^2+v1*q1/a
    -4*H0010/a+u2*q0/a)*epsilon^4, Vector):
> collect(XS,epsilon):
> u0:= 2-6/cosh(t)^2:
> v0:=12*tanh(t)/cosh(t)^2:
> u1:=0:
> v1:=-(6/7)*b*sinh(t)/(a*cosh(t))*v0:
> u2:=-(1/49)*(-210*a1*b+18*b^2+147*d)*sech(t)^2/a^2-(2/7)*(5*a1*b+7*d)/a^2:
> v2:=((3/7)*b^2/a^2+(3/2)*d/a^2-(5/14)*a1*b/a^2+(-(9/4)*d/a^2-(27/98)*b^2/a^2)/cosh(t)
    ^2)*v0:
```

By the following commands we plot the homoclinic orbits, the result is shown in Figure A.1.

```
> with(plots):
> for i to 10 do
> epsilon:=0.002*i;
> P[i] := plot([XS[1],XS[2],t=-200..200],numpoints=1000,color=black);
> end do:
> display(seq(P[i],i=1..10));
```

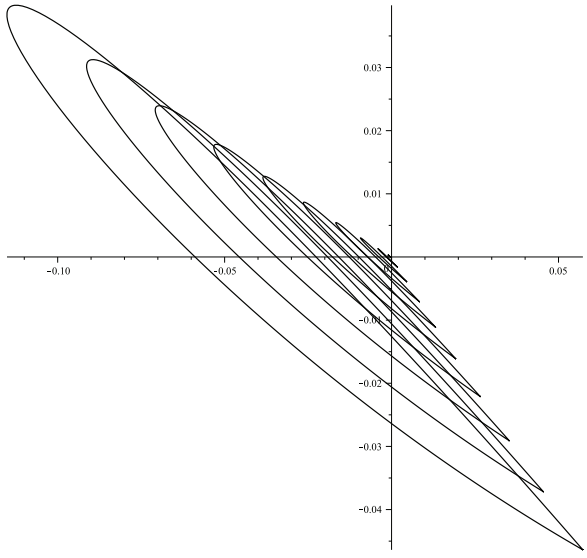

Figure A.1: Homoclinic orbits of (2.75). The Bogdanov-Takens point is $(0, 0)$.

APPENDIX B

Stability analysis using MATLAB

This appendix provides a part of the MATLAB codes that were used to study the monopoly model (6.11).

B.1 Bifurcation diagram Figure 6.1

The first MATLAB function defines the monopoly model

```
function M=monopoly(x,y,delta)
M1=y;
M2=y+delta*(3.6-2.4*(x+y)+0.6*(x^2+x*y+y^2)-0.05*(x^3+x^2*y+x*y^2+y^3));

M=[M1, M2];
```

To obtain Figure (6.1) we use the following commands

```
clc; clear all

d=[0:1e-2:4]; n=1e5; e=sqrt(3)-1e-5; Xu0=[3+e,3+e]; Xm0=[3,3]; Xl0=[3-e,3-e];

for j = 1:size(d,2)
   xu(j,1)=Xu0(1); yu(j,1)=Xu0(2);     xm(j,1)=Xm0(1); ym(j,1)=Xm0(2);
   xl(j,1)=Xl0(1); yl(j,1)=Xl0(2);
```

```
    for i = 2:n
      Xu=monopoly(xu(j,i-1),yu(j,i-1),d(j));  Xm=monopoly(xm(j,i-1),ym(j,i-1),d(j));
      Xl=monopoly(xl(j,i-1),yl(j,i-1),d(j));
      xu(j,i)=Xu(1);  yu(j,i)=Xu(2); xm(j,i)=Xm(1);  ym(j,i)=Xm(2);  xl(j,i)=Xl(1);  yl(j,
     i)=Xl(2);
    end
end
hold on
plot(d(:,:),xu(:,(n-200):n),'.b','MarkerSize',5);
plot(d(:,:),xm(:,(n-200):n),'.g','MarkerSize',5);
plot(d(:,:),xl(:,(n-200):n),'.r','MarkerSize',5);
axis([0 4 0 6])
%set(gcf,'Units','inches'); screenposition = get(gcf,'Position');
%set(gcf,'PaperPositionMode','Auto','PaperUnits','Inches','PaperSize',[screenposition
    (3:4)])
```

B.2 Largest Lyapunov exponent (method: I)

```
clc; clear all
format long
%
X0=[3+sqrt(3)-1e-5,3+sqrt(3)-1e-5];
delta=[1.7:0.01:4];       e=0.00001;
phi=0; %phi=pi/2; phi=pi; phi=3*pi/2;
%
k=100; N=100000;
for l=1:size(delta,2)
    X=X0;
    for j=1:k
        X=monopoly(X(1),X(2),delta(l));
    end
    Xh=[X(1)+e*cos(phi),X(2)+e*sin(phi)];
    X=monopoly(X(1),X(2),delta(l));
    Xh=monopoly(Xh(1),Xh(2),delta(l));
    d(1)=norm(Xh-X);
    for i=1:N
     Xh=[X(1)+e*(Xh(1)-X(1))/d(i), X(2)+e*(Xh(2)-X(2))/d(i)]; %Renormalization
     %
     X=monopoly(X(1),X(2),delta(l));
     Xh=monopoly(Xh(1),Xh(2),delta(l));
     d(i+1)=norm(X-Xh);
    end
    %The greatest Lyapunov exponent
    L0(l)=1/(N+1)*sum(log(d/e));
end
Lyapunov = [delta;L0];
%
hold on
plot(Lyapunov(1,:),Lyapunov(2,:),'-b','LineWidth',1.2);
line([0 4], [0 0]);
%--------------------------------------------------------------------------
```

B.3 Largest Lyapunov exponent (method: II)

The first function defines the Jacobian matrix of the monopoly model.

```
function Mjac=Mjac(x,y,delta)
fx=0;   fy=1;
gx=0+delta*(-2.4+0.6*(2*x+y)-0.05*(3*x^2+2*x*y+y^2));
gy=1+delta*(-2.4+0.6*(x+2*y)-0.05*(x^2+2*x*y+3*y^2));
Mjac=[fx,fy; gx,gy];
```

The largest Lyapunov exponents can be computed by running the following commands

```

clc; clear all

X0=[3+sqrt(3)-1e-5,3+sqrt(3)-1e-5];
delta = [0.01:0.01:4];
k=100;
N = 10000;
%
for j = 1:size(delta,2)
    X=X0;
    for l=1:k
        X=monopoly(X(1),X(2),delta(j));
    end
    phi=angle(complex(X(1),X(2)));
  for i = 1:N
      J=Mjac(X(1),X(2),delta(j));
      Dir=[cos(phi);sin(phi)];
      E=J*Dir;
      d=norm(E);
      s(i)=log(d);
      T2(i,j)=sum(s)/i;
      T1(i)=i;
      %Renormalization
      X=monopoly(X(1),X(2),delta(j));
      phi=angle(complex(E(1)/d,E(2)/d));
  end
  %The greatest Lyapunov exponent
  lya(j) = sum(s)/N;
end
%--------------------------------------------------------------------------
Lyapunov = [delta;lya];
%
hold on
line([0 4], [0 0]);
plot(Lyapunov(1,:),Lyapunov(2,:),'-b','LineWidth',2);
```

Bibliography

[1] E. Ahmed, M. Elettreby, and A. Hegazi. On Puu's incomplete information formulation for the standard and multi-team Bertrand game. *Chaos, Solitons & Fractals*, 30(5):1180 – 1184, 2006.

[2] B. Al-Hdaibat, W. Govaerts, Yu.A. Kuznetsov, and H. G. E. Meijer. Initialization of homoclinic solutions near Bogdanov-Takens points: Lindstedt-Poincaré compared with regular perturbation method. Submitted to *SIAM Journal on Applied Dynamical Systems*, 2015.

[3] B. Al-Hdaibat, W. Govaerts, and N. Neirynck. On periodic and chaotic behavior in a two-dimensional monopoly model. *Chaos, Solitons & Fractals*, 70:27 – 37, 2015.

[4] K. T. Alligood, T. D. Sauer, and J. A. Yorke. *Chaos: An Introduction to Dynamical Systems*. Springer-Verlag, New York, 1996.

[5] A. A. Andronov, E. A. Leontovich, I. I. Gordon, and A. G. Maier. *Qualitative Theory of Second-Order Dynamic Systems*. John Wiley & Sons, New York, 1973.

[6] V. I. Arnold. *Geometrical Methods in the Theory of Ordinary Differential Equations*. Springer-Verlag, 1983.

[7] D. K. Arrowsmith and C. M. Place. *An Introduction to Dynamical Systems*. Cambridge University Press, 1990.

[8] S. Askar. On complex dynamics of monopoly market. *Economic Modelling*, 31:586 – 589, 2013.

[9] W. J. Baumol and R. E. Quandt. Rules of thumb and optimally imperfect decisions. *The American Economic Review*, 54(2):pp. 23–46, 1964.

[10] A. S. Bazanella and R. Reginatto. Robustness margins for indirect field oriented control of induction motors. *IEEE Trans. Autom. Contr.*, 45(6):1226–1231, 2000.

[11] A. S. Bazanella and R. Reginatto. Instability mechanisms in indirect field oriented control drives: Theory and experimental results. In *IFAC World Congress*, volume 15, Part I, pages 1572–1572, Barcelona, Spain, 2002.

[12] J. Bechhoefer. The birth of period 3, revisited. *Mathematics Magazine*, 69(2):115–118, 1996.

[13] M. Belhaq, B. Fiedler, and F. Lakrad. Homoclinic connections in strongly self-excited nonlinear oscillators: The Melnikov function and the elliptic Lindstedt-Poincaré method. *Nonlinear Dynamics*, 23(1):67–86, 2000.

[14] M. Belhaq, F. Lakrad, and A. Fahsi. Predicting homoclinic bifurcations in planar autonomous systems. *Nonlinear Dynamics*, 18(4):303–310, 1999.

[15] W.-J. Beyn. Numerical analysis of homoclinic orbits emanating from a Takens-Bogdanov point. *IMA J. Numer. Anal.*, 14(3):381–410, 1994.

[16] W.-J. Beyn, A. R. Champneys, E. J. Doedel, W. Govaerts, Yu.A. Kuznetsov, and B. Sandstede. Numerical continuation, and computation of normal forms. In B. Fiedler, editor, *Handbook of Dynamical Systems, II*, pages 149–219. Elsevier Science, North Holland, 2002.

[17] W.-J. Beyn, T. Hüls, and Y. Zou. Numerical analysis of degenerate connecting orbits for maps. *International Journal of Bifurcation and Chaos*, 14(10):3385–3407, 2004.

[18] W.-J. Beyn and J.-M. Kleinkauf. The numerical computation of homoclinic orbits for maps. *SIAM J. Numer. Anal*, 34:1207–1236, 1996.

[19] S. Bindel, J. Demmel, and M. Friedman. Continuation of invariant subspaces for large bifurcation problems. Technical Report UCB/EECS-2006-13, EECS Department, University of California, Berkeley, Feb 2006.

[20] R. I. Bogdanov. Versal deformations of a singular point on the plane in the case of zero eigenvalues. *Functional Anal. Appl.*, 9:144–145, 1975.

[21] R. I. Bogdanov. Bifurcations of a limit cycle of a certain family of vector fields on the plane. In *Proceedings of Petrovskii Seminar, Vol. 2*, pages 23–35. Moscow State University, Moscow, 1976. In Russian (English translation: *Selecta Math. Soviet.* **1**, 1981, 373-388).

[22] J. Bovy. Lyapunov exponents and strange attractors in discrete and continuous dynamical systems. Theoretical Physics Project, KU Leuven University, Belgium, September 2004.

[23] F. Brauer and J. Nohel. *The Qualitative Theory of Ordinary Differential Equations.* Dover, New York, 1969.

[24] F. Brauer and A. C. Soudack. Stability regions and transition phenomena for harvested predator-prey systems. *J. Math. Biol*, 7:319–337, 1979.

[25] H. Broer. Normal forms in perturbation theory. In R. A. Meyers, editor, *Encyclopedia of Complexity and Systems Science*, pages 6310–6329. Springer New York, 2009.

[26] H. Broer, R. Roussarie, and C. Simó. Invariant circles in the Bogdanov-Takens bifurcation for diffeomorphisms. *Ergodic Theory and Dynamical Systems*, 16:1147–1172, 12 1996.

[27] H. Broer and G. Vegter. Subordinate Šil'nikov bifurcations near some singularities of vector fields having low codimension. *Ergodic Theory and Dynamical Systems*, 1984.

[28] R. Brown and L. O. Chua. Clarifying chaos: Examples and counterexamples. *International Journal of Bifurcation and Chaos*, 06(02):219–249, 1996.

[29] V. I. Bykov, G. S. Yablonskii, and V. F. Kim. On one simple model of kinetic self-oscillations in catalytic reaction of CO-oxidation. *Dokl. Sov. Math.*, pages 637–639, 1978.

[30] Y.Y. Cao, K.W. Chung, and J. Xu. A novel construction of homoclinic and heteroclinic orbits in nonlinear oscillators by a perturbation-incremental method. *Nonlinear Dynamics*, 64(3):221–236, 2011.

[31] A. R. Champneys and V. Kirk. The entwined wiggling of homoclinic curves emerging from saddle-node/Hopf instabilities. *Physica D: Nonlinear Phenomena*, 195(1–2):77 – 105, 2004.

[32] A. R. Champneys and Yu.A. Kuznetsov. Numerical detection and continuation of codimension-two homoclinic bifurcations. *International Journal of Bifurcation and Chaos*, 4(4):785–822, 1994.

[33] A. R. Champneys, Yu.A. Kuznetsov, and B. Sandstede. A numerical toolbox for homoclinic bifurcation analysis. *International Journal of Bifurcation and Chaos*, 6(5):867–887, 1996.

[34] J. P. Chávez. Starting homoclinic tangencies near 1:1 resonances. *International Journal of Bifurcation and Chaos*, 20(10):3157–3172, 2010.

[35] S.H. Chen, Y.Y. Chen, and K.Y. Sze. A hyperbolic perturbation method for determining homoclinic solution of certain strongly nonlinear autonomous oscillators. *Journal of Sound and Vibration*, 322(1–2):381–392, 2009.

[36] S.H. Chen, Y.Y. Chen, and K.Y. Sze. Homoclinic and heteroclinic solutions of cubic strongly nonlinear autonomous oscillators by hyperbolic Lindstedt-Poincaré method. *Science China Technological Sciences*, 53(3):692–702, 2010.

[37] S.H. Chen, X.M. Yang, and Y.K. Cheung. Periodic solutions of strongly quadratic non-linear oscillators by the elliptic Lindstedt-Poincaré method. *Journal of Sound and Vibration*, 227(5):1109–1118, 1999.

[38] Y.Y. Chen and S.H. Chen. Homoclinic and heteroclinic solutions of cubic strongly nonlinear autonomous oscillators by the hyperbolic perturbation method. *Nonlinear Dynamics*, 58(1-2):417–429, 2009.

[39] Y.Y. Chen, S.H. Chen, and K.Y. Sze. A hyperbolic Lindstedt-Poincaré method for homoclinic motion of a kind of strongly nonlinear autonomous oscillators. *Acta Mechanica Sinica*, 25(5):721–729, 2009.

[40] Y.Y. Chen, L.W. Yan, K.Y. Sze, and S.H. Chen. Generalized hyperbolic perturbation method for homoclinic solutions of strongly nonlinear autonomous systems. *Appl. Math. Mech. (English Ed.)*, 33(9):1137–1152, 2012.

[41] S.-N. Chow, C. Li, and D. Wang. *Normal Forms and Bifurcation of Planar Vector Fields*. Cambridge University Press, 1994.

[42] P. H. Coullet and E. A. Spiegel. Amplitude equations for systems with competing instabilities. *SIAM J. Appl. Math.*, 43:776–821, 1983.

[43] A. de Almeida. *Hamiltonian Systems: Chaos and Quantization*. Cambridge University Press, Cambridge, 1988.

[44] C. de Boor and B. Swartz. Collocation at Gaussian points. *SIAM Journal on Numerical Analysis*, 10(4):pp. 582–606, 1973.

[45] V. De Witte. *Computational Analysis of Bifurcations of Periodic Orbits*. PhD thesis, Ghent University, 2013.

[46] V. De Witte, F. Della Rossa, W. Govaerts, and Yu.A. Kuznetsov. Numerical periodic normalization for codim 2 bifurcations of limit cycles: Computational formulas, numerical implementation, and examples. *SIAM Journal on Applied Dynamical Systems*, 12(2):722–788, 2013.

[47] V. De Witte, W. Govaerts, Yu.A. Kuznetsov, and M. Friedman. Interactive initialization and continuation of homoclinic and heteroclinic orbits in MATLAB. *ACM Trans. Math. Software*, 38(3):Art. 18, 34, 2012.

[48] A. Delshams and R. Ramìrez-Ros. Poincaré-Melnikov-Arnold method for twist maps. In C. Simó, editor, *Hamiltonian Systems with Three or More Degrees of Freedom*, volume 533 of *NATO ASI Series*, pages 533–537. Springer Netherlands, 1999.

[49] J. W. Demmel, L. Dieci, and M. J. Friedman. Computing connecting orbits via an improved algorithm for continuing invariant subspaces. *SIAM J. Sci. Comput*, 22:81–94, 2000.

[50] R. Devaney. *An Introduction to Chaotic Dynamical Systems*. Westview Press, 2nd edition, 2003.

[51] A. Dhooge, W. Govaerts, and Yu.A. Kuznetsov. MATCONT: a MATLAB package for numerical bifurcation analysis of ODEs. *ACM Trans. Math. Software*, 29(2):141–164, 2003.

[52] A. Dhooge, W. Govaerts, Yu.A. Kuznetsov, H. G. E. Meijer, and B. Sautois. New features of the software MatCont for bifurcation analysis of dynamical systems. *Math. Comput. Model. Dyn. Syst.*, 14(2):147–175, 2008.

[53] L. Dieci and T. Eirola. On smooth decompositions of matrices. *SIAM J. Matrix Anal. Appl.*, 20(3):800–819, May 1999.

[54] L. Dieci and M. J. Friedman. Continuation of invariant subspaces. *Numerical Linear Algebra with Applications*, 8(5):317–327, 2001.

[55] E. J. Doedel and J. P. Kernévez. Auto: Software for continuation and bifurcation problems in ordinary differential equations. Applied mathematics report, California Institute of Technology, Pasadena CA, 1986. 226 pages.

[56] F. Dumortier, S. Ibánez, H. Kokubu, and C. Simó. About the unfolding of a hopf-zero singularity. *Discrete and Continuous Dynamical Systems*, 33(10):4435–4471, 2013.

[57] S. A. Elaydi. *Discrete Chaos: With Applications in Science and Engineering*. Chapman & Hall/CRC, 2nd edition, 2008.

[58] C. Elphick, E. Tirapegui, M. E. Brachet, P. H. Coullet, and G. Iooss. A simple global characterization for normal forms of singular vector fields. *Physica D*, 32:95–127, 1987.

[59] J. England, B. Krauskopf, and H. Osinga. Computing one-dimensional stable manifolds and stable sets of planar maps without the inverse. *SIAM Journal on Applied Dynamical Systems*, 3(2):161–190, 2004.

[60] M. Fečkan. Bifurcation and chaos in discontinuous and continuous systems. In Albert C.J. Luo and Nail H. Ibragimov, editors, *Nonlinear Physical Science*. Springer-Verlag, Berlin Heidelberg, 2011.

[61] M. Friedman, W. Govaerts, Yu.A. Kuznetsov, and B. Sautois. Continuation of homoclinic orbits in Matlab. In V. S. Sunderam, G. D. van Albada, P. M. A. Sloot, and J. J. Dongarra, editors, *Computational Science – ICCS 2005*, volume 3514 of *Lecture Notes in Computer Science*, pages 263–270. Springer Berlin Heidelberg, 2005.

[62] P. Gaspard. Local birth of homoclinic chaos. *Physica D: Nonlinear Phenomena*, 62(1–4):94 – 122, 1993.

[63] K. Geist, U. Parlitz, and W. Lauterborn. Comparison of different methods for computing Lyapunov exponents. *Progress of Theoretical Physics*, 83(5):875–893, 1990.

[64] V. Gelfreich. Chaotic zone in the Bogdanov-Takens bifurcation for diffeomorphisms. In H. Begehr, R. Gilbert, and M. Wong, editors, *Analysis and Applications - ISAAC 2001*, volume 10 of *International Society for Analysis, Applications and Computation*, pages 187–197. Springer, US, 2003.

[65] V. Gelfreich and V. Naudot. Analytic invariants associated with a parabolic fixed point in $x \in \mathbb{C}^2$. *Ergodic Theory and Dynamical Systems*, 28:1815–1848, 12 2008.

[66] V. Gelfreich and V. Naudot. Width of homoclinic zone for quadratic maps. *Experimental Mathematics*, 18(4):409–427, 2009.

[67] M. L. Glasser, V. G. Papageorgiou, and T. C. Bountis. Mel'nikov's function for two-dimensional mappings. *SIAM Journal on Applied Mathematics*, 49(3):pp. 692–703, 1989.

[68] F. Gordillo, F. Salas, R. Ortega, and J. Aracil. Hopf bifurcation in indirect field-oriented control of induction motors. *Automatica*, 38:829–835, 2002.

[69] W. B. Gordon. Period three trajectories of the logistic map. *Mathematics Magazine*, 69(2):118–120, 1996.

[70] W. Govaerts. *Numerical Methods for Bifurcations of Dynamical Equilibria*. SIAM, Philadelphia, PA, 2000.

[71] W. Govaerts, R. Khoshsiar Ghaziani, Yu.A. Kuznetsov, and H. G. E. Meijer. Numerical methods for two-parameter local bifurcation analysis of maps. *SIAM J. Sci. Comput.*, 29(6):2644–2667, Oct. 2007.

[72] W. Govaerts and Yu.A. Kuznetsov. Numerical continuation methods for dynamical systems. In B. Krauskopf, H. Osinga, and J. Galán-Vioque, editors, *Interactive Continuation Tools*, pages 51–75. Springer Netherlands, 2007.

[73] W. Govaerts and J. D. Pryce. Mixed block elimination for linear-systems with wider borders. *IMA Journal of Numerical Analysis*, 13(2):161–180, 1993.

[74] J.-M. Grandmont. Nonlinear difference equations, bifurcations and chaos: An introduction. *Research in Economics*, 62(3):122 – 177, 2008.

[75] P. Gray and S. Scott. Autocatalytic reactions in the isothermal, continuous stirred tank reactor: Isolas and other forms of multistability. *Chemical Engineering Science*, 38(1):29–43, 1983.

[76] P. Gray and S. Scott. Autocatalytic reactions in the isothermal, continuous stirred tank reactor: Oscillations and instabilities in the system A + 2B $\rightarrow$ 3B; B $\rightarrow$ C. *Chemical Engineering Science*, 39(6):1087–1097, 1984.

[77] P. Gray and S. Scott. Sustained oscillations and other exotic patterns of behavior in isothermal reactions. *The Journal of Physical Chemistry*, 89(1):22–32, 1985.

[78] J. Guckenheimer and P. Holmes. *Nonlinear Oscillations, Dynamical Systems and Bifurcations of Vector Fields*. Springer-Verlag, New York, 1983.

[79] D. Gulick. *Encounters with Chaos*. McGraw-Hill, New York, 1992.

[80] D. Hennig, K. O. Rasmussen, H. Gabriel, and A. Bülow. Solitonlike solutions of the generalized discrete nonlinear Schrödinger equation. *Physical Review E*, 54(5):5788–5801, 1996.

[81] E. Jury. "Inners" approach to some problems of system theory. *IEEE Transactions on Automatic Control*, 16(3):233–240, 1971.

[82] H. B. Keller. Numerical solution of bifurcation and nonlinear eigenvalue problems. In P. H. Rabinowitz, editor, *Applications of Bifurcation Theory*, pages 359–384, New York, 1977. Academic Press.

[83] A. I. Khibnik. LINLBF: A program for continuation and bifurcation analysis of equilibria up to codimenson three. In D. Roose, B. De Dier, and A. Spence, editors, *Continuation and Bifurcations: Numerical Techniques and Applicatins*, NATO ASI Series C313, pages 283–296. Kluwer Academic, 1990.

[84] R. Khoshsiar Ghaziani. *Bifurcations of Maps: Numerical Algorithms and Applications*. PhD thesis, Ghent University, 2008.

[85] R. Khoshsiar Ghaziani, W. Govaerts, Yu.A. Kouznetsov, and H. G. E. Meijer. Numerical continuation of connecting orbits of maps in MATLAB. *Journal of Difference Equations and Applications*, 15:849–875, 2009.

[86] S. Kolyada and L. Snoha. Some aspects of topological transitivity - a survey. *Proc. ECIT-94, Grazer Mathematische Berichte*, 334:3–35, 1997.

[87] Yu.A. Kuznetsov. Numerical normalization techniques for all codim 2 bifurcations of equilibria in ODEs. *SIAM J. Numer. Anal.*, 36:1104–1124, 1999.

[88] Yu.A. Kuznetsov. *Elements of Applied Bifurcation Theory*. Springer-Verlag, New York, 3rd edition, 2004.

[89] Yu.A. Kuznetsov. Practical computation of normal forms on center manifolds at degenerate Bogdanov–Takens bifurcations. *International Journal of Bifurcation and Chaos*, 15(11):3535–3546, 2005.

[90] Yu.A. Kuznetsov, W. Govaerts, E. J. Doedel, and A. Dhooge. Numerical periodic normalization for codim 1 bifurcations of limit cycles. *SIAM Journal on Numerical Analysis*, 43(4):1407–1435, 2006.

[91] Yu.A. Kuznetsov, H. G. E. Meijer, B. Al-Hdaibat, and W. Govaerts. Improved homoclinic predictor for Bogdanov-Takens bifurcation. *International Journal of Bifurcation and Chaos*, 24(4):1450057 (12 pages), 2014.

[92] Yu.A. Kuznetsov, H. G. E. Meijer, B. Al-Hdaibat, and W. Govaerts. Accurate approximation of homoclinic solutions in Gray-Scott kinetic model. *International Journal of Bifurcation and Chaos*, 25(9):1550125 (10 pages), 2015.

[93] Yu.A. Kuznetsov, H. G. E. Meijer, W. Govaerts, and B. Sautois. Switching to nonhyperbolic cycles from codim 2 bifurcations of equilibria in ODEs. *Physica D*, 237:3061–3068, 2008.

[94] C. Li., C. Rousseau, and X. Wang. A simple proof for the unicity of the limit cycle in the Bogdanov-Takens system. *Canad. Math. Bull.*, 33:84–92, 1990.

[95] T.-Y. Li and J. A. Yorke. Period three implies chaos. *The American Mathematical Monthly*, 82(10):985–992, 1975.

[96] M. Lines. *Nonlinear Dynamical Systems in Economics*. Springer, Vienna, 2005.

[97] A. C. J. Luo. *Regularity and Complexity in Dynamical Systems*. Springer, New York, 2012.

[98] A. Matsumoto and F. Szidarovszky. Discrete and continuous dynamics in nonlinear monopolies. *Applied Mathematics and Computation*, 232:632 – 642, 2014.

[99] W. Mazin, K. Rasmussen, E. Mosekilde, P. Borckmans, and G. Dewel. Pattern formation in the bistable Gray-Scott model. *Mathematics and Computers in Simulation*, 40(3-4):371–396, 1996.

[100] W. Mestrom. *Continuation of Limit Cycles in MATLAB*. Master's thesis, Utrecht University, 2002.

[101] J. Moiola and G. Chen. *Hopf Bifurcation Analysis: A Frequency Domain Approach*. World Scientific, Singapore, 1996.

[102] C. Morris and H. Lecar. Voltage oscillations in the barnacle giant muscle fiber. *Biophys. J.*, 35:1418–1450, 1991.

[103] P. J. Myrberg. Sur l'itération des polynômes réels quadratiques. *J. Math. Pures Appl.*, 9(41):339–351, 1962.

[104] A. K. Naimzada and G. Ricchiuti. Complex dynamics in a monopoly with a rule of thumb. *Applied Mathematics and Computation*, 203(2):921 – 925, 2008.

[105] A. H. Nayfeh. *Introduction to Perturbation Techniques*. John Wiley & Sons, New York, 1981.

[106] A. H. Nayfeh and B. Balachandran. *Applied Nonlinear Dynamics: Analytical, Computational and Experimental Methods*. Wiley-VCH, Germany, 1995.

[107] N. Neirynck, B. Al-Hdaibat, W. Govaerts, Yu.A. Kuznetsov, and H. G. E. Meijer. Using MatContM in the study of a nonlinear map in economics. *Journal of Physics: Series Proceedings*, 2015 (Accepted).

[108] H.-O. Peitgen, H. Jürgens, and D. Saupe. *Chaos and Fractals: New Frontiers of Science*. Springer-Verlag, New York, 2nd edition, 2004.

[109] L. Perko. *Differential Equations and Dynamical Systems*. Springer, 3rd edition, 2000.

[110] H. Poincaré. *Sur les propriétés de fonctions définies par les équations aux differences partielles*. Gauthier-Villars, Paris, 1879. 1re thèse.

[111] T. Puu. The chaotic monopolist. *Chaos, Solitons & Fractals*, 5(1):35 – 44, 1995.

[112] T. Puu. *Attractors, Bifurcations, and Chaos: Nonlinear Phenomena in Economics*. Springer-Verlag, Berlin, 2000.

[113] A. Riet. *A Continuation Toolbox in MATLAB*. Master's thesis, Utrecht University, 2000.

[114] A.J. Rodríguez-Luis, E. Freire, and E. Ponce. A method for homoclinic and heteroclinic continuation in two and three dimensions. In D. Roose, B. De Dier, and A. Spence, editors, *Continuation and Bifurcations: Numerical Techniques and Applications*, NATO ASI Series C313, pages 197–210. Kluwer Academic, 1990.

[115] P. Saha and S. Strogatz. The birth of period three. *Mathematics Magazine*, 68(1):42–47, 1995.

[116] F. Salas, F. Gordillo, and J. Aracil. Codimension-two bifurcations in indirect field oriented control of induction motor drives. *International Journal of Bifurcation and Chaos*, 18(3):779–792, 2008.

[117] F. Salas, R. Reginatto, F. Gordillo, and J. Aracil. Bogdanov-Takens bifurcation in indirect field oriented control of induction motor drives. In *Proc. CDC*, pages 4357–4362, Atlantis, Bahamas, 2004.

[118] M. Sandri. Numerical calculation of Lyapunov exponents. *The Mathematica Journal*, 6(3):78–84, 1996.

[119] H. Sedaghat. *Nonlinear Difference Equations: Theory with Applications to Social Science, Science Models*. Kluwer Academic Publishers, New York, 2003.

[120] Y. Shi and P. Yu. On chaos of logistic maps. *Dynamics of Continuous, Discrete and Impulsive Systems. Series B: Applications & Algorithms*, 14(2):175–195, 2007.

[121] A. Shil'nikov, G. Nicolis, and C. Nicolis. Bifurcation and predictability analysis of a low-order atmospheric circulation model. *International Journal of Bifurcation and Chaos*, 5(6):1701–1711, 1995.

[122] S. H. Strogatz. *Nonlinear Dynamics and Chaos*. Addison-Wesley, New York, 1994.

[123] F. Takens. Forced oscillations and bifurcations. *Comm. Math. Inst., Rijksuniversiteit Utrecht*, 2:1–111, 1974. Reprinted in *Global Analysis of Dynamical Systems*, Institute of Physics, Bristol, 2001, pp. 1–61.

[124] H. Thunberg. Periodicity versus chaos in one-dimensional dynamics. *SIAM Review*, 43(1):3–30, 2001.

[125] D. Ueyama. Dynamics of self-replicating patterns in the one-dimensional Gray-Scott model. *Hokkaido Math. J.*, 28(1):175–210, 02 1999. Hokkaido University, Department of Mathematics.

[126] D. van Kekem. *Homoclinic Orbits of Planar Maps: Asymptotics and Mel'nikov Functions*. Master's thesis, Utrecht University, January 2014.

[127] L. van Veen. Baroclinic flow and the Lorenz-84 model. *International Journal of Bifurcation and Chaos*, 13(8):2117–2139, 2003.

[128] J. Vandenameele. *Niet-lineaire Fenomenen in de Economie*. Master's thesis, Ghent University, 2014.

[129] P. F. Verhulst. Recherches mathématiques sur la loi d'accroissement de la population. *Nouveaux Mémoires de l'Académie Royale des Sciences et Belles-Lettres de Bruxelles*, 18:1–42, 1845.

[130] S. Wiggins. *Chaotic Transport in Dynamical Systems*. Springer-Verlag, New York, 1992.

[131] S. Wiggins. *Introduction to Applied Nonlinear Dynamical Systems and Chaos*. Springer-Verlag, New York, 2nd edition, 2003.

[132] A. Wolf, J. B. Swift, H. L. Swinney, and J. A. Vastano. Determining Lyapunov exponents from a time series. *Physica D: Nonlinear Phenomena*, 16(3):285 – 317, 1985.

[133] D. Xiao and S. Ruan. Bogdanov-Takens bifurcations in harvested predator-prey systems. *Fields Institute Communications*, 21:493–506, 1999.

[134] W.-B. Zhang. *Discrete Dynamical Systems, Bifurcations and Chaos in Economics*, volume 204 of *Mathematics in Science and Engineering*. Elsevier, 2006.

Acknowledgments

First of all, I must thank Allah (God) for giving me the vision, power, spirit and endurance to complete my PhD research.

I am deeply indebted to my supervisor Willy Govaerts for his fundamental role in my doctoral work. Willy, thank you for all of the guidance, assistance and expertise that you provided me during my PhD. I quite simply cannot imagine a better supervisor. I also want to thank Yuri Kuznetsov for his ideas and tremendous support which had a major influence on this thesis. Yuri, without your ideas and support it would not be possible to conduct this research.

Many thanks to Hil Meijer for his collaboration and insightful discussions during my research. He must be acknowledged for his crucial contribution to this thesis. I also have to thank the members of my PhD committee, Prof. Marnix Van Daele, Prof. Peter De Maesschalck, Prof. Hans De Meyer and Prof. Hans Vernaeve, for carefully reading my text and providing me with their comments.

Many thanks to my friends and colleagues for the great time and the cool discussions we had in Ghent. I enjoyed the atmosphere, their friendship, and their support. A special thank goes to Johan Steen, Hilmar Gudmundsson, Beatriz Sinova, Omar Ibrahim, Ahmed Atef, Xianming Sun, Diego Zapico, Mushthofa Mushthofa, Carmen Landuyt, Charlotte Sonck, Gustavo Torres, Holger Cevallos, Tim Decraecker, Virginie De Witte. I would like to thank my officemates Catherine Daveloose, Niels Neirynck, and Veerle Ledoux for their friendship and support during my research.

Last but not least, thanks to my family who always supported me. Your prayer for me was what sustained me thus far.

Thank you so much!

Bashir Al-Hdaibat
Ghent, Belgium

December 2015

Nederlandstalige samenvatting

Computationele Analyse van Dynamische Systemen:

Bogdanov-Takens Punten en een Economisch Model

door

Bashir Al-Hdaibat
Universiteit Gent, België

Promotoren:
Prof. dr. Willy Govaerts & Prof. dr. Yuri A. Kuznetsov

Het onderwerp van deze thesis is de bifurcatieanalyse van dynamische systemen, d.w.z. stelsels van gewone differentiaalvergelijkingen en geïtereerde afbeeldingen. Een hoofddoelstelling is de studie van de tak van homoclinische oplossingen die zijn oorsprong vindt in een generiek Bogdanov-Takens punt. Het probleem van de benadering van deze tak werd reeds intensief bestudeerd in de literatuur maar tot nog toe werd geen exacte oplossing gevonden, noch een hogere-orde benadering. Wij gebruiken de klassieke "blow-up" techniek om een gepaste normaalvorm in de buurt van een Bogdanov-Takens punt te herleiden tot een geperturbeerd Hamiltoniaans systeem. Met een reguliere perturbatiemethode en een veralgemening van de Lindstedt-Poincaré methode bekomen we twee expliciete derde-orde correcties van de niet-geperturbeerde homoclinische baan en parameterwaarde. We tonen aan dat beide methoden leiden tot dezelfde homoclinische parameterwaarde als de klassieke Melnikov methode en de vertakkingsmethode. We tonen ook aan dat de reguliere perturbatiemethode leidt tot een "parasitische kering" nabij het zadelpunt terwijl de Lindstedt-Poincaré oplossing dit merkwaardige verschijnsel niet vertoont. Dit maakt de Lindstedt-Poincaré methode beter geschikt voor numerieke implementatie. Om de normaalvorm in de centrale variëteit

te bekomen, gebruiken we de standaard parameter-afhankelijke reductie gecombineerd met een normalizatie, waarbij de Fredholm oplosbaarheid van de homologische vergelijking geëist wordt. Door het systematisch oplossen van alle lineaire stelsels die verschijnen in de Taylorontwikkeling van de homologische vergelijking corrigeren we een dubbelzinnigheid (fout) in de transformatie van de parameters die standaard voorkomt in de bestaande literatuur. We gebruiken verder de generieke homoclinische predictors om expliciet de homoclinische oplossingen in het kinetische Gray-Scott model te bekomen. We bespreken ook de implementatie van beide predictors in de Matlab continuatiesoftware MatCont en hun gebruik in vijf numerieke voorbeelden. Aansluitend hierop tonen we aan hoe de bekomen homoclinische predictors voor generieke differentiaalvergelijkingen gebruikt kunnen worden om de takken van homoclinische tangencies te continueren in de Bogdanov-Takens afbeelding.

In een tweede, korter deel van de thesis passen we bifurcatietheorie toe op het analyzeren van het dynamisch periodiek en chaotisch gedrag van een niet-lineair economisch model. Het gaat om een model voor een monopoliesituatie met kubische prijsfunctie en kwadratische marginale kostfunctie. We stellen fundamentele correcties voor aan vroegere studies van dit model en geven een volledige analytische beschrijving van alle cykels met periode 4. Met een numerieke continuatiemethode berekenen we takken van cykels met periode 5, 10, 13, 17 en bepalen de stabiliteitsgebieden van deze cykels.We tonen ook aan dat de 4-cykels weliswaar stabiel zijn in een groot parameterdomein maar nooit lineair asymptotisch stabiel. We gebruiken verder een niet-lineair criterium voor stabiliteit, analyse van het attractiedomein en simulatie om het exacte stabiliteitsgebied van de 4-cykels te bepalen. We corrigeren hiermee de incorrecte stabiliteitsanalyse in de literatuur die gebaseerd is op een (verkeerde) lineaire analyse van de stabiliteit. De berekening van de Lyapunov exponent bevestigt de bekomen resultaten.

De inhoud van deze thesis werd reeds gepubliceerd of is nu aangeboden voor publicatie, zie [2], [3], [107], [92] en [91].

List of Publications

- **B. Al-Hdaibat**, W. Govaerts, Yu.A. Kuznetsov & H.G.E. Meijer. Initialization of homoclinic solutions near Bogdanov-Takens points: Lindstedt-Poincaré compared with regular perturbation method. Submitted to: *SIAM Journal on Applied Dynamical Systems*, 2015.
- N. Neirynck, **B. Al-Hdaibat**, W. Govaerts, Yu.A. Kuznetsov & H.G.E. Meijer. Using MatContM in the Study of a Nonlinear Map in Economics. *Journal of Physics: Series Proceedings*, Accepted, 2015.
- Yu.A. Kuznetsov, H.G.E. Meijer, **B. Al-Hdaibat** & W. Govaerts. Accurate approximation of homoclinic solutions in Gray-Scott kinetic model. *International Journal of Bifurcation and Chaos*, 25(9), 1550125 (10 pages), 2015.
- **B. Al-Hdaibat**, W. Govaerts & N. Neirynck. On periodic and chaotic behavior in a two-dimensional monopoly model, *Chaos, Solitons & Fractals*. 70, 27-37, 2015.
- Yu.A. Kuznetsov, H.G.E. Meijer, **B. Al-Hdaibat** & W. Govaerts. Improved homoclinic predictor for Bogdanov-Takens bifurcation. *International Journal of Bifurcation and Chaos* 24, 1450057 (12 pages), 2014.
- **B. Al-Hdaibat** & W. Govaerts, (2014). *MatCont tutorial on starting up homoclinic orbits from a Bogdanov-Takens point*, MatCont version 5.3. Available on `http://sourceforge.net/projects/matcont/`

Conferences

- *New asymptotics of homoclinic orbits near Bogdanov-Takens bifurcation point* (May 2015). **Paper presented** at SIAM conference on applications of dynamical systems, Utah, US.
- *Chaos and periodic solutions in a dynamic monopoly model* (May 2015). **Paper presented** at the 8th CHAOS 2015 International Conference, Paris, France.
- *Practical initialization of homoclinic orbits from a Bogdanov-Takens point* (November 2014). **Poster presented** at the 3rd International Conference on Complex Dynamical Systems and Their Applications: New Mathematical Concepts and Applications in Life Sciences, Ankara, Turkey.